Εθνικό Μετσόβιο Πολυτεχνείο
Σχολή Πολιτικών Μηχανικών
Τομέας Γεωτεχνικής

National Technical University of Athens
School of Civil Engineering
Geotechnical Division

Διπλωματική Εργασία

Αγαλιανός Αθανάσιος - Σακελλαριάδης Λάμπρος

Επιβλέποντες

Καθηγητής Γ. Γκαζέτας

Επικ. Καθ. Ι. Αναστασόπουλος

Ιούλιος 2013

ΑΠΛΟΠΟΙΗΜΕΝΗ ΜΕΘΟΔΟΛΟΓΙΑ ΥΠΟΛΟΓΙΣΜΟΥ ΣΕΙΣΜΙΚΗΣ ΤΡΩΤΟΤΗΤΑΣ ΓΕΦΥΡΩΝ ΜΕ ΘΕΩΡΗΣΗ ΑΛΛΗΛΕΠΙΔΡΑΣΗΣ ΕΔΑΦΟΥΣ-ΚΑΤΑΣΚΕΥΗΣ

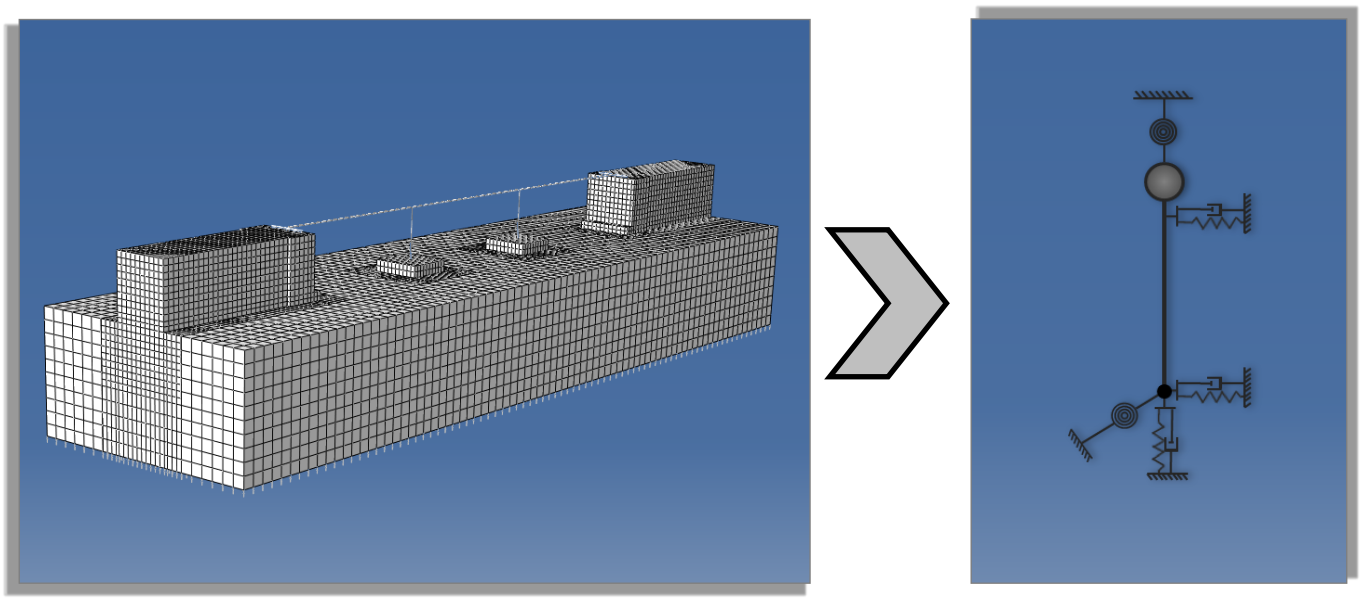

A SIMPLIFIED METHOD TO ESTIMATE SEISMIC VULNERABILITY OF BRIDGES CONSIDERING SOIL-STRUCTURE INTERACTION

Diploma Thesis

Agalianos Athanasios – Sakellariadis Lampros

Supervisors

Professor G. Gazetas

Assist. Prof. I. Anastasopoulos

July 2013

Ευχαριστίες

Ολοκληρώνοντας τη διπλωματική μας εργασία, νιώθουμε βαθιά την ανάγκη να ευχαριστήσουμε τους ανθρώπους που συνέβαλαν στην επίτευξη αυτού του στόχου.

Αρχικά, θα θέλαμε να ευχαριστήσουμε θερμά τον καθηγητή μας Γ. Γκαζέτα που μας τίμησε με την εμπιστοσύνη του και μας έδωσε την ευκαιρία να εργαστούμε υπό την επίβλεψη και την καθοδήγησή του. Η συναναστροφή μαζί του κατά τα χρόνια των σπουδών μας υπήρξε πολύτιμη και ιδιαίτερα διδακτική για εμάς.

Ιδιαίτερες ευχαριστίες οφείλουμε στον επίκουρο καθηγητή Ι. Αναστασόπουλο, για την εξαιρετική συνεργασία που αναπτύξαμε μαζί του όλους αυτούς τους μήνες. Η πολύτιμη καθοδήγηση, οι υποδείξεις και η αμέριστη συμπαράστασή του ήταν καθοριστικές για την επιτυχή ολοκλήρωση αυτής της εργασίας.

Θα θέλαμε επίσης να ευχαριστήσουμε τον επίκουρο καθηγητή Π. Αναστασόπουλο, για την σημαντική βοήθειά του. Η συμβολή του υπήρξε καθοριστική στη κατεύθυνση και τους στόχους της παρούσας εργασίας.

Νιώθουμε ακόμη την ανάγκη να ευχαριστήσουμε ιδιαίτερα το προσωπικό της εταιρίας ''Αττικές Διαδρομές'' για τη φιλοξενία που μας παρείχαν και την πρόθυμη βοήθειά τους.

Ολοκληρώνοντας, θα θέλαμε να ευχαριστήσουμε θερμά τον Δρ. Β. Δρόσο και τον υποψήφιο διδάκτορα Α. Τσάτση για τις συμβουλές και τη διαρκή βοήθειά τους. Βεβαίως, ευχαριστούμε πολύ και όλα τα υπόλοιπα μέλη του Εργαστηρίου Εδαφομηχανικής που μας στήριξαν ενεργά κατά τη διάρκεια της εργασίας αυτής.

Τέλος, νιώθουμε την ανάγκη να ευχαριστήσουμε τις οικογένειές μας και τους φίλους μας που βρίσκονται πάντα δίπλα μας στηρίζοντας τις προσπάθειές μας.

Απλοποιημένη Μεθοδολογία Υπολογισμού Σεισμικής Τρωτότητας Γεφυρών με Θεώρηση Αλληλεπίδρασης Εδάφους-Κατασκευής

Εκτενής Περίληψη

Οι συνέπειες ενός ισχυρού σεισμού σε ένα μητροπολιτικό δίκτυο αυτοκινητοδρόμων μπορούν να διακριθούν σε άμεσες και έμμεσες. Οι άμεσες αναφέρονται στις δομικές βλάβες των υποδομών του δρόμου ενώ οι έμμεσες στην επιδείνωση της λειτουργικότητας. Το τελευταίο μπορεί να είναι είτε λόγω της μείωσης της χωρητικότητας του αυτοκινητοδρόμου λόγω βλάβης των κρίσιμων υποδομών, είτε λόγω αύξησης της ζήτησης που οφείλεται σε δομικές βλάβες εντός του γειτονικού αστικού περιβάλλοντος.

Παρότι οι άμεσες συνέπειες ενός ισχυρού σεισμού δεν μπορούν εύκολα να αποφευχθούν, οι έμμεσες συνέπειες μπορεί να μετριαστούν αποτελεσματικά μέσω της ανάπτυξης και εφαρμογής ενός συστήματος ταχείας αντίδρασης. Ένα τέτοιο σύστημα έχει ως στόχο: (α) τη διασφάλιση της ασφάλειας των χρηστών του αυτοκινητόδρομου και την αποφυγή του αισθήματος πανικού, (β) την ελαχιστοποίηση του κλεισίματος του αυτοκινητόδρομου, και (γ) τη βελτιστοποίηση της λειτουργικότητας του δικτύου μετά το σεισμό.

Η ανάπτυξη ενός τέτοιου συστήματος απαιτεί: (α) την ακριβή εκτίμηση της σεισμικής επικινδυνότητας (β) την εκτίμηση της σεισμικής τρωτότητας των υποδομών ζωτικής σημασίας των αυτοκινητοδρόμων, όπως γέφυρες, σήραγγες, τοίχοι αντιστήριξης, επιχώματα και (γ) γνώση της τυπολογίας καθώς και όλες τις απαραίτητες πληροφορίες σχετικά με τη γεωμετρία και τις ιδιότητες των υλικών του δικτύου και των υποσυστημάτων του.

- **Εκτίμηση Σεισμικής Επικινδυνότητας**

Οι μέθοδοι που χρησιμοποιούνται για τον χαρακτηρισμό της σεισμικής επικινδυνότητας διακρίνονται σε προσδιοριστικούς και στοχαστικούς. Η προσέγγιση που επιλέγεται είναι η χρήση χαρακτηριστικών σεισμικών σεναρίων από τα οποία δημιουργούνται τα πεδία των αναμενόμενων σεισμικών διαταραχών τα οποία και εισάγονται στα μοντέλα κινδύνου.

Εξίσου σημαντική με την επιλογή χαρακτηριστικών σεισμικών σεναρίων είναι και η επιλογή των κατάλληλων μεγεθών έντασης της σεισμικής διαταραχής (Intensity Measures) σε σχέση με τις υπό εξέταση κατασκευές του αυτοκινητοδρόμου.

Σε αυτήν την κατεύθυνση επιλέχθηκαν 29 συνολικά πραγματικές καταγραφές οι οποίες κατά περίπτωση κλιμακώθηκαν με βάση το PGA από 0.1g έως 1.1g. Αντίστοιχα επιλέχθηκαν 19 συνολικά μεγέθη έντασης (IM) προκειμένου να διερευνηθεί η αποδότικότητά τους στην εκτίμηση των δομικών βλαβών στις υπό εξέταση κατασκευές μετά από ένα σεισμικό γεγονός.

- **Σεισμική Τρωτότητα Κρίσιμων Υποδομών Αυτοκινητοδρόμου**

Ένας τρόπος που χρησιμοποιείται ευρέως προκειμένου να εκφραστεί η σεισμική τρωτότητα των υποδομών ενός αυτοκινητοδρόμου, ειδικότερα στην περίπτωση των γεφυρών, είναι οι καμπύλες τρωτότητας (fragility curves). Οι καμπύλες αυτές περιγράφουν την πιθανότητα ένα δομικό στοιχείο να βρεθεί ή να υπερβεί μια συγκεκριμένη κατάσταση βλάβης (Damage State) για δεδομένη σεισμική ένταση. Οι καμπύλες αυτές διακρίνονται σε (α) καμπύλες που προκύπτουν με βάση την κρίση εμπειρογνωμόνων, (β) εμπειρικές με βάση τις καταστροφές μετά από σεισμούς και (γ) αναλυτικές που βασίζονται σε αριθμητικές αναλύσεις.

Αν και στην βιβλιογραφία είναι διαθέσιμη πληθώρα τέτοιων καμπυλών για γέφυρες συνήθως αυτές αναφέρονται σε ένα μόνο στοιχείο της γέφυρας το οποίο θεωρείται αντιπροσωπευτικό της συνολικής τρωτότητας. Ένα ακόμα χαρακτηριστικό των συγκεκριμένων καμπυλών είναι ότι χρησιμοποιούν ένα μέγεθος έντασης (IM), αυτό που κρίνεται ως το πλέον κατάλληλο για την υπό εξέταση κατασκευή.

Ένας ακόμα διαδεδομένος τρόπος έκφρασης της σεισμικής τρωτότητας κατασκευών είναι οι καμπύλες «αυξητικής δυναμικής ανάλυσης» (Incremental Dynamic Analysis curves). Οι καμπύλες αυτές προκύπτουν από αναλύσεις σε μία κατασκευή με κλιμακούμενη αύξηση της έντασης της καταγραφής που χρησιμοποιείται. Σε αυτή την περίπτωση χρησιμοποιούνται μεγέθη όπως ο λόγος απαιτούμενης προς διατιθέμενης πλαστιμότητας, προκειμένου να εκφραστεί η δομική βλάβη της κατασκευής ενώ όπως και στις καμπύλες τρωτότητας χρησιμοποιείται ένα μέγεθος έντασης του σεισμού.

- **Αποδοτικότητα Μεγεθών Έντασης (IM)**

Ένας κεντρικός στόχος της εργασίας είναι ο έλεγχος της αποδοτικότητας καθενός μεγέθους έντασης μεμονωμένα αλλά και ενδεχόμενης συσχέτισης περισσοτέρων στην εκτίμηση της αναμενόμενης δομικής βλάβης μετά από ένα σεισμικό γεγονός. Σε αυτή τη κατεύθυνση στο $2^{ο}$ κεφάλαιο της εργασίας χρησιμοποιήθηκε ένα χαρακτηριστικό βάθρο της γέφυρας Hanshin Expressway Fukae το οποίο έχει μελετηθεί διεξοδικά στο παρελθόν [Μ.Λώλη 2010].

Το βαθρο εξετάστηκε στην εγκάρσια διεύθυνση με θεώρηση μονοβάθμιου συστήματος (SDOF) με πάκτωση στη βάση. Αυτή είναι μια προσέγγιση ευρέως χρησιμοποιούμενη και βασίζεται στο γεγονός ότι η μάζα και η δυσκαμψία του στύλου είναι σημαντικά μικρότερη από την αντίστοιχη του καταστρώματος. Η ορθότητα αυτής της προσέγγισης εξετάζεται σε επόμενο στάδιο της εργασίας. Πραγματοποιήθηκαν συνολικά 377 αναλύσεις με βάση 29 πραγματικές καταγραφές οι οποίες κλιμακώθηκαν συναρτήσει του PGA. Στόχος της ανάλυσης ήταν να διερευνηθεί αν υπάρχει συσχέτιση ανάμεσα σε κάποιο μέγεθος έντασης (IM) από τα 19 που εξετάστηκαν και τους 6 δείκτες δομικής βλάβης που επιλέχθηκαν (Damage Indexes).

Λόγω του ότι δε παρατηρήθηκε σε κανένα από τα μεγέθη ικανοποιητική συσχέτιση εξετάστηκε η δυνατότητα συνδυασμού συγκεκριμένων IM προκειμένου να εκτιμηθεί συγκεκριμένο DI. Χάρη στη δουλειά του Π. Αναστασόπουλου, Επίκουρου Καθηγητή του τμήματος Πολιτικών Μηχανικών του Πανεπιστημίου της Νέας Υόρκης στο Μπάφαλο, με χρήση προχωρημένων οικονομετρικών μοντέλων προέκυψε εξίσωση η οποία συνδυάζει 6 IM και εκτιμά το μέγιστο αναμενόμενο drift. Η

προτεινόμενη εξίσωση παρουσιάζεται στο τέλος του 2ου κεφαλαίου, ενώ η ισχύς της ελέχθηκε σε 5 επιπλέον πραγματικές καταγραφές.

Σύμφωνα με μία απλοποιητική αλλά ευρέως χρησιμοποιούμενη υπόθεση ένα συστατικό μέρος της γέφυρας, όπως το βάθρο, θεωρείται αντιπροσωπευτικό της συνολικής τρωτότητας της γέφυρας. Αν υιοθετηθεί η συγκεκριμένη υπόθεση η προτεινόμενη εξίσωση μπορεί να περιγράψει τη συμπεριφορά της γέφυρας στο σύνολό της. Στη συνέχεια της εργασίας θα ελεγχθεί η ορθότητα της υπόθεσης διερευνώντας την επίδραση των υπόλοιπων συστατικών μερών της γέφυρας.

- **Κριτήριο Ισοδυναμίας Μονοβάθμιων συστημάτων**

Με στόχο την επέκταση της χρήσης της εξίσωσης που προέκυψε στο 2ο κεφάλαιο εξετάστηκε η δυνατότητα διατύπωσης κριτηρίου ισοδυναμίας ανάμεσα σε μονοβάθμια συστήματα. Η διερεύνηση που πραγματοποιήθηκε στο 3ο κεφάλαιο βασίζεται στη λογική υπόθεση ότι δύο μονοβάθμια συστήματα με ίδια ιδιοπερίοδο, επιτάχυνση διαρροής και πλαστιμότητα θα έχουν παρόμοια σεισμική συμπεριφορά. Η κοινή ιδιοπερίοδος εξασφαλίζει ότι η κάθε διαταραχή θα απαιτήσει την ίδια επιτάχυνση ελαστικά από τα δύο συστήματα ενώ η κοινή επιτάχυνση διαρροής εξασφαλίζει ότι τα 2 συστήματα θα εισέλθουν στην πλαστική περιοχή την ίδια χρονική στιγμή. Επιπρόσθετα έχοντας την ίδια πλαστιμότητα εξασφαλίζεται ότι και η τελική αστοχία θα συμπέσει.

Προκειμένου να εξεταστεί η ορθότητα της παραπάνω υπόθεσης δημιουργήθηκαν 2 συστήματα τα οποία έχουν την ίδια ιδιοπερίοδο, επιτάχυνση διαρροής και πλαστιμότητα με το μονοβάθμιο σύστημα που εξετάστηκε στο 2ο κεφάλαιο με τη διαφορά ότι στη μία περίπτωση η μάζα είναι διπλάσια ενώ στην άλλη το ύψος του μονοβάθμιου είναι το μισό. Στις δύο αυτές περιπτώσεις η διατομή του στύλου του μονοβάθμιου συστήματος αυξάνεται και μειώνεται αντίστοιχα προκειμένου η ιδιοπερίοδος να παραμείνει σταθερή.

Στη συνέχεια εξετάζεται η σεισμική συμπεριφορά των 2 αυτών μονοβάθμιων συστημάτων στις 29 καταγραφές που χρησιμοποιήθηκαν στο 2ο κεφάλαιο και συγκρίνεται με την αντίστοιχη του αρχικού μονοβάθμιου συστήματος. Το συμπέρασμα που εξάγεται είναι ότι τα 3 συστήματα σε σεισμούς που δεν εξάντλησαν τη διατιθέμενη πλαστιμότητα του συστήματος είχαν ιδιαίτερα

κοντινή συμπεριφορά. Προκειμένου να εξηγηθούν οι όποιες διαφορές παρατηρήθηκαν πραγματοποιήθηκε διερεύνηση στις καταγραφές εκείνες όπου οι αποκλίσεις ήταν μεγαλύτερες.

Το συμπέρασμα στο οποίο οδήγησε η διερεύνηση ήταν ότι οι αποκλίσεις οφείλονται κυρίως στις μη γραμμικότητες της ανωδομής (φαινόμενα P-δ) αλλά και στη μάζα των στύλων η οποία δεν είχε ληφθεί υπόψη στον υπολογισμό των ιδιοπεριόδων των συστημάτων. Η επίδραση των φαινομένων P-δ εξαρτάται τόσο από τη μάζα όσο και από το ύψος του μονοβάθμιου συστήματος, ενώ οι διαφορές γίνονται πιο έντονα αντιληπτές σε καταγραφές που εξαντλούν τη διατιθέμενη πλαστιμότητα του συστήματος. Η μάζα του στύλου αλλάζει την ιδιοπερίοδο του συστήματος με αποτέλεσμα να παρατηρούνται μικρές διαφορές στις ιδιοπεριόδους των μονοβάθμιων που εξετάστηκαν.

Ως τελικό συμπέρασμα για τους σκοπούς ενός συστήματος άμεσης απόκρισης μονοβάθμια συστήματα με ίδια ιδιοπερίοδο, επιτάχυνση διαρροής και πλαστιμότητα μπορούν να θεωρούνται ισοδύναμα. Άμεση συνέπεια αυτού του συμπεράσματος είναι η επέκταση της χρήσης της προτεινόμενης εξίσωσης όπως προέκυψε στο 2^{ο} κεφάλαιο σε ισοδύναμα συστήματα. Η ισχύς της εξίσωσης ελέχθηκε στα 3 ισοδύναμα συστήματα και παρουσιάζεται στο τέλος του 3^{ου} κεφαλαίου.

- **Επαλήθευση Κριτηρίου Ισοδυναμίας – Επίδραση Στατικού Συστήματος**

Στο 4^{ο} κεφάλαιο της εργασίας συγκρίνονται πραγματικά βάθρα γεφυρών του Ελληνικού αστικού αυτοκινητοδρόμου «ΑΤΤΙΚΗ ΟΔΟΣ» προκειμένου να επαληθευτεί το προτεινόμενο κριτήριο ισοδυναμίας μονοβάθμιων συστημάτων.

Αρχικά επιλέγονται 2 βάθρα και εξετάζονται στην εγκάρσια διεύθυνση. Όπως και στα προηγούμενα κεφάλαια γίνεται θεώρηση προβόλου. Τα δύο βάθρα έχουν παρόμοια ιδιοπερίοδο και σχετικά κοντινή επιτάχυνση διαρροής και διατιθέμενη πλαστιμότητα. Για τα 2 αυτά βάθρα ελέγχεται η σεισμική τους συμπεριφορά στις 29 καταγραφές που χρησιμοποιήθηκαν στα προηγούμενα κεφάλαια.

Από τη σύγκριση της συμπεριφοράς των 2 βάθρων προκύπτει επιβεβαίωση του προτεινούμενου κριτηρίου. Οι αποκλίσεις που παρατηρούνται οφείλονται στις διαφορές που παρουσιάζουν τα δύο

βάθρα ως προς την επιτάχυνση διαρροής και τη διατιθέμενη πλαστιμότητα. Παρόλα αυτά σε γενικές γραμμές τα βάθρα παρουσιάζουν παρόμοια συμπεριφορά.

Στη συνέχεια εξετάζεται η δυνατότητα επέκτασης του κριτηρίου και στη διαμήκη διεύθυνση. Επιλέγεται και πάλι βάθρο από γέφυρα του αυτοκινητοδρόμου «ΑΤΤΙΚΗ ΟΔΟΣ» που έχει παραπλήσια ιδιοπερίοδο στην διαμήκη διεύθυνση με την αντίστοιχη των προηγούμενων βάθρων στην εγκάρσια. Στη διαμήκη διεύθυνση γίνεται θεώρηση αμφίπακτου στύλου, που αποτελεί τον πλέον διαδεδομένο τρόπο εξέτασης ενός βάθρου στη διαμήκη διεύθυνση. Η ορθότητα της συγκεκριμένης υπόθεσης ελέγχεται σε επόμενο κεφάλαιο.

Εξετάζεται η σεισμική συμπεριφορά του αμφίπακτου βάθρου στις 29 καταγραφές και στη συνέχεια συγκρίνεται με την αντίστοιχη των βάθρων στην εγκάρσια. Το συμπέρασμα που προκύπτει από τη σύγκριση είναι ότι η σεισμική συμπεριφορά δεν εξαρτάται από το στατικό σύστημα. Επομένως δύο συστήματα με ίδια ιδιοπερίοδο, επιτάχυνση διαρροής και διατιθέμενη πλαστιμότητα θα έχουν παρόμοια σεισμική συμπεριφορά είτε πρόκειται για πρόβολο είτε για αμφίπακτο σύστημα και κατ' επέκταση για ενδιάμεσες καταστάσεις στροφικής δέσμευσης στην κορυφή του στύλου.

Ως εκ τούτου η ισχύς τόσο του προτεινόμενου κριτηρίου όσο και της αντίστοιχης εξίσωσης μπορεί να επεκταθεί και στη διαμήκη διεύθυνση.

- **Επίδραση Επιμέρους Συστατικών της Γέφυρας στη Συνολική Τρωτότητα**

Στο 5^{ο} κεφάλαιο εξετάζεται τόσο στην εγκάρσια όσο και στη διαμήκη διεύθυνση η επίδραση των υπολοίπων συστατικών μερών στη σεισμική συμπεριφορά της γέφυρας. Στόχος είναι να εξεταστεί σε ποιο βαθμό ένα συστατικό μέρος της γέφυρας, όπως το βάθρο, είναι αντιπροσωπευτικό της συνολικής τρωτότητας. Επίσης εξετάζεται σε ποιο βαθμό η θεώρηση προβόλου και αμφίπακτου στύλου είναι αντιπροσωπευτική της συμπεριφοράς του βάθρου της γέφυρας στην εγκάρσια και στη διαμήκη διεύθυνση αντίστοιχα.

Για το σκοπό αυτό αναπτύχθηκε ένα πλήρες μοντέλο μιας πραγματικής γέφυρας του αυτοκινητοδρόμου «ΑΤΤΙΚΗ ΟΔΟΣ», στο οποίο όπως και στις προηγούμενες περιπτώσεις

θεωρείται πάκτωση στη βάση των μεσοβάθρων και στη βάση των εφεδράνων στα ακρόβαθρα αγνοώντας την αλληλεπίδραση εδάφους κατασκευής. Η σεισμική συμπεριφορά της γέφυρας εξετάζεται στις ίδιες 29 καταγραφές και στις δύο διευθύνσεις.

Α) Διαμήκης Διεύθυνση

Η σεισμική συμπεριφορά της γέφυρας στη διαμήκη διεύθυνση αρχικά συγκρίνεται με αμφίπακτο σύστημα που έχει τις ίδιες ιδιότητες και χαρακτηριστικά με το βάθρο της γέφυρας. Λόγω των σημαντικών αποκλίσεων που παρατηρήθηκαν προκύπτει το συμπέρασμα ότι η επίδραση των υπολοίπων συστατικών μερών της γέφυρας είναι ιδιαίτερα σημαντική και δε μπορεί να αγνοηθεί. Επίσης συμπεραίνεται ότι η θεώρηση αμφίπακτου στύλου δεν περιγράφει ικανοποιητικά τη συμπεριφορά του βάθρου.

Αρχικά εξετάζεται η επίδραση των εφεδράνων. Η επίδραση αυτή έγκειται τόσο στη δυσκαμψία όσο και στην απόσβεση που προσδίδουν στο σύστημα. Διαδοχικά οι δύο αυτές παράμετροι προστίθενται στο αμφίπακτο σύστημα και ελέγχεται η σεισμική του συμπεριφορά. Από τη σύγκριση με το βάθρο του πλήρους μοντέλου παρατηρείται σημαντικά μεγαλύτερη σύγκλιση σε σχέση με πριν.

Το επόμενο συστατικό μέρος το οποίο λαμβάνεται υπόψη είναι το κατάστρωμα της γέφυρας. Υπολογίζεται τόσο η καμπτική δυσκαμψία όσο και η απόσβεση του καταστρώματος ενώ αντικαθίσταται η πάκτωση στη κορυφή του στύλου με ανάλογο στροφικό ελατήριο και αποσβεστήρα. Ελέγχοντας τη σεισμική συμπεριφορά του νέου συστήματος παρατηρείται σημαντική σύγκλιση με τη συμπεριφορά του βάθρου της γέφυρας.

Όπως προκύπτει από τα παραπάνω η θεώρηση αμφίπακτου στύλου δεν μπορεί να θεωρηθεί ακριβής προσέγγιση της συμπεριφοράς του βάθρου στη διαμήκη διεύθυνση και η συνεισφορά των υπολοίπων μερών της γέφυρας δεν μπορεί να αγνοηθεί.

Β) Εγκάρσια Διεύθυνση

Όπως στη διαμήκη έτσι και στην εγκάρσια διεύθυνση εξετάστηκε ο βαθμός στον οποίο η θεώρηση προβόλου προσεγγίζει τη σεισμική συμπεριφορά του βάθρου της γέφυρας. Από τη σύγκριση προέκυψαν σημαντικές αποκλίσεις γι αυτό και εξετάστηκε η συνεισφορά των υπολοίπων συστατικών μερών της γέφυρας.

Τα εφέδρανα στην εγκάρσια διεύθυνση πέρα από τη μετακινησιακή δυσκαμψία που προσφέρουν στο σύστημα προσφέρουν και στροφική λόγω της θέσης τους. Κάθε μία απ' αυτές όπως και η απόσβεση των εφεδράνων λαμβάνεται υπόψη διαδοχικά με τη προσθήκη γραμμικών μετακινησιακών και στροφικών ελατηρίων και αποσβεστήρων. Παρατηρείται σημαντική σύγκλιση, με την επίδραση της στροφικής δυσκαμψίας να δεσπόζει.

Το κατάστρωμα συμμετέχει στην εγκάρσια διεύθυνση μέσω της δυσκαμψίας του (στρεπτική) και της απόσβεσής του. Με την προσθήκη του αντίστοιχου στροφικού ελατηρίου και αποσβεστήρα παρουσιάζεται ικανοποιητική σύγκλιση με τη συμπεριφορά του βάθρου.

Όπως και στη διαμήκη διεύθυνση, η θεώρηση προβόλου δεν μπορεί να θεωρηθεί αντιπροσωπευτική της συμπεριφοράς του βάθρου στην εγκάρσια διεύθυνση και η συνεισφορά των υπολοίπων δομικών μελών της γέφυρας δεν μπορεί να αγνοηθεί.

Ένα ακόμα συμπέρασμα που προκύπτει από την ανάλυση που προηγήθηκε είναι ότι ένα μεμονωμένο συστατικό μέρος της γέφυρας, όπως ένα μεσόβαθρο, δεν προσεγγίζει με ακρίβεια την τρωτότητα του συνολικού συστήματος. Επομένως προκύπτει η ανάγκη για ανάπτυξη συστημάτων που λαμβάνουν υπόψη τη συνεισφορά και των υπόλοιπων συστατικών μερών της γέφυρας.

- **Αλληλεπίδραση Εδάφους-Κατασκευής**

Έχοντας εξετάσει τη συνεισφορά των διαφόρων δομικών συστατικών της γέφυρας και καταλήγοντας ότι δεν μπορεί να αγνοηθεί, επόμενος στόχος στο 6^{ο} κεφάλαιο είναι να εξεταστεί η ορθότητα της θεώρησης πακτωμένης βάσης των μεσοβάθρων και των ακροβάθρων. Προκειμένου να εξεταστεί η επιρροή της αλληλεπίδρασης εδάφους-κατασκευής αναπτύχθηκε τρισδιάστατο πλήρες μοντέλο της γέφυρας με επιφανειακή θεμελίωση. Οι εδαφικές συνθήκες είναι αντιπροσωπευτικές για το είδος θεμελίωσης της γέφυρας. Ακριβής είναι και η αναπαράσταση των τοίχων αντιστήριξης των ακροβάθρων προκειμένου να εξεταστεί κατά πόσο η θεώρηση πάκτωσης στα ακρόβαθρα είναι ρεαλιστική. Η μόνη διαφορά με τη πραγματική γέφυρα της Αττικής Οδού είναι ότι δεν προσομοιάστηκαν τα stoppers που υπάρχουν στα ακρόβαθρα. Αυτό έγινε διότι η

επίδρασή τους στη σεισμική συμπεριφορά της γέφυρας είναι δεσπόζουσα και με τον τρόπο αυτό ακυρώνει την επίδραση των υπόλοιπων δομικών συστατικών της.

Η σεισμική συμπεριφορά του πλήρους μοντέλου της γέφυρας λόγω του μεγάλου υπολογιστικού κόστους εξετάζεται σε 3 καταγραφές στη διαμήκη και εγκάρσια διεύθυνση. Στη συνέχεια συγκρίνεται με την αντίστοιχη συμπεριφορά της γέφυρας με θεώρηση πάκτωσης στα μεσόβαθρα και τα ακρόβαθρα. Απο τη σύγκριση προκύπτει ότι η θεώρηση πάκτωσης στη βάση των εφεδράνων ειναι ρεαλιστική. Οι μικρομετακινήσεις του τοίχου αντιστήριξης μπορούν να αγνοηθούν.

Αντίθετα η αλληλεπίδραση εδάφους-θεμελίου οδηγεί σε σημαντικές αποκλίσεις και δεν μπορεί να αγνοηθεί. Προκειμένου να ληφθεί υπόψη χωρίς να αυξηθεί σημαντικά το υπολογιστικό κόστος των αναλύσεων, για τα απλοποιητικά μοντέλα που αναπτύχθηκαν στο $5^{ο}$ κεφάλαιο η πάκτωση στη βάση των μοντέλων αντικαθίσταται με ελατήρια και αποσβεστήρες. Πρόκειται για μετακινησιακά και στροφικά ελατήρια και αποσβεστήρες που διαστασιολογούνται με βάση τις μεθοδολογίες (α) G.Gazetas (1983) και (β) I.Anastasopoulos & T.Kontoroupi (2013). Η συμπεριφορά των νέων μοντέλων συγκρίθηκε με την αντίστοιχη του βάθρου του πλήρους μοντέλου και παρατηρήθηκε σημαντική σύγκλιση σε σχέση με την θεώρηση πάκτωσης.

- **Προτεινόμενη Μεθοδολογία**

Όπως παρουσιάζεται εκτενώς στο $1^{ο}$ κεφάλαιο οι πιο διαδεδομένοι τρόποι εκτίμησης της σεισμικής τρωτότητας μιας γέφυρας είναι οι καμπύλες τρωτότητας (fragility curves) και οι καμπύλες «αυξητικής δυναμικής ανάλυσης» (Incremental Dynamic Analysis curves). Και στις δύο περιπτώσεις οι καμπύλες χρησιμοποιούν ένα μέγεθος έντασης (IM), ενώ στις περισσότερες περιπτώσεις ένα συστατικό μέρος της γέφυρας (βάθρο) θεωρείται αντιπροσωπευτικό της συνολικής τρωτότητας. Όταν επιλέγεται η χρήση πλήρους μοντέλου το υπολογιστικό κόστος αυξάνεται σημαντικά με αποτέλεσμα να χρησιμοποιούνται περιορισμένες καταγραφές.

Λαμβάνοντας υπόψη τις μεθόδους που είναι διαθέσιμες στη βιβλιογραφία και τα αποτελέσματα των αναλύσεων στα πλαίσια της παρούσας διπλωματικής εργασίας προτείνεται η ακόλουθη

απλοποιημένη μεθοδολογία υπολογισμού της σεισμικής τρωτότητας γεφυρών με θεώρηση αλληλεπίδρασης εδάφους κατασκευής:

Προκειμένου να υπολογιστεί η σεισμική τρωτότητα μίας γέφυρας δημιουργούνται απλοποιημένα μοντέλα στις δύο διευθύνσεις, όπως περιγράφεται αναλυτικά στο 5^{ο} κεφάλαιο, που λαμβάνουν υπόψη τη συνεισφορά όλων των συστατικών μερών της γέφυρας.

Η ανάπτυξη τέτοιων μοντέλων προϋποθέτει (i) την ανάλυση της διατομής ενός χαρακτηριστικού βάθρου της γέφυρας και (ii) τη γνώση της γεωμετρίας του καταστρώματος και των εφεδράνων προκειμένου να διαστασιολογηθούν μέσω αναλυτικών τύπων τα αντίστοιχα ελατήρια και οι αποσβεστήρες και να υπολογιστεί η μάζα του καταστρώματος.

Η αλληλεπίδραση εδάφους-κατασκευής λαμβάνεται υπόψη μέσω ελατηρίων και αποσβεστήρων που τοποθετούνται αντί πάκτωσης στη βάση των απλοποιημένων μοντέλων. Η διαστασιολόγηση τους γίνεται με βάση τους αναλυτικούς τύπους (Gazetas, 1983) που περιγράφονται στο 6^{ο} κεφάλαιο.

Η σεισμική συμπεριφορά των προτεινόμενων μοντέλων εξετάζεται σε ένα χαρακτηριστικό εύρος σεισμικών σεναρίων όπως οι 29 καταγραφές που χρησιμοποιήθηκαν στην παρούσα διπλωματική εργασία η επιλογή των οποίων αιτιολογείται στο 2^{ο} κεφάλαιο. Όπως ακολουθείται και στην μεθοδολογία ανάπτυξης καμπυλών τρωτότητας και καμπυλών «αυξητικής δυναμικής ανάλυσης» οι καταγραφές που επιλέγονται κλιμακώνονται συναρτήσει του PGA προκειμένου για κάθε στάθμη έντασης να υπάρχει μεγάλο εύρος καταγραφών με διαφορετικά χαρακτηριστικά.

Απο την βάση δεδομένων που προκύπτει με χρήση προχωρημένων οικονομετρικών μοντέλων παράγεται εξίσωση που συνδυάζει περισσότερα από ένα μεγέθη έντασης (IM) και εκτιμά με ικανοποιητική ακρίβεια ένα μέγεθος προσδιορισμού της δομικής βλάβης (DI) με τον τρόπο που αναπτύσσεται στο 2^{ο} κεφάλαιο.

- **Πλεονεκτήματα Μεθοδολογίας**

Η προτεινόμενη μεθοδολογία υιοθετεί στοιχεία από τις αντίστοιχες μεθοδολογίες που διατίθενται στη βιβλιογραφία, παρουσιάζει όμως δύο σημαντικές διαφορές:

Η πρώτη έγκειται στο γεγονός ότι δεν αναζητείται κατάλληλο μέγεθος έντασης της σεισμικής διαταραχής για τις υπό εξέταση κατασκευές. Αντίθετα επιλέγεται συνδυασμός συγκεκριμένων μεγεθών που αναφέρονται σε διαφορετικά χαρακτηριστικά της διαταραχής.

Η δεύτερη αναφέρεται στο μοντέλο που επιλέγεται ως αντιπροσωπευτικό του συστήματος της γέφυρας. Στις πλεον διαδεδομένες μεθόδους επιλέγεται είτε να χρησιμοποιηθεί ένα συστατικό της γέφυρας, όπως το βάθρο, ως αντιπροσωπευτικό της συνολικής τρωτότητας (με την απλοποιητική θεώρηση προβόλου/αμφίπακτου στις δύο διευθύνσεις) είτε αναπτύσσονται πλήρη μοντέλα γεφυρών. Στην πρώτη περίπτωση χρησιμοποιείται πλήθος καταγραφών με κλιμάκωση, ενώ στη δεύτερη λόγω μεγάλου υπολογιστικού κόστους οι καταγραφές είναι περιορισμένες. Αντίθετα στην προτεινόμενη μεθοδολογία τα απλοποιημένα μοντέλα στις δύο διευθύνσεις προσεγγίζουν ικανοποιητικά τη σεισμική συμπεριφορά του πλήρους συστήματος ενώ το υπολογιστικό κόστος παραμένει μικρό.

Ενδεικτικά για την ίδια καταγραφή από το σεισμό του Αιγίου η ανάλυση του πλήρους μοντέλου διήρκησε συνολικά 8 ώρες ενώ του προτεινόμενου μόλις 5 λεπτά. Επομένως είναι εφικτό να πραγματοποιηθούν πολύ περισσότερες αναλύσεις σε σχέση με το πλήρες σύστημα. Με τον τρόπο αυτό οι αβεβαιότητες σε σχέση με την ανωδομή αλλά και την αλληλεπίδραση εδάφους-κατασκευής αντισταθμίζονται σε ένα βαθμό από το πλήθος των σεισμικών σεναρίων που μπορούν να χρησιμοποιηθούν στο προτεινόμενο μοντέλο.

- **Πεδίο Εφαρμογής**

Η προτεινόμενη μεθοδολογία είναι δυνατόν να χρησιμοποιηθεί για τους σκοπούς ενός Συστήματος Άμεσης Απόκρισης (Rapid Response System). Στα πλαίσια του ερευνητικού προγράμματος RA.RE. (Rapid Response) σε συνεργασία του εργαστηρίου Εδαφομηχανικής του Εθνικού Μετσόβιου Πολυτεχνείου, του εργαστηρίου Θεμελιώσεων & Γεωτεχνικής Σεισμικής Μηχανικής του Αριστοτελείου Πανεπιστημίου Θεσσαλονίκης , της εταιρείας ‘’Όμιλος Τεχνικών Μελετών’’ και του αυτοκινητοδρόμου ‘’Αττικές Διαδρομές’’ προτείνεται να εξεταστεί η δυνατότητα εφαρμογής της εν λόγω μεθοδολογίας σε ένα σύνολο 180 γεφυρών κατά μήκος του δικτύου του αυτοκινητοδρόμου «Αττική Οδός».

Για τους σκοπούς του προγράμματος στα πλαίσια της παρούσας διπλωματικής εργασίας καταγράφηκαν στο σύνολό τους τα 180 τεχνικά έργα γεφυρών, κατηγοριοποιήθηκαν με ποιοτικά κριτήρια (πλήθος ανοιγμάτων, συνέχεια καταστρώματος, σύνδεση βάθρου-καταστρώματος) και στη συνέχεια δημιουργήθηκε μητρώο που περιλαμβάνει όλα τα βασικά γεωμετρικά στοιχεία των γεφυρών αλλά και στοιχεία που αφορούν τη θεμελίωση και τον αντισεισμικό τους σχεδιασμό.

Με βάση το μητρώο που δημιουργήθηκε είναι δυνατό να αναπτυχθούν τα προτεινόμενα απλοποιητικά μοντέλα και στη συνέχεια να παραχθούν εξισώσεις για τις 180 γέφυρες του δικτύου τόσο στη διαμήκη όσο και στην εγκάρσια διεύθυνση.

Table of Contents

INTRODUCTION

SCOPE OF THE THESIS

1. Earthquake Rapid Response System for Metropolitan Motorways

The consequences of a strong seismic event in a metropolitan motorway network can be distinguished in: (a) structural damage of motorway infrastructures, and (b) deterioration of serviceability. The latter can either be due to a decrease of motorway capacity due to damage of critical infrastructures, or to the increase of demand due to damage within the neighbouring urban environment.

Although the direct consequences of a strong earthquake cannot easily be avoided, the *indirect consequences* can be effectively mitigated through timely development and implementation of a rapid response system. Such a system aims to: (a) ensure the safety of motorway users and avoid panic, (b) minimize closure of the motorway, and (c) optimize system serviceability after the earthquake.

Evidently, emergency inspection of motorway infrastructures will be essential after a strong seismic event. However, prior knowledge of the seismic vulnerability of critical structures is necessary: (i) to rationally decide whether there is a need for emergency inspection, and (ii) to rationally allocate inspection teams, allowing for minimum disruption of traffic operations. Such prior knowledge of the seismic vulnerability of the motorway will enable prediction of potential damage distribution, facilitating the detection of sensitive areas within the network. This way, realistic seismic damage scenarios can be devised before-hand, to estimate the potential capacity deterioration of the motorway network, as well as the increased demand due to damage in neighbouring urban areas. Such scenarios can then be utilized to test before-hand (through traffic analysis simulation) the effectiveness of possible emergency response actions.

The development of such a system requires knowledge of: (a) of the accurate evaluation of the seismic hazard (b) the seismic vulnerability of critical motorway infrastructures, such as bridges, cut-and-cover and bored tunnels, retaining walls, cut slopes, and embankments; and (c) knowledge

of the typology and all necessary information regarding the geometric and material `properties of the network system and its subsystems.

1.1 Seismic Hazard Assessment

Various methods have been proposed to characterize the seismic hazard broadly categorized in *deterministic* and *probabilistic*. A significant amount of empirical correlations (broadly known as attenuation relationships or recently Ground Motion Prediction Equations–*GMPE*) can be found in the literature for estimation of ground motion characteristics, commonly expressed through spectral acceleration or displacement with regard to earthquake magnitude, distance from the source, soil and geologic site conditions (Figures I.1, I.2).

To model the consequences of failure to a motorway it is important to define seismic scenarios in a coherent and realistic manner. Traditional seismic hazard analysis, whilst effective in translating the hazard into a probabilistic formulation, is limited in the extent to which it can incorporate spatial coherency of the form needed for estimation of loss to spatially distributed portfolios. This approach becomes computationally and theoretically more complex when considering more than a few correlated sites or ground motions. So an alternative approach is the use of seismic scenarios, from which it is possible to create fields of expected ground motions, which are then input into seismic risk models.

The performance of a motorway network may be conditional upon failure of different elements, each responding differently to the ground motion. Certain components may respond adversely to strong accelerations, whilst other elements or larger structures may be sensitive to low period motions and ground displacements. Other may be mainly affected by permanent displacements (fault crossing, landslides). Hence, the characterization of ground motion and the associated permanent ground displacements constitute a crucial element for the assessment of the risk of isolated structures. Many intensity measures (IM) have been developed and are readily available in the literature.

1.2 Seismic Vulnerability of critical Motorway Infrastructures

A widely used way to express vulnerability of a motorway infrastructure , especially referring to bridges, are fragility curves, which describe the probability of an element at risk, to be in or to exceed different damage states for a given seismic intensity. They can be classified as : (a) generic–based on expert judgment [e.g., ATC-13, ATC-25], (b) empirical–based mainly on surveys after earthquakes [Basoz et al., 1999; Shinozuka et al., 2000a], and (c) analytical–based on numerical simulation [Shinozuka et al., 2000b; Elnashai et al., 2004; Nielson & DesRoches, 2007]. Although such a plethora of fragility curves for bridges is readily available in the literature, they typically refer to a single bridge component as representative of the overall fragility. Another more recent approach to express vulnerability is Incremental Dynamic Analysis (IDA) curves, which express the correlation between an IM and a Damage Measure (DM) for a specific accelerogram while the intensity increases.

Bridges represent a particular challenge in the analysis of seismic risk of motorways. Failure of a bridge may occur due to either strong seismic shaking or ground deformation, or a combination of both. The response of a bridge due to strong shaking may vary according to many different factors including span and skewness, in addition to the common situation whereby the fundamental period of a column differs in the longitudinal and transverse direction. For a portfolio of bridges within a region, the vast disparity in bridge geometry, construction type and method (including design code level) limit the extent to which the structural models can be adequately described. Consequently the gain in efficiency for using complex spectral IMs may be offset by the uncertainty in the structural model. Modeling infrastructure and complex systems presents a challenge in this approach (Figure I.3, I4).

One of the main purposes of the analysis is to highlight the most crucial parameters affecting the vulnerability, including (but not limited to): the typology of the structural system, P-Δ effects, the characteristics of the ground motion, and the magnitude of ground-induced deformation.

2. Proposal of the thesis:

A simplified method to estimate the seismic vulnerability of bridges considering soil-structure interaction

The number and the variety of bridges of a metropolitan motorway make the computational effort to estimate precisely the seismic vulnerability of each one of them, unprofitable. In addition to this, the necessity to take into account the contribution of each component of a bridge as well as the interaction between them to the seismic response of the whole bridge, leads to very complicated models. Hence the need for classification of bridges and subsequently the creation of a simplified model which has the similar seismic performance with the original bridge is one of the key objectives of the present thesis (Figure I.5).

In order to examine the seismic performance of a bridge, it is very important to keep in mind that the structural damage due to different records from different earthquakes might be different even having the same IM. This is due to the characteristics (frequency contents, phase, duration, etc.) of the input ground motion. In order to take into account the effect of each one of these characteristics, a variety of real records of varying intensity and characteristics has to be selected. On the other hand the fact that each IM may describe different characteristics of the motion, some of which may be more adverse for the structure or system under consideration indicates the need to explore the effectiveness of each of the different IM's or a combination of some specific.

2.1 Main Structure of the Thesis

One common way to estimate the fragility of a bridge is to consider a single bridge component as representative of the overall fragility. In most cases a bridge pier is considered as a SDOF system and its seismic performance is thought to be a close representation of the performance of the whole bridge in the transverse direction.

The scope of this thesis is to examine numerically the possibility to estimate the seismic performance of such a system when a seismic event occurs but also the impact of each component of the bridge that a SDOF doesn't include.

At first to a SDOF system of a single bridge pier that has been examined in the past [Marianna Loli 2008] from 29 real records, on which PGA was normalized to different excitation levels, non-linear time history analyses were performed, in order to obtain the damage indices. This task aims to show if it is possible to estimate the damage of the pier using a single IM or a combination of some specific.

The next step was to compare this model to another two concept bridge piers with different geometry, stiffness and mass at the top, but the same natural period (T), design acceleration (Sa) and ductility (μ). The purpose of this investigation is the development of a criterion by which two systems will be considered equivalent in order to extend the results of the previous analysis.

In order to validate the results of the above analysis three real piers from different bridges of the Greek metropolitan motorway "Attiki Odos", with close natural period, design acceleration, and ductility were modeled and non-linear time history analyses were performed, in order to compare their performance. Another objective was to examine the way that static system affects.

The following challenge is to examine at what level a SDOF system represent the bridge pier at the longitudinal and transverse direction. To examine this, a real bridge is modeled and tested in order to compare the performance of the bridge pier with the SDOF system. In the same vein the effect of each component of the bridge (bearings, deck) is measured and more complicated models are created and examined in both directions.

The last parameter to be taken into account was Soil-Structure Interaction. For this purpose a complete 3D model of a bridge was developed and examined in ABAQUS finite element code. Comparing this model with the fixed base bridge and the relevant systems the impact of SSI is quantified.

The final conclusions of the work preceded are summarized in a simplified method to estimate the seismic vulnerability of bridges. This method is tested in a variety of bridges of the Attiki Odos motorway.

Introduction

Figures

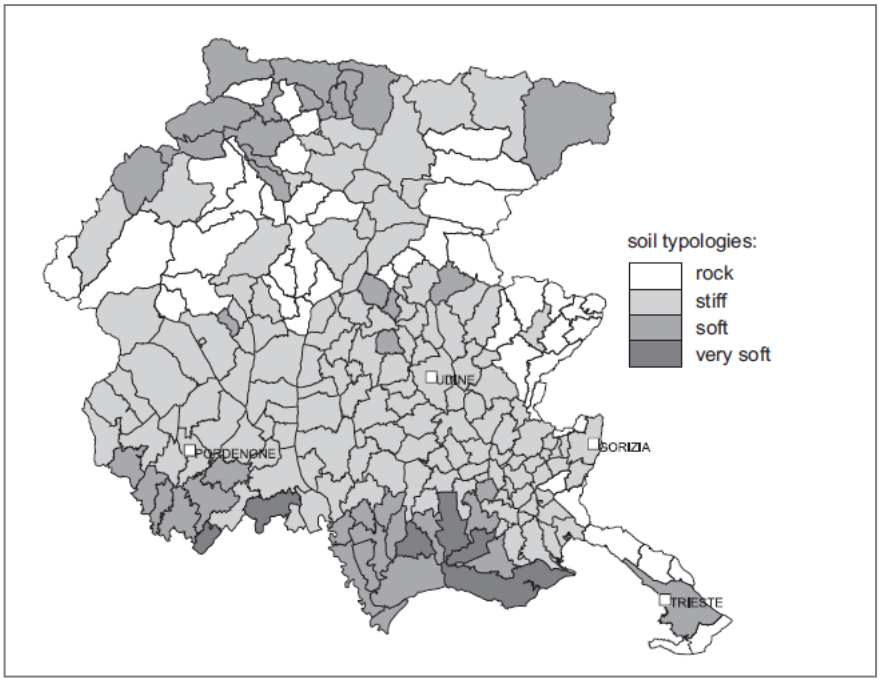

Figure I.1 Soil typologies of the municipalities of the Friuli–Venezia Giulia Region [Seismic risk assessments and GIS technology: applications to infrastructures in the Friuli–Venezia Giulia region Codermatz, Nicolich, Slejko 2003]

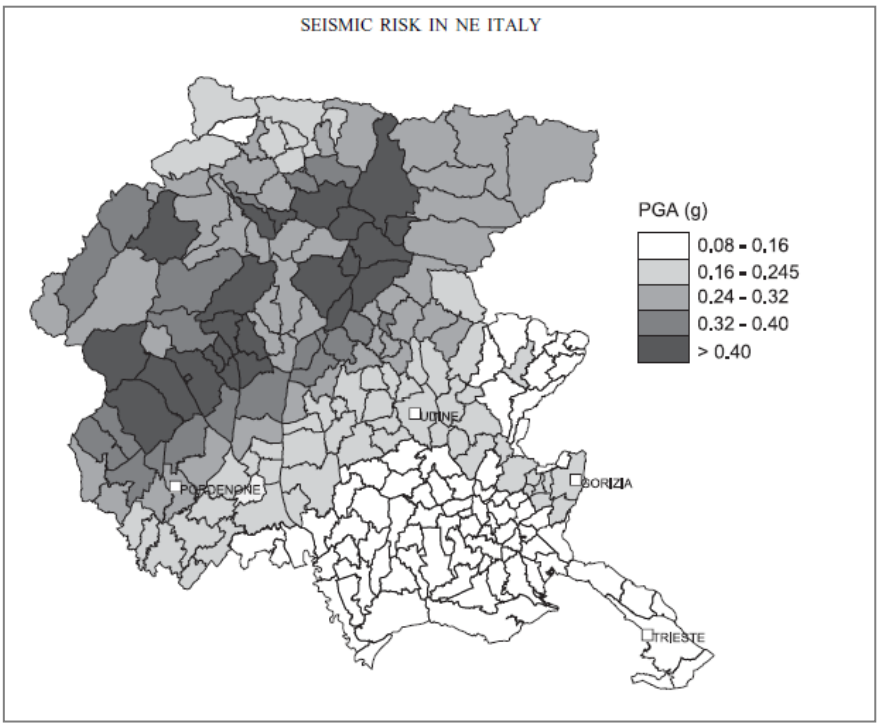

Figure I.2 Soil dependent seismic hazard map of Italy in terms of PGA with a 475-year return period [Seismic risk assessments and GIS technology: applications to infrastructures in the Friuli–Venezia Giulia region Codermatz, Nicolich, Slejko 2003]

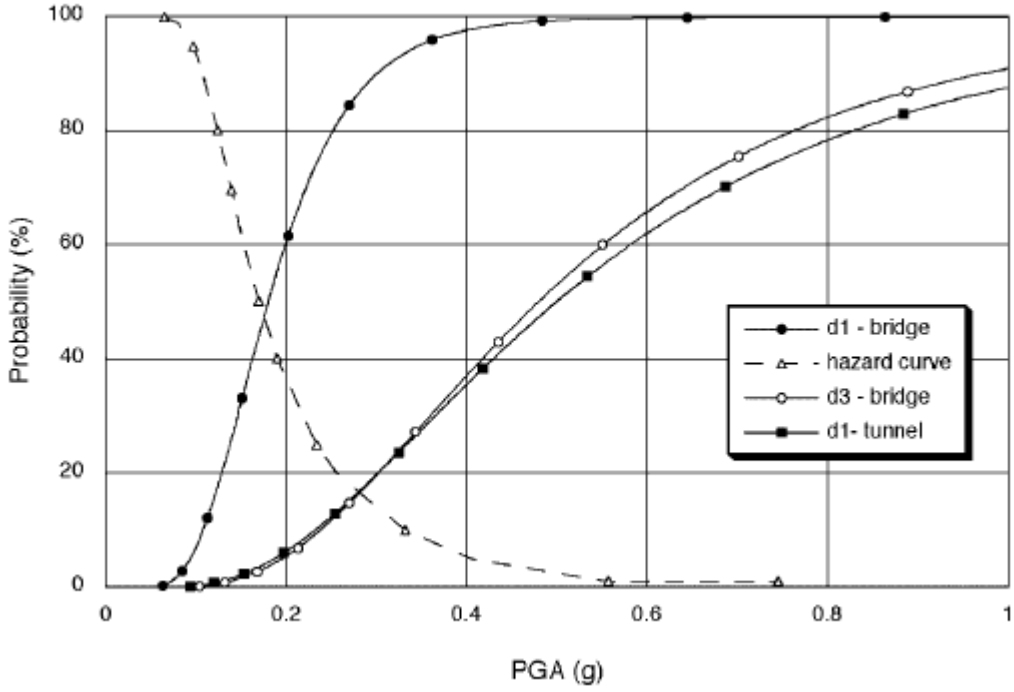

Figure I.3 Fragility curves for a bridge (d1, d3 damage states), fragility curve for a tunnel (d1 damage state), hazard curve, in terms of a 50-year exceedance probability [Seismic risk assessments and GIS technology: applications to infrastructures in the Friuli–Venezia Giulia region Codermatz, Nicolich, Slejko 2003]

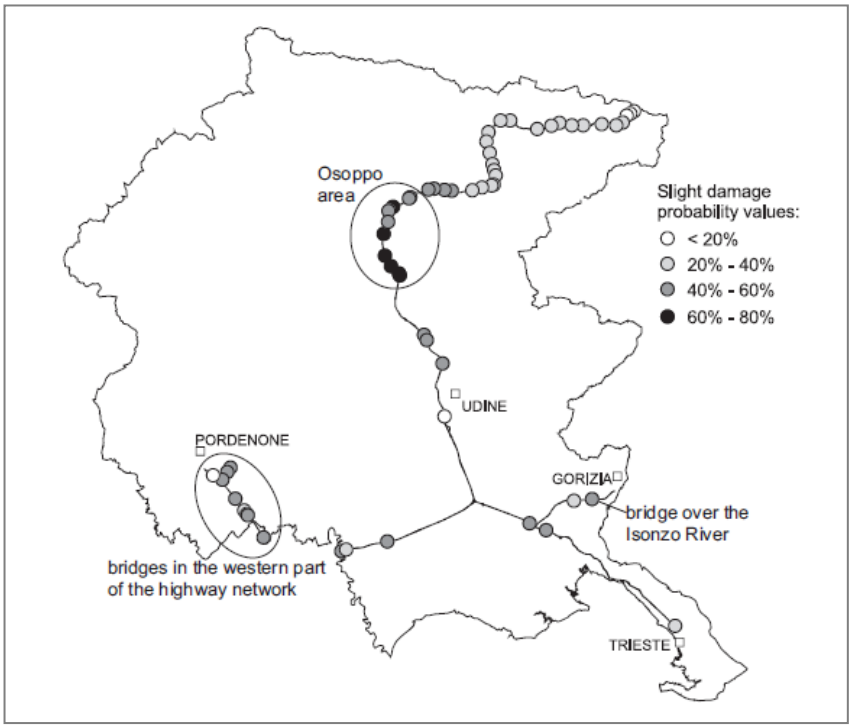

Figure I.4 A 50-year probability of observing a slight damage for the bridges of the regional highway network [Seismic risk assessments and GIS technology: applications to infrastructures in the Friuli–Venezia Giulia region Codermatz, Nicolich, Slejko 2003]

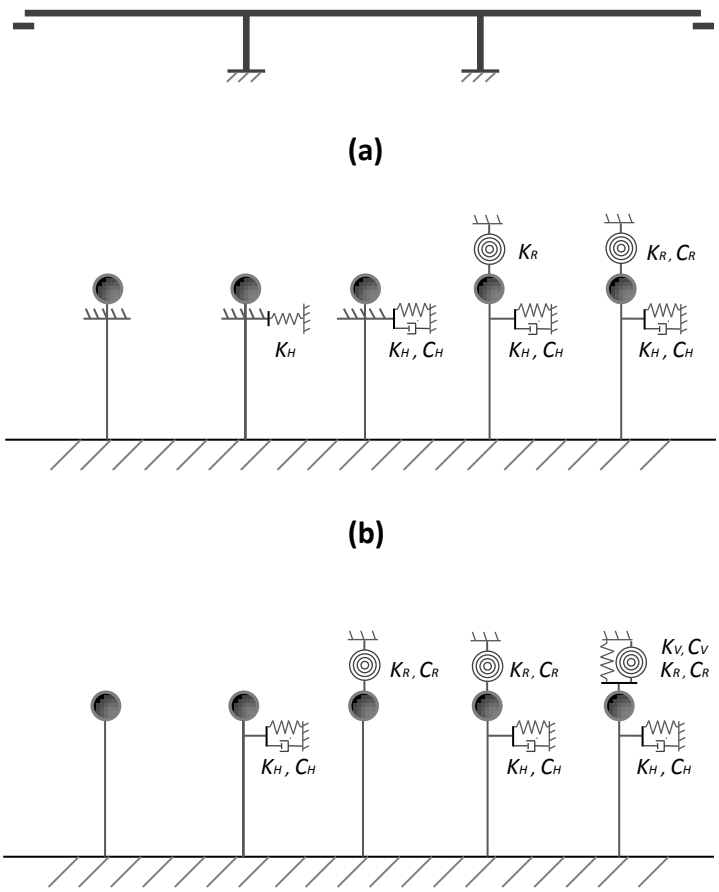

Figure I.5 (a) Whole Bridge and simplified systems in **(b)** longitudinal and **(c)** transverse direction

CHAPTER 1

LITERATURE REVIEW

FRAGILITY CURVES – IDA CURVES

1.1 Fragility Curves

A widely used way to express vulnerability of a motorway infrastructure , especially referring to bridges, are fragility curves, which describe the probability of an element at risk, to be in or to exceed different damage states for a given seismic intensity. They can be classified as: (a) generic–based on expert judgment [e.g., ATC-13, ATC-25], (b) empirical–based mainly on surveys after earthquakes [Basoz & Kiremidjian, 1997; Yamazaki et al., 1999; Shinozuka et al., 2000b; Kiureghian, 2002], and (c) analytical–based on numerical simulation [Shinozuka et al., 2000b; Karim & Yamazaki, 2002; Elnashai et al., 2004; Nielson & DesRoches, 2007;]. Although such a plethora of fragility curves for bridges is readily available in the literature, they typically refer to a single bridge component as representative of the overall fragility.

1.1.1 Fragility functions

One of the key links in the risk assessment methodology is to estimate the damage to the lifeline components. This is done by estimating the performance of the various highway bridges in the network as a function of a ground motion intensity parameter. This bridge performance is commonly represented in either a damage probability matrix or a fragility function.

A fragility function is a conditional probability that gives the likelihood that a structure will meet or exceed a specified level of damage for a given ground motion parameter. This conditional probability is given in the following equation:

$$Fragility = P[S > LS \mid IM = y] \qquad (1)$$

where S is the response measure of the bridge or bridge component, LS is the limit state or damage level of the bridge or bridge component, IM is the ground motion intensity measure and y is the realization of the chosen ground motion intensity measure. One can see from this formulation that given a scenario earthquake, a prediction of the damage level may be made for each bridge for which a fragility function is defined.

This probabilistic way of estimating structural damage was used in the evaluation of nuclear facility vulnerabilities in the late 1970's and early 1980's and since then has expanded into other areas of structural engineering. The 1985 ATC-13 report presented this probability of damage in the discrete form of damage probability matrices which were later followed by the introduction of continuous cumulative distribution functions or fragility curves in the 1991 ATC-25 report as well as the first release of the FEMA funded HAZUS software in 1997. There are many different methodologies that have been employed in the determination of these structural fragilities, a synopsis of which will be given in the following sections.

1.1.2 Generic fragility curves

Generic fragility curves are based on expert judgment. A typical example of developing generic fragility curves is the ATC-13 report (ATC, 1985) developed by the Applied Technology Council (ATC) of California, USA. In October 1982 the Federal Emergency Management Agency (FEMA) awarded Applied Technology Council (ATC) a contract to develop earthquake damage evaluation data for facilities in California. FEMA was planning to use these data and companion loss estimation and inventory methodology to estimate the economic impacts of a major California earthquake. Because the required earthquake damage, loss and inventory data were not available in the literature, ATC and FEMA agreed that the best way to develop the required data was to draw on the experience and judgment of seasoned earthquake engineers. The ATC put together a panel of 42 experts, four of which were for bridges, whom they could query concerning the various components of a typical Californian infrastructure.

The questionnaires that were created queried the experts on the probability of a bridge being in one of seven damage states for a given Modified-Mercalli Intensity (MMI) value. They also asked the experts to rate themselves on their experience in the field on a scale from zero to ten. After the questionnaires were completed and analyzed, the results were given back to the experts for a second look. They were permitted to consider the overall results and compare them with their initial responses and make any modifications they felt were necessary. These results were then compiled and reported as the probability damage matrices (DPM) for bridges in the ATC-13 report (ATC, 1985) and were subsequently used in the ATC-25 report (ATC, 1991). (Table 1.1, Figures 1.1)

1.1.3 Empirical fragility curves

Empirical fragility curves are based mainly on surveys after earthquakes. Following the 1989 Loma Prieta and 1994 Northridge earthquakes empirical bridge fragility curves became more common as a direct result of more complete ground motion and bridge damage data. Empirical fragility curves are generated from actual earthquake data. This methodology has been presented and demonstrated by several groups of people for the Loma Prieta and Northridge earthquakes such as Basoz and Kiremidjian (1997), Kiureghian (2002), Shinozuka et al. (2000b) and by Yamazaki et al. (1999) for the 1995 Kobe earthquake.

Although there are some slight variations in the methods used by the aforementioned groups they are conceptually the same. The procedure requires that a post-earthquake assessment be performed where a damage state would be assigned to all the bridges that belong to the bridge class being considered. A shake map, that geographically defines the ground motion in terms of some intensity measure, such as peak ground acceleration (PGA) is used to assign each bridge to a damage state and a given ground motion intensity in a damage frequency matrix. Table 1.2 is an example of a damage frequency matrix that was assembled by Basoz and Kiremidjian (1997) for all multi-span bridge types as they performed in the Northridge earthquake. Thus a percentage of the overall bridge class inventory may be displayed for each damage state at each ground motion intensity level as shown in Table 1.3.

This information can be used in any number of ways. Basoz and Kiremidjian (1997) used a logistic regression analysis to generate the fragility curves shown in Figure 1.2 from the damage matrices shown in Tables 1.2, 1.3. Shinozuka et. al (2000b) recommends using the Maximum Likelihood method in conjunction with hypothesis and goodness of fit tests to estimate the parameters of the two parameter lognormal probability distribution while Kiureghian (2002) used a Bayesian approach and the Likelihood function to accomplish this task.

Although this method is relatively straight forward it has limitations. The first limitation is that it is difficult to get an adequate number bridges belonging to one bridge class that lie in a particular damage state to get statistically significant results (Shinozuka, 2000b). Thus it is often required to group classes together to get enough bridges in a given damage state and hence reduces the usefulness of the fragility curves. However, these empirical fragility curves can still be used to

calibrate/validate analytical fragility curves which will be discussed hereafter (Basoz and Kiremidjian, 1999).

Another limitation that Basoz and Kiremidjian (1997) noted in their generation of fragility curves for several classes of bridges in both the Loma Prieta and Northridge earthquakes was that the ground motion intensity (Shake maps) were different depending upon who generated them. They received two different maps with different values for the Northridge earthquake (USGS and WCFS) and three different maps for the Loma Prieta earthquake (observed, Boore and Joyner, Campbell).

Yet another limitation of empirical fragility curves is that when post-earthquake assessments of bridges are made and damage levels assigned, there is often a discrepancy between the damage levels that any two different inspectors would assign (Basoz and Kiremidjian, 1997). Thus another source of uncertainty is entered into the curves.

1.1.4 Analytical fragility curves

Analytical fragility curves are based on numerical simulation. When actual bridge damage and ground motion data are not available, analytical fragility curves must be used to assess the performance of highway bridges. There have been many researchers that have developed analytical fragility curves for bridges. As previously mentioned, a fragility curve is a conditional probability that specifies the likelihood of a structure or structural component reaching or exceeding a damage state for a specified ground motion intensity. Since damage states are related to structural capacity and the ground motion intensity parameter is related to structural demand, the fragility can then be described as the probability that the seismic demand will exceed the structural capacity. This probability of failure is represented in the following equation (Melchers, 1999):

$$p_f = P\left[\frac{S_d}{S_c} \geq 1\right] \tag{2}$$

where *pf* is the probability of exceeding a specific damage state, *Sd* is the structural demand and *Sc* is the structural capacity or damage state.

This probability is generally modeled as a lognormal probability distribution. This model is chosen because it has shown to be a good fit in the past and is convenient for manipulation using conventional probability theory (Wen et al., 2003). In addition, when the structural capacity and

demand roughly fit a normal or lognormal distribution, using the central limit theorem, it can be said that the composite performance will be lognormally distributed (Kottegoda and Rosso, 1997). Thus the fragility curve can be represented by a lognormal cumulative distribution function which is given in the following equation (Melchers, 1999):

$$p_f = \Phi\left[\frac{ln\left(S_d/S_c\right)}{\sqrt{\beta_d^2+\beta_c^2}}\right] \quad (3)$$

where *Sc* is the median value of the structural capacity defined for the damage state, β*c* is the dispersion or lognormal standard deviation of the structural capacity, *Sd* is the seismic demand in terms of a chosen ground motion intensity parameter, βd is the logarithmic standard deviation for the demand and Φ[•] is the standard normal distribution function.

Using the above equation it can be seen that the structural demand and capacity must be modeled to generate analytical fragility curves. Figure 1.3 presents the basic flow of analytical fragility curve generation using non-linear time history analysis. Although there are some variations to this methodology that are used, this represents the basic overall procedure. The first step is to obtain a suite of ground motions that is appropriate and representative of the target geographic area and captures the uncertainty inherent in ground motions such as the magnitude and the epicentral distances. Next, the structural properties (material strengths and geometric values) are probabilistically sampled for a base bridge model. This will be done N times thus generating N nominally identical but statistically different bridge samples. Then the ground motions are paired with the bridge simulations and a non-linear time history analysis is performed. For each simulation, the peak structural responses for key elements (i.e. column's ductility, bearing deformation, abutment displacement, etc.) are collected. Using the peak bridge component responses, a probabilistic seismic demand model is generated by using a regression analysis of the ground motion parameters and the peak structural response. The capacity or limit state of each component is combined with the seismic demand in the above equation to generate the fragility curves. The next few sections will discuss each of these steps in more depth.

Typical analytical Fragility curves from the work of Karim & Yamazaki (2001) are shown on Figure 1.4 while analytical fragility curves from the work of Choi & Nielson are presented on Figure 1.5.

1.1.4.1 Selection of ground motion time-histories

As part of the probabilistic seismic demand analysis (PSDA), a suite of ground motion time histories must be obtained for use therein. The composition of this suite is a function of the requirements of the PSDA methodology chosen. For instance, if the PSDA is being performed for bridges in Southern California then a suite of time histories may be assembled from strong ground motion records from the area. In work done by Mackie and Stojanovic (2003), they assemble four suites of 20 ground motions each having different magnitudes and epicentral distances.

When the PSDA is being used for regions where little or no strong ground motion records are available, such as the Mid-America region of the U.S., it becomes necessary to use outside records or create synthetic time histories by sampling on ground motion parameter random variables. There have been a number of groups that have generated synthetic ground motions for use in this region (Wen and Wu, 2001; Herrmann and Akinci, 1999; Hwang et al., 2000c).

The number of ground motions required for the analysis also varies depending on the methodology used. In work done by Hwang et al. (2000c) and Choi (2002) a suite of ground motions containing 100 records was used. Shome et al. (1998) state that the lognormal assumption for the model allows suites containing 20 ground motions are sufficient to achieve the required confidence levels, while Wen et al. (2003) assert that suites with as few as ten ground motions are adequate to capture the structural response.

Another issue that arises is the question of what ground motion intensity parameter best captures the response and minimizes the dispersion of that response. The traditional intensity parameters that have been used are MMI (ATC, 1985) and PGA (FEMA, 1997), but Mackie and Stojanovic (2003) point out that there are up to 22 different ground motion intensity parameters that could be used. These parameters range from geometric properties (epicentral distance) to peak motion quantities (PGA, PGV, PGD) to spectral quantities (Sa, Sv, Sd) to energy based quantities (Mw). However, they state along with others, that the spectral quantities at the fundamental period of the structure, such as spectral acceleration, velocity and displacements, produce better results than do peak ground motion quantities such as peak ground acceleration, velocity and displacement (Wen et al., 2003; Mackie and Stojanovic, 2003; Hwang et al., 2000b).

It is interesting to note that although most fragility work done now with respect to buildings is done using spectral quantities, the bridge community is still predominantly using PGA as the intensity measure. This reluctance of the highway bridge community to switch to spectral values is in part due to the challenges associated with their use. One of these challenges is the difficulty in comparing the fragility of various bridges types. When the bridge types have different fundamental periods, the fragility comparisons must be done at a specific ground motion. Also to use the fragility curves in a risk assessment program it is imperative that the fundamental period of the structure be known. This is not always possible when the bridge information is pulled out of the NBI database. In addition to the challenges of implementation, some in the transportation arena assert that there is very little difference in the transportation network loss calculations as well as the dispersion of the results when the use of PGA and Sa is compared (Tri-Center Workshop, 2003).

1.1.4.2 Bridge model simulation

A base bridge analytical model needs to be created that is representative of the target structure. It should be noted that this not a trivial task. In fact, Song and Ellingwood (2001) recommended that less time should be spent developing more efficient Monte Carlo sampling techniques and more time should be focused on generating better models, indicating that the modeling procedure plays a very important role in the outcome of the model. Different structural properties that define the bridge model, such as concrete compressive strength, yield strength of the reinforcing steel, deck mass, deck gap width, column height and span length will need to be defined probabilistically. These structural properties should each be assigned a probability distribution to account for their uncertainty. Then using a sampling technique such as Importance Sampling (Melchers, 1989) or Latin Hypercube sampling (Ayyub and Lai, 1989), these structural parameters can be sampled based on their distributions to create a required number of nominally identical but statistically different bridge samples. Not all structural properties need to be treated probabilistically. A sensitivity analysis of the various structural properties is generally performed to indicate which ones should be treated probabilistically and which ones may be treated deterministically.

As previously mentioned, the model generation is not a trivial task. Whenever an analytical model is created the assumptions and modeling format are a major concern. The general consensus in the field of structural engineering is that the simpler the model the better off you are. However, caution must also be used so as not to oversimplify.

1.1.4.3 Transverse vs. Longitudinal

When generating the analytical models for bridges, assumptions and simplifications are often made to make the analyses more feasible. A full three dimensional model of a bridge may be generated but the analysis becomes extremely computationally expensive when it is used in a Monte Carlo simulation. Therefore much of the work done to date has simplified the models by modeling the bridges in two dimensions. This requires the bridges to be modeled in both the transverse and longitudinal directions. In an attempt to cut down further on the amount of work required to adequately quantify a bridge response, it is advantageous to explore whether or not one loading direction controls the response of the bridge.

There have been a number of studies that indicate that the longitudinal direction controls the response of the bridge (Choi, 2002; Rashidi and Saadeghvaziri, 1997) while others maintain that the loading in the transverse direction controls the damage of the bridge (Cheng et al, 1998; Saadeghvaziri and Rashidi, 1998). There are yet others that believe that a bridge must be modeled in three dimensions and have the longitudinal and transverse responses combined in some fashion to adequately represent the system (Jernigan and Hwang, 2002; ATC, 1991; Yashinski, 1999; Hwang et al, 2000b). It is clear from the many different views on this issue that there is no definite methodology that should be used for the analytical modeling of bridges.

1.1.4.4 Vulnerable bridge components

There are a number of different vulnerable components in a bridge system which include the columns/piers, fixed and expansion bearings, abutments and foundations. Almost all of the previous work for fragility analysis of bridges has assumed that the columns/piers are the only vulnerable component (ie. the fragility of the column is equivalent to the fragility of the entire bridge system) (Dutta and Mander, 1998; Hwang et al, 2000b; Hwang et al, 2000c; Mander and Basoz, 1999; Shinozuka et al, 2000a; Shinozuka et al, 2000b). However, previous work has shown that the steel fixed bearing is the most fragile component for the multi-span simply supported steel girder bridge at all of the damage states. This trend varies for different bridge types. For example, the columns for the multi-span continuous pre-stressed concrete girder bridge typical to Mid-America are the most fragile bridge component in the moderate, extensive and complete damage states (Choi, 2002). This indicates that it is important to include all major vulnerable components

when doing a fragility analysis of a bridge. If the assumption was made that the column damage states were representative of the damage states of the entire bridge, it is likely that this would result in an underestimation of the overall bridge system fragility.

1.1.4.5 Seismic demand

There are several different methodologies that have been proposed for the analysis of the seismic demand of a structure ranging from simplistic in nature to labor intensive. Some of these methods are using probabilistic response spectra in conjunction with the NBI data (Dutta and Mander, 1998; FEMA, 1999), using an elastic spectral analysis couched in a capacity/demand ratio formulation (Jernigan and Hwang, 2002; Hwang et al., 2000b), using a reduced response spectrum (Shinozuka et al., 2000b), using non-linear time history analysis in incremental dynamic analysis (IDA) (Mackie and Stojanovic, 2003) and using non-linear time history analysis to perform a probabilistic seismic demand analysis (Hwang and Huo, 1998; Hwang et al., 2000c; Choi, 2002; Mackie and Stojanovic, 2001; Song and Ellingwood, 2001; Wen et. al, 2003). It appears that the majority of the seismic demand modeling work to date has been using non-linear time history analyses using Monte Carlo simulation techniques. It is also the most reliable method available (Shinozuka et al., 2000a).

As shown in Figure 1.3, a probabilistic seismic demand model (PSDM) must be generated if the non-linear time history approach is to be used. This is done through a probabilistic seismic demand analysis (PSDA) which relies heavily upon the first three steps in Figure 1.3. As previously mentioned these steps would be to combine a suite of ground motions with a suite of bridge samples to create ground motion-bridge pairs. These pairs are then analyzed using a finite element analysis package. For each analysis, the maximum response quantities of interest, such as column curvature ductility (μθ) and the bearing and abutment deformations (δb, δa), are recorded and plotted versus the ground motion intensity parameter value, as seen in Figure 1.6. A linear regression of the form shown in Equation 4 is then performed to determine the seismic demand, Sd, as a function of the ground motion intensity measure (IM) for each of the bridge components. This is shown in Equation 5, where a and b are the unknown regression coefficients.

$$\ln(S_d) = b\ln(IM) + \alpha \tag{4}$$

$$S_d = IM^b e^a \tag{5}$$

This seismic demand, Sd, is the first half of the input to the fragility function, Equation 3. The structural capacity or limit states must also be acquired as will be addressed in the next section.

1.1.4.6 Structural capacity and damage states

As previously mentioned, the other part of fragility modeling requires something to be known about the capacity or limit states of the structure. To facilitate further discussion about the structural capacity a brief discussion on damage or limit states is required. A limit state is defined as the capacity that a structure or structural component has before reaching a specified level of damage or deformation. These limit states, which have traditionally been given in qualitative terms, are defined and discretized differently by various researchers. For example, the ATC-13 and ATC-25 reports list seven damage states (ATC, 1985; ATC, 1991). HAZUS reports five damage states (FEMA, 1997) and Hwang and Huo (1998) used two. It should be noted that it appears as if the majority of users appear to use the qualitative damage states as given by HAZUS.

The qualitative limit state descriptions work well for fragility curves that are based on expert judgment and empirical methods, but quantitative descriptions are needed for use in analytical models. The question of what response quantities (deformations, ductilities, material response etc.) will result in the qualitative description for the various damage states needs to be answered. There have been a number of tests and analytical procedures implemented to address this issue. Dutta and Mander (1998) in addition to Akkari and Duan (2000) used static pushover with plastic analysis to get deterministic capacity values with assumed dispersion values with many others following similar paths (Choi, 2002; Shinozuka et al., 2000b; Hwang and Huo, 1998; Hwang and Jaw, 1990; Hwang et al., 2000c). Shinozuka et al. (2000a) used a capacity spectrum analysis while others recommended the use of an incremental dynamic analysis (IDA) to calculate the capacity against collapse (Wen et al., 2003). An example of a quantitative equivalent to the qualitative descriptions of the bridge component limit states is presented in Table 1.4. These are the limit states that Choi (2002) used in his work for developing fragility curves for bridges in Mid-America. This table shows the median values of the limit states that were used in conjunction with the dispersions that were recommended by HAZUS 97.

There have been numerous studies done on the behavior of reinforced concrete bridge piers and columns to assist in the quantification of pier/column limit states (Kowalsky, 2000; Park et al., 1982;

Ghosn and Chen, 1991). However, there have not been many studies on the response of other vulnerable bridge components, such as bearings (Mander et al., 1996) and abutments (Goel and Chopra, 1997). Therefore expert or professional judgment is still required in defining the capacity limit states of bridge components.

1.1.4.7 Component vs. System fragility

The process that is explained in Figure 1.3 is the process to generate fragility curves for the individual bridge components. It is necessary, however, to obtain an overall bridge or system fragility for use in the risk assessment process. This can be performed through a crude Monte Carlo simulation but is considerably more computationally expensive. An alternative would be to combine the component fragility curves to get the system (bridge) fragility curve. This, however, requires information about the stochastic dependence between the damage states of the various bridge components. Using first-order reliability theory, an upper and lower bound on the system fragility can be easily determined. The lower bound is the maximum component fragility while the upper bound is a combination of all of the component fragilities. These bounds are given in Equation 5 where P(Fi) is the probability of failure for each component and P(Fsys) is the probability of failure for the entire system.

$$\max_{i=1}^{m}[P(F_i)] \le P(F_{sys}) \le 1 - \prod_{i=1}^{m}[1 - P(F_i)] \tag{6}$$

These first-order bounds are valid for a series type system where a failure of one the components constitutes a failure of the system (Melchers, 1999). When a bridge is modeled in the longitudinal direction, it in fact behaves like a series system. The lower bound represents the probability of failure for a system whose components are all fully stochastically dependent and provides an un-conservative estimate for the fragilities of the subject bridges. The upper bound assumes that the components are all statistically independent and provides a conservative estimate on the overall bridge fragility. The upper bound estimate to the system fragility gets better as the difference between the upper and lower bound decreases. When the bridge is modeled in the transverse direction, it is no longer solely a series system but rather a combination of parallel and serial

components. Therefore if transverse analysis is required, the implementation of more complex second-order reliability techniques will be required.

1.2 Incremental Dynamic Analysis (IDA) Curves

In the wake of the damage brought by the 1994 Northridge earthquake, the SAC/FEMA project was launched to resolve the issue of poor performance of steel moment-resisting frames due to the fracturing beam-column connections. Within the creative environment of research cooperation, the idea of subjecting a structure to a wider range of scaling emerged. Initially, the method was called Dynamic Pushover and it was conceived as a way to estimate a proxy for the global collapse of the structure. It was later recognized that such a method would also enable checking for multiple limit-states, e.g. for life-safety, as is the standard for most seismic design methods, but also for lower and higher levels of intensity that represent different threat levels, such as immediate-occupancy and collapse-prevention. Thus, the idea for Incremental Dynamic Analysis was born by researchers Vamvatsikos & Cornell (2002) at the John A. Blume Earthquake Research Center of Stanford University.

Incremental Dynamic Analysis (IDA) is a computational analysis method for performing a comprehensive assessment of the behavior of structures under seismic loads. It has been developed to build upon the results of probabilistic seismic hazard analysis in order to estimate the seismic risk faced by a given structure. It can be considered to be the dynamic equivalent of the static pushover analysis.

IDA involves performing multiple nonlinear dynamic time history analyses of a structural model under a suite of ground motion records, each scaled to several levels of seismic intensity. The scaling levels are appropriately selected to force the structure through the entire range of behavior, from elastic to inelastic and finally to global dynamic instability, where the structure essentially experiences collapse. Appropriate post processing can present the results in terms of IDA curves, one for each ground motion record, of the seismic intensity, typically represented by a scalar Intensity Measure (IM), versus the structural response, as measured by an Engineering Demand Parameter (EDP).

Possible choices for the IM are scalar (or rarely vector) quantities that relate to the severity of the recorded ground motion and scale linearly or nonlinearly with its amplitude. The IM is properly chosen well so that appropriate hazard maps (hazard curves) can be produced for them by probabilistic seismic hazard analysis. Possible choices are the peak ground acceleration, peak ground velocity or Arias intensity, but the most widely used is the 5%-damped spectral acceleration at the first-mode period of the structure.

The EDP can be any structural response quantity that relates to structural, non-structural or contents' damage. Typical choices are the maximum (over all stories and time) interstorey drift, the individual peak storey drifts and the peak floor accelerations.

IDA grew out of the typical practice of scaling accelerograms by multiplying with a constant factor to represent more or less severe ground motions than the ones that were recorded at a site. Since the natural recordings available are never enough to cover all possible needs, scaling is a simple, yet potentially problematic method (if misused) to "fill-in" gaps in the current catalog of events. Still, in most cases, researchers would scale only a small set of three to seven records and typically only once, just to get an estimate of response in the area of interest.

Typical IDA curves from the work of Vamvatsikos & Cornell (2002) are shown in Figure 1.7.

Chapter 1

Figures

	Modified Mercalli Intensity					
Damage State	VI	VII	VIII	IX	X	XI
1-None	~ 0	~ 0	~ 0	~ 0	~ 0	~ 0
2-Slight	0.23	0.02	~ 0	~ 0	~ 0	~ 0
3-Light	0.78	0.98	0.83	0.28	0.03	0.01
4-Moderate	~ 0	~ 0	0.16	0.72	0.85	0.45
5-Heavy	~ 0	~ 0	~ 0	0.01	0.12	0.54
6-Major	~ 0	~ 0	~ 0	~ 0	~ 0	~ 0
7-Destroyed	~ 0	~ 0	~ 0	~ 0	~ 0	~ 0

Table 1.1 Damage Probability matrix for C1 building class from ATC-13 (class 20,high-rise concrete moment frame)

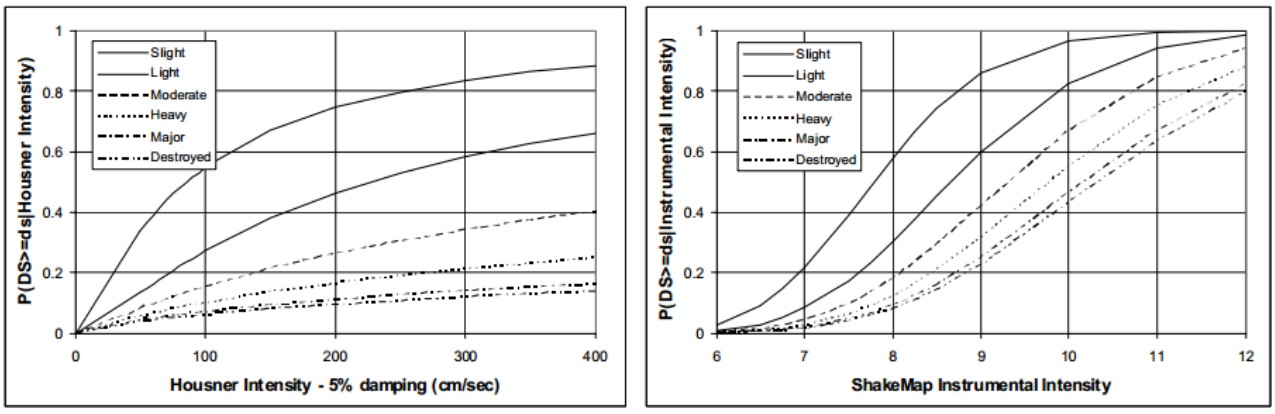

Figure 1.1 Fragility curves for C1 buildings, ATC-13 damage states and parameters *IH* and *IMM*

	USGS Peak Ground Acceleration (g)						
Observed Damage	0.15 –0.2	0.2 - 0.3	0.3 - 0.4	0.4 - 0.5	0.5 - 0.6	0.6 - 0.7	0.7 - 0.8
None	194	262	150	31	10	15	17
Minor	2	8	16	2	6	4	2
Moderate	1	8	8	9	6	5	1
Major	0	6	0	5	5	3	1
Collapse	0	0	0	0	0	0	0
Total	197	284	174	47	27	27	21
	USGS Peak Ground Acceleration (g)						
Observed Damage	0.8 - 0.9	0.9 - 1.0	1.0 - 1.1	1.1 - 1.2	1.2 - 1.3	1.3 - 1.4	Total
None	18	7	9	1	0	1	717
Minor	0	5	1	1	0	0	47
Moderate	4	7	3	0	0	0	52
Major	1	9	0	0	0	0	30
Collapse	2	1	1	0	0	0	4
Total	25	29	14	2	0	1	848

Table 1.2 Damage Frequency Matrix for Multi-Span Bridges (Basoz and Kiremidjian, 1997)

	USGS Peak Ground Acceleration (g)						
Observed Damage	0.15 –0.2	0.2 - 0.3	0.3 - 0.4	0.4 - 0.5	0.5 - 0.6	0.6 - 0.7	0.7 - 0.8
None	98.48	92.25	86.21	65.96	37.04	55.56	80.95
Minor	1.02	2.82	9.20	4.26	22.22	14.81	9.52
Moderate	0.51	2.82	4.60	19.15	22.22	18.52	4.76
Major	0	2.11	0	10.64	18.52	11.11	4.76
Collapse	0	0	0	0	0	0	0
	USGS Peak Ground Acceleration (g)						
Observed Damage	0.8 - 0.9	0.9 - 1.0	1.0 - 1.1	1.1 - 1.2	1.2 - 1.3	1.3 - 1.4	
None	72.00	24.14	64.29	50	0	100	
Minor	0	17.24	7.14	50	0	0	
Moderate	16.00	24.14	21.43	0	0	0	
Major	4.00	31.03	0	0	0	0	
Collapse	8.00	3.45	7.14	0	0	0	

Table 1.3 Damage Probability Matrix for Multi-Span Bridges (%) (Basoz and Kiremidjian, 1997)

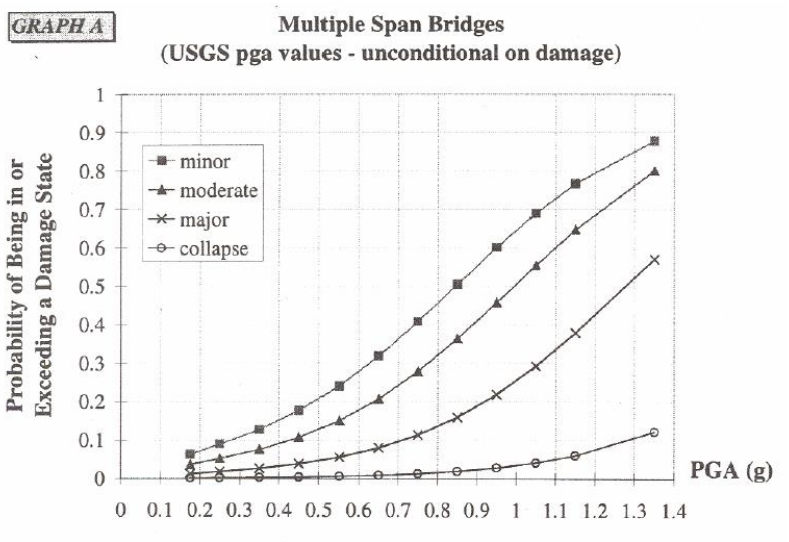

Figure 1.2 Fragility curves using logistic regression analyses (Basoz and Kiremidjian, 1997)

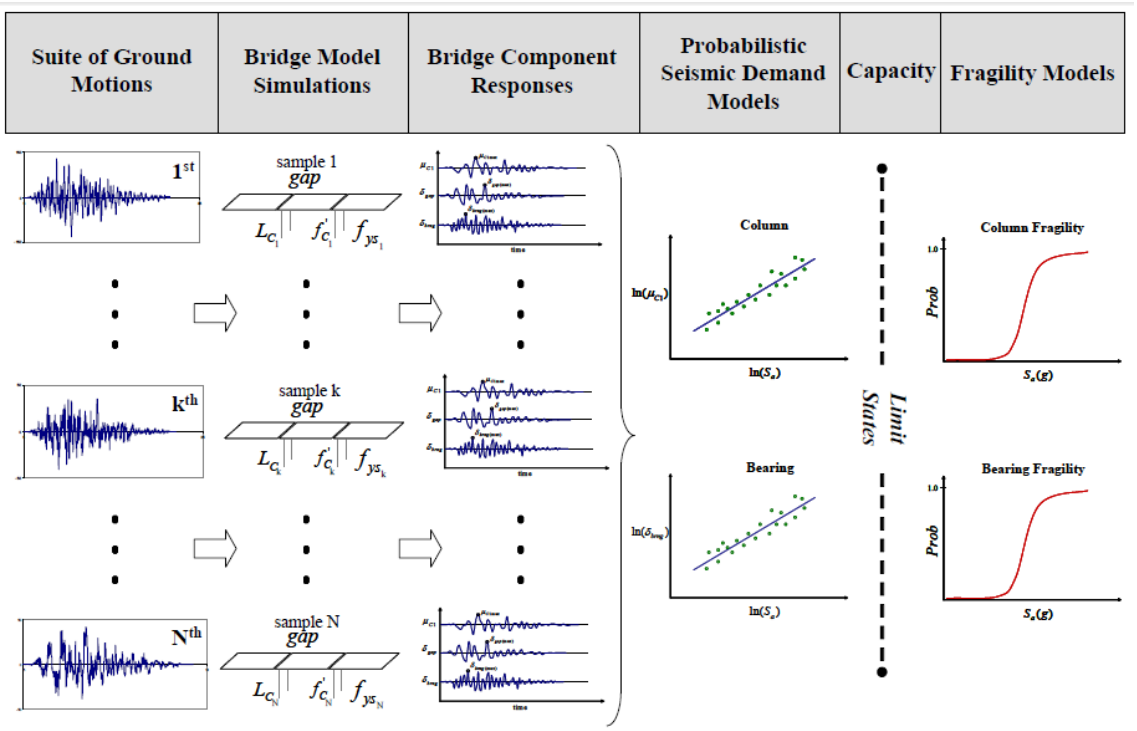

Figure 1.3 Analytical Fragility curve Generation using Non-linear Time History Analysis

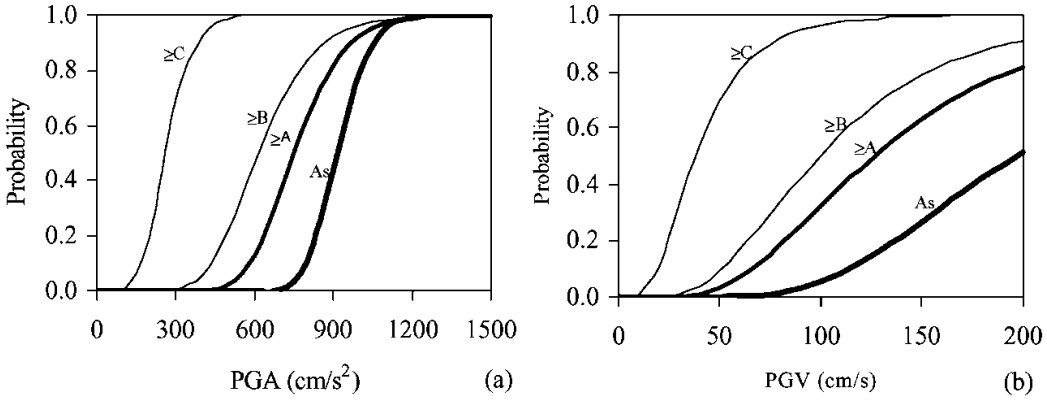

Figure 1.4 Typical analytical Fragility curves from the work of Karim & Yamazaki (2001) with respect to **(a)** PGA and **(b)** PGV obtained from the records of Kobe earthquake

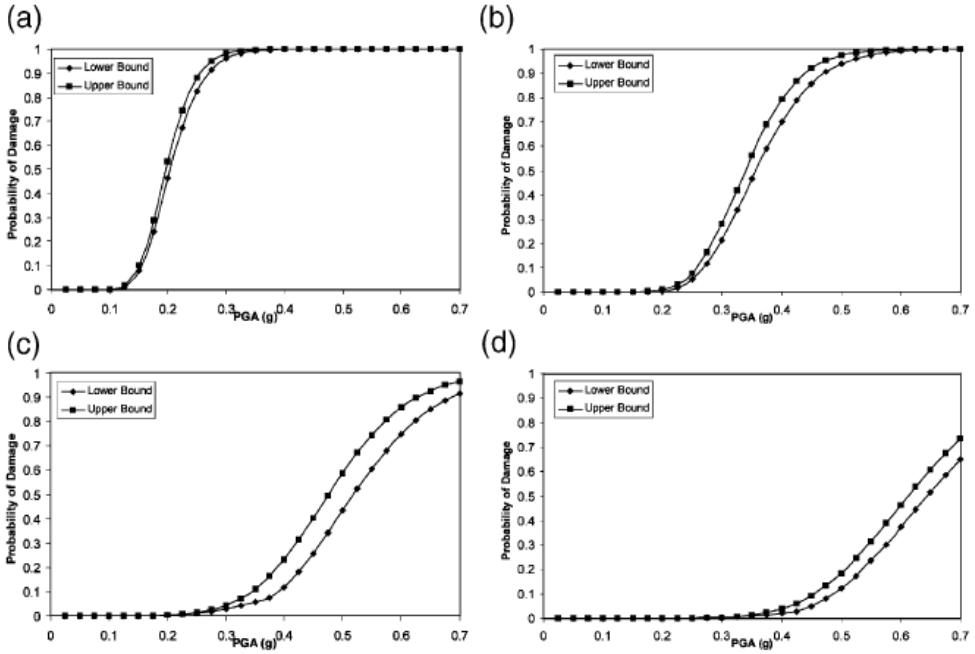

Figure 1.5 Typical analytical Fragility curves from the work of Choi & Nielson (2004) for **(a)** slight damage, **(b)**moderate damage, **(c)** extensive damage and **(d)** complete damage

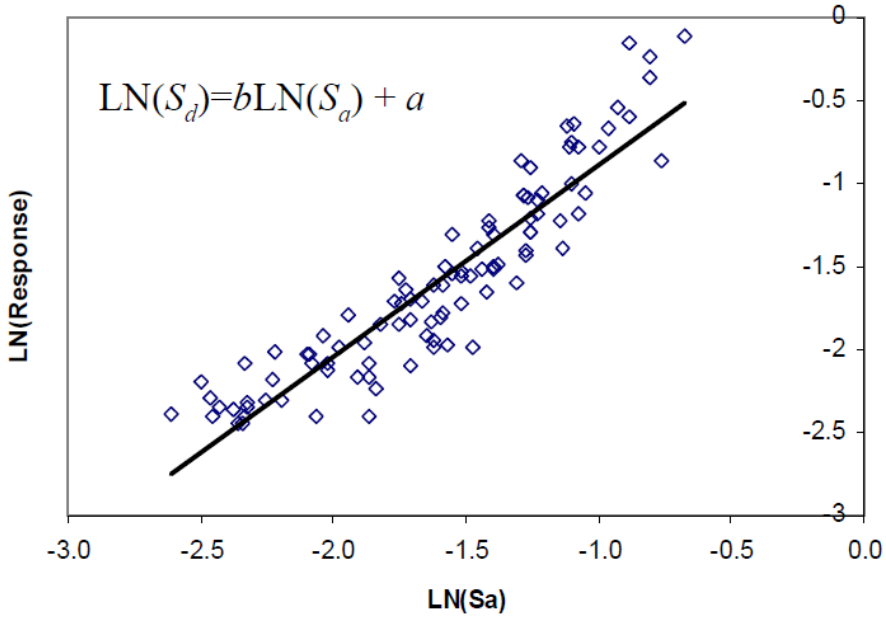

Figure 1.6 Probabilistic seismic demand model (PSDM) using Sa at the fundament period of the bridge

Damage State		Slight Damage	Moderate Damage	Extensive Damage	Complete Damage
Columns	(μ)	1.0<μ<2.0	2.0<μ<4.0	4.0<μ<7.0	7.0<μ
Steel Bearings	(δ, mm)	1<δ<6	6<δ<20	20<δ<40	40<δ
Expansion Bearings	(δ, mm)	δ<50	50<δ<100	100<δ<150	150<δ<255
Fixed Dowels	(δ, mm)	8<δ<100	100<δ<150	150<δ<255	255<δ
Expansion Dowels	(δ, mm)	δ<30	30<δ<100	100<δ<150	150<δ<255

Table 1.4 Definition of Limit States for Bridge Components (Choi, 2002)

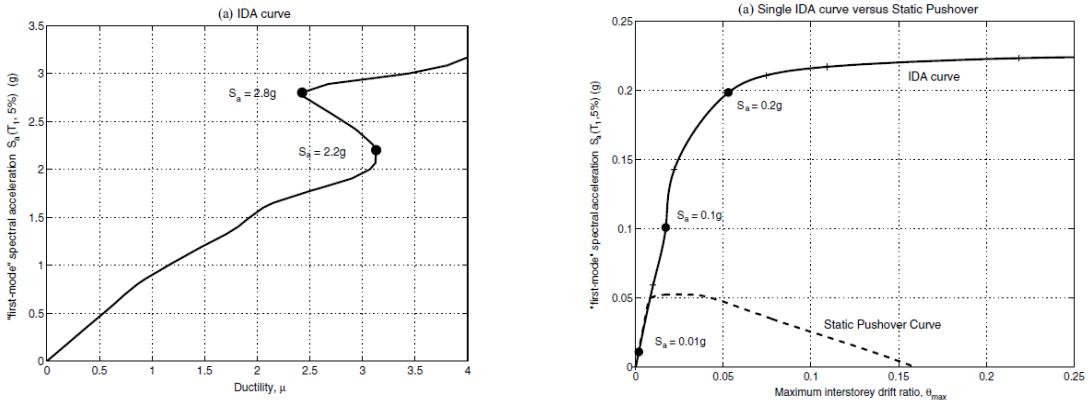

Figure 1.7 Typical Incremental Dynamic Analysis (IDA) curves from the work of Vamvatsikos and Cornell (2002)

CHAPTER 2

SEISMIC PERFORMANCE OF S-DOF SYSTEM EFFECTIVENESS OF IM's & DPI's

2.1 Seismic Hazard

2.1.1 Selection of acceleration time histories

The fact that the structural damage due to different records from different earthquakes might be different even having the same IM indicates the importance of various characteristics of the input ground motion. Frequency contents, phase, duration etc. have such a significant effect on the performance of the structure that they cannot be ignored.

In order to take into account the effect of each one of these characteristics, 29 real records from earthquakes of varied intensity and characteristics are used as input excitation. Additionally in each one of these records Peak Ground Acceleration (PGA) is scaled from 0.1g to 1.2g. Finally a range of 377 acceleration time histories is used in order to examine a Single Degree of Freedom (SDOF) system to different excitation levels but also to time histories with different characteristics.

2.1.2 Selection of Intensity Measures (IM) and Damage Potential Indexes (DPI)

The Peak Ground Acceleration (PGA) and Peak Ground Velocity (PGV) are commonly used indices to describe the severity of the earthquake ground motion. However, it is well known that a large PGA is not always followed by severe structural damage, especially for long period structures. Similarly, a large PGV is not always followed by severe structural damage, especially for input motions which include permanent fault displacements. Other indices of earthquake ground motion, e.g., Peak Ground Displacement (PGD), time duration of strong motion (Td), spectrum intensity (SI) , and spectral characteristics, can be considered in damage estimation.

In this direction, a total of nineteen IM's and DPI's were selected each of which describes a different characteristic of the earthquake. Ten of them (PGA, PGV, PGD, IA, ARMS, VRMS, DRMS, IC, SMA, SMV) which are directly correlated to the acceleration, velocity and displacement time history were calculated first and then were compared and validated with the results of the software

SEISMOSIGNAL. Furthermore another nine DPI's (IH, SE, CAV, ASI, VSI, A95, TP, TMEAN, Dsig) were extruded from SEISMOSIGNAL in order to take into account more parameters of the ground motion. All these parameters are presented in detail and are listed in Table 2.1.

2.2 Seismic Performance of a bridge pier

2.2.1 Model used

A single-degree-of-freedom (SDOF) model of a bridge pier similar to the Hanshin Expressway Fukae bridge [M.Loli 2008], is used to calculate the seismic excitation applied at the level of the deck. This is a rational approximation as the mass and the stiffness of the pier are significantly lower than the mass and the stiffness of the deck. Both the calculation of the natural period of the system and the static and dynamic loading assume fixed base conditions. With reference to Figure 2.1 the equivalent oscillator has the following characteristics:

- ✓ m = 1200 Mgr
- ✓ h = 12 m
- ✓ I = $\frac{\Pi d^4}{64}$
- ✓ d = 3 m
- ✓ T = 0.48s

2.2.2 Method of Analysis

A total of 377 series of two dimensional finite element analyses are performed for the S-DOF model using the ABAQUS code. The mass point (m = 1200 Mgr) is located 12 m above the foundation level and is connected to the footing with linear beam elements of circular section (r = 1.5 m) in order to take into account the flexural deformation of the superstructure.

The response of the SDOF system to static and dynamic loading is investigated in terms of nonlinear behavior. For all stages of analysis, P–δ effects are taken into consideration. The elastoplastic pier behavior is described with Von Mises yielding criterion with nonlinear kinematic hardening and associative plastic flow rules. This model is originally used to stimulate the inelastic

behavior of metals subjected to cyclic loading. Although the aforementioned elastoplastic model is not appropriate for the stress–strain relationship of reinforced concrete, its parameters can be calibrated to match the pier response in the macroscopic moment-curvature level. To simulate the softening behavior of the reinforced concrete section after ultimate capacity is reached a special user subroutine is encoded in ABAQUS. The parameters of the model are calibrated using the following methodology:

2.2.3 Pier Behavior

- **Pier Section Reinforcement**

The reinforcement of the pier base circular section (D = 3 m) was calculated according to the provisions of the Greek Code for Reinforced Concrete (ΕΚΩΣ, 2000) for columns with large capacity demands. For acceleration A = 0.24 g, considering a (ductility-based) behavior factor q = 2 with an elastic (fixed-base) vibration period T = 0.48 s and soil conditions characterized as "B" the design spectral acceleration is SA = 0.3g. The computed reinforcement [M.Loli 2008] of the pier section for concrete C30 and Steel S400 is:

longitudinal 100 Ø32

transverse Ø13/8.

- **Moment-Curvature Analysis**

The section is also analyzed using the USC_RC program (Moment-Curvature, Force-Deflection, and Axial Force-Bending Moment Interaction Analysis of Reinforced Concrete Members". University of South California, 2001). The geometric characteristics and the reinforcement of the section used in the analysis are depicted in Figure 2.2.

The Mander model (Mander et al., 1984) is used to simulate the stress–strain relationship of confined concrete. The analysis doesn't take into account the hardening behavior of steel and the material strength values refer to the design values (fcd, fsd). The moment curvature relationship for

the pier section as derived from the analysis with the USC_RC program, considering the softening behavior of concrete, is shown in Figure 2.3. The point of "failure", when the ultimate moment capacity is reached, is highlighted in the diagram as well as the point when yielding initiates (εy = fy/Es ≈0.002).

- **Calibration of the Kinematic Hardening Model for the Pier Elements**

The nonlinear kinematic hardening model provided by ABAQUS with Von Mises yield surface is used to simulate the nonlinear elastoplastic behavior of the pier elements. The parameters of the model are calibrated in order to match the moment–curvature relationship of the concrete section as derived from the analysis with the USC_RC program.

The bending moment of a circular section is by definition related to the normal stresses σ with the following expression:

$$M = 2\int_0^{\Pi}\int_0^{d/2} \sigma r^2 \sin\theta \, dr d\theta$$

For the maximum yield stress σy this relationship gives:

$$M_y = 2\,\sigma_y \int_0^{\pi} \frac{r^2}{3}\sin\theta \,\Big|_0^{d/2} d\theta$$

$$M_y = \frac{1}{6}\sigma_y d^3$$

The maximum yield stress according to the kinematic hardening model is given by the following expression:

$$\sigma_y = \frac{c}{\gamma} + \sigma_0$$

In which the initial kinematic hardening modulus C is equal to the modulus of elasticity E.

The calibration of the model parameters (σ_0, C, γ) is implemented with regard to the aforementioned constitutive relationships for monotonic loading of the pier elements. Figure 2.4 shows the comparison between the moment curvature relationship derived from the monotonic

loading of the pier elements with the calibrated kinematic parameters and the moment curvature relationship calculated with USC_RC.

2.2.4 Dynamic Loading

A nonlinear dynamic time history analysis is conducted to the S-DOF system, using 29 real earthquake records. The records are presented in Figure 2.5. In all cases the excitations are applied at the fixed base. Each record is scaled by PGA from 0.1g to 1.2g in order to examine the performance of the pier to different excitation levels. The results obtained from the analysis are the displacement both at the base and the top of the pier but also the moment and curvature time history at the fixed base of the SDOF system.

In order to quantify the structural damage of each excitation, the maximum and the residual drift and drift ratio were calculated but also the ductility demanded in terms of curvature. (μ_{demand}). The drift time history is calculated by abstracting from the displacement at the top of the pier, the displacement at the fixed base. The maximum and the residual drift ratio are calculated by dividing the maximum and the residual drift respectively, to the height of the SDOF system. It is widely accepted that the maximum and the residual drift and drift ratio can be representative of the structural damage depending on the typology of the bridge tested. Ductility is extracted from the moment-curvature curve of each analysis by dividing the maximum value of curvature demanded with the value of curvature when yielding initiates. An alternative way to express the structural damage in terms of ductility is the ratio $\frac{\mu_{demand}}{\mu_{capacity}}$. This is the way that is considered to be more appropriate because it takes into account the ductility capacity of the system. Ductility capacity ($\mu_{capacity}$) is calculated by dividing the curvature at the point of "failure", when the ultimate moment capacity is reached, with the curvature when yielding initiates. In this case the ductility capacity of the system in terms of curvature is $\frac{\mu_{demand}}{\mu_{capacity}}$ =16.6.

Finally the maximum drift, residual drift, maximum drift ratio, residual drift ratio and $\frac{\mu_{demand}}{\mu_{capacity}}$ are selected as Damage Indexes (DI) to describe the structural damage of the S-DOF system while the 19 IM's and DPI's selected ''capture'' the characteristics and the excitation level of each record.

The model used in ABAQUS code is presented on Figure 2.11 at the end of Chapter 2 as its deformed shape for JMA_000 record.

2.3 Effectiveness of IM's and DPI's

2.3.1 Database

The results of the previous analysis are aggregated and classified in a database that includes all of the 19 IM's and 6 DI's for each one of the 377 acceleration time histories. (Table 2.2)

2.3.2 Effectiveness of a single IM and DI

Having completed the whole set of the analyses, the next step is to compare the effectiveness of each IM to estimate a single DI. The graphs, exported for each IM, aim to show the correlation between a specific IM and a specific DI. Some indicative graphs are presented in Figures 2.6, 2.7 and show the correlation between 2 DI's (max drift ration and μd/μc) with 4 IM's (PGV, AI, HI, ASI). It is observed that each individual IM is unable to predict the expected structural damage as there is no satisfactory correlation between an IM and a DI. So the previous analysis leads to the conclusion that you cannot predict the structural damage of a SDOF system by considering only one IM.

2.3.3 Correlation between IM's and DI's

The fact that an individual IM cannot be used to estimate the structural damage of every structure was expected and is generally accepted. In most cases investigation aims to show which one of the IM's is more suitable for the particular structure under consideration. On this task a different approach is attempted.

In an effort to deal with this fact it was attempted to correlate more than one IM's using advanced econometric methods. Thanks to the work of P. Anastasopoulos, Assistant Professor at the Department of Civil, Structural and Environmental Engineering at State University of New York at Buffalo, the following equation was generated:

$$Drift max\ ratio = e^{1.68068703+0.00000203935 \cdot PGV^2+0.21425116 \cdot \sqrt{IA}-0.59155881 \cdot \frac{1}{\sqrt{ASI}}+0.06021123 \cdot \sqrt{VSI}+0.00475847 \cdot \frac{1}{\sqrt{TP^2}}-1.36230326 \cdot \frac{1}{\sqrt{Tmean}}-0.13138765\sqrt{Dsig}}$$

The deviations between the results of the analysis and the one predicted from the equation are presented in Figure 2.8 as well as the spread of these results.

With a closer look, it is noticed that the seven Intensity Measures used in the equation are related with different characteristics of the ground motion. More specific, PGV and Arias Intensity are related with the velocity and acceleration time history while ASI and VSI are related with the spectral acceleration and velocity respectively. Predominant Period (T_P) , Mean Period (Tmean) and Significant Duration (D_{sig}) are also a part of the equation, considering the parameter of the duration of the ground motion in an attempt to provide correlation between the various Intensity Measures. This enhances the belief that all the characteristics of the ground motion affect in a different way the performance of the structure and therefore cannot be ignored.

2.3.4 Efficiency of the equation

It is important to keep in mind that this equation is only a first attempt to estimate a specific Damage Index using a combination of IM's. Also the database used in order to extrude this equation includes results of records that demanded ductility much larger than the capacity of the system. Therefore it is possible to achieve an even better approach excluding the results that are not part of our interest ($\mu_{demand} \gg \mu_{capacity}$).

The following step was to examine the effectiveness of the developed equation. For this purpose for another 5 real records a series of non-linear time history analyses were performed, in order to obtain the damage indices and compare them with the relevant results of the equation. Figures 2.9, 2.10 present the deviations between the observed results of the analysis and the predicted one of the equation while the results are collected on Table 2.3.

In general terms such an equation is considered to be a very satisfactory way to estimate the structural damage of S-DOF systems when a seismic event occurs, as far as a rapid response system is concerned. For the purposes of a rapid response system, structural damage is characterized by

some specific damage states (No damage, Slight damage, Moderate damage, Extensive damage, Complete damage). As a result it is not so important to estimate precisely the structural damage but it is satisfactory to be close enough to it.

As a next step it will be attempted to extend the use of the equation to equivalent systems but also to improve the equation in order to take into account the effect of each component of the bridge.

Chapter 2

Figures

Seismological Index	***Definition***
Peak Ground Acceleration, ***PGA***	*Highest absolute peak in the acceleration time-history.*
Peak Ground Velocity, ***PGV***	*Highest absolute peak in the velocity time-history.*
Peak Ground Displacement, ***PGD***	*Highest absolute peak in the displacement time-history.*
RMS Acceleration, A_{RMS}	$A_{RMS} = \sqrt{\frac{\int A^2(t)dt}{T_D}}$ *TD = length of record, A(t) = ground acceleration.*
RMS Velocity, V_{RMS}	$V_{RMS} = \sqrt{\frac{\int V^2(t)dt}{T_D}}$ *TD = length of record, V(t) = ground acceleration.*
RMS Displacement, D_{RMS}	$D_{RMS} = \sqrt{\frac{\int D^2(t)dt}{T_D}}$ *TD = length of record, D(t) = ground acceleration.*
Arias Intensity, I_A	$I_A = \frac{\pi}{2g} \int A^2(t)\,dt$ *A(t)= ground acceleration.*
Characteristic Intensity, I_C	$I_C = (A_{RMS})^{\frac{3}{2}} \sqrt{T_D}$ T_D *= length of record.*
Specific Energy Density, S_E	$S_E = \frac{V_S \rho_S}{4} \int V^2(t)dt$ *VS = wave velocity, ρS = mass density.*
Cumulative Absolute Velocity, ***CAV***	$CAV = \sum_{i=1}^{N} H\,(PGA_i - A_{min}) \int_{t_i}^{t_{i+1}} \lvert A(t)\rvert dt$ *N = number of 1-second time windows in the time series, PGAi = PGA of time window i, ti = start time of window i, Amin = acceleration threshold (user-defined but commonly 0.025g), and H(x) = Heaviside step function (unity for x>0 and 0 otherwise).*

Acceleration Spectrum Intensity, ***ASI***	$ASI=\int S_A(5\%,T)dT$ *SA(5%,T) = spectral acceleration for 5% damping, T = natural period.*
Velocity Spectrum Intensity, ***VSI***	$VSI=\int S_V(5\%,T)dT$ *SA(5%,T) = spectral acceleration for 5% damping, T = natural period.*
Housner Intensity, I_H	$I_H = \int_{0.1}^{2.5} S_v\,(T,\xi = 5\%)\ \mathrm{dT}$ *SV (T, ξ) = pseudo-velocity spectrum.*
Sustained Maximum Acceleration, ***SMA***	*The third highest absolute peak in the acceleration time-history.*
Sustained Maximum Velocity, ***SMV***	*The third highest absolute peak in the velocity time-history.*
Acceleration Parameter A_{95}	*The level of acceleration which contains up to 95% of the Arias Intensity.*
Predominant Period, T_P	*The period of the maximum spectral 5% damping acceleration*
Mean Period, T_{mean}	$T_{mean} = \frac{\sum\left(\frac{C_i^2}{f_i}\right)}{\sum C_i^2}$ *Ci = Fourier amplitude for frequency fi in the range 0.25–20 Hz.*
Significant Duration, D_{sig}	*is the interval of time between the accumulation of 5% and 95 % of Arias Intensity.*

Table 2.1 List of Intensity Measures and Damage Potential Indexes

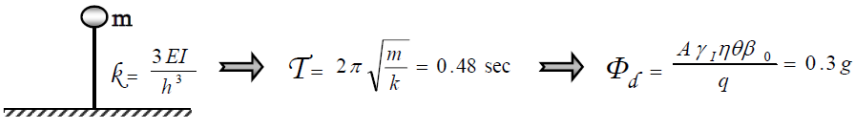

Figure 2.1 SDOF approximation and estimation of the design seismic acceleration developed at the center of mass

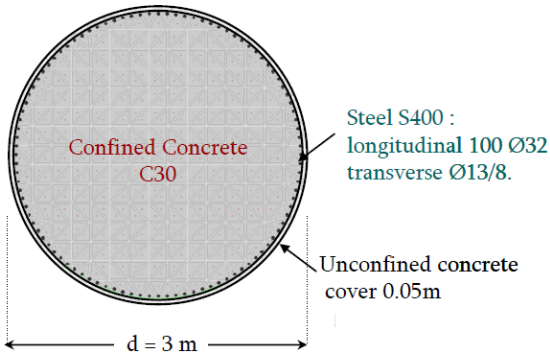

Figure 2.2 The geometric characteristics and the reinforcement of the bridge pier section

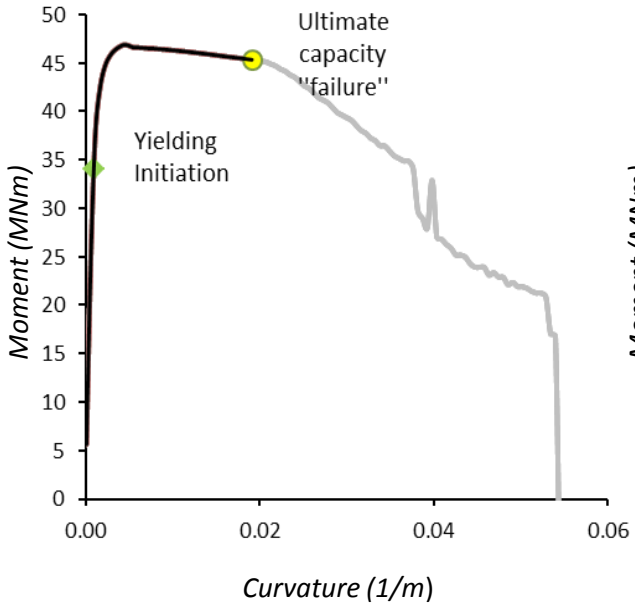

Figure 2.3 Moment-Curvature relationship for the pier section as derived from the analysis with the USC_RC

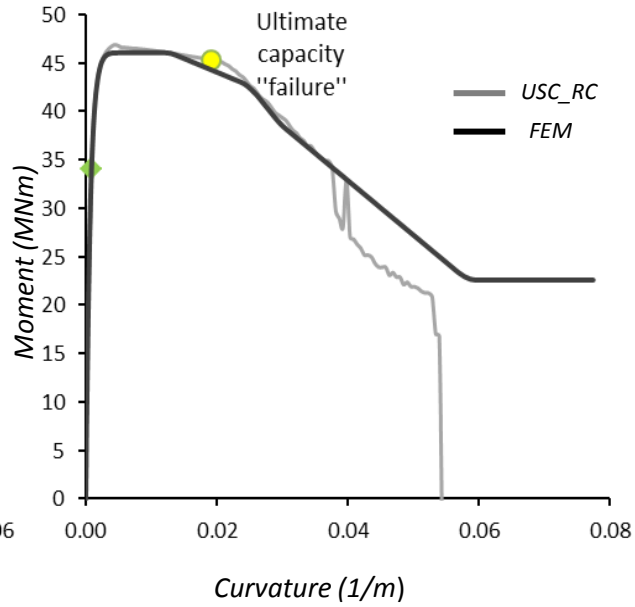

Figure 2.4 Comparison of the moment-curvature curves using the USC_RC program and calibrated finite element model with kinematic hardening law

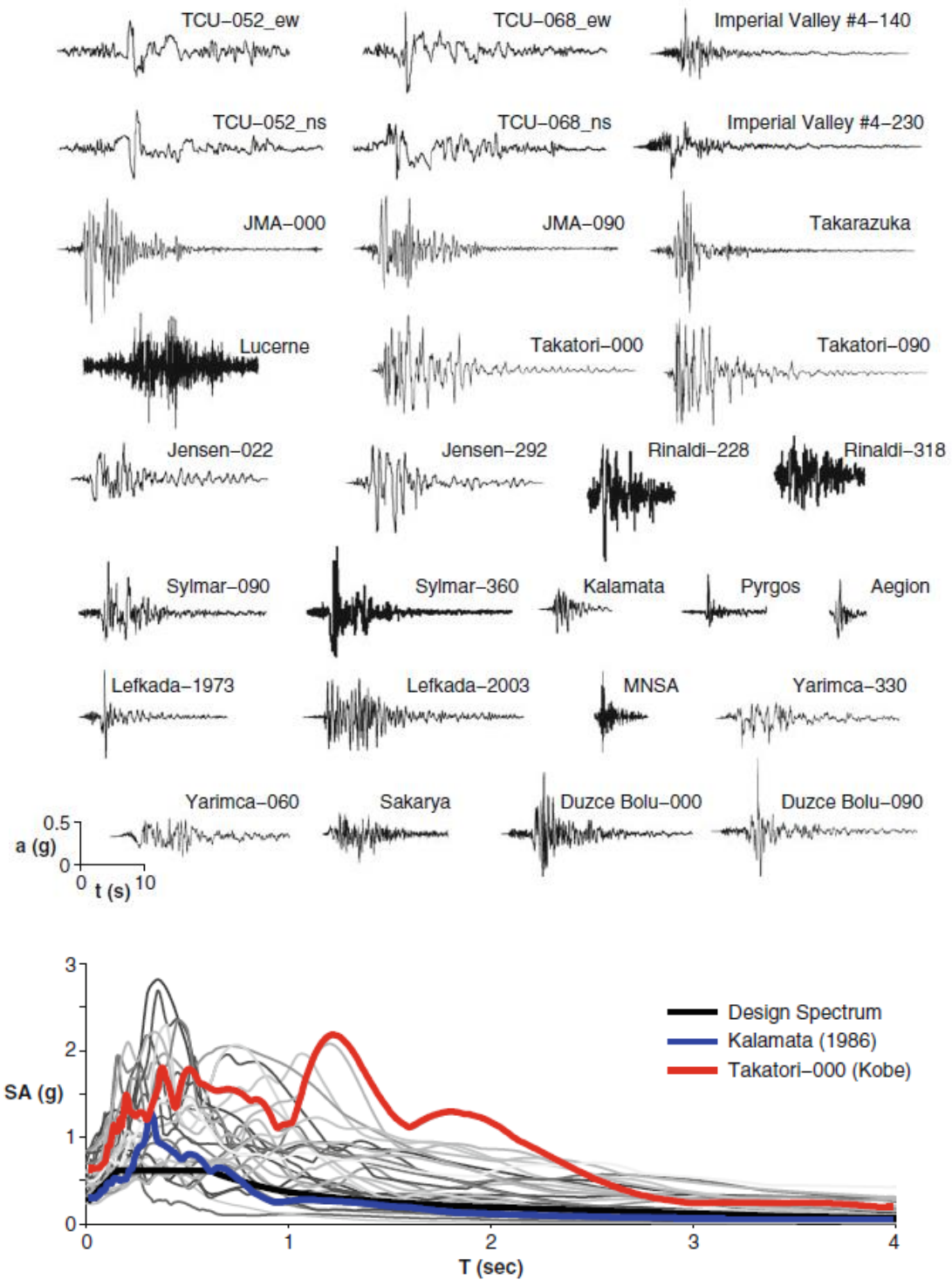

Figure 2.5 Real earthquake records used for analysis of the two bridge systems, along with their elastic spectra and the design spectrum of the investigated bridge

REAL RECORDS	IM-DPI																		
	PGA (g)	PGV (cm/s)	PGD (cm)	Arms (g)	Vrms (cm/s)	Drms (cm)	IA (m/s)	Ic	SE (cm^2/s)	CAV (cm/s)	ASI (g*s)	VSI (cm)	IH (cm)	SMA (g)	SMV (cm/s)	A95 (g)	TP (s)	Tmean (s)	Dsig (s)
TAKATORI_000	0.61	127	36	0.15	31	10	8.63	0.29	23523	2399	0.53	580	586	0.48	70	0.60	1.2	1.1	11.3
TAKATORI_090	0.62	121	33	0.14	27	9	8.09	0.28	18263	2114	0.71	505	511	0.57	77	0.60	0.2	1.0	9.9
JMA_000	0.82	81	18	0.14	16	4	8.38	0.27	7582	2021	0.72	417	362	0.62	55	0.80	0.3	0.6	8.1
JMA_090	0.60	74	20	0.12	14	4	5.42	0.21	5047	1681	0.54	292	262	0.56	39	0.59	0.4	0.6	9.5
TAKARAZUKA_090	0.69	85	17	0.11	14	4	3.93	0.17	3935	1103	0.69	312	298	0.53	50	0.69	0.5	0.6	3.6
MNSA	0.51	15	4	0.08	3	2	0.75	0.06	86	347	0.27	51	40	0.34	14	0.51	0.2	0.2	3.0
PYRGOS	0.44	20	2	0.05	3	1	0.33	0.03	82	226	0.28	64	37	0.09	4	0.44	0.3	0.3	3.6
AEGIO	0.39	38	5	0.08	8	2	0.52	0.05	324	247	0.27	106	86	0.19	13	0.38	0.5	0.5	1.5
KALAMATA	0.27	24	6	0.07	7	2	0.73	0.06	451	421	0.30	103	93	0.20	21	0.27	0.3	0.5	3.7
LEFKADA_2003	0.43	36	51	0.11	10	33	3.97	0.17	1914	1461	0.50	149	126	0.39	31	0.42	0.5	0.5	9.2
LEFKADA_1973	0.53	55	12	0.07	8	2	1.35	0.08	1145	610	0.41	206	154	0.09	12	0.53	0.5	0.6	4.9
TCU_052EW	0.35	175	476	0.08	52	291	2.65	0.12	71112	1416	0.21	317	377	0.27	136	0.35	1.1	1.6	14.7
TCU_052NS	0.44	220	787	0.08	62	601	2.78	0.12	118132	1439	0.27	381	414	0.16	171	0.43	1.1	1.5	15.6
TCU_068EW	0.49	273	716	0.08	67	516	3.02	0.13	129572	1467	0.46	301	346	0.45	137	0.48	0.4	1.5	11.8
TCU_068NS	0.35	289	891	0.09	97	589	2.98	0.13	203859	1528	0.25	260	286	0.28	115	0.34	0.8	1.3	12.7
RINALDI_228	0.84	166	28	0.20	30	10	7.31	0.31	10769	1575	0.65	510	457	0.62	46	0.83	0.7	0.7	7.0
RINALDI_318	0.47	73	20	0.15	21	7	3.89	0.19	5404	1282	0.51	299	297	0.41	60	0.47	0.3	0.6	7.3
JENSEN_022	0.42	106	43	0.09	24	12	2.61	0.12	11701	1200	0.29	284	309	0.29	74	0.41	0.8	1.2	11.0
JENSEN_292	0.59	99	24	0.13	24	6	5.56	0.22	11316	1522	0.45	504	462	0.44	71	0.58	1.1	1.0	5.6
SYLMAR_090	0.60	78	17	0.12	19	7	2.54	0.14	4358	932	0.42	259	261	0.35	49	0.60	0.5	0.8	5.7
SYLMAR_360	0.84	129	32	0.18	29	11	4.84	0.24	8398	1084	0.82	390	388	0.28	42	0.84	0.4	0.7	4.6
DUZE-BOLU_000	0.73	56	24	0.11	14	9	3.68	0.16	3762	1282	0.64	235	211	0.44	41	0.72	0.3	0.5	8.4
DUZE-BOLU_090	0.82	62	13	0.09	13	5	2.37	0.12	3192	933	0.48	255	237	0.33	26	0.82	0.4	0.7	7.9
LUCERNE_000	0.70	31	34	0.12	7	19	5.16	0.20	1344	1937	0.38	111	92	0.59	29	0.69	0.1	0.2	13.1
YARIMCA_060	0.23	90	198	0.06	26	151	1.31	0.07	17757	996	0.22	150	156	0.19	84	0.23	0.5	1.3	13.3
YARIMCA_330	0.32	87	149	0.06	22	105	1.32	0.07	12357	1010	0.22	169	175	0.23	47	0.32	0.4	1.3	15.0
SAKARYA_TRANS	0.33	81	211	0.07	27	170	1.14	0.07	11883	724	0.26	134	129	0.23	57	0.32	0.3	0.5	7.9
IV#04_140	0.49	37	20	0.05	8	7	1.34	0.06	2470	827	0.36	188	177	0.27	34	0.48	0.2	0.7	6.7
IV#04_230	0.36	77	59	0.04	16	13	0.93	0.05	9556	758	0.24	148	180	0.24	43	0.36	0.2	1.3	10.3

REAL RECORDS	Damage Indexes					
	Dmax	Dres	Drift max ratio (%)	Drift res ratio (%)	μ demand Cu	μ d/ μ c
TAKATORI_000	0.57	0.55	4.8	4.6	43.19	2.57
TAKATORI_090	0.45	0.35	3.8	2.9	39.37	2.34
JMA_000	0.32	0.22	2.6	1.8	15.82	0.94
JMA_090	0.28	0.26	2.3	2.2	14.89	0.89
TAKARAZUKA_090	0.16	0.02	1.3	0.2	7.76	0.46
MNSA	0.01	0.00	0.1	0.0	0.22	0.01
PYRGOS	0.03	0.01	0.2	0.1	0.59	0.03
AEGIO	0.06	0.00	0.5	0.0	1.59	0.09
KALAMATA	0.07	0.03	0.6	0.2	2.11	0.13
LEFKADA_2003	0.07	0.03	0.6	0.2	2.36	0.14
LEFKADA_1973	0.16	0.13	1.4	1.0	7.76	0.46
TCU_052EW	0.14	0.04	1.1	0.3	8.12	0.48
TCU_052NS	0.26	0.22	2.2	1.8	14.74	0.88
TCU_068EW	0.31	0.23	2.6	1.9	19.00	1.13
TCU_068NS	0.12	0.06	1.0	0.5	5.18	0.31
RINALDI_228	0.34	0.29	2.8	2.4	15.80	0.94
RINALDI_318	0.10	0.02	0.8	0.1	4.61	0.27
JENSEN_022	0.25	0.20	2.1	1.6	16.26	0.97
JENSEN_292	0.33	0.29	2.7	2.4	13.34	0.79
SYLMAR_090	0.20	0.17	1.6	1.4	12.10	0.72
SYLMAR_360	0.20	0.08	1.7	0.7	10.53	0.63
DUZE-BOLU_000	0.09	0.05	0.7	0.4	4.25	0.25
DUZE-BOLU_090	0.24	0.17	2.0	1.4	13.41	0.80
LUCERNE_000	0.05	0.02	0.4	0.1	0.95	0.06
YARIMCA_060	0.05	0.02	0.4	0.1	1.50	0.09
YARIMCA_330	0.07	0.02	0.6	0.2	2.78	0.17
SAKARYA_TRANS	0.05	0.00	0.4	0.0	1.07	0.06
IV#04_140	0.11	0.04	0.9	0.3	5.03	0.30
IV#04_230	0.06	0.02	0.5	0.1	1.71	0.10

Table 2.2 Results of the dynamic analysis for 29/377 acceleration time histories including all of the 19 IM's and 6 DI's

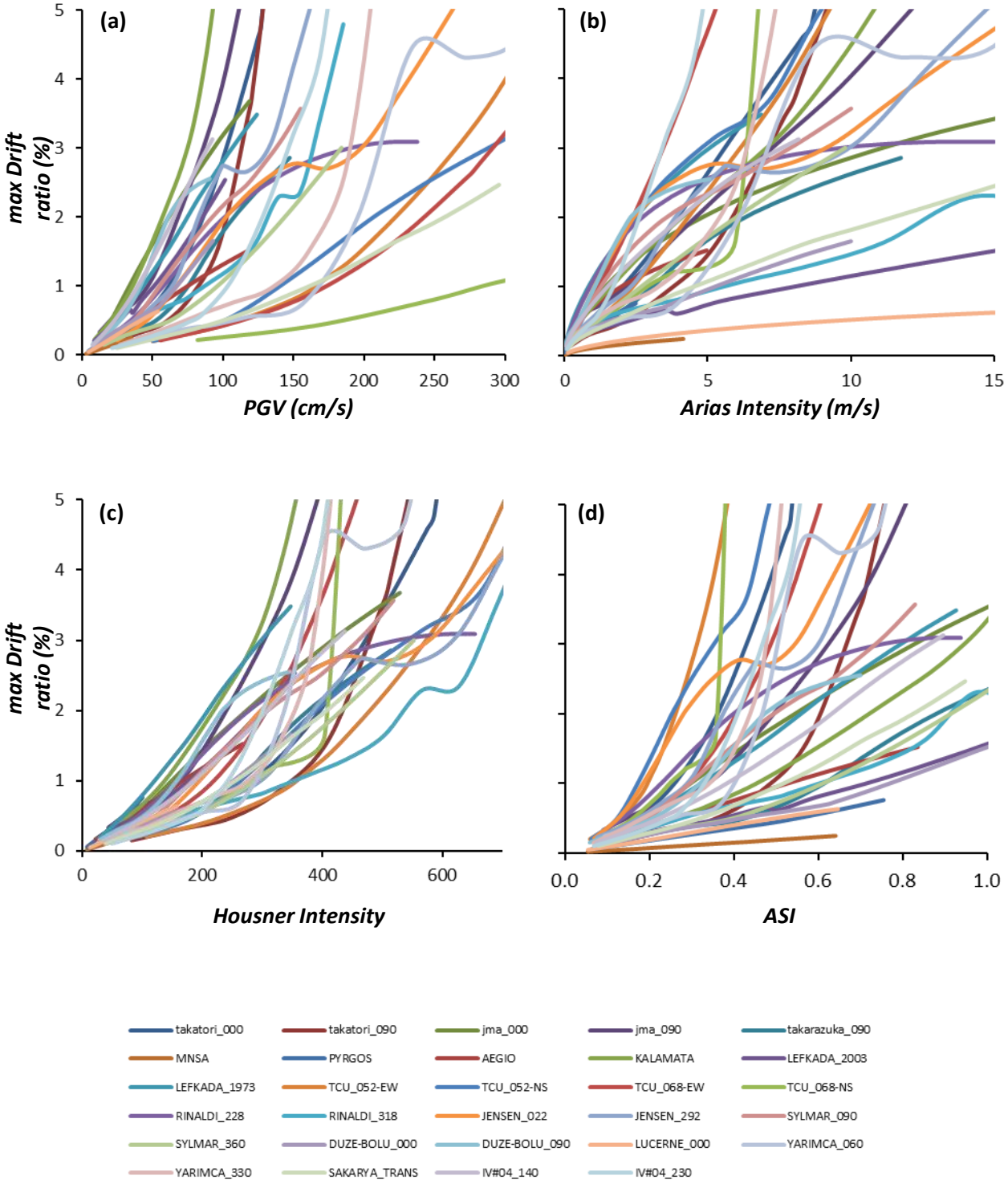

Figure 2.6 Max drift correlated with **(a)** PGV, **(b)** Arias Intensity, **(c)** Housner Intensity, **(d)** ASI

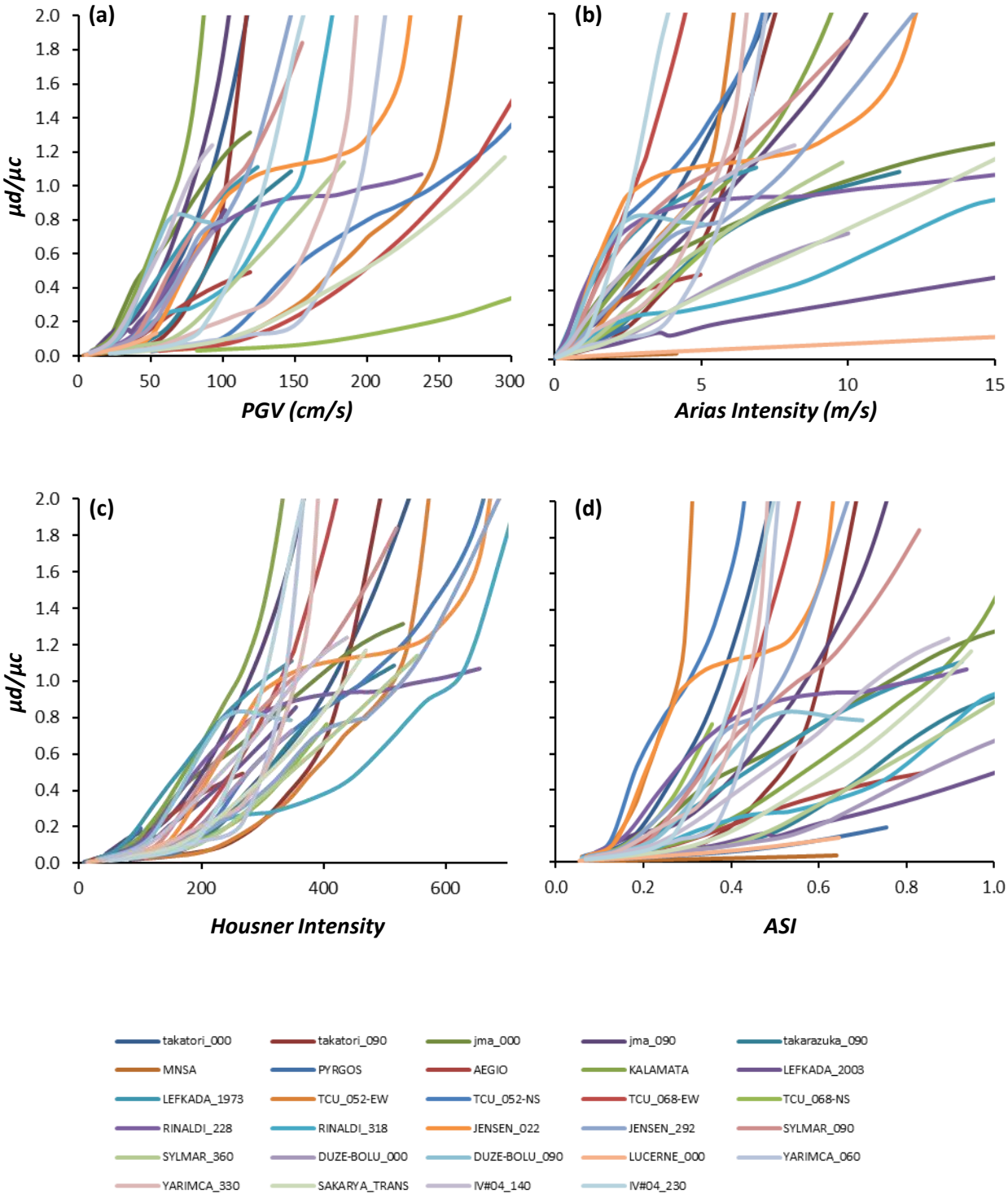

Figure 2.7 Max drift correlated with **(a)** PGV, **(b)** Arias Intensity, **(c)** Housner Intensity, **(d)** ASI

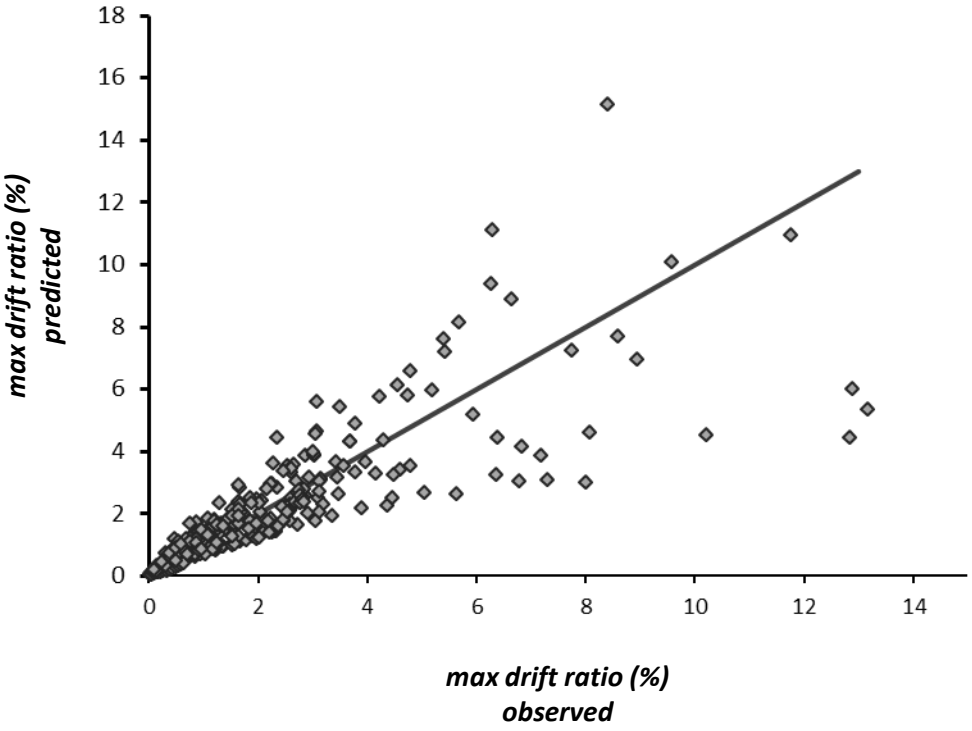

Figure 2.8 Deviations between the observed results of the analysis and the predicted of the equation in terms of maximum drift ratio

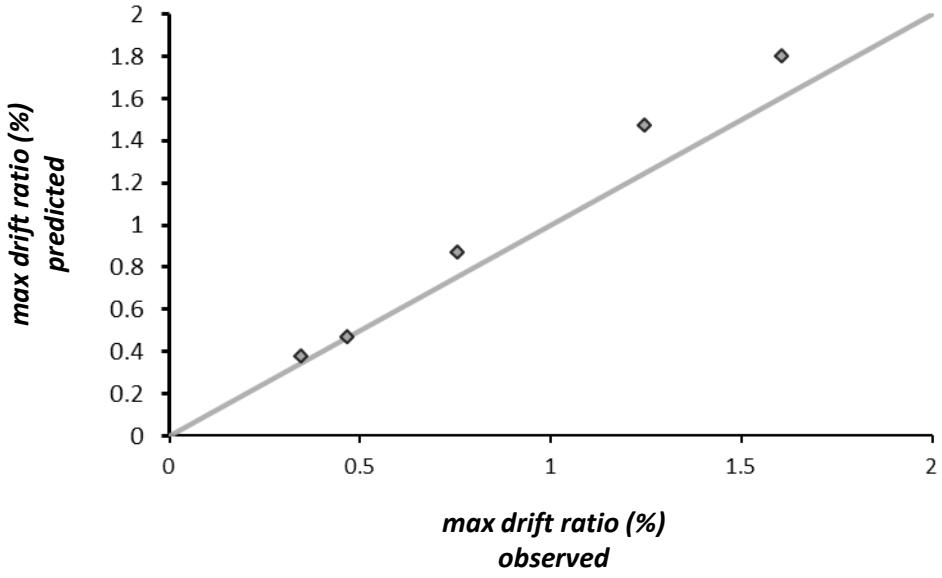

Figure 2.9 Deviations between the observed results of the analysis and the predicted of the equation in terms of maximum drift ratio for 5 real records out of the database

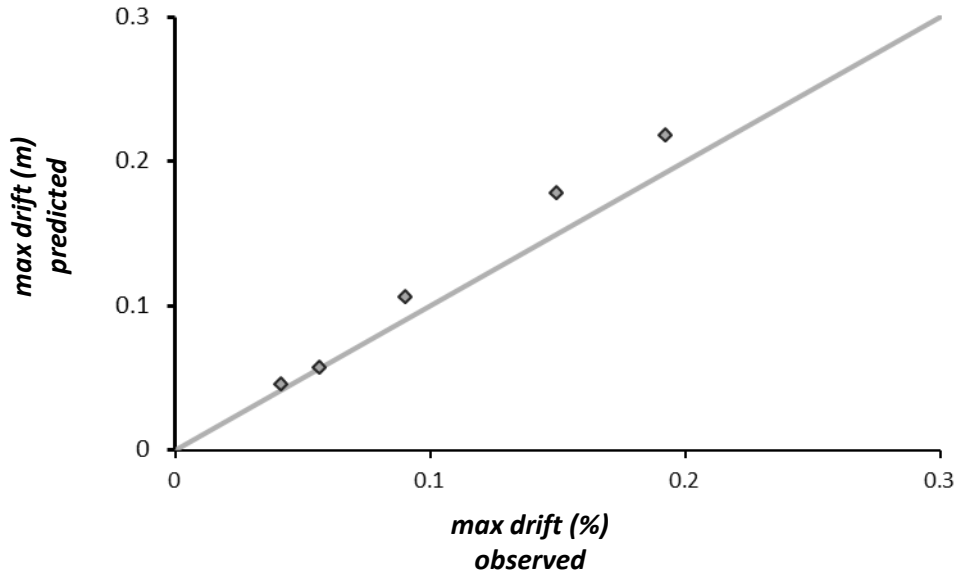

Figure 2.10 Deviations between the observed results of the analysis and the predicted of the equation in terms of maximum drift ratio for 5 real records out of the database.

real records used	*Results Observed (Analysis)*		*Results Estimated (Equation)*		*Deviations*	
	Drift ratio (%)	Dmax (m)	Drift ratio (%)	Dmax (m)	Drift ratio (%)	Dmax (m)
IZMIT_090	0.35	0.04	0.38	0.05	0.03	0.00
KARAKYR_000	0.76	0.09	0.87	0.11	0.11	0.01
NAHANNI_010	0.47	0.06	0.47	0.06	0.00	0.00
PAC_164	1.61	0.19	1.80	0.22	0.19	0.02
TABAS_LN	1.25	0.15	1.47	0.18	0.22	0.03

	Deviations	
	Drift ratio (%)	*Dmax (m)*
max	0.22	0.03
average	0.11	0.01

Table 2.3 Comparison between the results of the analysis and the estimations of the equation

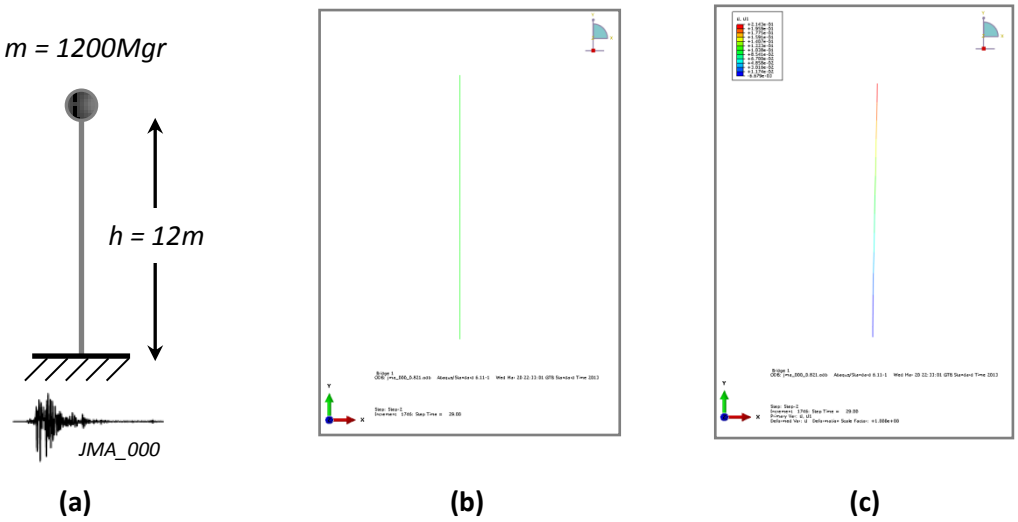

Figure 2.11 (a),(b) Model used in ABAQUS code **(c)** Deformed shape for JMA_000 record

CHAPTER 3

CRITERION OF EQUIVALENCE BETWEEN S-DOF SYSTEMS

3.1 The main concept

The previous analysis proved that it is possible to estimate the structural damage of a bridge pier due to an earthquake considered as S-DOF system, by correlating some specific IM's of the ground motion. Assuming that a single component of the bridge, such as a pier, can be representative of the seismic performance of the whole bridge, it is possible to estimate the structural damage of the whole system.

Due to the high number of bridges of a metropolitan motorway, it is necessary to categorize them and analyze some of them as representative of the others. In the same vein if a single bridge pier can be considered as representative of the overall fragility, arises the need to develop a criterion of equivalence between two piers of different bridges.

This task aims to compare the system that was examined previously with other S-DOF systems of different geometry, stiffness and mass, obtain the results and examine the way that each of these parameters affects. The main purpose is the development of equivalent S-DOF systems if possible in order to extend the results of the previous analysis.

The following investigation is based on the logical assumption that two S-DOF systems with the same Natural Period (T), Design Spectral Acceleration (SA) and Ductility in terms of curvature ($\mu_{capacity}$), are expected to have close enough seismic performance.

3.2 Impact of Mass

3.2.1 Model used

In S-DOF systems with a fixed base the natural period depends only on the mass at the top and the stiffness of the pier. The latter in the case of circular pier depends on the height of the pier and the diameter of the section of the pier. In this case in order to examine the impact of mass, an extreme

case is selected. The mass of the system is doubled while the height of the pier and the natural period remain the same. This leads to an increase of the diameter of the section from 3m to 3.57m.

The selected system has the following characteristics:

- ✓ m = 2400 Mgr
- ✓ h = 12 m
- ✓ D = 3.57 m
- ✓ T=0.48 s

The system used is presented on Figure 3.1(b).

- **Pier Section Reinforcement**

The reinforcement of the pier base circular section (D = 3.57 m) was calculated according to the provisions of the Greek Code for Reinforced Concrete (ΕΚΩΣ, 2000) for columns with large capacity demands. Design spectral acceleration depends only on Natural Period, soil conditions and behavior factor q. So assuming the same soil conditions and behavior factor with the previous case, the design acceleration remains: SA=0.3g. The fact that the design spectral acceleration and the height of the pier remain the same while the mass is doubled leads to double Ultimate Moment as well.

The computed reinforcement of the pier section for concrete C30 and Steel S400 is:

longitudinal 98 Ø41

transverse Ø13/5.

The geometric characteristics and the reinforcement of the section used in the analysis are depicted in Figure 3.2.

- **Section Analysis**

The same constitutive model is calibrated to match the pier response in the macroscopic moment–curvature level. The moment curvature relationship is derived from static concrete section analysis using the USC_RC software, which uses the Mander model (Mander et al. 1988) to simulate the stress–strain relationship of confined concrete. The moment-curvature curve derived from section

analysis is compared with the calibrated one and is presented on Figure 3.3. For a better overview and comparison of the two systems, the normalized moment-curvature curve and Force-Displacement curve of both systems is presented on Figure 3.4.

3.2.2 Dynamic analysis

- **Results of the Analysis - Comparison of the two Systems**

The selected system was tested under nonlinear dynamic time history analysis using the same 29 real earthquake records. The seismic performance of the system is compared with the relevant of the system with half a mass. This task aims to examine the impact of mass on two systems with the same natural period, design spectral acceleration and ductility in terms of curvature.

The results can be divided into two parts. The first one includes the 26 of 29 records in which the ductility demanded did not exceed the ductility capacity of the system. In these records the average deviation of the two systems in terms of $\frac{\mu_{demand}}{\mu_{capacity}}$ is 4% while the maximum is 11% and so it can be deduced in general terms that the two systems are equivalent. In the other 3 records both systems exceed their ductility capacity and the deviations observed are higher than before but in this case they are less important due to the fact that the damage-state of both systems will be Severe Damage or Collapse. Graphs of the performance of the two systems in terms of: (i) max drift (ii) residual drift and (iii)$\frac{\mu_{demand}}{\mu_{capacity}}$, are presented on Figure 3.5 while the relevant deviations are collected on Table 3.1.

- **Interpretation of deviations observed**

In an attempt to adopt natural period, design spectral acceleration and ductility as a criterion of equivalence of S-DOF systems, arises the need to explain the deviations observed even if they do not appear to be prohibitive for our purpose.

For two of the cases that the greater deviations were observed, (takatori_000 record and takatori_090 record) the factors that explain the deviations between the two systems were investigated. The deviations of the two systems, in these two records, in terms of drift time history

are presented on Figures 3.6(a), 3.7(a). At first in an attempt to give an explanation both systems were tested under these specific time histories but the analysis did not take into account the P-δ effects. The impact of P-δ effects in a case of a ground motion that exceeds the ductility capacity of the system seems to be an explanation. The new drift time histories are presented on Figures 3.6(b), 3.7(b). As a first review the two systems now have a much closer performance but still seem to be affected by another factor.

The second attempt to explain the deviations was to test both systems under these two records but the analysis does not take into account the mass of the pier itself. The calculation of the natural period of both systems took into account only the mass at the top of the pier and ignored the mass of the pier itself. As a result these two systems do not have precisely the same natural period and also the axial force at the base of each pier is not exactly the same. The results of the analysis are presented on Figures 3.6(c), 3.7(c).

The final step was to ignore both P-δ effects and the mass of the pier for the two systems. The results of this approach are presented on Figures 3.6(d), 3.7(d) and show that the seismic performance of the two S-DOF systems is almost the same for these two strong records that exceeded system's capacity.

So the impact of mass lies mainly in the different P-δ effects observed on the two systems. Also it can be deduced that the different mass of the pier (due to the increase of the diameter of the section) between two S-DOF systems leads the natural period and the axial load at the base of the pier to be slightly different. These two factors explain the deviations to the seismic performance of these systems. However these deviations are of no particular significance for the purpose of assessment of structural damage when a seismic event occurs and as a result they can be ignored.

3.2.3 Effectiveness of the equation

From the previous analysis it can be deduced that two S-DOF systems with the same natural period, design spectral acceleration, ductility capacity and height have equivalent seismic performance even if the mass at the top of the pier is doubled. In order to extend the results of the previous analysis and examine the effectiveness of the equation, the obtained results of the system with the double mass are compared with the relevant results of the equation. The deviations are presented

on Table 3.2. Figure 3.8 shows graphically the effectiveness of the equation on the systems examined.

3.3 Impact of Height

3.3.1 Model used

Since mass was proven not to have a significant impact on the seismic performance of two "equivalent" systems, the next step was to investigate the impact of height. In this direction the third S-DOF system was selected to have half the height of the previous two while the mass and the natural period remained the same, which of course is an extreme case. This assumption leads to a decrease of the diameter of the section from 3m to 1.78m.

The selected system has the following characteristics:

- ✓ m = 1200 Mgr
- ✓ h = 6 m
- ✓ D = 1.78 m
- ✓ T=0.48 s

The system used is presented on Figure 3.1(c).

- **Pier Section Reinforcement**

The reinforcement of the pier base circular section (D = 1.78 m) couldn't be calculated according to the provisions of the Greek Code for Reinforced Concrete (ΕΚΩΣ, 2000) for columns with large capacity demands. This is due to the fact that the axial load exceeds the permitted value by the code for the cross-sectional area.

Therefore the chosen model is an ideal case which has the same natural period, design spectral acceleration and ductility capacity as before. The moment-curvature curve was calibrated to match the pier response using the same constitutive model. For a better overview and comparison of this

system with the two systems analyzed before, the normalized moment-curvature curve and force-displacement curve of the three systems, derived from pushover analysis, is presented on Figure 3.9.

- **Impact of meshing – Sensitivity analysis**

The two systems compared in the previous section had the same height. Therefore there was no need to take into account the impact of meshing. In this case, that the system's height is half the height of the previous two, there was a need to investigate whether or not meshing affects the results of the analysis. So for the first system examined, four series of pushover analyses were performed. On these four cases the length of the pier's beam element was 0.125m, 0.25m, 0.5m and 1m in order to examine the effect of the length and the number of the elements. The results are presented on Figure 3.10. It can be deduced that the number and the length of the elements of the pier doesn't affect the results of the analysis in the area of our interest. The main impact of meshing lies in the length of the plastic hinge at the base of the pier and as a result in the final curvature of the system. However up to the point that the ductility capacity of the system exceeds, meshing doesn't affect at all.

3.3.2 Dynamic analysis

- **Results of the Analysis - Comparison of the three Systems**

The selected system was tested under nonlinear dynamic time history analysis using the same 29 real earthquake records. The seismic performance of the system is compared to both the previous systems. This task aims to examine the impact of height on S-DOF systems with the same natural period, design spectral acceleration and ductility capacity in terms of curvature.

In comparison with the first system (m=1200Mgr, h=12m, d=3m) the results can be divided into two parts. The first one includes the 24 of 29 records on which the ductility demanded did not exceed the ductility capacity of the system in both systems. In these records the average deviation in terms of $\frac{\mu_{demand}}{\mu_{capacity}}$ of the two systems was 4% while the maximum was 15% and so it can be deduced

in general terms that the two systems are equivalent. On the other 5 records both systems almost exceeded their ductility capacity and the deviations observed were higher than before but in this case they are less important due to the fact that the damage-state of both systems will be Severe Damage or Collapse. Graphs of the seismic performance of the two systems in terms of:

(i)max drift, (ii)residual drift and (iii)$\frac{\mu_{demand}}{\mu_{capacity}}$, are presented on Figure 3.11 while the relevant deviations are collected on Table 3.3.

In comparison with the second system (m=2400Mgr, h=12m, d=3.57m) the results can be divided into two parts as well. The first one includes the 22 of 29 records on which the ductility demanded did not exceed the capacity of the system in both systems. In these records the average deviation in terms of $\frac{\mu_{demand}}{\mu_{capacity}}$ of the two systems was 2% while the maximum is 19% and so it can be deduced in general terms that the two systems are equivalent. On the other 7 records both systems almost exceed their ductility capacity and the deviations observed were higher than before but in this case they are less important due to the fact that the damage-state of both systems will be Severe Damage or Collapse. Graphs of the seismic performance of the two systems in terms of: (i)max drift, (ii)residual drift and (iii)$\frac{\mu_{demand}}{\mu_{capacity}}$ are presented on Figure 3.12 while the relevant deviations are collected on Table 3.4.

- **Interpretation of deviations observed**

Exactly as the previous case, arises the need to explain the deviations observed even if they do not appear to be prohibitive for our purpose. For the case with the greater deviations (takatori_000 record) the factors that resulted in them were investigated.

Following the same approach as before, P-δ effects were ignored for the first system and the one with the half height. The results of this approach are presented on Figure 3.13 and show that the seismic performance of the two S-DOF systems is almost the same for this strong record that exceeded system's capacity.

So the impact of height lies mainly in the different P-δ effects observed in the two systems. Also it can be deduced that the different mass of the pier (due to the decrease of the diameter of the section) between two S-DOF systems leads the natural period and the axial load at the base of the

pier to be slightly different. In this case the impact of axial load is even more important than before due to the decrease of the diameter of the section. These two factors explain the deviations to the seismic performance of these systems. However these deviations are of no particular significance for the purpose of assessment of structural damage and as a result these three systems can be considered as equivalent.

It is important to be mentioned that equivalent behavior doesn't mean same destructiveness. For example same drift for these piers means half drift ratio in one case. However it seems possible to estimate a specific damage index for both cases and extrude destructiveness separately.

3.3.3 Effectiveness of the equation

Such as before the obtained results of the system with the half height are compared with the relevant results of the equation in order to examine the effectiveness of the equation. The deviations between the obtained and the estimated results are presented on Table 3.2 and graphically on Figure 3.8.

3.4 Criterion of equivalence

The aim of all the previous tasks was to compare S-DOF systems with different mass, geometry and stiffness but the same natural period, design spectral acceleration and ductility capacity, in order to examine whether or not these three parameters can constitute a criterion of equivalence. In general terms the seismic performance of these three S-DOF systems was quite the same. The deviations observed do not seem to be of great importance as far as a rapid response system is concerned.

Moreover it is important to keep in mind that the systems examined are extreme and ideal cases. For example to consider double mass or half height to a S-DOF system would probably lead to a change in most of cases of the natural period of the pier, due to the regulations of the code for reinforced concrete (ΕΚΩΣ, 2000). However these systems were selected this way in order to extend this criterion even in extreme cases. So the deviations are expected to be smaller in more realistic cases.

From the previous analysis it can be deduced that two S-DOF systems with the same:

- ✓ Natural Period (T)
- ✓ Design Spectral Acceleration (Sa)
- ✓ Ductility capacity in terms of curvature ($\mu_{capacity}$)

are expected to have almost equivalent seismic performance. In addition if the pier is considered to be a close representation of the overall fragility of the bridge, the above conclusion can be extended to the whole bridge.

At the end of the chapter are presented the three models examined in ABAQUS code and their deformed shape for Rinaldi_228 record (Figure 3.14).

Chapter 3

Figures

$T=0.48s$, $SA=0.3g$, $\mu_{capacity}=16.6$

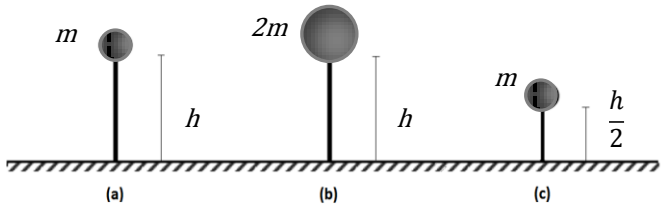

Figure 3.1 Three S-DOF Systems with the same natural period (T) , design spectral acceleration (SA) and ductility in terms of curvature ($\mu_{capacity}$)

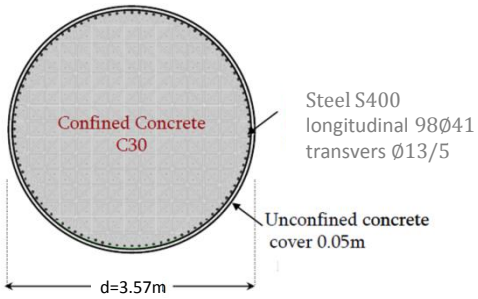

Figure 3.2 The geometric characteristics and the reinforcement of system's (b) section

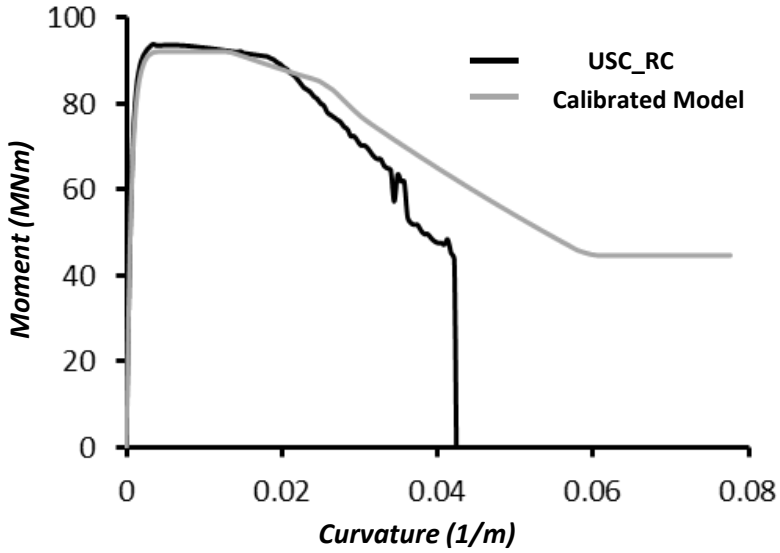

Figure 3.3 Comparison of moment–curvature curves using USC_RC program and calibrated finite element model with kinematic hardening law for *system (b)*

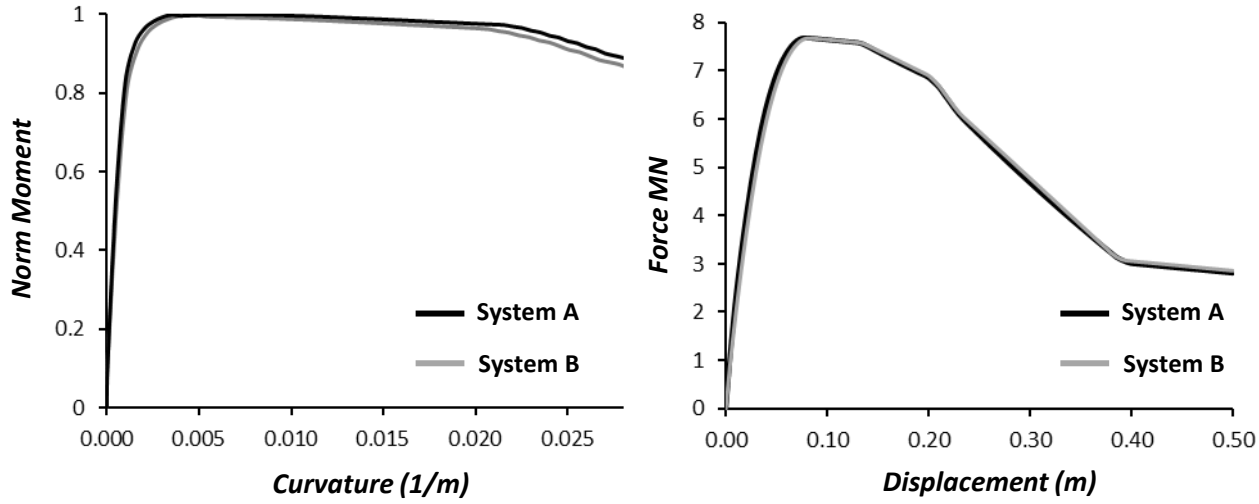

Figure 3.4 (a) , (b) Normalized Moment-Curvature curve and Force-Displacement curve

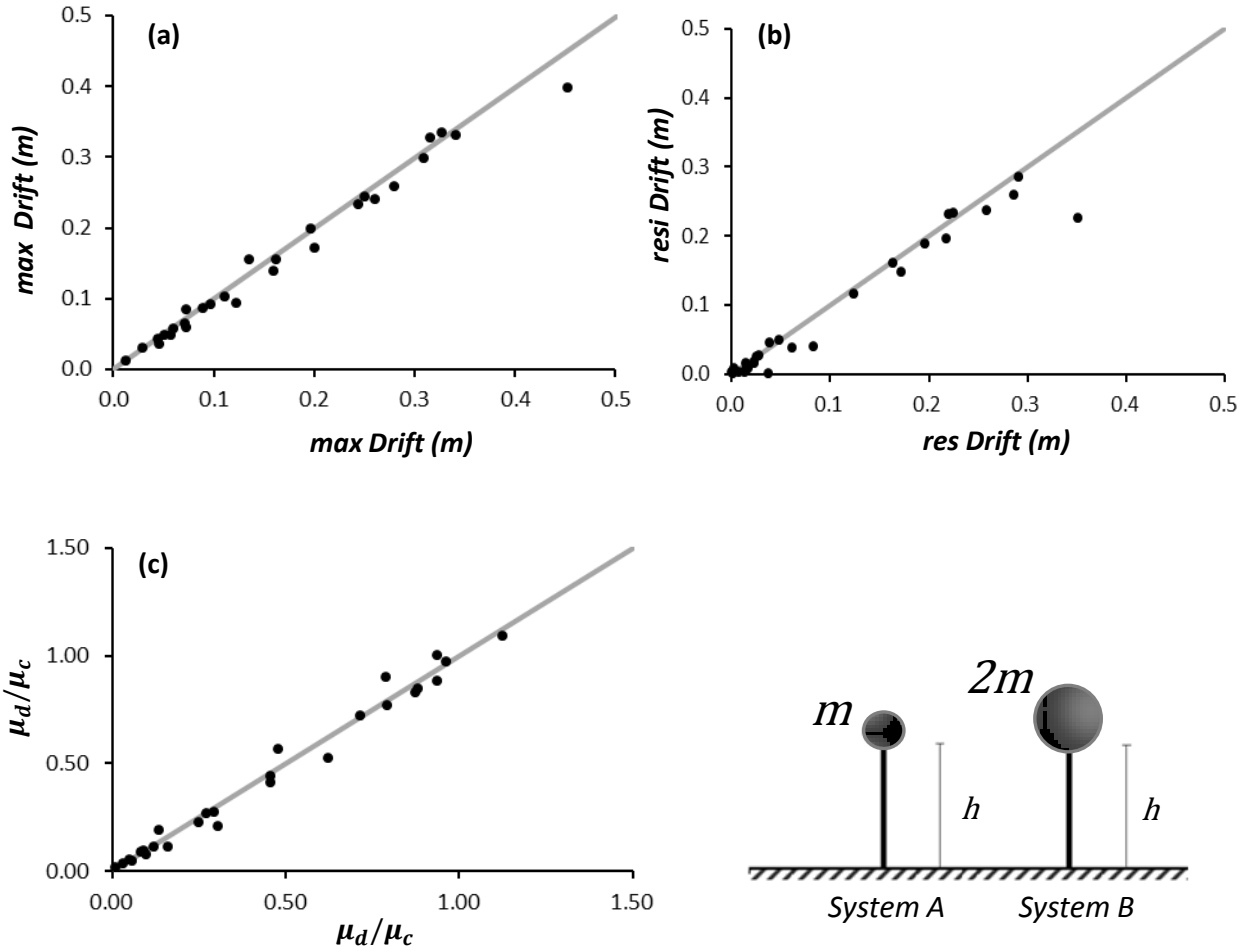

Figure 3.5 (a), (b), (c) Deviations in terms of *max Drift* , *residual Drift* and $\mu_{demand}/\mu_{capacity}$

	Deviations between System A - System B					
	max Drift (m)	*maxDrift ratio (%)*	*Drift res (m)*	*Drift res ratio (%)*	*μ demand*	*μ d / μ c*
TAKATORI_000	0.06	0.52	0.16	1.29	8.35	0.50
JMA_090	0.02	0.18	0.02	0.21	0.70	0.04
MNSA	0.00	0.00	0.00	0.00	0.01	0.00
KALAMATA	0.01	0.06	0.00	0.02	0.28	0.02
TCU68NS	0.03	0.26	0.03	0.22	1.74	0.10
RINALDI_228	0.01	0.10	0.03	0.24	0.97	0.06
SYLMAR_360	0.03	0.24	0.05	0.39	1.72	0.10
TAKATORI_090	0.06	0.46	0.13	1.07	5.75	0.34
JMA_000	0.01	0.08	0.01	0.07	1.00	0.06
TAKARAZUKA_090	0.02	0.17	0.01	0.08	0.85	0.05
PYRGOS	0.00	0.00	0.01	0.05	0.02	0.00
AEGIO	0.00	0.02	0.00	0.04	0.01	0.00
LEFKADA_2003	0.01	0.08	0.00	0.02	0.82	0.05
LEFKADA_1973	0.01	0.07	0.01	0.08	0.35	0.02
TCU52EW	0.02	0.15	0.04	0.31	1.34	0.08
TCU52NS	0.02	0.18	0.02	0.19	0.86	0.05
TCU68EW	0.01	0.09	0.01	0.06	0.70	0.04
RINALDI_318	0.01	0.05	0.01	0.09	0.13	0.01
JENSEN_292	0.01	0.06	0.01	0.06	1.79	0.11
JENSEN_022	0.01	0.07	0.01	0.07	0.02	0.00
SYLMAR_090	0.00	0.01	0.01	0.04	0.01	0.00
DUZE_000	0.00	0.02	0.00	0.01	0.47	0.03
YARIMCA_060	0.00	0.03	0.01	0.11	0.07	0.00
YARIMCA_330	0.01	0.12	0.01	0.06	0.87	0.05
SAKARYA	0.01	0.10	0.00	0.01	0.34	0.02
LUCERNE_000	0.00	0.03	0.00	0.01	0.04	0.00
IV#04_140	0.01	0.07	0.00	0.04	0.46	0.03
IV#04_230	0.01	0.09	0.01	0.08	0.44	0.03
DUCE_090	0.01	0.09	0.03	0.22	0.48	0.03

	max Drift (m)	*maxDrift ratio(m)*	*Drift res(m)*	*Drift res ratio(m)*	*μ demand*	*μ d / μ c*
max	0.06	0.52	0.16	1.29	8.35	0.50
average	0.01	0.12	0.02	0.18	1.06	0.06
max (μd/μc<1)	0.03	0.26	0.05	0.39	1.79	0.11
average (μd/μc<1)	0.01	0.09	0.01	0.11	0.61	0.04

Table 3.1 Deviations between System A and System B

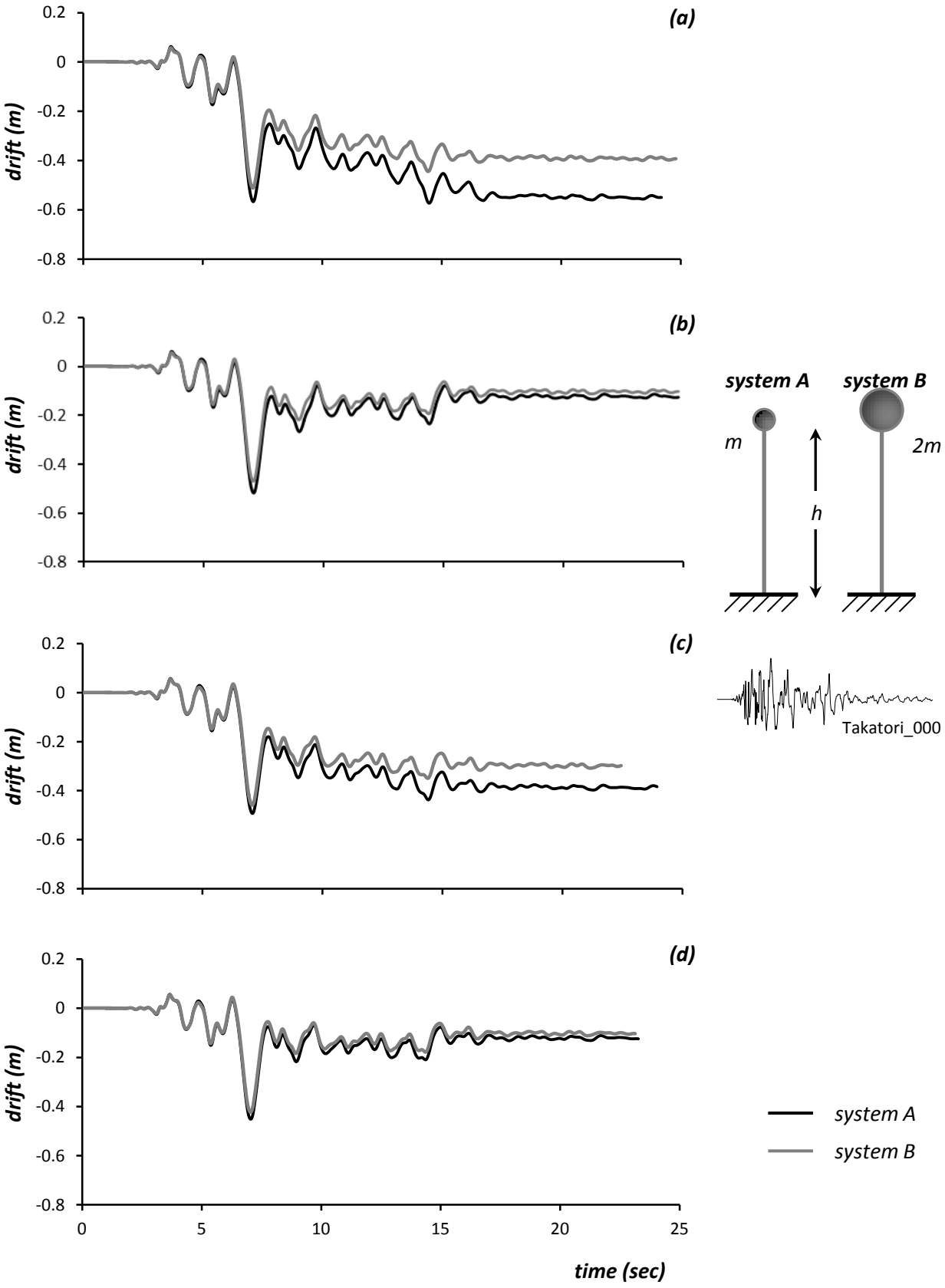

Figure 3.6 Comparison of system A and B in terms of drift time history **(a)** accounting for the P – δ effects and gravity, **(b)** ignoring P-δ effects, **(c)** ignoring pier's density and **(d)** ignoring both P-δ effects and pier's density when the two systems are subjected to the Takatori_000 record

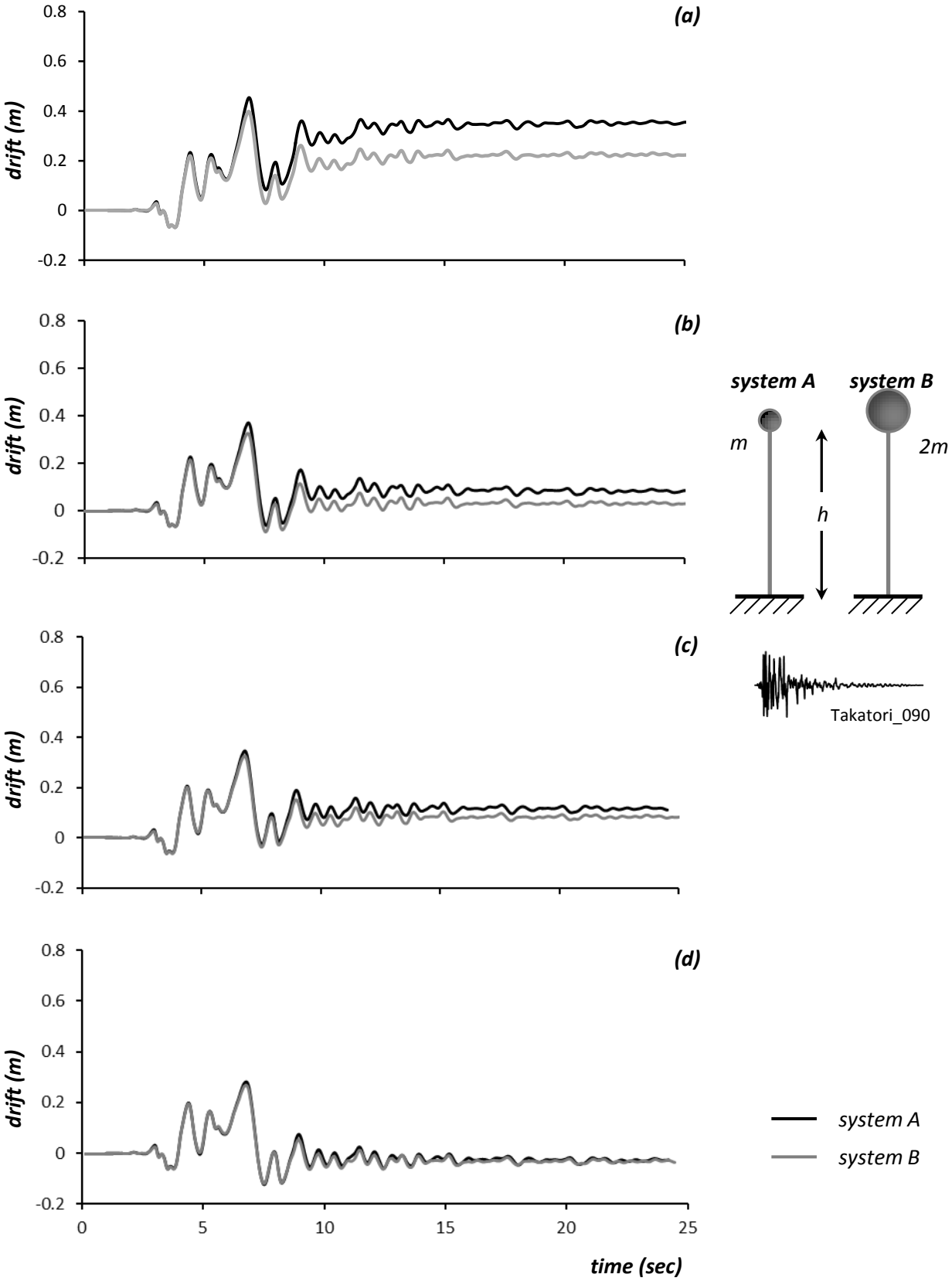

Figure 3.7 Comparison of system A and B in terms of drift time history **(a)** accounting for the P – δ effects and gravity, **(b)** ignoring P-δ effects, **(c)** ignoring pier's density and **(d)** ignoring both P-δ effects and pier's density when the two systems are subjected to the Takatori_090 record

	DEVIATIONS BETWEEN OBSERVED AND PREDICTED DRIFT			
	Drift maximum deviation (m)	*Drift ratio maximum deviation (%)*	*Drift average deviation (m)*	*Drift ratio average deviation (%)*
System A	0.12	0.98	0.04	0.32
System B	0.10	0.81	0.04	0.33
System C	0.18	3.00	0.04	0.34

Table 3.2 Deviations between the observed results of the analysis and the predicted ones of the proposed equation

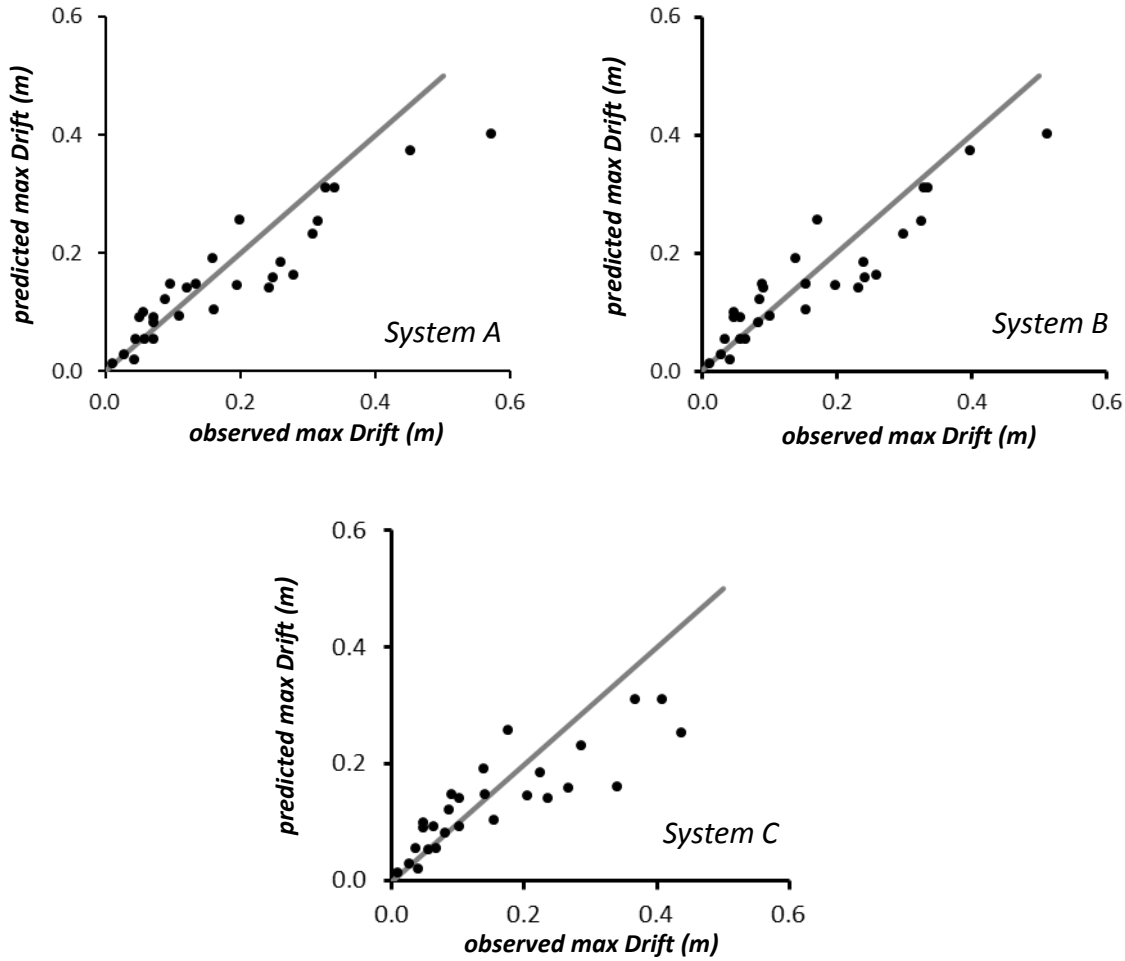

Figure 3.8 Deviations between the observed results of the analysis and the predicted ones of the proposed equation

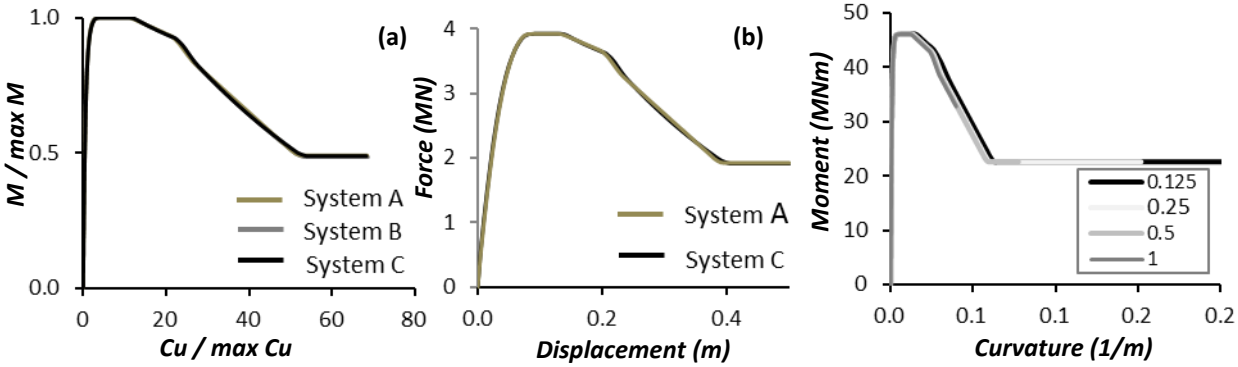

Figure 3.9 (a) Normalized Moment-Curvature and **(b)** Force-Displacement curve

Figure 3.10 Sensitivity analysis-4 different lengths of elements

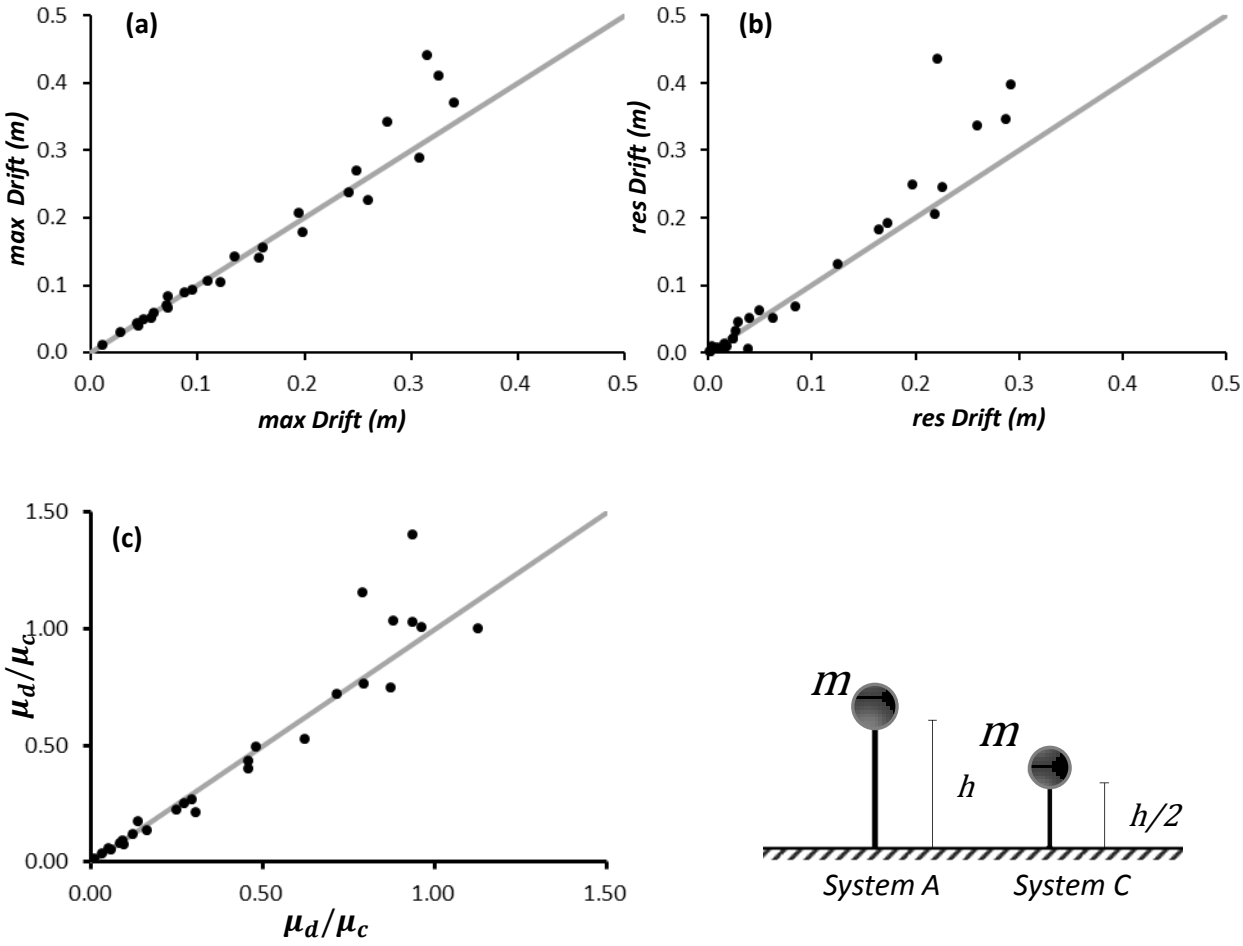

Figure 3.11 (a), (b), (c) Deviations in terms of *max Drift* , *residual Drift* and $\mu_{demand}/\mu_{capacity}$

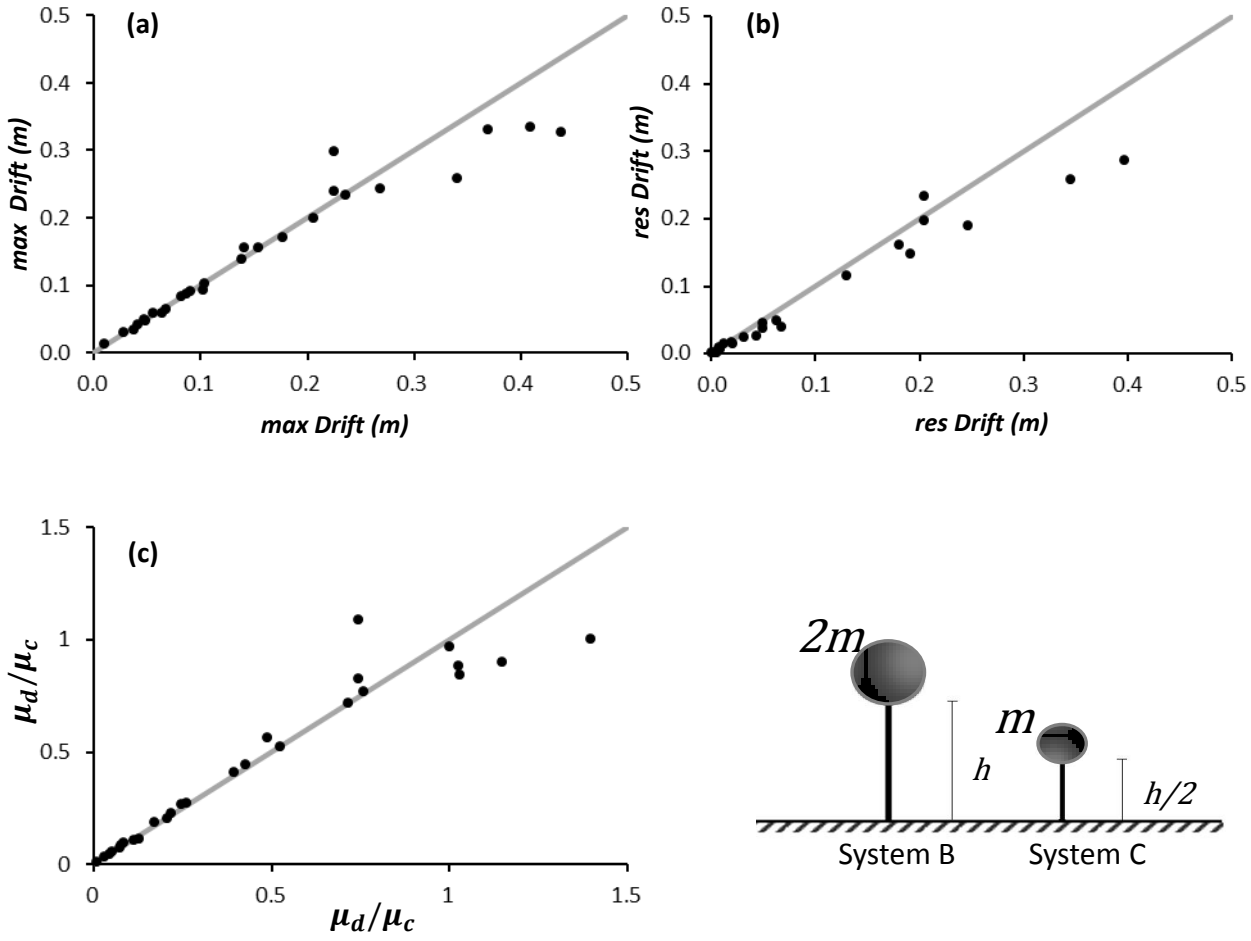

Figure 3.12 (a), (b), (c) Deviations in terms of *max Drift* , *residual Drift* and $\mu_{demand}/\mu_{capacity}$

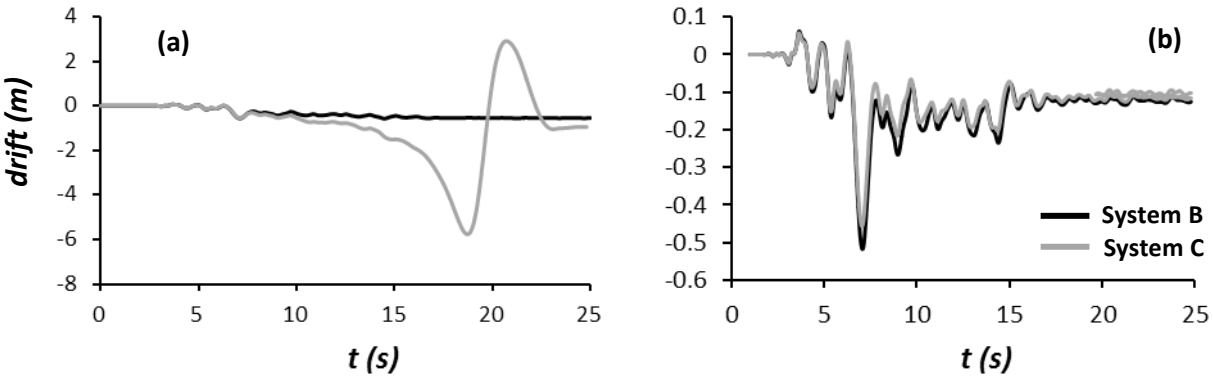

Figure 3.13 Drift time history of both systems on takatori_000 record **(a)** with *p-δ effects and* ***(b)*** without *p-δ effects*

	Deviations Betwenen System A - System C					
	max Drift (m)	***maxDrift ratio (%)***	***Drift res (m)***	***Drift res ratio (%)***	***μ demand***	***μ d / μ c***
TAKATORI_000	5.19	43.28	0.40	3.37	1160.23	69.06
JMA_090	0.06	0.52	0.08	0.63	2.44	0.15
MNSA	0.00	0.01	0.00	0.00	0.02	0.00
KALAMATA	0.00	0.02	0.00	0.03	0.18	0.01
TCU68NS	0.02	0.16	0.01	0.11	1.67	0.10
RINALDI_228	0.03	0.24	0.06	0.49	1.48	0.09
SYLMAR_360	0.02	0.18	0.02	0.14	1.65	0.10
TAKATORI_090	0.28	2.35	0.38	3.18	38.89	2.31
JMA_000	0.12	1.03	0.22	1.79	7.70	0.46
TAKARAZUKA_090	0.02	0.16	0.00	0.03	1.05	0.06
PYRGOS	0.00	0.00	0.00	0.02	0.01	0.00
AEGIO	0.00	0.02	0.00	0.03	0.09	0.01
LEFKADA_2003	0.01	0.08	0.01	0.12	0.57	0.03
LEFKADA_1973	0.01	0.06	0.01	0.05	0.53	0.03
TCU52EW	0.01	0.05	0.03	0.28	0.12	0.01
TCU52NS	0.04	0.29	0.01	0.12	2.18	0.13
TCU68EW	0.02	0.17	0.02	0.16	2.20	0.13
RINALDI_318	0.00	0.04	0.01	0.08	0.39	0.02
JENSEN_292	0.08	0.69	0.10	0.87	6.02	0.36
JENSEN_022	0.02	0.16	0.05	0.42	0.62	0.04
SYLMAR_090	0.01	0.08	0.02	0.13	0.01	0.00
DUZE_000	0.00	0.01	0.01	0.11	0.54	0.03
YARIMCA_060	0.00	0.02	0.01	0.08	0.14	0.01
YARIMCA_330	0.01	0.07	0.00	0.04	0.56	0.03
SAKARYA	0.01	0.06	0.00	0.01	0.25	0.01
LUCERNE_000	0.00	0.02	0.00	0.03	0.04	0.00
IV#04_140	0.01	0.05	0.01	0.08	0.56	0.03
IV#04_230	0.01	0.07	0.01	0.06	0.44	0.03
DUCE_090	0.01	0.05	0.02	0.16	0.59	0.04

μd/μc < 1	***max Drift (m)***	***maxDrift ratio (%)***	***Drift res (m)***	***Drift res ratio (%)***	***μ demand***	***μ d / μ c***
max	0.12	1.03	0.22	1.79	7.70	0.46
average	0.02	0.16	0.03	0.23	1.15	0.07

Table 3.3 Deviations between System A and System C

	Deviations Betwenen System B - System C					
	max Drift (m)	***maxDrift ratio (%)***	***Drift res (m)***	***Drift res ratio (%)***	***μ demand***	***μ d / μ c***
TAKATORI_000	5.26	43.80	0.56	4.66	1168.58	69.56
JMA_090	0.08	0.69	0.10	0.84	3.13	0.19
MNSA	0.00	0.01	0.00	0.01	0.02	0.00
KALAMATA	0.00	0.04	0.01	0.06	0.11	0.01
TCU68NS	0.01	0.10	0.01	0.11	0.07	0.00
RINALDI_228	0.04	0.34	0.09	0.73	2.46	0.15
SYLMAR_360	0.01	0.06	0.03	0.24	0.07	0.00
TAKATORI_090	0.34	2.81	0.51	4.25	44.64	2.66
JMA_000	0.11	0.94	0.21	1.71	6.70	0.40
TAKARAZUKA_090	0.00	0.01	0.01	0.05	0.19	0.01
PYRGOS	0.00	0.00	0.00	0.03	0.03	0.00
AEGIO	0.00	0.00	0.00	0.00	0.09	0.01
LEFKADA_2003	0.00	0.00	0.02	0.14	0.25	0.01
LEFKADA_1973	0.00	0.01	0.02	0.13	0.18	0.01
TCU52EW	0.01	0.10	0.00	0.03	1.22	0.07
TCU52NS	0.01	0.11	0.01	0.07	1.32	0.08
TCU68EW	0.07	0.60	0.03	0.24	5.74	0.34
RINALDI_318	0.00	0.02	0.00	0.02	0.26	0.02
JENSEN_292	0.08	0.63	0.11	0.93	4.23	0.25
JENSEN_022	0.03	0.22	0.06	0.49	0.61	0.04
SYLMAR_090	0.01	0.07	0.02	0.17	0.00	0.00
DUZE_000	0.00	0.01	0.01	0.12	0.08	0.00
YARIMCA_060	0.00	0.01	0.00	0.03	0.08	0.00
YARIMCA_330	0.01	0.06	0.00	0.03	0.32	0.02
SAKARYA	0.00	0.04	0.00	0.00	0.09	0.01
LUCERNE_000	0.00	0.00	0.00	0.02	0.00	0.00
IV#04_140	0.00	0.02	0.00	0.04	0.10	0.01
IV#04_230	0.00	0.02	0.00	0.02	0.00	0.00
DUCE_090	0.00	0.04	0.04	0.37	0.11	0.01

μd/μc < 1	***max Drift (m)***	***maxDrift ratio (%)***	***Drift res (m)***	***Drift res ratio (%)***	***μ demand***	***μ d / μ c***
max	0.11	0.94	0.21	1.71	6.70	0.40
average	0.02	0.14	0.03	0.25	0.83	0.05

Table 3.4 Deviations between System B and System C

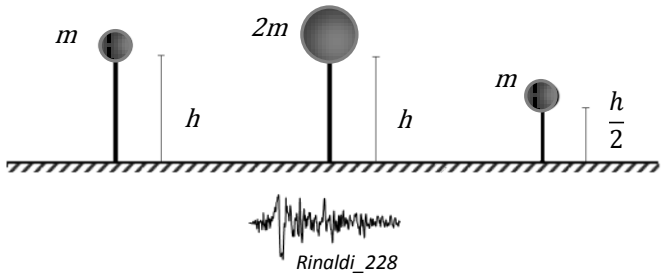

(a)

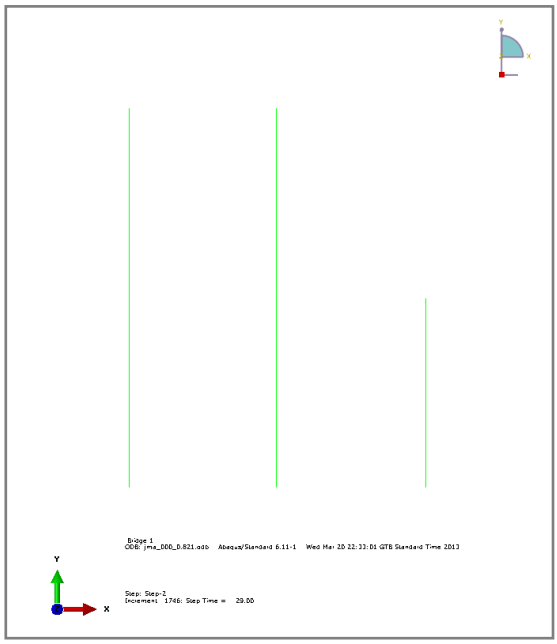

(b)

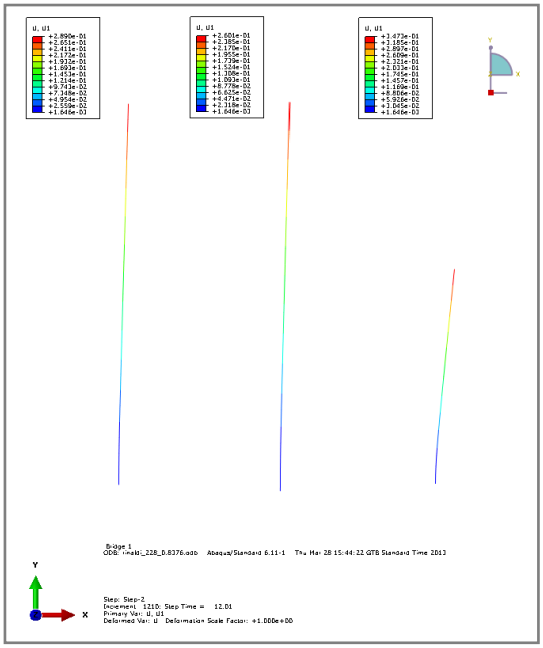

(c)

Figure 3.14 (a),(b) 3 Models compared in ABAQUS code **(c)** Deformed shape for Rinaldi_228 record

CHAPTER 4

COMPARISON BETWEEN THREE REAL PIERS

VALIDATION OF THE CRITERION

4.1 Validation of the proposed criterion

The results of the previous analysis proved that three ideal S-DOF systems with extremely different geometry and mass at the top, but the same natural period, design spectral acceleration and ductility capacity, have almost the same seismic performance.

The following step was to compare real piers of bridges of the Greek metropolitan motorway "ATTIKI ODOS" with close natural period, design spectral acceleration and ductility capacity in order to validate the above conclusion. In addition, the impact of the static system had to be examined in order to see whether or not this criterion can be used for any static system.

4.2 1st Pier – Transverse Direction

4.2.1 Model Used

- **Equivalent Oscillator**

The first pier selected was the 1st pier of the bridge: *A01_TE20*, of the Greek metropolitan motorway "ATTIKI ODOS". The impact of the deck corresponds only on the mass at the top of the pier. The stiffness of the deck in both directions is ignored. Both the geometry of the bridge and the section of the deck are presented on Figure 4.2. The pier is examined in the transverse direction and is considered as SDOF system. The final system has the following characteristics:

- ✓ m = 1166 Mgr
- ✓ h = 8.8 m
- ✓ D = 2 m
- ✓ T = 0.636 s

The system used is presented on Figure 4.1(a).

- **Pier Reinforcement**

The reinforcement of the pier base circular section (D = 2 m) was calculated according to the provisions of the Greek Code for Reinforced Concrete (ΕΚΩΣ, 2000) for columns with large capacity demands. For an elastic (fixed-base) vibration period *T* = 0.636 s and soil conditions characterized as "B", the design spectral acceleration is estimated according to the following formula (E.A.K. 2000):

$$\Phi_d(T) = \gamma_i A \frac{n\,\theta\,\beta_o}{q} \left(\frac{T_2}{T}\right)^{2/3} = 0.13g$$

assuming the following parameters:

- A = 0.16g
- q = 3
- γ_1 = 1.00
- β_o = 2.5
- θ = 1.00
- ζ=5%, n= 1

The computed reinforcement [DOMI OE-STATHOPOULOS-FARROS & all.] of the pier section for concrete C25 and Steel S500 is:
longitudinal 64Ø25
transverse Ø13/8.6

The section of the pier is presented on Figure 4.3.

- **Section Analysis**

The moment curvature relationship is derived as before from static concrete section analysis using the USC_RC software. The same constitutive model that was used in all the previous cases is

calibrated to match the pier response in the macroscopic moment–curvature level. The moment-curvature curve derived from section analysis is compared with the calibrated one and is presented on Figure 4.4.

From this moment-curvature curve it can be deduced that the specific designer has overdesigned the pier. As a result the acceleration on which yielding initiates is larger than the design spectral acceleration and is equal to ***0.18g*****.** This fact may leads to a modification of the proposed criterion. It is more appropriate to use the acceleration on which yielding initiates for each pier than its design spectral acceleration due to the fact that it is very common the designers to overdesign the pier. Ductility capacity of the system in terms of curvature was calculated $\boldsymbol{\mu_{capacity} = 11.8}$.

The computation of the acceleration on which yielding initiates is based on section analysis of the pier which implies the knowledge of the longitudinal and transverse reinforcement of the pier. So for a long list of bridges the computational effort may be prohibitive. On the other hand the hypothesis that design spectral acceleration is close enough to the actual acceleration that yielding initiates is not the most accurate approach.

On this task the actual yielding acceleration is used in order to compare the piers examined. However the hypothesis that design spectral acceleration is close to the actual yielding acceleration is adopted, due to the high computational effort of the latter.

4.2.2 Dynamic Analysis

The selected pier was tested under nonlinear dynamic time history analysis using the same 29 real earthquake records. The seismic performance of the system is expressed in terms of maximum drift, residual drift and $\frac{\mu_{demand}}{\mu_{capacity}}$. The results are presented on Table 4.1.

4.3 2nd Pier – Transverse Direction

4.3.1 Model Used

- **Equivalent Oscillator**

The second pier was selected in order to have approximately the same natural period with the first one. Eventually the 1st pier of the bridge: *A07_TE11*, of the Greek metropolitan motorway "ATTIKI ODOS" was selected. The impact of the deck corresponds only on the mass at the top of the pier. As before the stiffness of the deck in both directions is ignored. Both the geometry of the bridge and the section of the deck are presented on Figure 4.5. The pier is examined in the transverse direction and is considered as a SDOF system. The final system has the following characteristics:

- ✓ m = 356 Mgr
- ✓ h = 6.5 m
- ✓ D = 1.2 m
- ✓ T = 0.643 s

The system used is presented on Figure 4.1(b).

- **Pier Reinforcement**

The reinforcement of the pier base circular section (D = 1.2 m) was calculated according to the provisions of the Greek Code for Reinforced Concrete (ΕΚΩΣ, 2000) for columns with large capacity demands. For acceleration *A* = 0.16 g, considering a (ductility-based) behavior factor *q* = 3 with an elastic (fixed-base) vibration period *T* = 0.643 s and soil conditions characterized as "B" the design spectral acceleration is estimated to be: $\Phi_d = 0.13g$ as in the previous case.

The computed reinforcement [OMETE AE] of the pier section for concrete C35 and Steel S500 is:
longitudinal 40Ø25
transverse Ø13/5.5

The section of the pier is presented on Figure 4.6.

- **Section Analysis**

The moment curvature relationship is derived as before from static concrete section analysis using the USC_RC software. The same constitutive model that was used in all the previous cases is calibrated to match the pier response in the macroscopic moment–curvature level. The moment-curvature curve derived from section analysis is compared with the calibrated one and is presented on Figure 4.7.

Exactly as in the previous case the designer has overdesigned the pier. As a result the actual yielding acceleration is $a_y = 0.21g$ even larger than in the previous case. Ductility capacity in terms of curvature was calculated $\boldsymbol{\mu_{capacity} = 17.1}$ which is almost 45% larger than in the previous case. Even if it is a small sample, a trend to overdesign the piers is observed and also a deviation in the ductility capacity of the piers. Due to the provisions of the Greek Code for Reinforced Concrete (ΕΚΩΣ, 2000) for columns with large capacity demands, $\mu_{capacity}$ is not expected to be less than 11. Also in most cases the ductility capacity is not expected to be larger than 18. So these two piers illustrate the highest deviation expected in terms of ductility.

4.3.2 Dynamic Analysis

The selected pier was tested under nonlinear dynamic time history analysis using the same 29 real earthquake records. The seismic performance of the system is expressed in terms of maximum drift, residual drift *and* $\frac{\mu_{demand}}{\mu_{capacity}}$. The results are presented on Table 4.2.

4.4 Comparison between the two piers

The seismic performance of the two piers was compared and the results in terms of maximum drift, residual drift and $\frac{\mu_{\text{demand}}}{\mu_{\text{capacity}}}$ are presented on Figure 4.8 while the relevant deviations are collected on Table 4.3.

It can be deduced from these results that the two systems have a close enough seismic performance. The first one for each of the ground motions seems to be more vulnerable. This was

expected due to the fact that the first pier's yielding acceleration is less than the relative of the second pier. Moreover the ductility of the first pier is also lower than the ductility of the second. These two factors have the greatest impact on the deviations observed between the two piers. In this case that the yielding acceleration of the second pier is 17% higher than the first one and the ductility of the second pier is 45% higher than the relative of the first one, the average deviation observed in terms of $\frac{\mu_{demand}}{\mu_{capacity}}$ was 22%. However in cases of piers with closer ductility it is expected to have even closer seismic performance.

It is important to be mentioned that in records of low and medium intensity (records that demanded up to 50% of the ductility capacity of the piers) the deviations observed were much lower. More specific the maximum deviation observed in terms of $\frac{\mu_{demand}}{\mu_{capacity}}$ was 19% while the average was 7%.

The previous analysis proved that the two piers examined cannot be considered as equivalent and that the deviations in yielding acceleration and ductility capacity have a significant effect in the seismic performance of the pier. However the deviations observed are not prohibitive for the purposes of a rapid response system in which the destructiveness of a ground motion is described through damage states, even in this case that the ductility of the two piers is quite different.

4.5 Impact of static system

In order to examine the impact of the static system another pier was selected and tested, but in this case in the longitudinal direction. Due to the stiffness of the deck in this direction it is widely accepted to represent the pier not as a SDOF system but as a system in which the rotational degree of freedom at the top of the pier is fixed.

In order to test the effectiveness of the proposed criterion in such a system, a pier with a natural period in the longitudinal direction close to the natural period of the previous cases in the transverse direction was selected.

4.5.1 3rd Pier – Longitudinal Direction

The third pier was selected in order to have approximately the same natural period with the previous two piers but this time in the longitudinal direction. Eventually the 1st pier of the bridge: *A04_TE12*, of the Greek metropolitan motorway "ATTIKI ODOS" was selected. The impact of the deck corresponds both on the mass at the top of the pier and on the fixity on the rotational degree of freedom at the top of the pier. Both the geometry of the bridge and the section of the deck are presented on Figure 4.9. The pier is examined in the longitudinal direction and is represented as a system with fixed rotational degree of freedom at top. The final system has the following characteristics:

- ✓ m = 296.4 Mgr
- ✓ h = 11 m
- ✓ D = 1.2 m
- ✓ T = 0.65 s

The system used is presented on Figure 4.1(c).

- **Pier Reinforcement**

The reinforcement of the pier base circular section (D = 1.2 m) was calculated according to the provisions of the Greek Code for Reinforced Concrete (ΕΚΩΣ, 2000) for columns with large capacity demands. For acceleration *A* = 0.16 g, considering a (ductility-based) behavior factor *q* = 3.5 with an elastic (fixed-base) vibration period *T* = 0.65 s and soil conditions characterized as "B" the design spectral acceleration is estimated to be: $\Phi_d = 0.08g$, lower than the previous cases.

The computed reinforcement [OMETE AE] of the pier section for concrete C35 and Steel S500 is:
longitudinal 28Ø25
transverse Ø13/11.5

The section of the pier is presented on Figure 4.10.

- **Section Analysis**

The moment curvature relationship is derived as before from static concrete section analysis using the USC_RC software. The same constitutive model that was used in all the previous cases is calibrated to match the pier response in the macroscopic moment–curvature level. The moment-curvature curve derived from section analysis is compared with the calibrated one and is presented on Figure 4.11.

As in the previous case the designer has overdesigned the pier. As a result the actual yielding acceleration is $a_y = 0.23g$ which is 28% larger than the first pier and 9% larger than the second pier. Ductility capacity in terms of curvature was calculated $\boldsymbol{\mu_{capacity} = 13.3}$ which is almost 12% larger than the one of the first pier and 34% lower than the one of the third.

The characteristics of the third pier are closer to the second pier in terms of acceleration that yielding initiates. Therefore it was considered more appropriate to compare the seismic performance of these two piers.

4.5.2 Dynamic Analysis

The selected pier was tested under nonlinear dynamic time history analysis using the same 29 real earthquake records. The seismic performance of the system is expressed in terms of maximum drift, residual drift and $\frac{\mu_{demand}}{\mu_{capacity}}$. The results are presented on Table 4.4.

4.5.3 Comparison between the two piers

The seismic performance of the two piers was compared and the results in terms of maximum drift, residual drift and $\frac{\mu_{\mathrm{demand}}}{\mu_{\mathrm{capacity}}}$ are presented on Figure 4.12 while the relevant deviations are collected on Table 4.5.

From the comparison between the two piers examined, it is observed that in this case the seismic performance of these systems is much closer than in the previous case. Due to this fact it can be

deduced that static system has almost no impact in the seismic performance of two systems with approximately the same natural period, yielding acceleration and ductility capacity.

The decrease on the deviations was expected. The fact that the third pier has less ductility capacity than the second is hedged by the acceleration on which yielding initiates that in the case of the third pier is 9% larger than the relative of the second. This seems to be the most appropriate explanation for the similar seismic performance of the two systems.

4.6 Validation of the proposed criterion

In addition to the comparison of three ideal and extremely different (in terms of mass, geometry and stiffness) piers, the comparison of three real cases of bridge piers proved that natural period, yielding acceleration and ductility capacity can be used as a criterion of equivalence between two piers. In addition it was shown that this criterion can be used both in longitudinal and transverse direction.

Furthermore, if a single bridge pier can be considered as representative of the overall fragility of the bridge, this criterion could be the basis for the classification of a portfolio of bridges. In this direction, one of the key objectives of this study is to examine whether or not the impact of the rest components of the bridge to its seismic performance can be ignored. Therefore in the following tasks it will be examined on which level a single pier can be representative of the overall fragility of the bridge.

At the end of the chapter are presented the three piers examined in ABAQUS code and their deformed shape for Yarimca_060 record (Figure 4.13).

Chapter 4

Figures

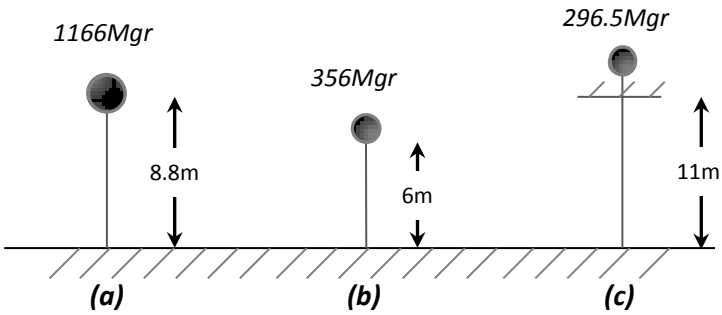

Figure 4.1 Three piers examined **(a)** A01_TE20 **(b)** A07_TE11 **(c)** A04_TE12

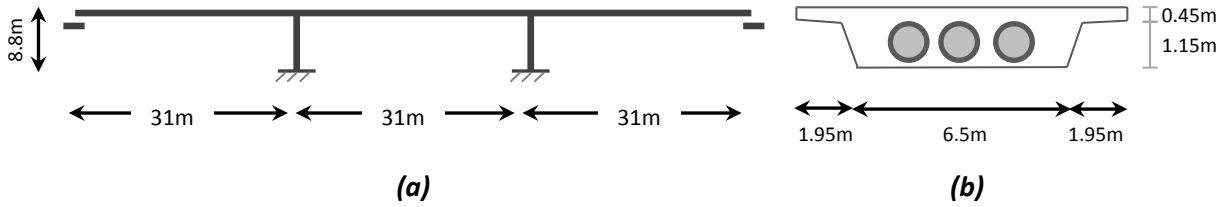

Figure 4.2 (a) geometry of the bridge and **(b)** section of the deck

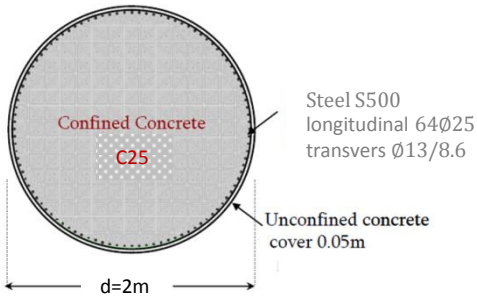

Figure 4.3 Geometric characteristics and reinforcement of pier's section

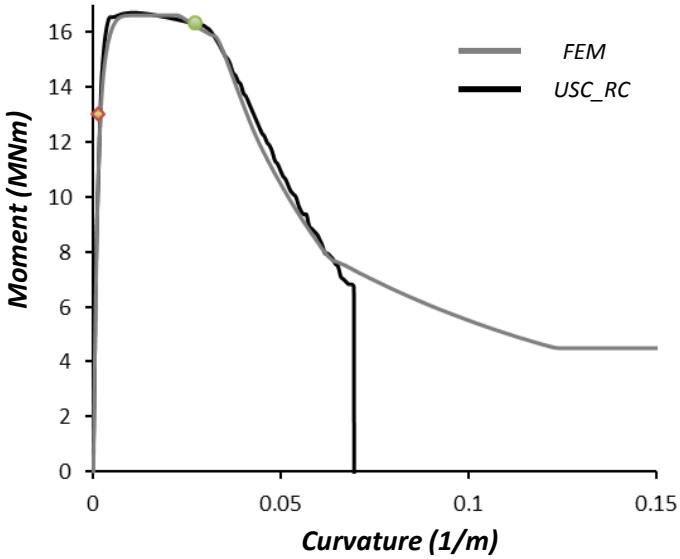

Figure 4.4 Comparison of moment–curvature curves using USC_RC program and calibrated finite element model

	SEISMIC PERFORMANCE					
	max Drift (m)	*maxDrift ratio (%)*	*Drift res (m)*	*Drift res ratio(%)*	*μ demand*	*μ d / μ c*
TAKATORI_000	8.20	93.23	5.16	58.59	2199.26	184.81
JMA_090	2.72	30.95	2.72	30.95	438.17	36.82
MNSA	0.02	0.28	0.00	0.01	0.44	0.04
KALAMATA	0.07	0.81	0.05	0.62	1.92	0.16
TCU68NS	8.19	93.07	3.86	43.88	2077.64	174.59
RINALDI_228	0.36	4.05	0.20	2.29	15.98	1.34
SYLMAR_360	0.31	3.53	0.06	0.73	13.55	1.14
TAKATORI_090	8.20	93.23	5.66	64.36	2245.35	188.69
JMA_000	0.20	2.26	0.05	0.55	8.98	0.75
TAKARAZUKA_090	0.18	2.09	0.05	0.60	9.27	0.78
PYRGOS	0.03	0.29	0.00	0.04	0.46	0.04
AEGIO	0.05	0.62	0.00	0.03	1.24	0.10
LEFKADA_2003	0.10	1.15	0.06	0.74	3.06	0.26
LEFKADA_1973	0.15	1.73	0.13	1.52	6.46	0.54
TCU52EW	8.18	93.01	2.96	33.62	1854.96	155.88
TCU52NS	0.36	4.13	0.01	0.11	19.02	1.60
TCU68EW	8.18	92.95	0.30	3.36	2955.09	248.33
RINALDI_318	0.28	3.16	0.13	1.51	17.75	1.49
JENSEN_292	8.16	92.73	3.05	34.66	2009.33	168.85
JENSEN_022	0.38	4.33	0.38	4.26	42.86	3.60
SYLMAR_090	0.27	3.03	0.23	2.58	16.19	1.36
DUZE_000	0.15	1.67	0.11	1.23	7.04	0.59
YARIMCA_060	0.16	1.77	0.14	1.60	7.92	0.67
YARIMCA_330	0.22	2.44	0.20	2.27	12.47	1.05
SAKARYA	0.07	0.74	0.01	0.12	2.57	0.22
LUCERNE_000	0.05	0.55	0.01	0.06	1.01	0.08
IV#04_140	0.17	1.89	0.16	1.82	8.61	0.72
IV#04_230	0.27	3.05	0.24	2.74	15.43	1.30
DUCE_090	0.17	1.95	0.16	1.82	7.68	0.65

Table 4.1 Seismic performance of pier of bridge A01_TE20

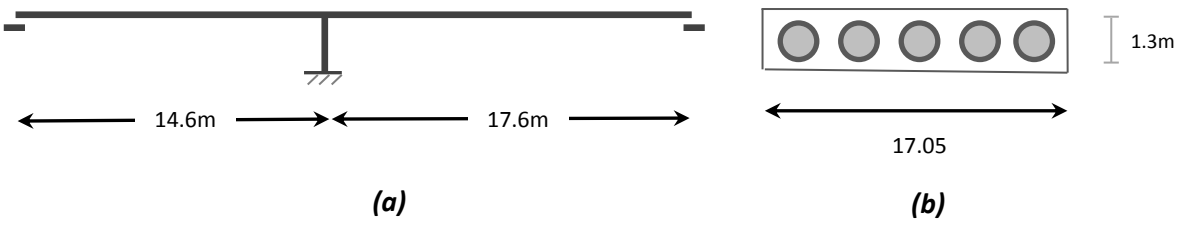

Figure 4.5 (a) geometry of the bridge and **(b)** section of the deck

Figure 4.6 Geometric characteristics and reinforcement of pier's section

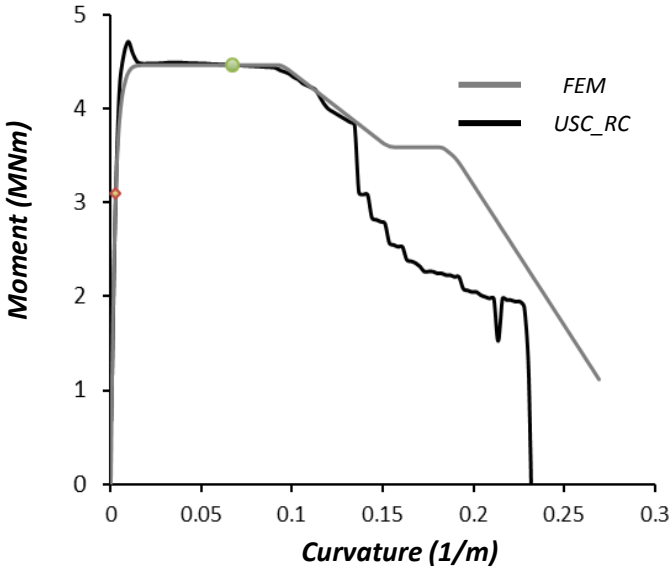

Figure 4.7 Comparison of moment–curvature curves using USC_RC program and calibrated finite element model

	SEISMIC PERFORMANCE					
	max Drift (m)	*maxDrift ratio (%)*	*Drift res (m)*	*Drift res ratio(%)*	*μ demand*	*μ d / μ c*
TAKATORI_000	6.26	104.29	1.89	31.47	2784.30	162.82
JMA_090	0.61	10.12	0.60	9.97	38.44	2.25
MNSA	0.02	0.31	0.00	0.02	0.36	0.02
KALAMATA	0.07	1.09	0.03	0.51	1.75	0.10
TCU68NS	6.27	104.47	4.69	78.15	1733.70	101.39
RINALDI_228	0.31	5.25	0.03	0.49	16.01	0.94
SYLMAR_360	0.30	4.99	0.18	2.98	15.08	0.88
TAKATORI_090	6.25	104.25	4.45	74.09	1661.83	97.18
JMA_000	0.25	4.12	0.19	3.20	12.87	0.75
TAKARAZUKA_090	0.19	3.12	0.10	1.68	10.56	0.62
PYRGOS	0.03	0.45	0.00	0.07	0.54	0.03
AEGIO	0.06	0.96	0.00	0.06	1.47	0.09
LEFKADA_2003	0.09	1.47	0.06	1.04	3.05	0.18
LEFKADA_1973	0.17	2.89	0.16	2.70	8.45	0.49
TCU52EW	0.40	6.75	0.32	5.29	23.79	1.39
TCU52NS	0.31	5.23	0.11	1.84	18.45	1.08
TCU68EW	6.25	104.19	0.81	13.49	3505.06	204.97
RINALDI_318	0.21	3.58	0.01	0.22	13.45	0.79
JENSEN_292	6.26	104.37	3.38	56.37	2341.83	136.95
JENSEN_022	0.33	5.45	0.29	4.85	19.35	1.13
SYLMAR_090	0.24	3.99	0.21	3.50	15.70	0.92
DUZE_000	0.14	2.37	0.12	1.93	8.03	0.47
YARIMCA_060	0.15	2.58	0.13	2.24	8.19	0.48
YARIMCA_330	0.14	2.40	0.09	1.52	8.51	0.50
SAKARYA	0.07	1.10	0.02	0.31	1.83	0.11
LUCERNE_000	0.04	0.72	0.01	0.09	0.96	0.06
IV#04_140	0.15	2.50	0.13	2.17	8.54	0.50
IV#04_230	0.21	3.48	0.16	2.67	13.07	0.76
DUCE_090	0.19	3.09	0.17	2.91	9.13	0.53

Table 4.2 Seismic performance of pier of bridge A07_TE11

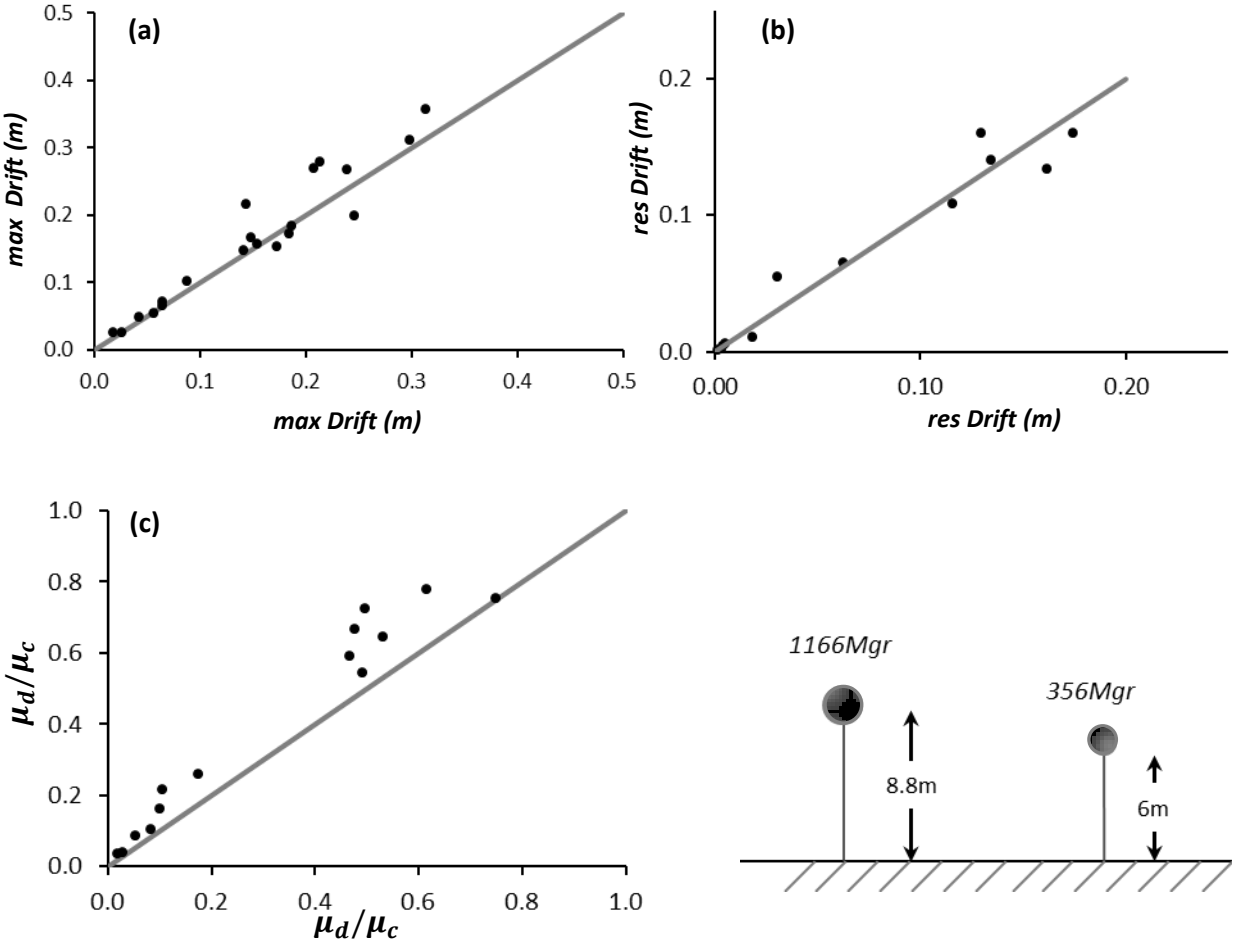

Figure 4.8 (a), (b), (c) Deviations in terms of *max Drift* , *residual Drift* and $\mu_{demand}/\mu_{capacity}$

μd < μc	*max Drift (m)*	*Drift res (m)*	*μ demand*	*μ d / μ c*
max	0.07	0.17	4.30	0.71
average	0.02	0.05	1.20	0.20

Table 4.3 Deviations between the two piers

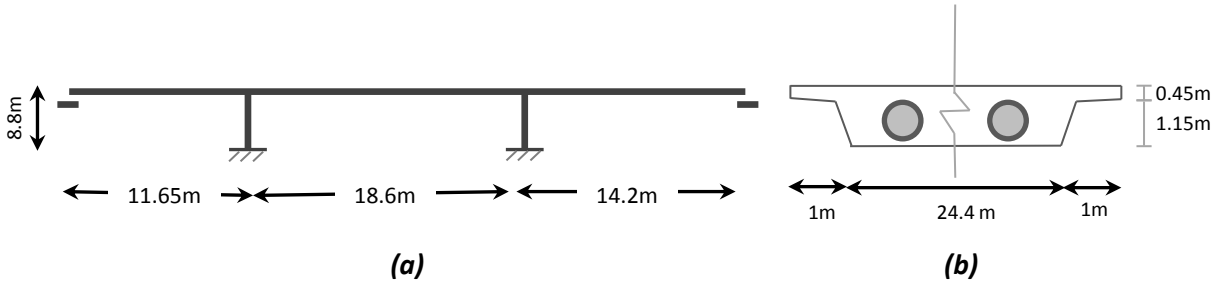

Figure 4.9 (a) geometry of the bridge and **(b)** section of the deck

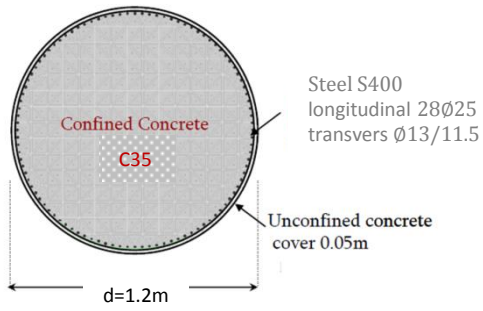

Figure 4.10 Geometric characteristics and reinforcement of pier's section

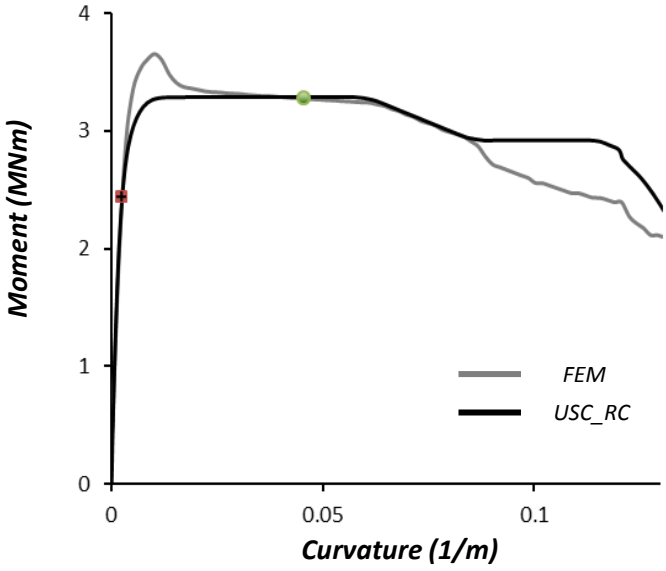

Figure 4.11 Comparison of moment–curvature curves using USC_RC program and calibrated finite element model

	SEISMIC PERFORMANCE					
	max Drift (m)	*maxDrift ratio (%)*	*Drift res (m)*	*Drift res ratio(%)*	*μ demand*	*μ d / μ c*
TAKATORI_000	0.54	4.94	0.51	4.65	20.92	1.57
JMA_090	0.31	2.79	0.28	2.57	13.16	0.99
MNSA	0.02	0.21	0.00	0.00	0.35	0.03
KALAMATA	0.06	0.58	0.04	0.35	1.24	0.09
TCU68NS	0.35	3.19	0.23	2.14	21.54	1.62
RINALDI_228	0.32	2.94	0.09	0.78	13.16	0.99
SYLMAR_360	0.29	2.67	0.12	1.07	11.70	0.88
TAKATORI_090	0.50	4.50	0.48	4.39	18.44	1.39
JMA_000	0.19	1.76	0.00	0.01	7.71	0.58
TAKARAZUKA_090	0.18	1.65	0.04	0.35	8.21	0.62
PYRGOS	0.03	0.24	0.00	0.04	0.40	0.03
AEGIO	0.05	0.50	0.00	0.03	0.99	0.07
LEFKADA_2003	0.09	0.82	0.05	0.48	2.16	0.16
LEFKADA_1973	0.16	1.44	0.13	1.15	6.03	0.45
TCU52EW	0.40	3.63	0.02	0.18	19.24	1.45
TCU52NS	0.32	2.90	0.18	1.61	15.46	1.16
TCU68EW	0.84	7.67	0.84	7.65	57.01	4.29
RINALDI_318	0.24	2.14	0.02	0.17	11.53	0.87
JENSEN_292	0.47	4.24	0.41	3.75	25.27	1.90
JENSEN_022	0.32	2.91	0.27	2.47	16.01	1.20
SYLMAR_090	0.22	1.96	0.17	1.57	11.51	0.87
DUZE_000	0.14	1.32	0.08	0.69	6.21	0.47
YARIMCA_060	0.14	1.30	0.11	1.04	5.87	0.44
YARIMCA_330	0.15	1.35	0.08	0.70	7.12	0.54
SAKARYA	0.07	0.60	0.02	0.15	1.32	0.10
LUCERNE_000	0.05	0.44	0.00	0.02	0.83	0.06
IV#04_140	0.13	1.21	0.10	0.87	5.39	0.41
IV#04_230	0.21	1.94	0.14	1.26	10.53	0.79
DUCE_090	0.17	1.57	0.14	1.26	6.59	0.50

Table 4.4 Seismic performance of pier of bridge A04_TE12

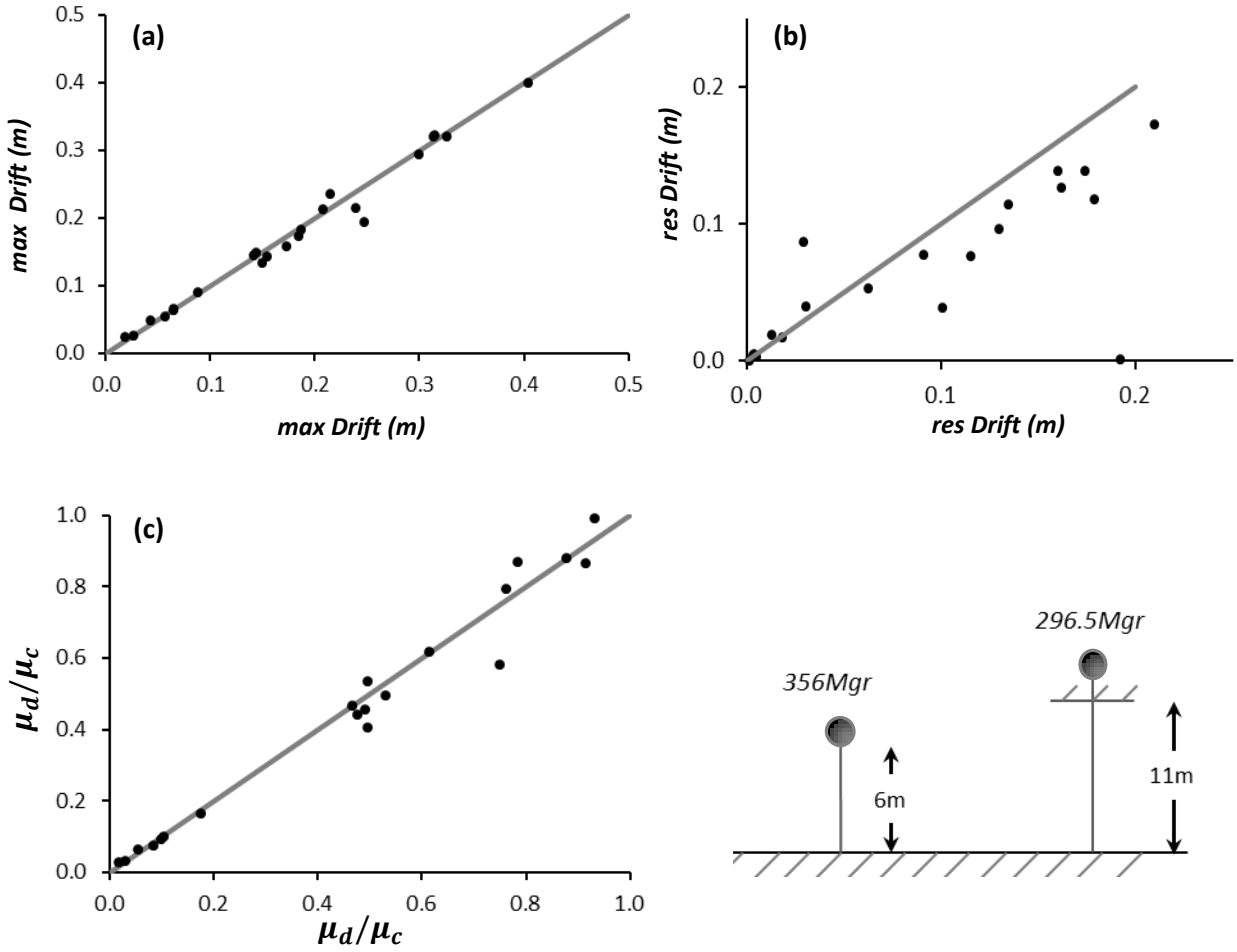

Figure 4.12 (a), (b), (c) Deviations in terms of *max Drift* , *residual Drift* and $\mu_{demand}/\mu_{capacity}$

μd < μc	*max Drift (m)*	*Drift res (m)*	*μ demand*	*μ d / μ c*
max	0.05	0.19	5.16	0.17
average	0.01	0.03	1.94	0.03

Table 4.5 Deviations between the two piers

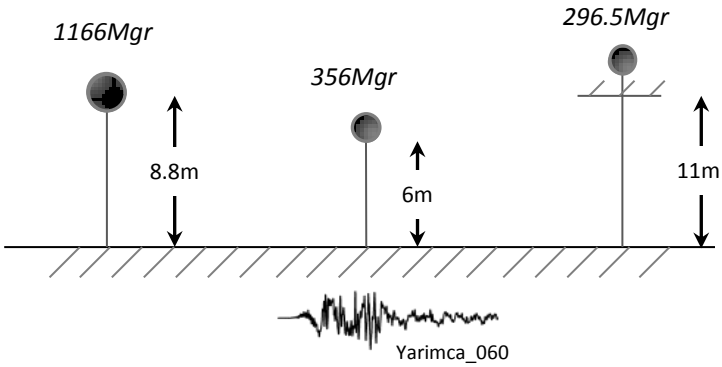

(a)

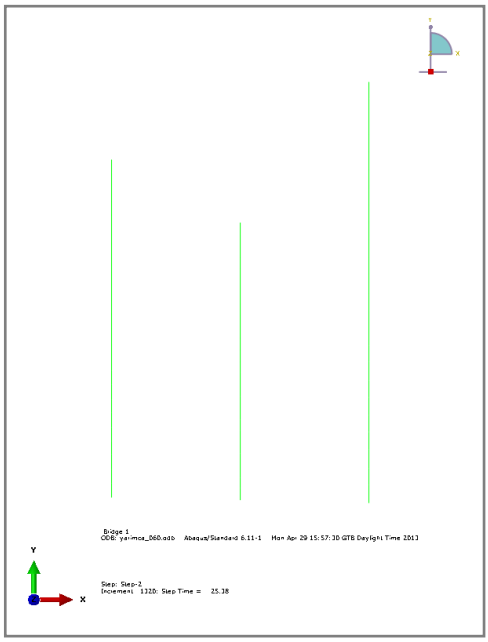

(b)

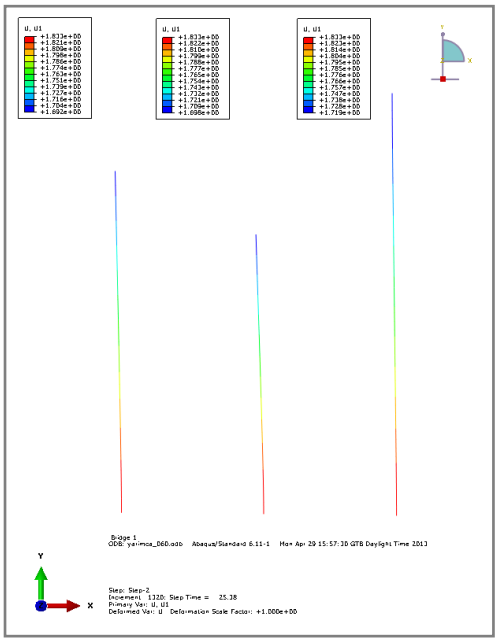

(c)

Figure 4.13 (a),(b) The 3 Models compared in ABAQUS code **(c)** Deformed shape for Yarimca_060 record

CHAPTER 5

IMPACT OF EACH COMPONENT OF A BRIDGE TO THE OVERALL FRAGILITY – DEVELOPMENT OF EQUILAVENT SYSTEMS

5.1 Introduction

One of the key objectives of the current study is to examine whether or not the impact of the various components of a bridge on its seismic performance can be ignored. Therefore it had to be examined on which level a single pier can be representative of the overall fragility of the bridge. For this purpose a specific bridge was chosen in order to compare the seismic performance of the whole bridge with the performance of its pier, both in transverse and longitudinal direction.

5.1.1 Selected bridge

The bridge selected was the A01_TE20 bridge of the Greek metropolitan motorway ''*ATTIKI ODOS*''. The reason that led to this choice was that it is a simple and at the same time common case. Its simplicity lies in the symmetry of the bridge and the circular section of the pier. Also each pier consists of a single column which is monolithically connected to the deck while there are bearings at the abutments.

- **Model Used**

Three-dimensional analytical model was generated using the finite element platform ANSYS. Typical details taken from examined bridge plans were used to generate this model. The superstructure of the bridge is modeled using linear elastic beam elements in a lumped centerline model as shown in Figure 5.1. The piers are modeled using also nonlinear beam elements. The hysteretic behavior of the piers is described through the moment-curvature curve. Truss elements of one meter length are used to model the behavior of the bearings in both the transverse and longitudinal direction while linear springs and dampers are used in the vertical direction. The abutments are ignored in this case and the bearings are considered to be fixed. In order to place the bearings in their exact position, rigid elements were used with selected nodes in the exact place of each bearing. Furthermore in this task the base of the pier is considered fixed and the impact of foundation and soil-structure interaction (SSI) is ignored.

As far as bearings are concerned both in longitudinal and transverse direction truss elements were chosen. The fact that truss elements have both stiffness and damping make them more appropriate solution in comparison to springs and extra dashpots. Moreover by using truss elements it is possible to simulate the nonlinear behavior of the bearings after a certain deformation. Also dashpots are designed with a damping coefficient appropriate for a specific deformation, so truss elements simulate better the behavior of the bearings. Truss elements work with an axial force that depends on their axial strain, so while the value of $\frac{Axial\ deformation}{Length\ of\ truss\ element}$ increases, after a while they do not perform in the expected way. In order to be sure for the results of our analysis it had to be examined whether or not the expected deformations affects the performance of the truss elements used. For this purpose a pushover analysis was performed in order to extrude the Force-Displacement curve of the truss element. The curve is presented on Figure 5.3. It can be deduced that even for the maximum expected displacements (Takatori records) truss elements of one meter length work appropriately.

- **Piers Reinforcement**

The reinforcement of the piers base circular section (D = 2 m) was calculated according to the provisions of the Greek Code for Reinforced Concrete (ΕΚΩΣ, 2000) for columns with large capacity demands. For acceleration *A* = 0.16 g, considering a (ductility-based) behavior factor *q* = 3 with an elastic (fixed-base) vibration period *T* = 0.55s and soil conditions characterized as "B" the design spectral acceleration is estimated to be: $\Phi_d = 0.13g$.
The computed reinforcement of the pier section was taken from the examined bridge plans [DOMI OE-STATHOPOULOS-FARROS & all.] and for concrete C25 and Steel S500 is:

longitudinal 64Ø25
transverse Ø13/8.6

The section of the pier is presented on Figure 5.2.

- **Section Analysis – Moment Curvature curve**

The behavior of the pier with the computed reinforcement is described through the moment-curvature curve. This curve is derived from static concrete section analysis using the USC_RC software. The moment curvature curve is presented on Figure 5.4.

5.1.2 Aims of this task

This task aims to test both in longitudinal and transverse direction the seismic performance of this specific bridge and to compare it with the performance of a single pier of the bridge. At first the seismic performance of the bridge is compared in transverse direction with a S-DOF system that represents a single pier and in longitudinal with a pier with fixed rotational degree of freedom at the top to considerate the stiffness of the deck. Therefore new models are created in order to take into account the impact of each of the bridge components.

5.2 Longitudinal Direction

5.2.1 Performance of the bridge under low, moderate and strong seismic shaking

The seismic performance of this bridge was tested under nonlinear dynamic time history analysis using the same 29 real earthquake records as before. The seismic performance of the system is expressed in terms of maximum drift, residual drift and $\frac{\mu_{demand}}{\mu_{capacity}}$. Still only 9 of these records were finally used. This is due to the fact that the rest of the records demanded twice or even more the ductility capacity of the system. In order to have a wider variety of records 16 of the rejected records were scaled based on PGA to 50%. Finally the results of the 25 records used to describe the seismic performance of the whole bridge in the longitudinal direction are presented on Table 5.1. The chosen records demanded up to 125% of the ductility capacity of the system.

5.2.2 First Model used to represent bridge's pier in Longitudinal Direction

- **Model Used**

At first a pier with fixed rotational degree of freedom at the top and fixed base was chosen. This assumption is the most common way to represent a bridge pier in the longitudinal direction and is based on the fact that the stiffness of the deck is much higher than the pier's, so it limits the rotation at the top of the pier.

The mass of the deck is distributed at the top of the pier according to the stiffness of the pier. In longitudinal direction the stiffness of the bridge is calculated according to the following equation:

$$K_{Bridge} = K_{left\ Bearings} + K_{left\ Pier} + K_{right\ Pier} + K_{right\ Bearings}$$

So the mass that is distributed to the pier is:

$$M_{pier} = M_{deck} * \frac{K_{Pier}}{K_{Bridge}} \quad (K_{pier} = \frac{12*EI}{h^3})$$

Finally the system of the pier with fixed rotational degree of freedom at the top has the following characteristics:

- ✓ m = 1361 Mgr
- ✓ h = 8.8 m
- ✓ D = 2 m

A very important factor, in order to achieve the right comparison between the bridge's pier and this system that aims to represent pier's behavior, is the correct placement of the mass. So placing the mass at the top of the pier (8.8m height) would be an important mistake because moment at the base of the pier would be dramatically different in the two cases. Therefore the mass is placed at the actual height of deck's center of mass (9.67m height). Rigid elements are used to connect the mass element with the top of the pier. However the rotational fixity is still imposed at the top of the pier. The system used is presented on Figure 5.5(a).

- **Pushover Analysis**

Static pushover analysis is performed in order to compare this model with the pier of the whole system in terms of Force-Displacement at the top of the pier. The relevant curves are presented on Figure 5.6.

- **Seismic Performance**

The seismic performance of this system was examined under nonlinear dynamic time history analysis using the 25 records (9 real records, 16 scaled real records) selected before. The results of the analysis are compared with the performance of the relevant pier of the model of the whole bridge and are presented on Table 5.2. The maximum deviation observed in terms of $\frac{\mu_{demand}}{\mu_{capacity}}$, in 23 of the 25 records that demanded less ductility than the capacity of the system, is 32% while the average is 11%. In the other two records the deviations observed are dramatically larger. A first conclusion from this specific analysis is that it seems that ignoring the impact of the rest components of the bridge, the deviations observed are of high importance.

The deviations in terms of maximum drift, residual drift and $\frac{\mu_{\text{demand}}}{\mu_{\text{capacity}}}$ are graphically presented on Figure 5.7 while their maximum and average values are collected on Table 5.3. From these graphs another fact of great importance is observed. The impact of the rest components of the bridge cannot be characterized as beneficial or adverse in general. Their impact depends on the specific ground motion and its characteristics and this is another reason that proves that these components should be taken into account.

Therefore the following step is to examine one by one the impact of the rest components of the bridge.

5.2.3 Second Model used – Impact of bearing's stiffness

The first component of the bridge that is taken into account is the bearings. As in the model of the whole bridge the abutments are fixed, the impact of bearings is specified on their stiffness while damping will be examined in the following section.

- **Model Used**

The model used is similar to the previous one with two differences. The first one is the adding of a linear elastic displacement spring at the top of the pier. The stiffness of the specific spring is equal to the stiffness of the four bearings of the one abutment.

$$K_{spring} = 4 * K_{Bearing} = 5200 \frac{KN}{m}$$

The second difference with the first model used is the mass at the top of the pier. Also, in this case as before the mass is distributed according to the stiffness of the model. The stiffness of this model is higher than the previous one and equals to:

$$K_{system} = K_{pier} + K_{abutment}$$

The stiffness of the bearing is calculated by the following equation:

$$K_{bearing} = n * \frac{G * A}{t}$$

assuming the following parameters:

- n : number of bearings
- G : 1 MPa
- A : section area of bearing
- t : thickness of elastic part of bearing

It is obvious that the stiffness of this system is half the stiffness of the whole bridge. So the mass at the top of pier is half the mass of the deck and this is the second difference. As in the previous case, mass element is placed at the right position at deck's mass center.

On the other hand the displacement spring is placed at the top of the pier (8.8m height) while the rotational degree of freedom at the top of the pier remains fixed.

Finally the system of the pier with fixed rotational degree of freedom at the top has the following characteristics:

- ✓ m = 1408 Mgr
- ✓ h = 8.8 m
- ✓ D = 2 m

The system used is presented on Figure 5.5(b).

- **Pushover Analysis**

Static pushover analysis is performed in order to compare this model with the pier of the whole system of the bridge in terms of Force-Displacement at the top of the pier. The relevant curves are presented on Figures 5.8.

- **Seismic Performance**

The seismic performance of this system was examined under nonlinear dynamic time history analysis using the same 25 records (9 real records, 16 scaled real records) as before. The results of the analysis are compared with the performance of the relevant pier of the model of the whole bridge and are presented on table 5.4. In this case, in the 23 of the 25 records that demanded less ductility than the capacity of the system, the maximum deviation observed in terms of $\frac{\mu_{demand}}{\mu_{capacity}}$ was 30%, only 2% less than before, while the average deviation remains 11%. However in the two records that demanded ductility higher than the capacity of the system the results are far different than before. In the record of JMA_000, $\frac{\mu_{demand}}{\mu_{capacity}}$ is decreased from 365% to 26% while in the record of LEFKADA_2003 from 71% to 22%.

- **Impact of bearing's stiffness**

From these results it can be deduced that bearings offer an important overstrength to the system when the ductility capacity of the system is exceeded, which points out the important impact of the bearings to the seismic performance of a bridge as bearings may prevent the total collapse of the bridge.

The deviations in terms of maximum drift, residual drift and $\frac{\mu_{demand}}{\mu_{capacity}}$ between the second system and the whole bridge are graphically presented on Figure 5.9 while their maximum and average values are collected on Table 5.5. From these graphs it can be deduced as before that the impact of the rest components of the bridge cannot be characterized as beneficial or adverse in general. Their impact depends on the specific ground motion and its characteristics and this is another factor that should be taken into account.

Therefore it is important to considerate the rest components of the bridge. This investigation aims to minimize the deviations to the seismic performance of the whole bridge and the proposed system.

5.2.4 Third Model used – Impact of bearing's damping

This task aims to examine the impact of bearing's damping. This is the second parameter of the bearings that may affect the seismic performance of the bridge.

- **Model Used**

The model used is similar to the previous one with the addition of a horizontal dashpot at the top of the pier (8.8m height). The model is presented on Figure 5.5(c). The damping coefficient of the dashpot that represents the damping of the four bearings of the abutment is calculated by the following equation:

$$c_{bearing} = \frac{2 * k * \xi}{\omega}$$

assuming the following parameters:

- K : stiffness of bearings
- ξ : 5%
- ω_{bridge} : $2\pi / T_{bridge\ long}$

The stiffness of the system remains half the stiffness of the whole bridge. So the mass at the top of pier is half the mass of the deck as previously. The rotational degree of freedom at the top of the pier remains fixed while the system has the same deformational-spring and the same characteristics.

- **Pushover Analysis**

Static pushover analysis is performed in order to compare this model to the pier of the whole system in terms of Force-Displacement at the top of the pier. The relevant curves are presented on Figure 5.10.

- **Seismic Performance**

The seismic performance of this system was examined under nonlinear dynamic time history analysis using the same 25 records (9 real records, 16 scaled real records) as before. The results of the analysis are compared with the performance of the relevant pier of the model of the whole bridge and are presented on Table 5.6. The deviations are graphically presented on Figure 5.11 while their maximum and average values are collected on Table 5.7. It is observed that they are almost the same with the previous case. Comparing the second to the third model the maximum deviation in terms of $\frac{\mu_{demand}}{\mu_{capacity}}$ is 1.3%, so it can be concluded that these two systems are equivalent.

- **Impact of bearing's damping**

The addition of bearing's damping to the system was not proven to be of great importance. The seismic performance is almost the same with the previous case in which damping was ignored.

5.2.5 Fourth Model used – Impact of deck's rotational stiffness

The following step was to take into account the deck of the bridge. The deck of the bridge affects the seismic performance of the whole system both with the damping of its material and its rotational stiffness. At first the rotational stiffness of the deck is examined to find out on what level the fixed rotational degree of freedom that was assumed in the previous cases is close to reality.

- **Rotational stiffness of the deck in longitudinal direction – Rotational Spring**

In order to estimate the rotational stiffness of the deck in longitudinal direction a rotational pushover analysis is performed to the entire system of the bridge. An angle of 0.01 rad is applied on the top of the two piers. In order to exclude the effect of the pier's stiffness, each pier is replaced with a vertical spring that represents its axial stiffness. The results of the analysis are expressed in a moment-angle curve that is presented on Figure 5.12. From this curve the rotational stiffness of the deck is extruded which equals to: $K_{rotational}$=21990200 KNm/rad.

- **Literature Formulation**

The rotational stiffness of the deck can also be calculated with one of the known methods of structural analysis if you consider the deck of the bridge as a continuous beam with simply supports at the top of the piers and the bearings of the abutments. In this case that the deck is considered as a three equal span continuous beam, the rotational (bending) stiffness of the deck is calculated by the following formula:

$$K_{rotational} = \frac{9EI}{L}$$

assuming the following parameters:

- E=30000000 KPa, the Young's elastic modulus
- I=2.72 m^4, the I_{11}moment of inertia of the deck
- L=31 m, the length of each span

The rotational stiffness of the deck using the above formulation equals to $K_{rotational}$=23690323 KNm/rad which is very close to the one extruded by the pushover analysis of the deck of the bridge model. This small deviation is due to the consideration of simply supports at the top of the piers and the bearings of the abutments, instead of vertical springs which stiffness is the axial stiffness of the piers and the bearings respectively. Finally the stiffness of the rotational spring that is added to

the top of the simple model is the one calculated by the literature formulation. In this way the development of the complete model of the bridge in a finite element code is avoided.

- **Model Used**

The 4th model used is similar to the 3rd one with the addition of a rotational spring at the top of the pier (8.8m height). The horizontal spring of the previous system remains at the top of the pier while the dashpot is removed as it was proven not to have a significant impact.

The stiffness of the system remains half the stiffness of the whole bridge. So the mass at the top of pier is half the mass of the deck as previously. This system is presented on figure 5.5(d).

- **Pushover Analysis**

Static pushover analysis is performed in order to compare this model with the pier of the whole system in terms of Force-Displacement at the top of the pier and Moment-Curvature at the base of the pier. The relevant curves are presented on Figures 5.13.

- **Seismic Performance**

The seismic performance of this system was examined under nonlinear dynamic time history analysis using the same 25 records (9 real records, 16 scaled real records) as before. The results of the analysis are compared with the performance of the relevant pier of the model of the whole bridge and are presented on Table 5.8. The deviations are graphically presented on Figure 5.14 while their maximum and average values are collected on Table 5.9. In this case the deviations observed are smaller than in the previous one. Comparing the fourth model to the whole bridge the maximum deviation in terms of $\frac{\mu_{demand}}{\mu_{capacity}}$ is 26%, while the average is 7% in 23 cases that didn't exceed system's ductility capacity. Compared to the relevant deviations of the previous system, the maximum deviation decreased in this case by 8%, while the average by 5%.

- **Impact of deck's rotational stiffness**

From the previous results it is obvious that adding the actual rotational stiffness of the deck in the top of the pier instead of fixity on the rotational degree of freedom, decreases the deviations between the pier of the whole system and the system that aims to represent it. Another factor that has to be examined is the computational effort to ''build'' each of the examined system. This factor has to be considered, in addition to deviations, in order to select the most appropriate model to represent the bridge's pier.

5.2.6 Fifth Model used – Impact of deck's damping

The last parameter that was taken into account was the damping of the material of the bridge's deck. The damping coefficient of the dashpot that represents the damping of the material of the deck is calculated by the following equation:

$$c_{deck\ rotational} = \frac{2 * k * \xi}{\omega}$$

assuming the following parameters:

- K :rotational stiffness of deck
- ξ : 5%
- ω_{bridge} : $2\pi/T_{bridge\_long}$

The rotational dashpot is placed at the top of the pier in addition to the rotational spring.

- **Model Used**

The 5th model used is similar to the 4th one with the addition of a rotational dashpot at the top of the pier (8.8m height).Rotational and horizontal springs of the previous system remain at the top of the pier while the dashpot that represents the damping of the bearings is added as to have an even more complete model.

The stiffness of this system remains half the stiffness of the whole bridge. So the mass at the top of pier is half the mass of the deck as previously. The system is presented on Figure 5.5(e).

- **Pushover Analysis**

Static pushover analysis is performed in order to compare this model to the pier of the entire system of the bridge in terms of Force-Displacement at the top of the pier and Moment-Curvature at the base of the pier. The relevant curves are presented on Figures 5.15.

- **Seismic Performance**

The seismic performance of the last system was examined under nonlinear dynamic time history analysis using the same 25 records (9 real records, 16 scaled real records) as before. The results of the analysis are compared as previously with the performance of the relevant pier of the model of the whole bridge and are presented on Table 5.10. . The deviations are graphically presented on Figure 5.16 while their maximum and average values are collected on Table 5.11. Comparing the fifth model to the entire model of the bridge, the maximum deviation in terms of $\frac{\mu_{demand}}{\mu_{capacity}}$ is 15%, while the average is 5%. Compared to the relevant deviations of the previous system, the maximum deviation is decreased in this case by 11% while the average by 2%.

- **Impact of deck's damping**

The adding of the rotational dashpot at the top of the pier decreases the deviations between the pier of the whole system and the system that aims to represent it. However adding the rotational dashpot at the top increases the computational effort to ''build'' the equivalent model.

5.3 Transverse Direction

5.3.1 Performance of the bridge under low, moderate and strong seismic shaking

The bridge *A01_TE20* of the Greek metropolitan motorway *ATTIKI ODOS* is also examined in the transverse direction using the same three-dimensional analytical model. The same 25 records are used in order to test the seismic performance of the bridge under nonlinear dynamic time history analysis in the transverse direction. The chosen records demanded from 2% up to 160% of the ductility capacity, so they are a representative sample. The seismic performance of the system is expressed in terms of maximum drift, residual drift and $\frac{\mu_{demand}}{\mu_{capacity}}$. The results of the analysis are presented on Table 5.12.

5.3.2 First Model used to represent bridge's pier in Transverse Direction

- **Model Used**

A single-degree-of-freedom (SDOF) model of the bridge pier is used to estimate the seismic excitation applied at the level of the deck in the transverse direction. This is a very common and rational approximation as the mass and the stiffness of the pier are significantly lower than the mass and the stiffness of the deck.

The mass of the deck is distributed at the top of the pier according to the stiffness of the pier. In transverse direction the stiffness of the bridge is calculated according to the following equation:

$$K_{Bridge} = K_{left\ Bearings} + K_{left\ Pier} + K_{right\ Pier} + K_{right\ Bearings}$$

So the mass that is distributed to the pier is:

$$M_{pier} = M_{deck} * \frac{K_{Pier}}{K_{Bridge}} \quad (K_{pier} = \frac{3*EI}{h^3})$$

Finally the SDOF system that represents the bridge's pier has the following characteristics:

- ✓ m = 1237.5 Mgr
- ✓ h = 8.8 m
- ✓ D = 2 m

As in the previous tasks a very important factor, in order to have the proper comparison between the bridge's pier and this S-DOF system is the correct placement of the mass. Mass is placed at the actual height of deck's center of mass (9.67m height). Rigid elements are used to connect the mass element to the top of the pier. The system used is presented on Figure 5.17(a).

- **Pushover Analysis**

Static pushover analysis is performed in order to compare this SDOF model to the pier of the whole system in terms of Force-Displacement at the top of the pier. The relevant curves are presented on Figure 5.18.

- **Seismic Performance**

The seismic performance of this S-DOF system was examined under nonlinear dynamic time history analysis using the same 25 records. (9 real records, 16 scaled real records) that were selected before. The results of the analysis are presented on Table 5.13. In 8 of the 25 cases S-DOF system totally collapsed while the pier of the bridge has barely or even not exceeded its ductility capacity.

The average deviation observed in terms of $\frac{\mu_{demand}}{\mu_{capacity}}$, in the rest 17 records is 29%. The results of this specific analysis show that S-DOF system cannot itself represent the seismic performance of the pier in transverse direction. By ignoring the impact of the rest components of the bridge the deviations observed are great.

The deviations in terms of terms of maximum drift, residual drift and $\frac{\mu_{demand}}{\mu_{capacity}}$ are graphically presented on Figure 5.19 while their maximum and average values are collected on Table 5.14.

Therefore the following step is to include one by one the impact of the rest components of the bridge.

5.3.3 Second Model used – Impact of bearing's stiffness & damping

As in the longitudinal direction, the first component of the bridge that was taken into account was the bearings. In this case both the stiffness and the damping of the bearings in transverse direction are examined.

- **Model Used**

The second model used is the same S-DOF system with the previous case only with two added components. The first one is the adding of a linear elastic displacement spring at the top of the pier. The stiffness of the specific spring equals to the stiffness of the four bearings of the one abutment as in longitudinal direction.

$$K_{spring} = 4 * K_{bearing} = 5200 \frac{KN}{m}$$

As a result:

$$K_{system} = K_{pier} + K_{abutments} = \frac{K_{bridge}}{2}$$

The second component that was added is a horizontal dashpot in the transverse direction. The damping coefficient of the dashpot that represents the damping of the material of the bearings is calculated by the following equation:

$$c_{bearing} = \frac{2 * k * \xi}{\omega}$$

assuming the following parameters:

- K : stiffness of bearings
- ξ : 5%
- ω_{bridge} : $2\pi / T_{bridge\ trans}$

The increase of system's stiffness results in the mass that is distributed at the top of the pier. As a result the mass of the second system is half the mass of the deck.

Both spring and dashpot are placed on the top of the pier (8.8m height) while the rotational degree of freedom at the top of the pier remains unrestrained.

Finally the system has the following characteristics:

- ✓ m = 1408 Mgr
- ✓ h = 8.8 m
- ✓ D = 2 m

The system used is presented on Figure 5.17(b).

- **Pushover Analysis**

Static pushover analysis is performed in order to compare this model to the pier of the whole system in terms of Force-Displacement at the top of the pier. The relevant curves are presented on Figure 5.20.

- **Seismic Performance**

The seismic performance of this system was examined under nonlinear dynamic time history analysis using the same 25 records. The results of the analysis (Table 5.15) are compared to the performance of the relevant pier of the model of the whole bridge. In this case, although total collapse is prevented in most cases because of the spring, the maximum deviation in terms of $\frac{\mu_{demand}}{\mu_{capacity}}$ is 500%, while the average is 100%.

- **Impact of bearing's stiffness**

It is evident that this system cannot describe the seismic performance of the pier. Nevertheless the adding of the horizontal spring and the dashpot prevents the system from total collapse that was observed in the previous case.

The deviations in terms of terms of maximum drift, residual drift, $\frac{\mu_{demand}}{\mu_{capacity}}$ between this second system and the whole bridge, are graphically presented on Figure 5.21 while their maximum and average values are collected on Table 5.16. Therefore it is important to take into account the rest components of the bridge such as the deck. In transverse direction the bearings, because of their position, also offer significant moment stability to the system.

5.3.4 Third Model used – Impact of bearing's moment stability & deck's torsional stiffness

This task aims to examine on which level the assumption of unrestrained rotational degree of freedom at the top of the pier represents the pier in transverse direction. For this purpose both the horizontal spring and the dashpot are removed from the system in order to ignore their impact and a rotational spring and a dashpot are added.

- **Model Used**

This model is similar to the S-DOF system that was examined at first, with the difference of adding a rotational spring and a dashpot at the top of the pier (8.8m height). The rotational spring represents both the rotational stiffness of the bearings and the torsional stiffness of the deck. The bearings add rotational stiffness to the system due to their position. The axial loading of the bearings in the transverse direction leads to an important stability moment that should be taken into account. Also the rotational dashpot at the top of the pier represents the impact of deck's rotational damping.

- **Rotational Pushover of the deck**

As in longitudinal direction, a rotational pushover analysis is performed to the entire system of the bridge in order to extrude the rotational stiffness that has to be added to the examined system. An angle of 0.01 rad is applied on the top of the two piers. In order to exclude the effect of the pier's stiffness, piers are replaced with vertical springs that represent their axial stiffness. The results of the analysis are expressed in a Moment-Angle curve that is presented on Figure 5.23. From this curve the rotational stiffness that has to be added to the examined system is extruded which is equal to: $K_{rotational}$=2655080 KNm/rad. This rotational stiffness includes the effect of both the bearings and the deck.

- **Literature Formulations**

The torsional stiffness of the deck can be calculated using the following literature formulation:

$$T = K_{torsional} * \Theta \, , \, K_{torsional} = \frac{J}{L} * G$$

assuming the following parameters:

- T: torque (KNm)
- θ: angle of twist (rad)
- $J = 8.183m^4$: Torsion constant of deck's section
- $G = 12.5\ GPa : Shear\ modulus$
- L=31m : Length of the element the torque is being applied to or over

As far as the bearings are concerned their actual position is presented on Figure 5.22. The rotational stiffness that is added to the system due to the position of the bearings can be calculated by the following equation:

$$K_{Rotational_{Bearings}} = 2 * K_v * ({L_1}^2 + {L_2}^2)$$

assuming the following parameters:

- $K_V : Vertical\ stiffness\ of\ bearings$
- $L_1, L_2 : Transverse\ distance\ of\ bearings\ from\ the\ center\ of\ gravity\ of\ deck$

The overall rotational stiffness of the system can be calculated by the following equation:

$$\frac{1}{K_{rotational}} = \frac{1}{K_{Torsional-deck}} + \frac{1}{K_{rotational-bearings}}$$

$$\Rightarrow K_{rotational} = \frac{K_{bearings} * K_{deck}}{K_{bearings} + K_{deck}} = 2728633 \text{ KNm/rad}$$

As far as damping is concerned, a rotational dashpot is added at the top of the pier as in longitudinal direction. The damping coefficient of the dashpot is calculated by the following equation:

$$c_{deck\ rotational} = \frac{2 * k * \xi}{\omega}$$

assuming the following parameters:

- K :rotational stiffness of deck
- ξ : 5%
- ω_{bridge} : $2\pi/T_{bridge\_trans}$

Finally the rotational stiffness that was calculated by the equations is used and not the one from the rotational pushover analysis. It is obvious that by using equations instead of pushover analysis the computational effort to ''build'' the model is minimized.

The system has the following characteristics:

- ✓ m = 1237.5 Mgr
- ✓ h = 8.8 m
- ✓ D = 2 m

The system used is presented on Figure 5.17(c).

- **Pushover Analysis**

Static pushover analysis is performed in order to compare this model to the pier of the whole system in terms of Force-Displacement at the top of the pier. The relevant curves are presented on Figures 5.24.

- **Seismic Performance**

The seismic performance of the system was examined under nonlinear dynamic time history analysis using the same 25 records. The results of the analysis (Table 5.17) are compared to the performance of the relevant pier of the model of the whole bridge. In this case, the maximum deviation in terms of $\frac{\mu_{demand}}{\mu_{capacity}}$ is 50%, while the average is 13%.

- **Impact of system's rotational stiffness**

The deviations in terms of terms of maximum drift, residual drift and $\frac{\mu_{demand}}{\mu_{capacity}}$ between this third model and the whole bridge are graphically presented on Figure 5.25 while their maximum and average values are collected on Table 5.18.

Compared to the previous two models it is obvious that the seismic performance of this model is much closer to the one of the pier. However the deviations in some cases remain significant, which implies the need to take into account the impact of the rest components of the bridge.

Although it can be deduced that system's rotational stiffness are of great importance compared to the horizontal stiffness and it cannot be ignored.

5.3.5 Fourth Model used – Combination of 2nd & 3rd model

In the previous task it was proven that bridge's rotational stiffness affects significantly the seismic behavior of the pier in transverse direction. For this reason the 4th model takes into account both the horizontal and rotational stiffness of the bridge combining the two previous models.

- **Model Used**

This model is a combination of the two previous ones. At the top of the pier (8.8m height) a horizontal spring and a dashpot are placed but also a rotational spring and a dashpot as they were calculated before. The mass as in the second case is half the mass of the deck.

The system used is presented on Figure 5.17(d).

- **Pushover Analysis**

Static pushover analysis is performed in order to compare this model to the pier of the whole system in terms of Force-Displacement at the top of the pier. The relevant curves are presented on Figure 5.26.

- **Seismic Performance**

The seismic performance of the system was examined under nonlinear dynamic time history analysis using the same 25 records. The results of the analysis (Table 5.19) are compared to the performance of the relevant pier of the model of the whole bridge. In this case, the maximum deviation in terms of $\frac{\mu_{demand}}{\mu_{capacity}}$ is 26%, while the average is 7%. It is important to be mentioned that in cases that didn't exceed the system's ductility capacity the maximum deviation is 16% while the average is 5%.

- **Impact of system's horizontal & rotational stiffness**

The deviations in terms of maximum drift, residual drift and $\frac{\mu_{demand}}{\mu_{capacity}}$ between this fourth model and the whole bridge are graphically presented on Figure 5.27 while their maximum and average values are collected on Table 5.20.

It can be deduced that a system that takes into account both the horizontal and the rotational stiffness but also the horizontal and rotational damping added to the system by the bearings and the deck of the bridge, has a similar seismic performance to the pier.

5.3.6 Fifth Model used –Impact of deck's vertical stiffness & damping

- **Model Used**

The 5th model is similar to the previous one, with the difference of adding a vertical spring and a vertical dashpot at the top of the pier (8.8m height). The vertical spring represents the vertical stiffness of the deck while the vertical dashpot the damping of the material of the deck.

- **Vertical Pushover of the deck**

A vertical pushover analysis is performed to the entire system of the bridge in order to extrude the vertical stiffness that has to be added to the examined system. A displacement of 0.05 m is applied on the top of the two piers. In order to exclude the effect of the pier's stiffness, piers are replaced with vertical springs that represent their axial stiffness. The results of the analysis are expressed in a Force-Displacement curve that is presented on Figure 5.28. From this curve the vertical stiffness that has to be added to the examined system is extruded which equals to: $K_{vertical}$=15658 KN/m.

- **Pushover Analysis**

Static pushover analysis is performed in order to compare this model to the pier of the whole system in terms of Force-Displacement at the top of the pier. The relevant curves are presented on Figure 5.29.

- **Seismic Performance**

The seismic performance of the system was examined under nonlinear dynamic time history analysis using the same 25 records. The results of the analysis (Table 5.21) are compared to the performance of the relevant pier of the model of the whole bridge. In this case, the maximum deviation in terms of $\frac{\mu_{demand}}{\mu_{capacity}}$ remains 26%, while the average 7% as well.

- **Impact of deck's vertical stiffness & damping**

The deviations in terms of maximum drift, residual drift and $\frac{\mu_{\mathrm{demand}}}{\mu_{\mathrm{capacity}}}$ between the fifth model and the whole bridge are graphically presented on Figure 5.30 while their maximum and average values are collected on Table 5.22.

The results are almost the same to the previous case so the vertical stiffness of the deck and the damping of its material don't seem to affect the seismic performance of the pier.

At the end of the chapter are presented both bridge and five systems examined in ABAQUS code and their deformed shape for Takarazuka_000 record (scaled by PGA 50%) in longitudinal and transverse direction (Figures 5.31, 5.32).

Chapter 5

Figures

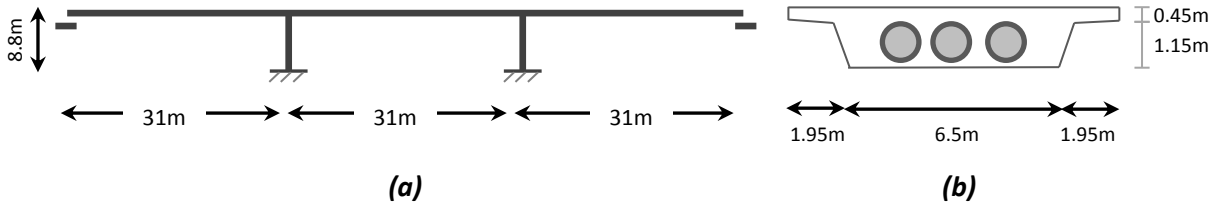

Figure 5.1 (a) geometry of the bridge and **(b)** section of the deck

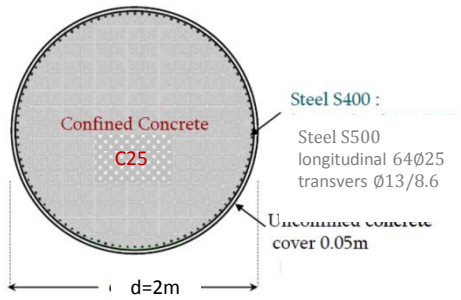

Figure 5.2 The geometric characteristics and the reinforcement of pier's section

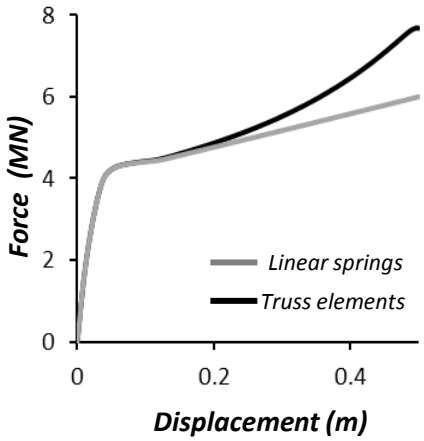

Figure 5.3 Pushover analysis comparison between bearing as linear springs and truss elements

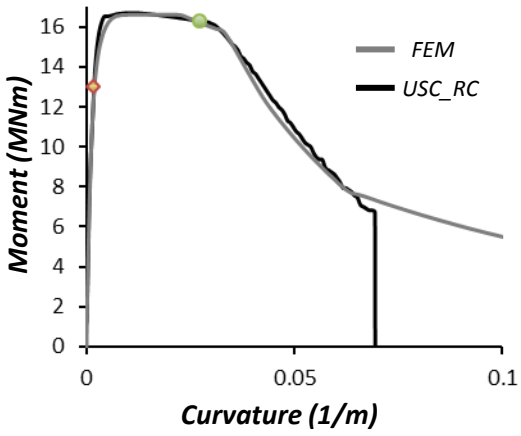

Figure 5.4 Comparison of moment–curvature curves using USC_RC program and calibrated finite element model

	SEISMIC PERFORMANCE					
	max Drift (m)	*maxDrift ratio (%)*	*Drift res (m)*	*Drift res ratio(%)*	*μ demand*	*μ d / μ c*
JMA_090	0.08	0.95	0.06	0.64	10.10	0.89
MNSA	0.01	0.14	0.01	0.06	0.47	0.04
KALAMATA	0.04	0.45	0.02	0.18	2.69	0.24
TCU68NS	0.02	0.20	0.00	0.02	0.51	0.05
SYLMAR_360	0.05	0.61	0.03	0.30	6.89	0.60
JMA_000	0.11	1.28	0.02	0.18	14.15	1.24
TAKARAZUKA_090	0.05	0.62	0.03	0.30	6.25	0.55
PYRGOS	0.03	0.30	0.01	0.07	0.91	0.08
AEGIO	0.05	0.57	0.01	0.07	4.59	0.40
LEFKADA_2003	0.09	1.05	0.01	0.07	12.32	1.08
LEFKADA_1973	0.05	0.52	0.01	0.08	3.22	0.28
TCU52EW	0.03	0.30	0.01	0.08	0.86	0.08
TCU52NS	0.02	0.23	0.00	0.03	0.78	0.07
TCU68EW	0.09	0.98	0.06	0.74	9.63	0.84
RINALDI_318	0.03	0.33	0.00	0.04	2.92	0.26
JENSEN_022	0.03	0.39	0.02	0.18	2.67	0.23
SYLMAR_090	0.06	0.70	0.04	0.49	7.61	0.67
DUZE_000	0.04	0.43	0.00	0.03	4.84	0.42
YARIMCA_060	0.05	0.57	0.02	0.18	7.77	0.68
YARIMCA_330	0.01	0.17	0.00	0.05	0.55	0.05
SAKARYA	0.04	0.43	0.01	0.12	3.48	0.31
LUCERNE_000	0.03	0.33	0.01	0.08	2.89	0.25
IV#04_140	0.03	0.30	0.00	0.05	0.95	0.08
IV#04_230	0.04	0.47	0.02	0.21	4.14	0.36
DUCE_090	0.06	0.70	0.01	0.15	5.84	0.51

Table 5.1 Seismic performance of pier of bridge A01_TE20 in longitudinal direction

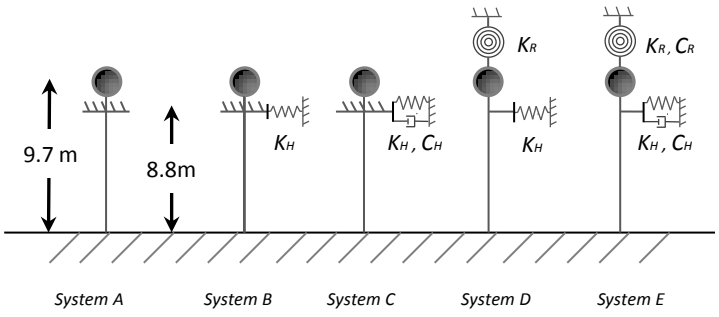

Figure 5.5 Five systems examined

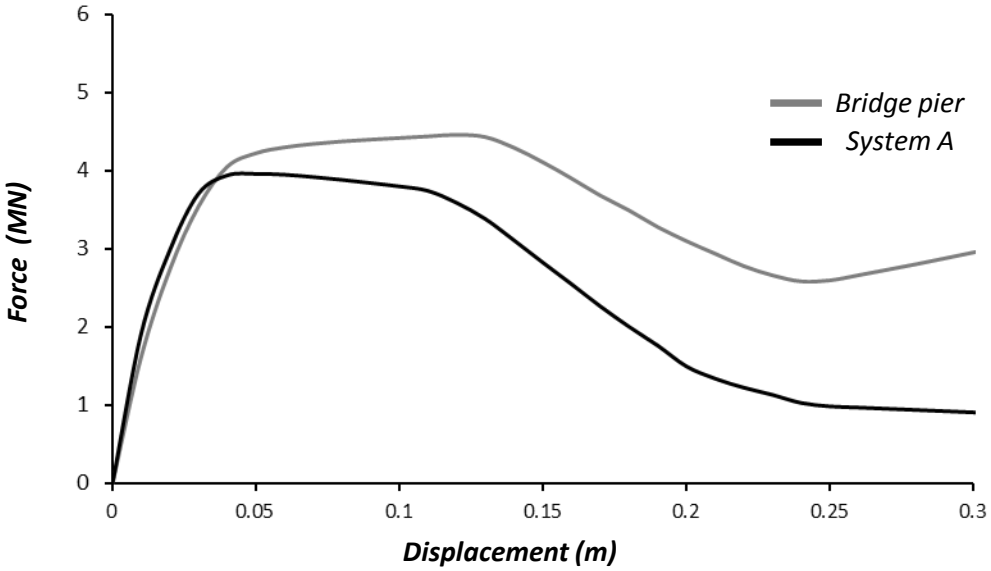

Figure 5.6 Force-Displacement curve from Pushover analysis for Bridge Pier and System A

	SEISMIC PERFORMANCE					
	max Drift (m)	*maxDrift ratio (%)*	*Drift res (m)*	*Drift res ratio(%)*	*μ demand*	*μ d / μ c*
JMA_090	0.11	1.26	0.10	1.15	12.04	1.06
MNSA	0.01	0.17	0.01	0.09	0.49	0.04
KALAMATA	0.04	0.40	0.00	0.02	2.37	0.21
TCU68NS	0.02	0.22	0.02	0.20	0.68	0.06
SYLMAR_360	0.09	0.99	0.04	0.49	10.54	0.92
JMA_000	0.45	5.08	0.44	5.04	55.69	4.89
TAKARAZUKA_090	0.05	0.55	0.02	0.28	4.67	0.41
PYRGOS	0.03	0.30	0.00	0.01	1.14	0.10
AEGIO	0.05	0.54	0.02	0.20	4.25	0.37
LEFKADA_2003	0.15	1.74	0.15	1.68	20.38	1.79
LEFKADA_1973	0.04	0.46	0.01	0.06	2.65	0.23
TCU52EW	0.04	0.43	0.03	0.31	2.62	0.23
TCU52NS	0.02	0.24	0.00	0.05	0.99	0.09
TCU68EW	0.07	0.82	0.06	0.69	7.50	0.66
RINALDI_318	0.06	0.65	0.04	0.42	4.86	0.43
JENSEN_022	0.02	0.28	0.00	0.05	1.81	0.16
SYLMAR_090	0.05	0.59	0.04	0.47	5.73	0.50
DUZE_000	0.03	0.36	0.01	0.16	2.21	0.19
YARIMCA_060	0.05	0.52	0.00	0.04	5.42	0.48
YARIMCA_330	0.03	0.35	0.01	0.10	2.32	0.20
SAKARYA	0.03	0.33	0.01	0.11	3.22	0.28
LUCERNE_000	0.03	0.36	0.01	0.06	1.85	0.16
IV#04_140	0.02	0.23	0.00	0.05	1.01	0.09
IV#04_230	0.06	0.68	0.05	0.53	5.84	0.51
DUCE_090	0.06	0.73	0.02	0.26	6.15	0.54

Table 5.2 Seismic performance of system A

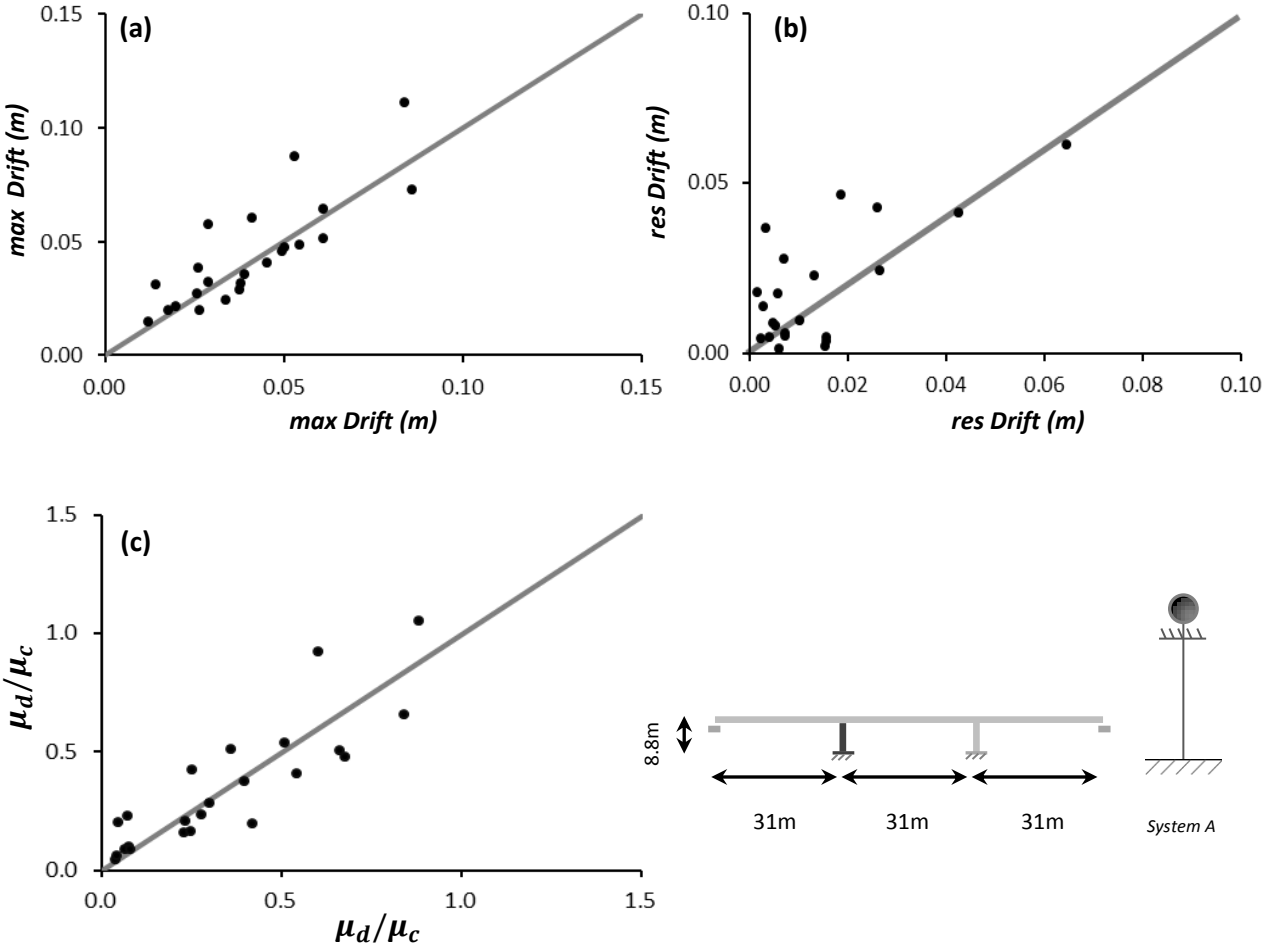

Figure 5.7 (a), (b), (c) Deviations in terms of *max Drift* , *residual Drift* and $\mu_{demand}/\mu_{capacity}$ between bridge's pier and system A (longitudinal direction)

μd < μc	*max Drift (m)*	*Drift res (m)*	*μ demand*	*μ d / μ c*
max	0.03	0.04	3.65	0.32
average	0.01	0.01	1.20	0.11

Table 5.3 Deviations between bridge's pier and system A

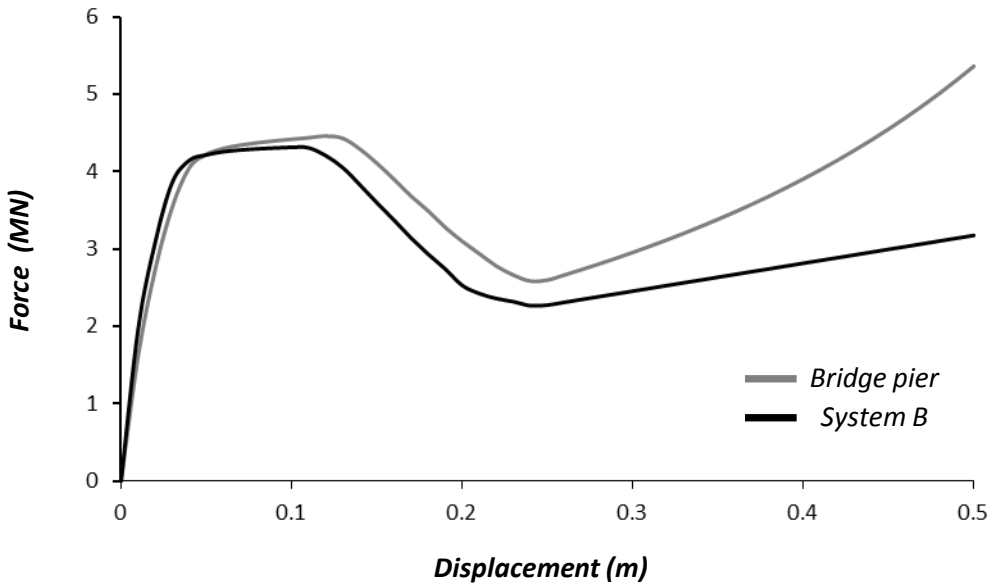

Figure 5.8 Force-Displacement curve from Pushover analysis for Bridge Pier and System B

	SEISMIC PERFORMANCE					
	max Drift (m)	***maxDrift ratio (%)***	***Drift res (m)***	***Drift res ratio(%)***	***μ demand***	***μ d / μ c***
JMA_090	0.07	0.84	0.02	0.27	7.14	0.63
MNSA	0.02	0.19	0.01	0.14	0.56	0.05
KALAMATA	0.04	0.40	0.00	0.03	2.53	0.22
TCU68NS	0.02	0.24	0.02	0.18	0.77	0.07
SYLMAR_360	0.09	0.97	0.02	0.17	10.31	0.90
JMA_000	0.13	1.53	0.01	0.07	16.10	1.41
TAKARAZUKA_090	0.05	0.55	0.02	0.23	4.62	0.41
PYRGOS	0.03	0.30	0.01	0.07	1.14	0.10
AEGIO	0.05	0.54	0.02	0.22	4.33	0.38
LEFKADA_2003	0.11	1.25	0.01	0.15	14.80	1.30
LEFKADA_1973	0.04	0.47	0.01	0.11	2.72	0.24
TCU52EW	0.04	0.42	0.03	0.30	2.47	0.22
TCU52NS	0.02	0.25	0.01	0.08	0.82	0.07
TCU68EW	0.07	0.81	0.06	0.64	7.23	0.63
RINALDI_318	0.06	0.64	0.04	0.41	4.71	0.41
JENSEN_022	0.02	0.28	0.01	0.15	1.82	0.16
SYLMAR_090	0.04	0.48	0.03	0.30	4.64	0.41
DUZE_000	0.03	0.36	0.00	0.04	2.37	0.21
YARIMCA_060	0.05	0.58	0.02	0.19	5.98	0.52
YARIMCA_330	0.03	0.33	0.01	0.06	2.00	0.18
SAKARYA	0.03	0.34	0.00	0.04	3.30	0.29
LUCERNE_000	0.03	0.34	0.00	0.01	1.57	0.14
IV#04_140	0.02	0.22	0.01	0.09	0.93	0.08
IV#04_230	0.06	0.70	0.02	0.22	6.01	0.53
DUCE_090	0.06	0.73	0.02	0.19	6.31	0.55

Table 5.4 Seismic performance of system B

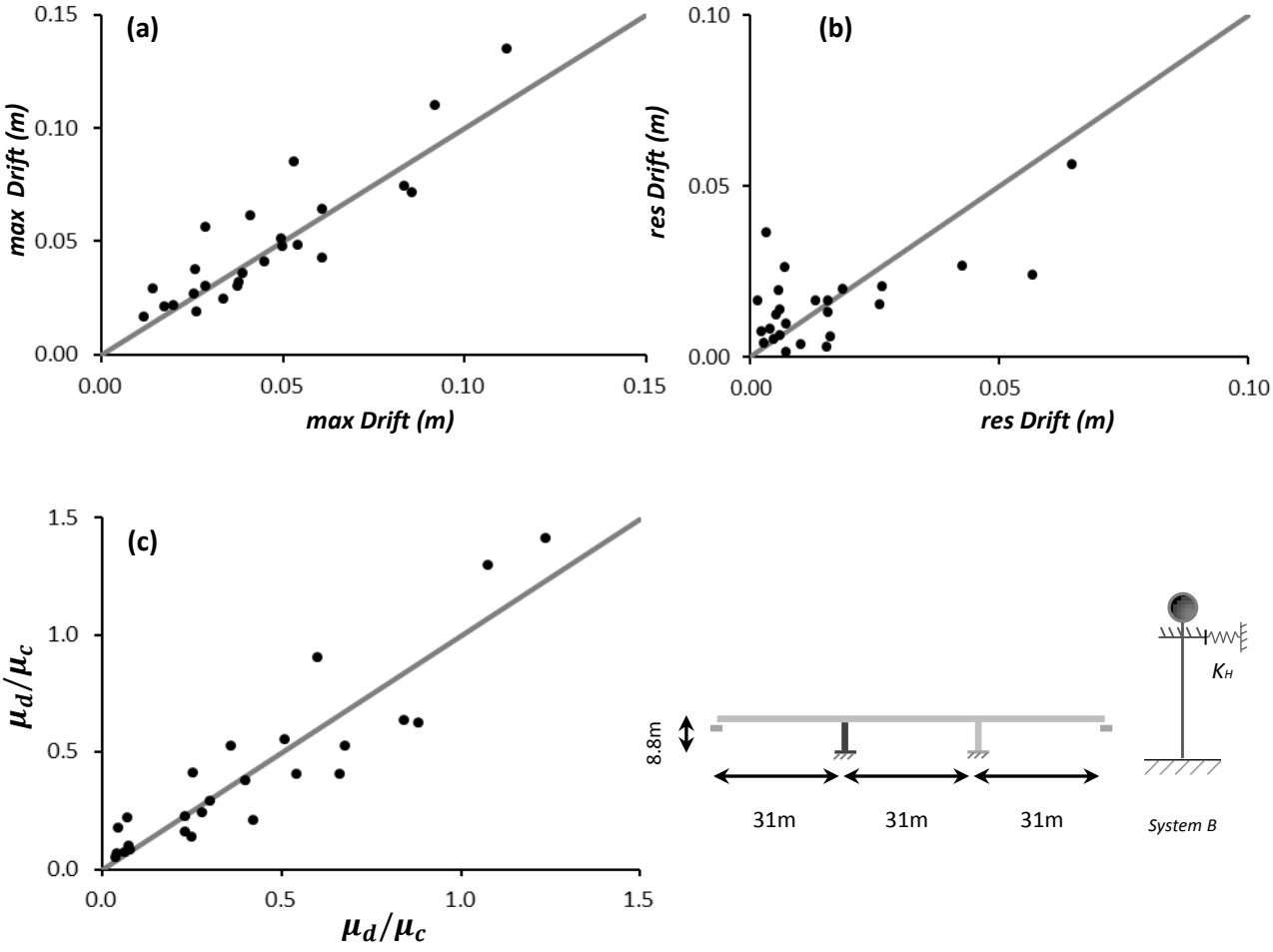

Figure 5.9 (a), (b), (c) Deviations in terms of *max Drift* , *residual Drift* and $\mu_{demand}/\mu_{capacity}$ between bridge's pier and system B (longitudinal direction)

μd < μc	*max Drift (m)*	*Drift res (m)*	*μ demand*	*μ d / μ c*
max	0.03	0.03	3.42	0.30
average	0.01	0.01	1.25	0.11

Table 5.5 Deviations between bridge's pier and system B

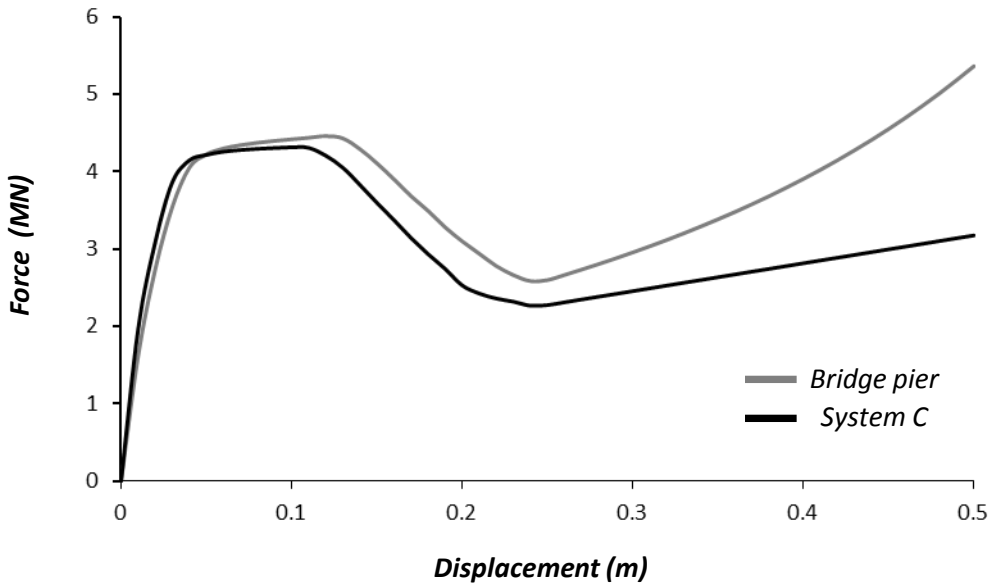

Figure 5.10 Force-Displacement curve from Pushover analysis for Bridge Pier and System C

	SEISMIC PERFORMANCE					
	max Drift (m)	*maxDrift ratio (%)*	*Drift res (m)*	*Drift res ratio(%)*	*μ demand*	*μ d / μ c*
JMA_090	0.07	0.84	0.04	0.40	7.24	0.64
MNSA	0.02	0.18	0.01	0.14	0.55	0.05
KALAMATA	0.04	0.40	0.00	0.03	2.53	0.22
TCU68NS	0.02	0.23	0.02	0.18	0.73	0.06
SYLMAR_360	0.08	0.96	0.02	0.18	10.29	0.90
JMA_000	0.13	1.53	0.01	0.07	16.11	1.41
TAKARAZUKA_090	0.05	0.55	0.02	0.24	4.59	0.40
PYRGOS	0.03	0.30	0.01	0.07	1.14	0.10
AEGIO	0.05	0.54	0.02	0.22	4.30	0.38
LEFKADA_2003	0.11	1.24	0.01	0.16	14.71	1.29
LEFKADA_1973	0.04	0.46	0.01	0.09	2.70	0.24
TCU52EW	0.04	0.41	0.03	0.29	2.32	0.20
TCU52NS	0.02	0.24	0.01	0.08	0.73	0.06
TCU68EW	0.07	0.81	0.06	0.63	7.16	0.63
RINALDI_318	0.06	0.63	0.04	0.40	4.60	0.40
JENSEN_022	0.02	0.28	0.01	0.14	1.78	0.16
SYLMAR_090	0.04	0.49	0.03	0.30	4.63	0.41
DUZE_000	0.03	0.36	0.00	0.05	2.38	0.21
YARIMCA_060	0.05	0.57	0.01	0.17	5.92	0.52
YARIMCA_330	0.03	0.34	0.01	0.08	2.04	0.18
SAKARYA	0.03	0.34	0.00	0.04	3.26	0.29
LUCERNE_000	0.03	0.34	0.00	0.00	1.59	0.14
IV#04_140	0.02	0.22	0.01	0.10	0.92	0.08
IV#04_230	0.06	0.69	0.02	0.25	5.93	0.52
DUCE_090	0.06	0.72	0.02	0.19	6.27	0.55

Table 5.6 Seismic performance of system C

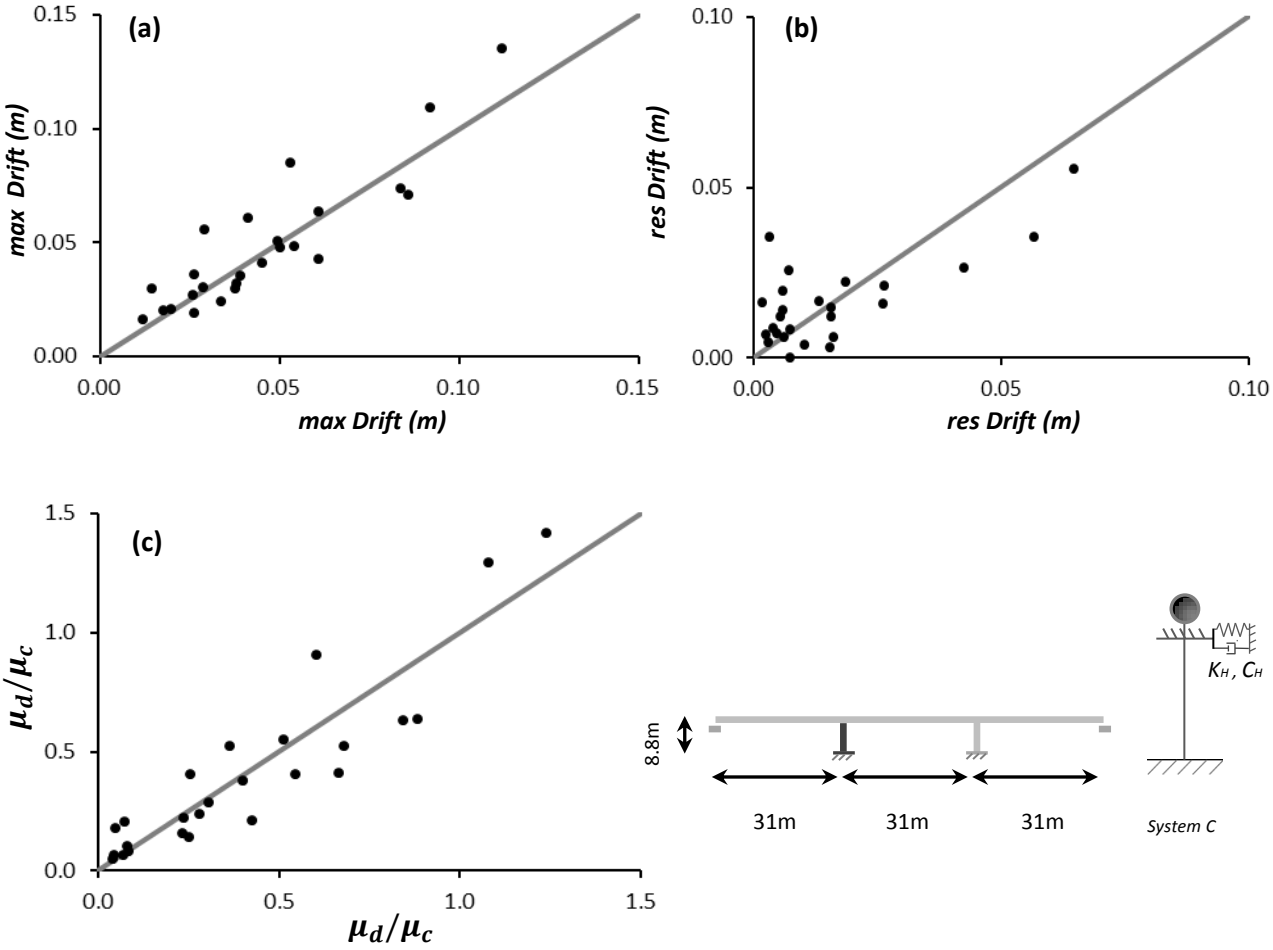

Figure 5.11 (a), (b), (c) Deviations in terms of *max Drift* , *residual Drift* and $\mu_{demand}/\mu_{capacity}$ between bridge's pier and system C (longitudinal direction)

μd < μc	max Drift (m)	Drift res (m)	μ demand	μ d / μ c
max	0.03	0.03	3.40	0.30
average	0.01	0.01	1.24	0.11

Table 5.7 Deviations between bridge's pier and system C

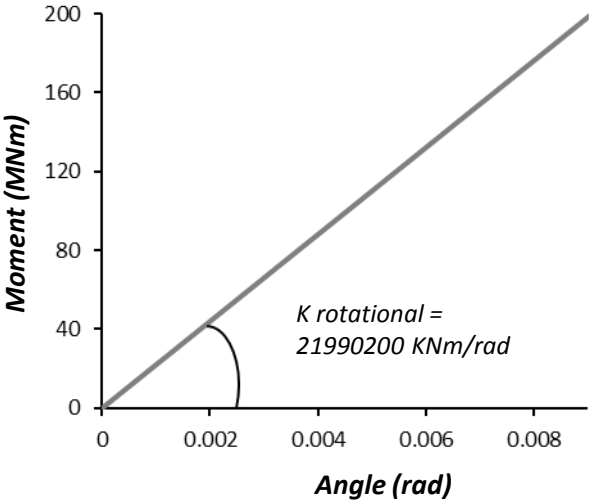

Figure 5.12 Rotational Pushover Moment-Angle curve

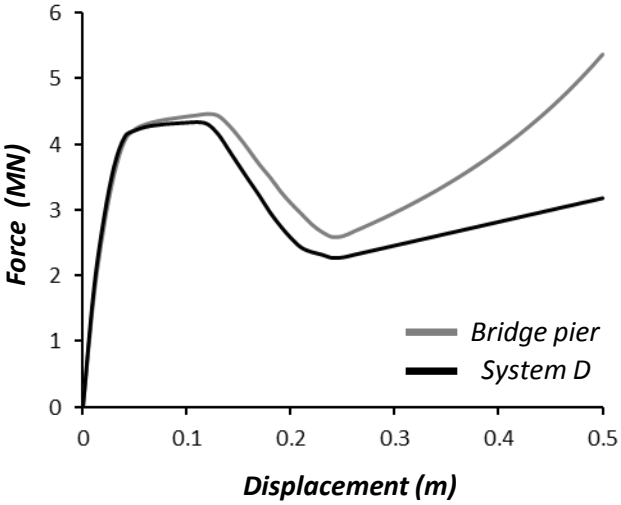

Figure 6.13 Force-Displacement curve from Pushover analysis for Bridge Pier and System D

	SEISMIC PERFORMANCE					
	max Drift (m)	*maxDrift ratio (%)*	*Drift res (m)*	*Drift res ratio(%)*	*μ demand*	*μ d / μ c*
JMA_090	0.11	1.22	0.02	0.17	12.46	1.09
MNSA	0.01	0.15	0.01	0.08	0.44	0.04
KALAMATA	0.04	0.44	0.01	0.14	2.54	0.22
TCU68NS	0.02	0.26	0.01	0.16	1.06	0.09
SYLMAR_360	0.06	0.71	0.02	0.28	7.83	0.69
JMA_000	0.12	1.33	0.02	0.23	14.14	1.24
TAKARAZUKA_090	0.06	0.65	0.03	0.36	6.63	0.58
PYRGOS	0.03	0.31	0.01	0.07	1.10	0.10
AEGIO	0.05	0.60	0.01	0.06	4.95	0.43
LEFKADA_2003	0.12	1.31	0.01	0.06	15.29	1.34
LEFKADA_1973	0.05	0.56	0.01	0.14	3.63	0.32
TCU52EW	0.03	0.34	0.01	0.07	1.18	0.10
TCU52NS	0.02	0.26	0.00	0.05	0.76	0.07
TCU68EW	0.09	1.01	0.06	0.68	9.58	0.84
RINALDI_318	0.03	0.38	0.00	0.02	4.04	0.35
JENSEN_022	0.04	0.42	0.01	0.09	3.74	0.33
SYLMAR_090	0.08	0.86	0.04	0.50	9.89	0.87
DUZE_000	0.04	0.47	0.01	0.15	4.97	0.44
YARIMCA_060	0.05	0.59	0.01	0.11	7.61	0.67
YARIMCA_330	0.01	0.16	0.00	0.02	0.48	0.04
SAKARYA	0.05	0.51	0.01	0.15	4.61	0.40
LUCERNE_000	0.03	0.32	0.01	0.11	2.58	0.23
IV#04_140	0.03	0.31	0.01	0.14	1.56	0.14
IV#04_230	0.06	0.67	0.03	0.30	6.60	0.58
DUCE_090	0.07	0.81	0.00	0.04	7.24	0.63

Table 5.8 Seismic performance of system D

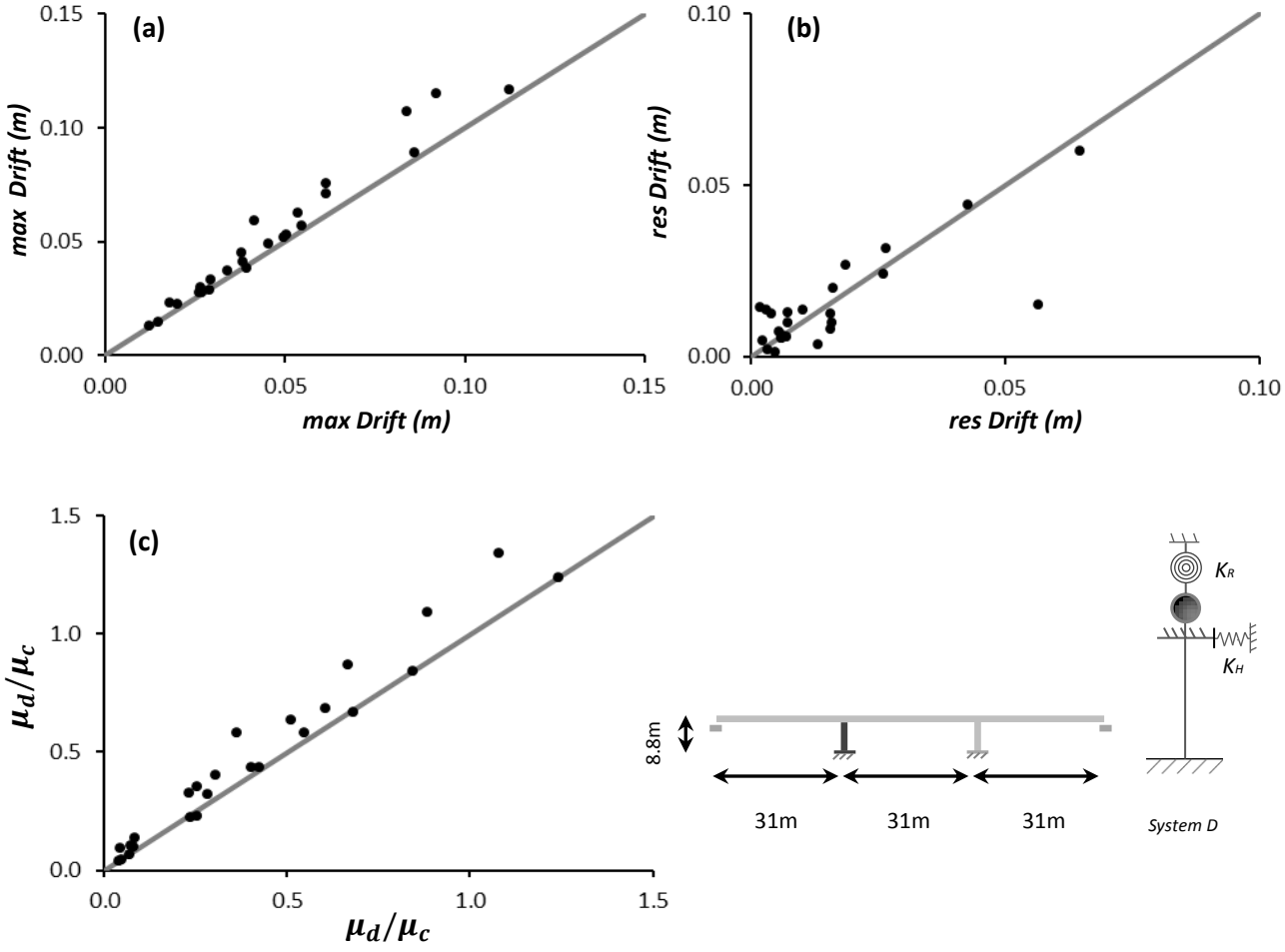

Figure 5.14 (a), (b), (c) Deviations in terms of *max Drift* , *residual Drift* and $\mu_{demand}/\mu_{capacity}$ between bridge's pier and system C (longitudinal direction)

μd<μc	*max Drift (m)*	*Drift res (m)*	*μ demand*	*μ d / μ c*
max	0.02	0.04	2.97	0.26
average	0.01	0.01	0.78	0.07

Table 5.9 Deviations between bridge's pier and system D

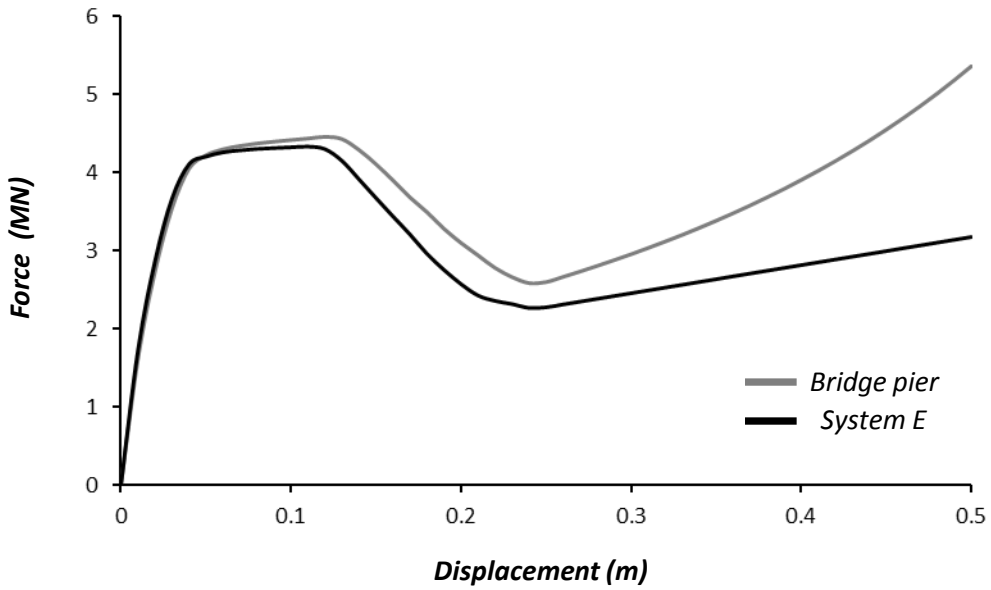

Figure 5.15 Force-Displacement curve from Pushover analysis for Bridge Pier and System E

	SEISMIC PERFORMANCE					
	max Drift (m)	*maxDrift ratio (%)*	*Drift res (m)*	*Drift res ratio(%)*	*μ demand*	*μ d / μ c*
JMA_090	0.10	1.13	0.02	0.20	11.44	1.00
MNSA	0.01	0.14	0.01	0.08	0.42	0.04
KALAMATA	0.04	0.43	0.01	0.16	2.51	0.22
TCU68NS	0.02	0.21	0.01	0.08	0.72	0.06
SYLMAR_360	0.06	0.70	0.03	0.36	7.76	0.68
JMA_000	0.12	1.33	0.02	0.20	14.07	1.23
TAKARAZUKA_090	0.05	0.62	0.03	0.32	6.09	0.53
PYRGOS	0.03	0.31	0.01	0.07	1.05	0.09
AEGIO	0.05	0.58	0.01	0.07	4.72	0.41
LEFKADA_2003	0.11	1.29	0.01	0.07	14.99	1.31
LEFKADA_1973	0.05	0.55	0.01	0.09	3.55	0.31
TCU52EW	0.03	0.32	0.01	0.07	1.05	0.09
TCU52NS	0.02	0.24	0.00	0.01	0.74	0.07
TCU68EW	0.08	0.96	0.06	0.66	9.32	0.82
RINALDI_318	0.03	0.35	0.00	0.05	3.79	0.33
JENSEN_022	0.04	0.41	0.02	0.20	3.49	0.31
SYLMAR_090	0.07	0.83	0.05	0.54	9.25	0.81
DUZE_000	0.04	0.46	0.01	0.14	4.57	0.40
YARIMCA_060	0.05	0.55	0.00	0.02	6.87	0.60
YARIMCA_330	0.01	0.16	0.00	0.04	0.46	0.04
SAKARYA	0.04	0.46	0.01	0.11	3.90	0.34
LUCERNE_000	0.03	0.31	0.00	0.00	2.54	0.22
IV#04_140	0.03	0.31	0.00	0.01	1.36	0.12
IV#04_230	0.05	0.62	0.03	0.34	5.84	0.51
DUCE_090	0.07	0.77	0.01	0.06	6.69	0.59

Table 5.10 Seismic performance of system E

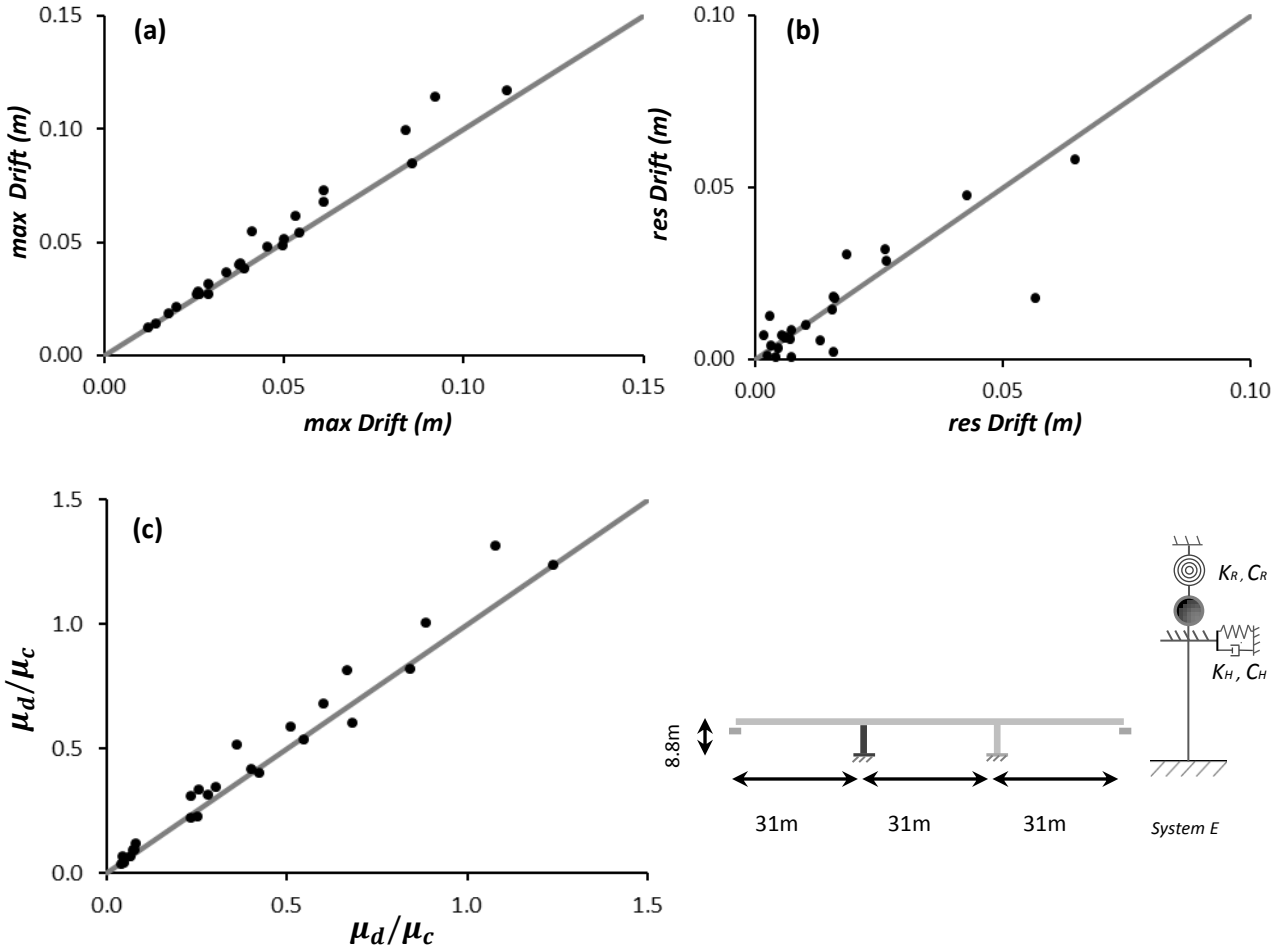

Figure 5.16 (a), (b), (c) Deviations in terms of *max Drift* , *residual Drift* and $\mu_{demand}/\mu_{capacity}$ between bridge's pier and system E (longitudinal direction)

μd < μc	*max Drift (m)*	*Drift res (m)*	*μ demand*	*μ d / μ c*
max	0.02	0.04	1.70	0.15
average	0.00	0.01	0.53	0.05

Table 5.11 Deviations between bridge's pier and system E

	SEISMIC PERFORMANCE					
	max Drift (m)	*maxDrift ratio (%)*	*Drift res (m)*	*Drift res ratio(%)*	*μ demand*	*μ d / μ c*
JMA_090	0.10	1.15	0.02	0.27	13.34	1.17
MNSA	0.01	0.16	0.00	0.03	0.25	0.02
KALAMATA	0.05	0.60	0.01	0.12	4.30	0.38
TCU68NS	0.06	0.63	0.00	0.05	4.60	0.40
SYLMAR_360	0.08	0.88	0.02	0.27	6.08	0.53
JMA_000	0.14	1.61	0.06	0.63	18.12	1.59
TAKARAZUKA_090	0.06	0.73	0.01	0.08	5.76	0.51
PYRGOS	0.02	0.25	0.00	0.04	0.57	0.05
AEGIO	0.05	0.54	0.02	0.26	3.02	0.26
LEFKADA_2003	0.05	0.53	0.01	0.07	6.37	0.56
LEFKADA_1973	0.06	0.71	0.01	0.14	4.70	0.41
TCU52EW	0.05	0.52	0.00	0.01	3.43	0.30
TCU52NS	0.11	1.20	0.03	0.29	13.92	1.22
TCU68EW	0.08	0.95	0.01	0.11	7.04	0.62
RINALDI_318	0.06	0.73	0.02	0.23	6.84	0.60
JENSEN_022	0.09	0.97	0.00	0.02	12.46	1.09
SYLMAR_090	0.09	1.02	0.02	0.26	11.69	1.03
DUZE_000	0.04	0.50	0.01	0.12	3.45	0.30
YARIMCA_060	0.07	0.78	0.01	0.10	9.21	0.81
YARIMCA_330	0.04	0.46	0.01	0.11	2.70	0.24
SAKARYA	0.05	0.55	0.00	0.03	4.05	0.36
LUCERNE_000	0.04	0.43	0.00	0.01	2.47	0.22
IV#04_140	0.04	0.46	0.00	0.03	3.72	0.33
IV#04_230	0.08	0.93	0.02	0.17	7.78	0.68
DUCE_090	0.09	1.04	0.01	0.16	9.86	0.86

Table 5.12 Seismic performance of pier of bridge A01_TE20 in transverse direction

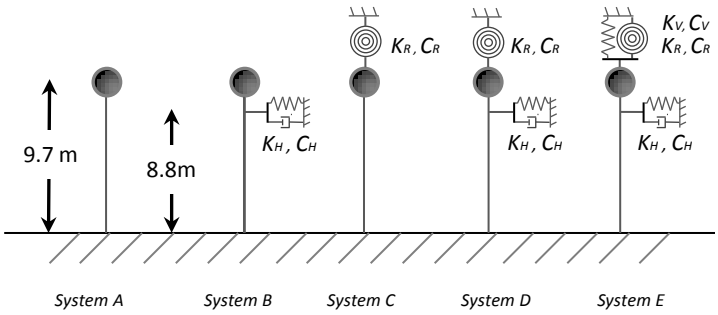

Figure 5.17 Five systems examined

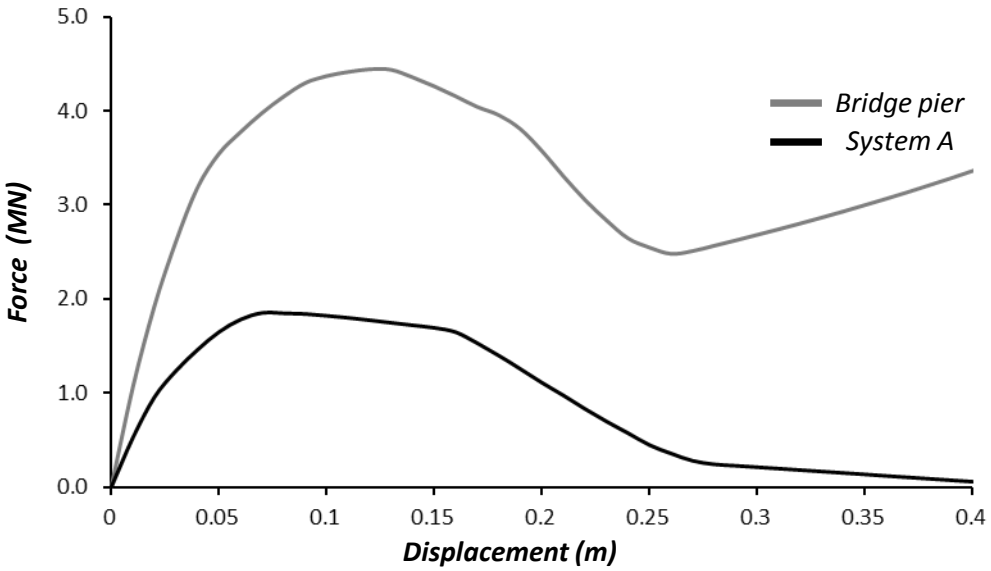

Figure 5.18 Force-Displacement curve from Pushover analysis for Bridge Pier and System A

	SEISMIC PERFORMANCE					
	max Drift (m)	***maxDrift ratio (%)***	***Drift res (m)***	***Drift res ratio(%)***	***μ demand***	***μ d / μ c***
JMA_090	0.09	1.03	0.07	0.85	9.08	0.80
MNSA	0.03	0.36	0.01	0.11	0.58	0.05
KALAMATA	0.08	0.94	0.08	0.93	5.02	0.44
TCU68NS	8.69	98.70	8.60	97.78	6130.60	537.77
SYLMAR_360	0.12	1.40	0.07	0.79	8.09	0.71
JMA_000	0.08	0.92	0.08	0.87	10.28	0.90
TAKARAZUKA_090	0.12	1.32	0.09	1.01	12.05	1.06
PYRGOS	0.02	0.24	0.01	0.08	0.33	0.03
AEGIO	0.05	0.59	0.00	0.02	0.98	0.09
LEFKADA_2003	0.74	8.39	0.74	8.39	90.85	7.97
LEFKADA_1973	0.06	0.70	0.02	0.23	3.28	0.29
TCU52EW	8.69	98.70	7.91	89.93	5938.66	520.94
TCU52NS	8.68	98.69	8.67	98.52	6031.81	529.11
TCU68EW	8.68	98.69	7.82	88.87	5993.58	525.75
RINALDI_318	0.16	1.84	0.16	1.84	19.05	1.67
JENSEN_022	8.69	98.70	6.46	73.45	4380.22	384.23
SYLMAR_090	0.11	1.27	0.09	0.99	10.30	0.90
DUZE_000	0.06	0.64	0.01	0.14	5.67	0.50
YARIMCA_060	8.69	98.69	8.04	91.34	5924.78	519.72
YARIMCA_330	0.09	1.00	0.08	0.93	5.41	0.47
SAKARYA	0.10	1.13	0.08	0.94	10.62	0.93
LUCERNE_000	0.06	0.63	0.04	0.50	4.78	0.42
IV#04_140	0.06	0.72	0.02	0.21	3.31	0.29
IV#04_230	8.68	98.69	2.69	30.61	6045.00	530.26
DUCE_090	0.17	1.95	0.17	1.95	21.67	1.90

Table 5.13 Seismic performance of system A

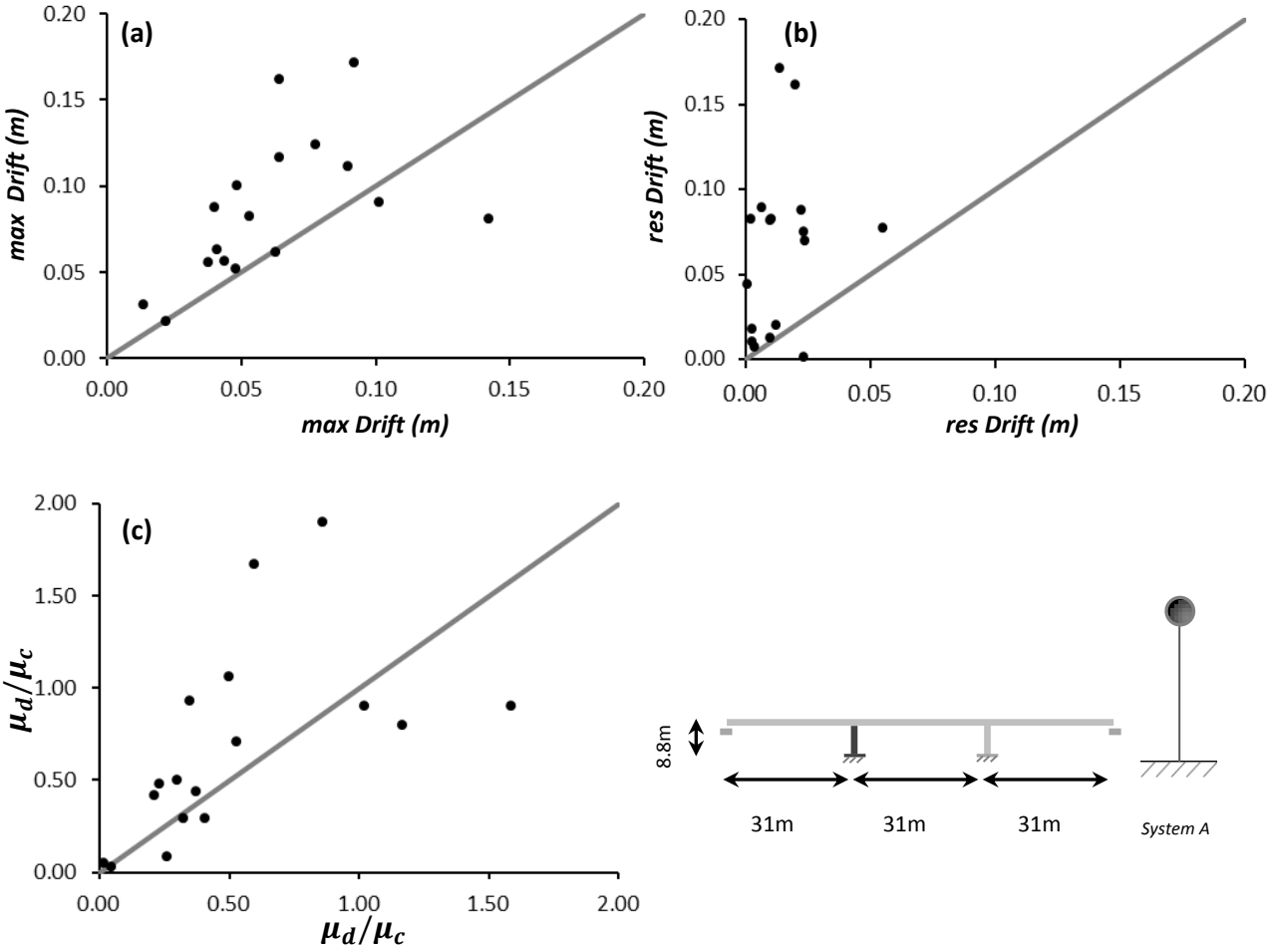

Figure 5.19 (a), (b), (c) Deviations in terms of *max Drift* , *residual Drift* and $\mu_{demand}/\mu_{capacity}$ between bridge's pier and system A (transverse direction)

μd < μc	*max Drift (m)*	*Drift res (m)*	*μ demand*	*μ d / μ c*
max	8.64	8.64	6126.01	537.37
average	2.46	2.07	1621.42	142.23

Table 5.14 Deviations between bridge's pier and system A

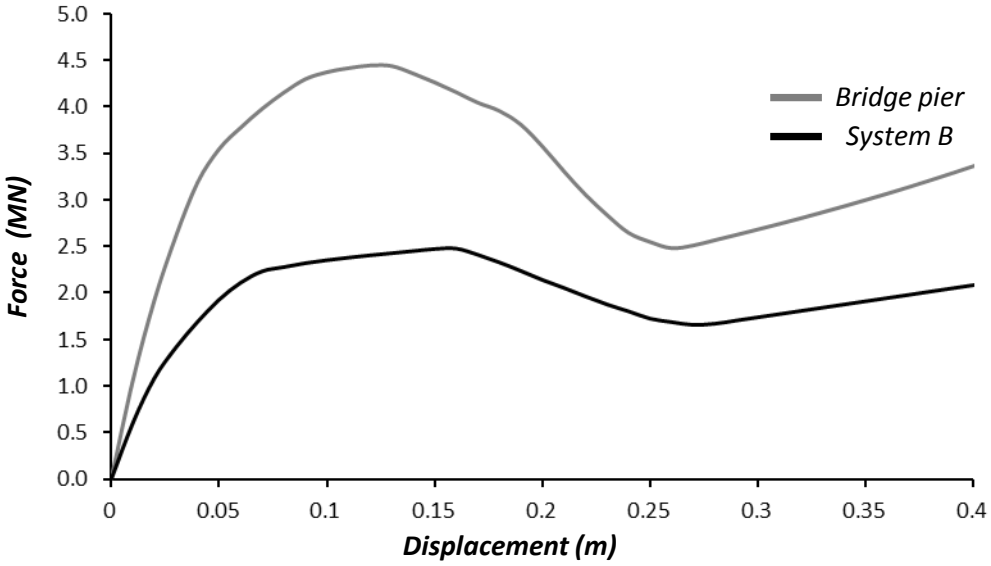

Figure 5.20 Force-Displacement curve from Pushover analysis for Bridge Pier and System B

	SEISMIC PERFORMANCE					
	max Drift (m)	***maxDrift ratio (%)***	***Drift res (m)***	***Drift res ratio(%)***	***μ demand***	***μ d / μ c***
JMA_090	0.07	0.83	0.00	0.02	5.75	0.50
MNSA	0.03	0.31	0.02	0.17	0.51	0.04
KALAMATA	0.06	0.72	0.04	0.46	2.67	0.23
TCU68NS	0.28	3.19	0.01	0.06	36.90	3.24
SYLMAR_360	0.12	1.37	0.00	0.05	18.40	1.61
JMA_000	0.09	0.98	0.00	0.02	12.01	1.05
TAKARAZUKA_090	0.15	1.69	0.04	0.45	17.25	1.51
PYRGOS	0.02	0.25	0.00	0.00	0.32	0.03
AEGIO	0.05	0.58	0.02	0.17	0.95	0.08
LEFKADA_2003	0.09	1.00	0.03	0.30	8.26	0.72
LEFKADA_1973	0.06	0.70	0.00	0.02	3.33	0.29
TCU52EW	0.48	5.43	0.01	0.12	61.05	5.36
TCU52NS	0.37	4.22	0.03	0.32	45.27	3.97
TCU68EW	0.35	4.00	0.01	0.12	46.28	4.06
RINALDI_318	0.13	1.44	0.03	0.30	14.72	1.29
JENSEN_022	0.15	1.68	0.01	0.08	21.82	1.91
SYLMAR_090	0.10	1.09	0.04	0.45	7.40	0.65
DUZE_000	0.06	0.67	0.01	0.09	6.01	0.53
YARIMCA_060	0.24	2.74	0.02	0.22	27.47	2.41
YARIMCA_330	0.08	0.96	0.03	0.32	4.69	0.41
SAKARYA	0.10	1.10	0.01	0.07	9.93	0.87
LUCERNE_000	0.06	0.68	0.01	0.08	4.97	0.44
IV#04_140	0.05	0.59	0.00	0.01	2.70	0.24
IV#04_230	0.45	5.15	0.00	0.00	57.39	5.03
DUCE_090	0.10	1.10	0.00	0.00	10.89	0.95

Table 5.15 Seismic performance of system B

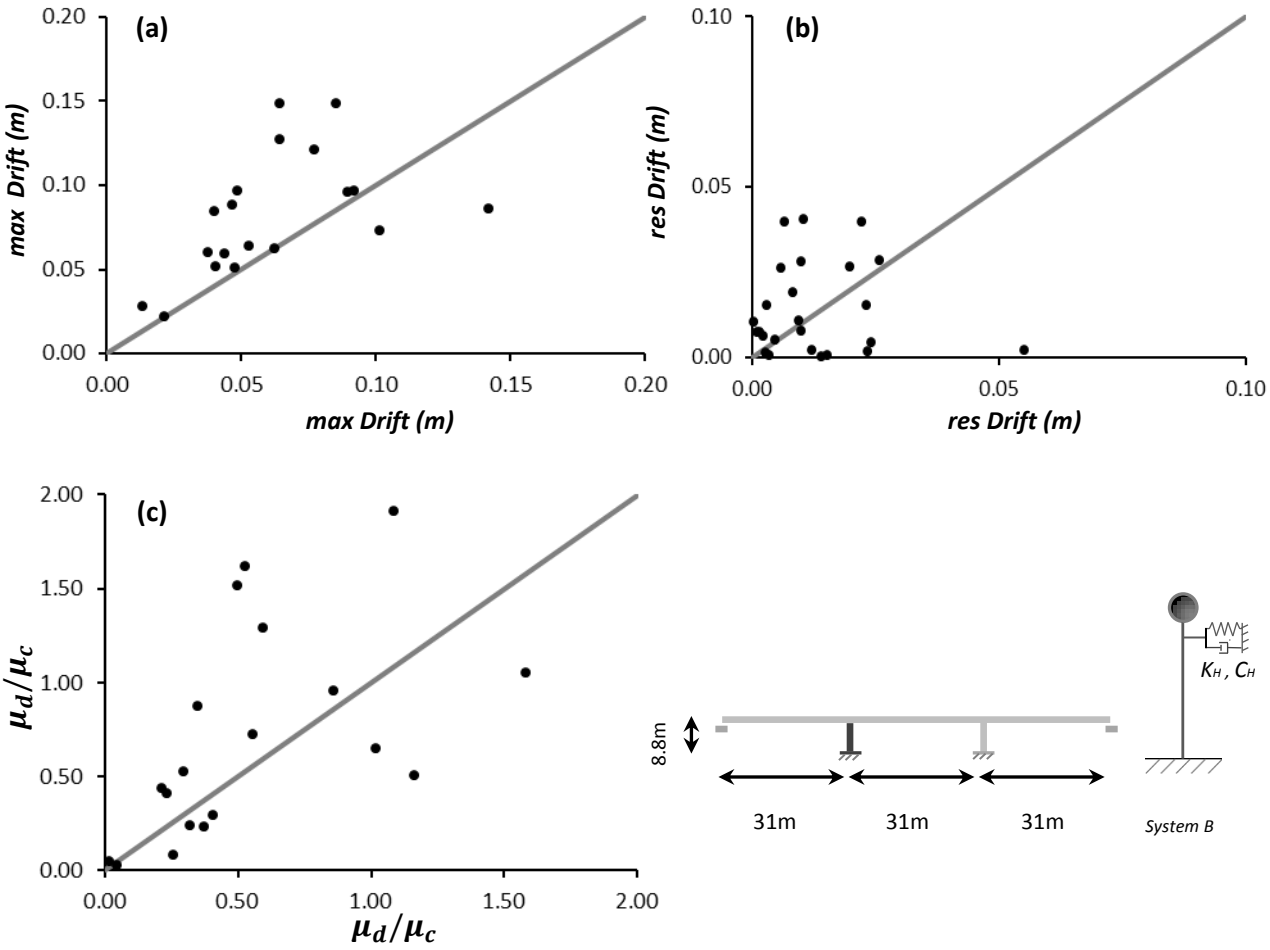

Figure 5.21 (a), (b), (c) Deviations in terms of *max Drift* , *residual Drift* and $\mu_{demand}/\mu_{capacity}$ between bridge's pier and system B (transverse direction)

μd < μc	*max Drift (m)*	*Drift res (m)*	*μ demand*	*μ d / μ c*
max	0.43	0.03	57.62	5.05
average	0.09	0.01	11.96	1.05

Table 5.16 Deviations between bridge's pier and system B

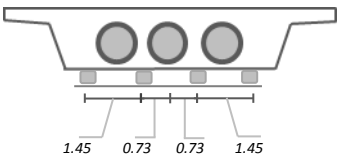

Figure 5.22 Actual position of bearings

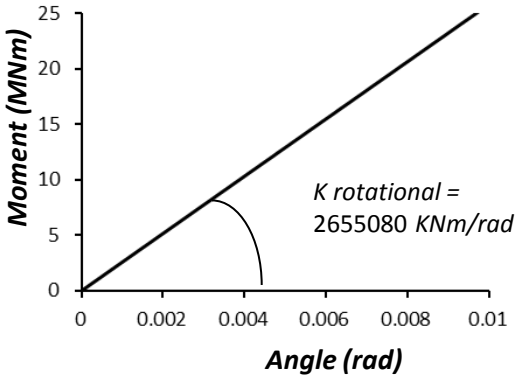

Figure 5.23 Rotational Pushover Moment-Angle curve

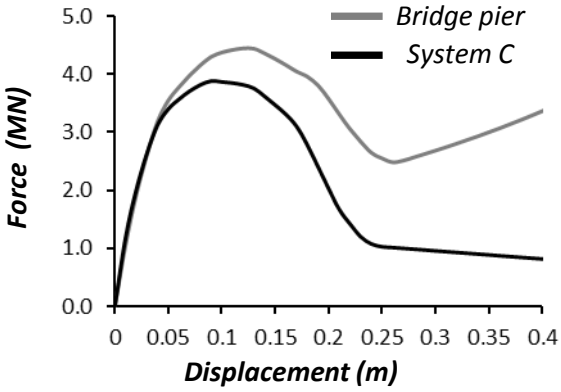

Figure 5.24 Force-Displacement curve from Pushover analysis for Bridge Pier and System C

	SEISMIC PERFORMANCE					
	max Drift (m)	***maxDrift ratio (%)***	***Drift res (m)***	***Drift res ratio(%)***	***μ demand***	***μ d / μ c***
JMA_090	0.11	1.26	0.04	0.41	14.47	1.27
MNSA	0.01	0.15	0.00	0.02	0.25	0.02
KALAMATA	0.07	0.82	0.02	0.18	6.55	0.57
TCU68NS	0.04	0.43	0.02	0.22	3.38	0.30
SYLMAR_360	0.07	0.76	0.02	0.27	5.47	0.48
JMA_000	0.17	1.94	0.10	1.08	21.85	1.92
TAKARAZUKA_090	0.05	0.56	0.00	0.05	4.52	0.40
PYRGOS	0.03	0.33	0.01	0.09	1.18	0.10
AEGIO	0.05	0.62	0.00	0.04	3.86	0.34
LEFKADA_2003	0.05	0.62	0.01	0.12	6.40	0.56
LEFKADA_1973	0.07	0.74	0.00	0.04	4.96	0.43
TCU52EW	0.04	0.48	0.01	0.11	2.71	0.24
TCU52NS	0.09	0.99	0.02	0.24	10.75	0.94
TCU68EW	0.08	0.87	0.01	0.07	6.04	0.53
RINALDI_318	0.06	0.64	0.01	0.07	6.19	0.54
JENSEN_022	0.08	0.93	0.00	0.05	11.56	1.01
SYLMAR_090	0.05	0.60	0.00	0.05	5.68	0.50
DUZE_000	0.05	0.54	0.00	0.02	3.29	0.29
YARIMCA_060	0.08	0.92	0.02	0.20	11.03	0.97
YARIMCA_330	0.03	0.36	0.00	0.04	1.58	0.14
SAKARYA	0.04	0.47	0.01	0.15	2.68	0.24
LUCERNE_000	0.04	0.46	0.01	0.13	1.97	0.17
IV#04_140	0.04	0.50	0.01	0.09	1.91	0.17
IV#04_230	0.06	0.72	0.01	0.15	5.29	0.46
DUCE_090	0.08	0.87	0.02	0.18	7.54	0.66

Table 5.17 Seismic performance of system C

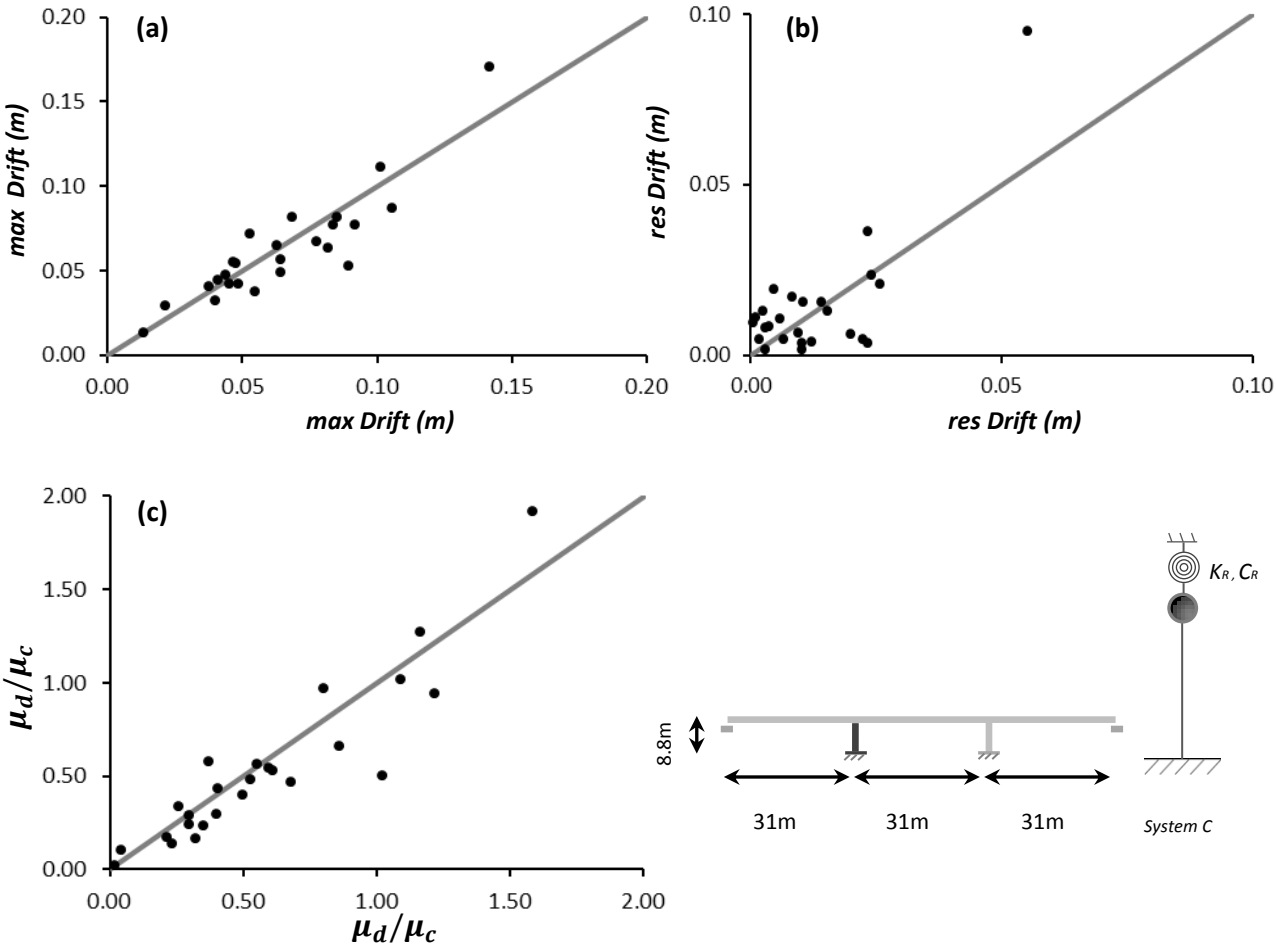

Figure 5.25 (a), (b), (c) Deviations in terms of *max Drift* , *residual Drift* and $\mu_{demand}/\mu_{capacity}$ between bridge's pier and system C (transverse direction)

μd < μc	*max Drift (m)*	*Drift res (m)*	*μ demand*	*μ d / μ c*
max	0.04	0.02	6.01	0.53
average	0.01	0.01	1.37	0.12

Table 5.18 Deviations between bridge's pier and system C

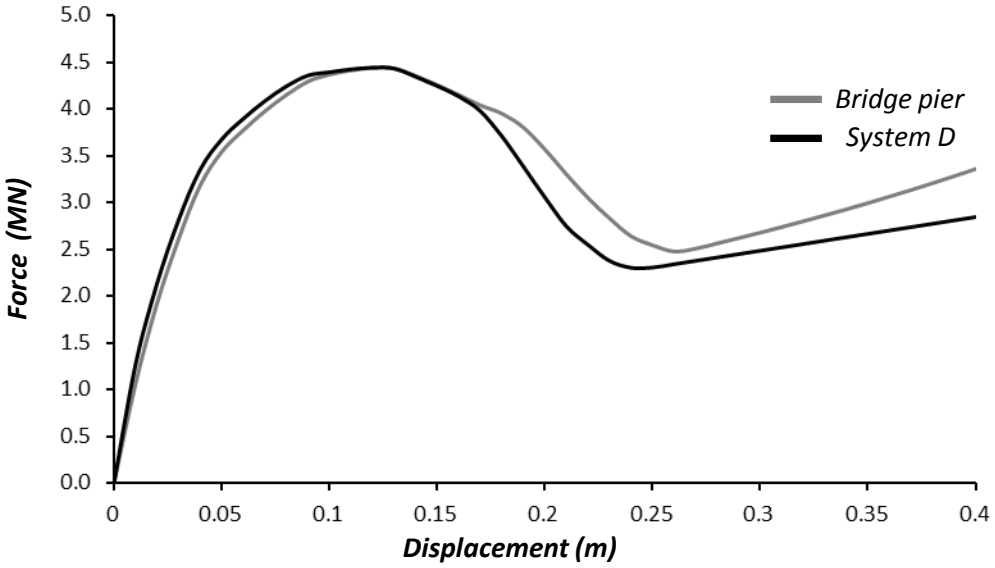

Figure 5.26 Force-Displacement curve from Pushover analysis for Bridge Pier and System D

	SEISMIC PERFORMANCE					
	max Drift (m)	***maxDrift ratio (%)***	***Drift res (m)***	***Drift res ratio(%)***	***μ demand***	***μ d / μ c***
JMA_090	0.10	1.17	0.02	0.26	13.54	1.19
MNSA	0.01	0.15	0.00	0.02	0.25	0.02
KALAMATA	0.07	0.79	0.01	0.17	6.15	0.54
TCU68NS	0.04	0.47	0.01	0.09	2.84	0.25
SYLMAR_360	0.08	0.86	0.02	0.27	7.32	0.64
JMA_000	0.16	1.78	0.00	0.04	19.99	1.75
TAKARAZUKA_090	0.06	0.71	0.00	0.03	5.66	0.50
PYRGOS	0.03	0.32	0.01	0.16	0.89	0.08
AEGIO	0.05	0.62	0.01	0.08	3.93	0.34
LEFKADA_2003	0.05	0.57	0.00	0.05	7.29	0.64
LEFKADA_1973	0.07	0.77	0.01	0.13	5.43	0.48
TCU52EW	0.04	0.46	0.01	0.16	3.13	0.27
TCU52NS	0.10	1.17	0.03	0.34	13.26	1.16
TCU68EW	0.08	0.89	0.00	0.02	6.35	0.56
RINALDI_318	0.06	0.72	0.01	0.12	7.16	0.63
JENSEN_022	0.10	1.18	0.01	0.13	15.46	1.36
SYLMAR_090	0.09	1.01	0.02	0.27	11.88	1.04
DUZE_000	0.05	0.53	0.00	0.04	3.78	0.33
YARIMCA_060	0.08	0.92	0.01	0.12	10.84	0.95
YARIMCA_330	0.04	0.47	0.00	0.05	2.83	0.25
SAKARYA	0.04	0.50	0.01	0.12	3.88	0.34
LUCERNE_000	0.04	0.48	0.00	0.03	3.06	0.27
IV#04_140	0.05	0.53	0.00	0.01	2.84	0.25
IV#04_230	0.08	0.91	0.02	0.23	7.66	0.67
DUCE_090	0.09	1.00	0.01	0.12	9.31	0.82

Table 5.19 Seismic performance of system D

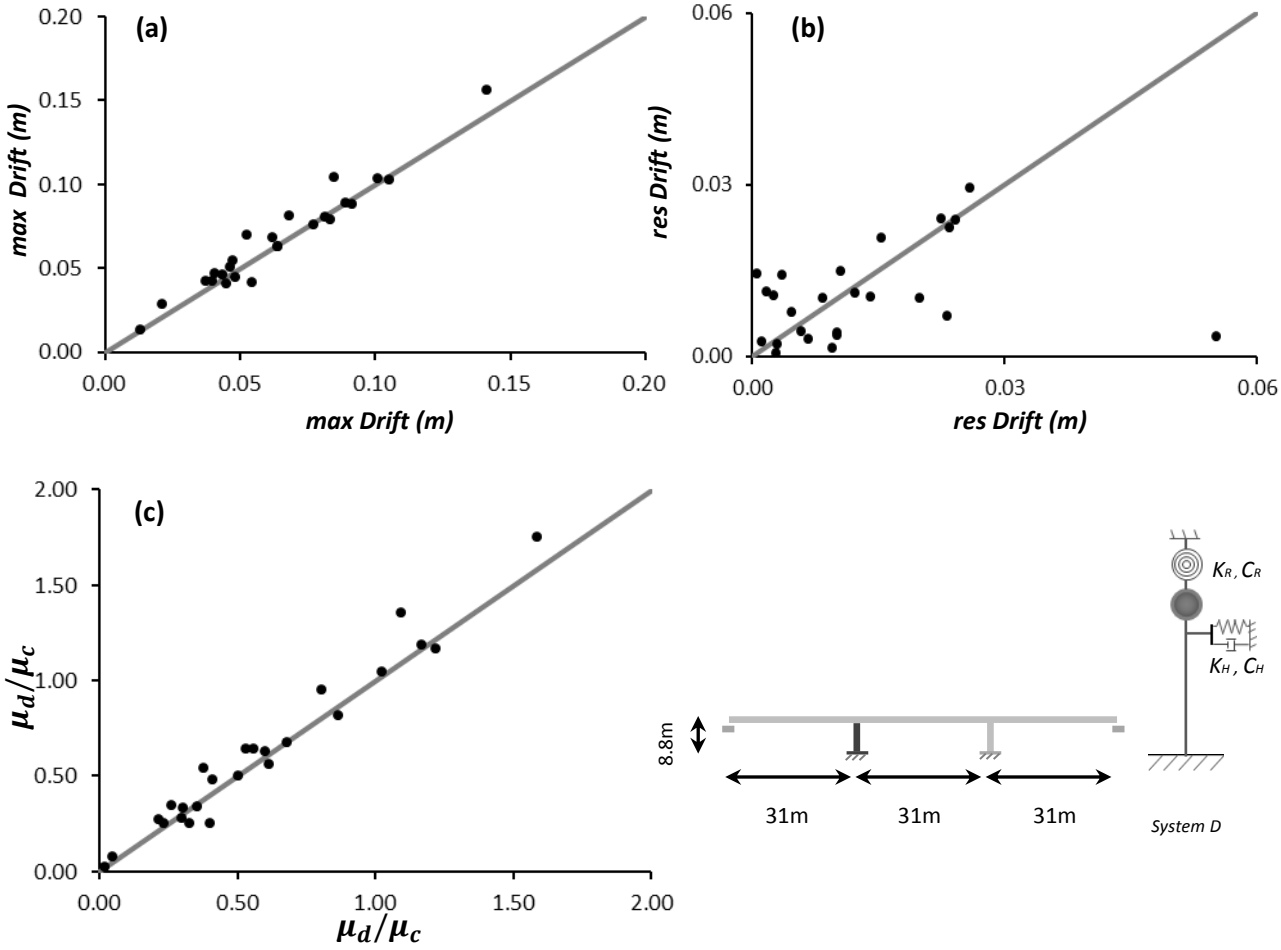

Figure 5.27 (a), (b), (c) Deviations in terms of *max Drift* , *residual Drift* and $\mu_{demand}/\mu_{capacity}$ between bridge's pier and system D (transverse direction)

$\mu d < \mu c$	*max Drift (m)*	*Drift res (m)*	*μ demand*	*μ d / μ c*
max	0.02	0.02	1.85	0.16
average	0.01	0.01	0.68	0.06

Table 5.20 Deviations between bridge's pier and system D

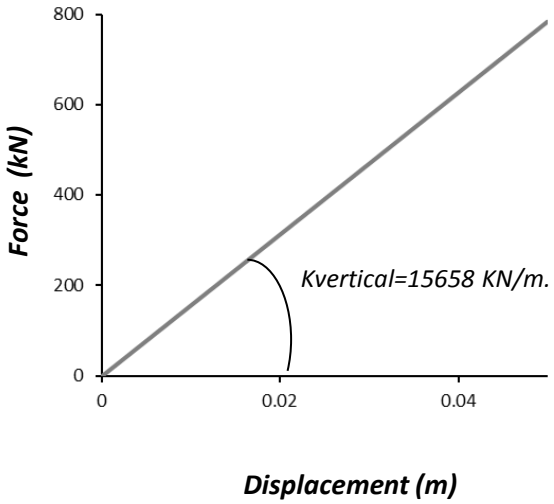

Figure 5.28 Force-Displacement curve from vertical Pushover analysis for Bridge A01_TE20

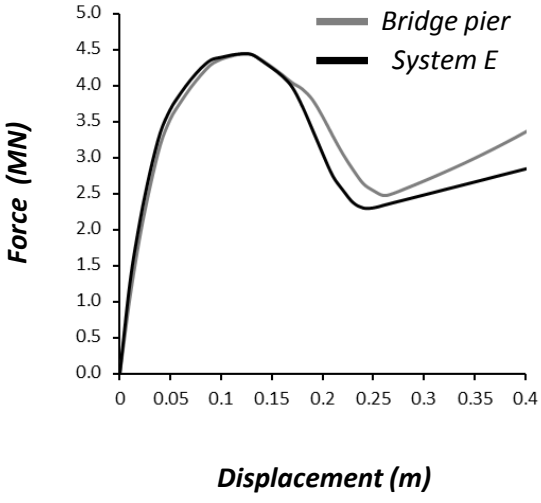

Figure 5.29 Force-Displacement curve from Pushover analysis for Bridge Pier and System E

	SEISMIC PERFORMANCE					
	max Drift (m)	*maxDrift ratio (%)*	*Drift res (m)*	*Drift res ratio(%)*	*μ demand*	*μ d / μ c*
JMA_090	0.10	1.18	0.02	0.26	13.57	1.19
MNSA	0.01	0.15	0.00	0.02	0.25	0.02
KALAMATA	0.07	0.79	0.02	0.17	6.19	0.54
TCU68NS	0.04	0.47	0.01	0.09	2.84	0.25
SYLMAR_360	0.08	0.86	0.02	0.27	7.32	0.64
JMA_000	0.16	1.77	0.00	0.04	19.94	1.75
TAKARAZUKA_090	0.06	0.72	0.00	0.04	5.74	0.50
PYRGOS	0.03	0.32	0.01	0.16	0.89	0.08
AEGIO	0.05	0.62	0.01	0.08	3.93	0.34
LEFKADA_2003	0.05	0.57	0.00	0.05	7.36	0.65
LEFKADA_1973	0.07	0.77	0.01	0.12	5.43	0.48
TCU52EW	0.04	0.46	0.01	0.16	3.13	0.27
TCU52NS	0.10	1.17	0.03	0.34	13.27	1.16
TCU68EW	0.08	0.90	0.00	0.02	6.35	0.56
RINALDI_318	0.06	0.72	0.01	0.12	7.16	0.63
JENSEN_022	0.10	1.18	0.01	0.13	15.45	1.36
SYLMAR_090	0.09	1.01	0.02	0.28	11.88	1.04
DUZE_000	0.05	0.53	0.00	0.04	3.76	0.33
YARIMCA_060	0.08	0.93	0.01	0.12	11.02	0.97
YARIMCA_330	0.04	0.48	0.00	0.04	2.84	0.25
SAKARYA	0.04	0.50	0.01	0.12	3.87	0.34
LUCERNE_000	0.04	0.48	0.00	0.03	3.06	0.27
IV#04_140	0.05	0.53	0.00	0.00	2.81	0.25
IV#04_230	0.08	0.91	0.02	0.23	7.65	0.67
DUCE_090	0.09	1.00	0.01	0.12	9.31	0.82

Table 5.21 Seismic performance of system E

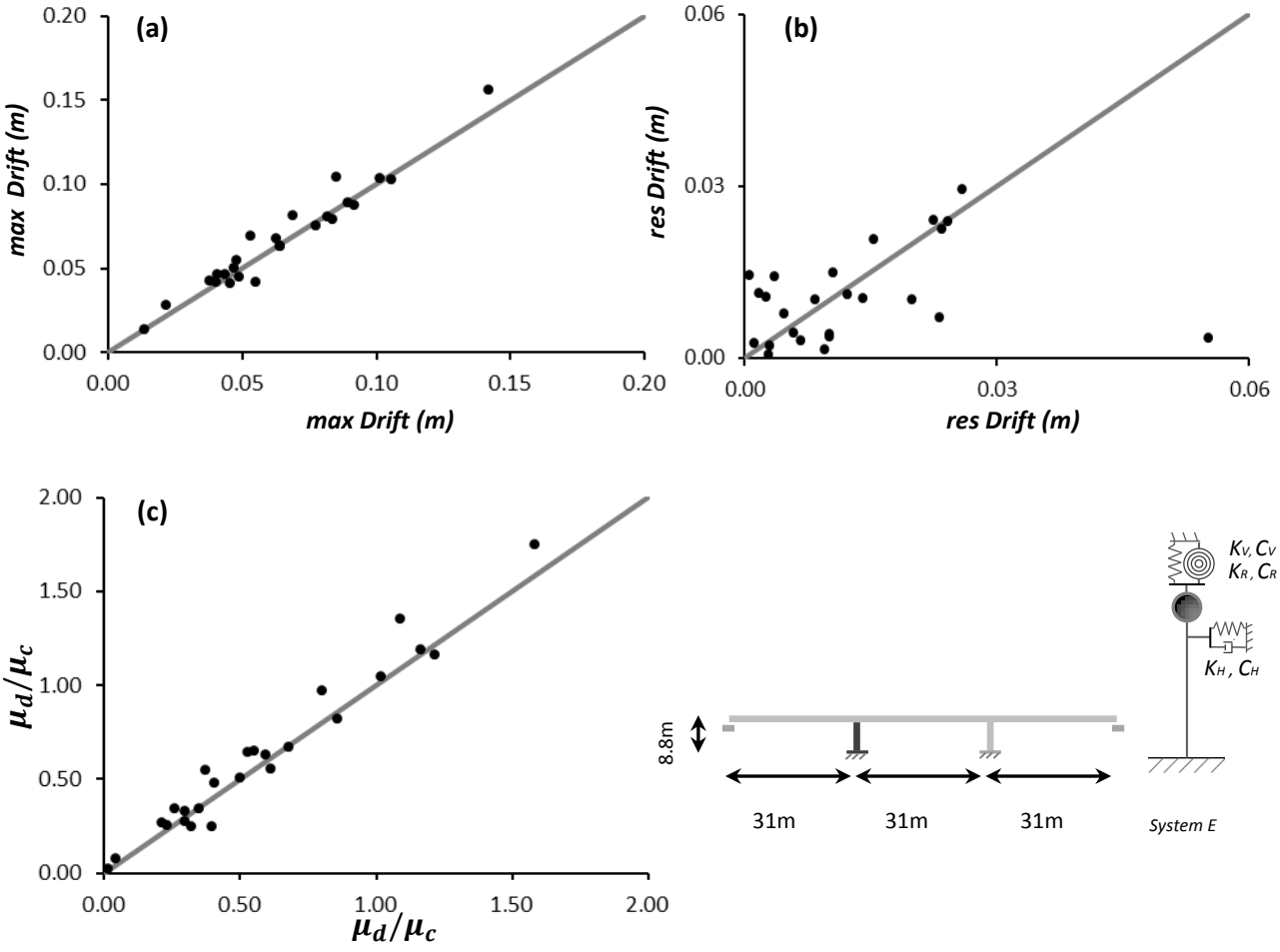

Figure 5.30 (a), (b), (c) Deviations in terms of *max Drift* , *residual Drift* and $\mu_{demand}/\mu_{capacity}$ between bridge's pier and system E (transverse direction)

μd < μc	*max Drift (m)*	*Drift res (m)*	*μ demand*	*μ d / μ c*
max	0.02	0.02	1.89	0.17
average	0.01	0.01	0.69	0.06

Table 5.22 Deviations between bridge's pier and system E

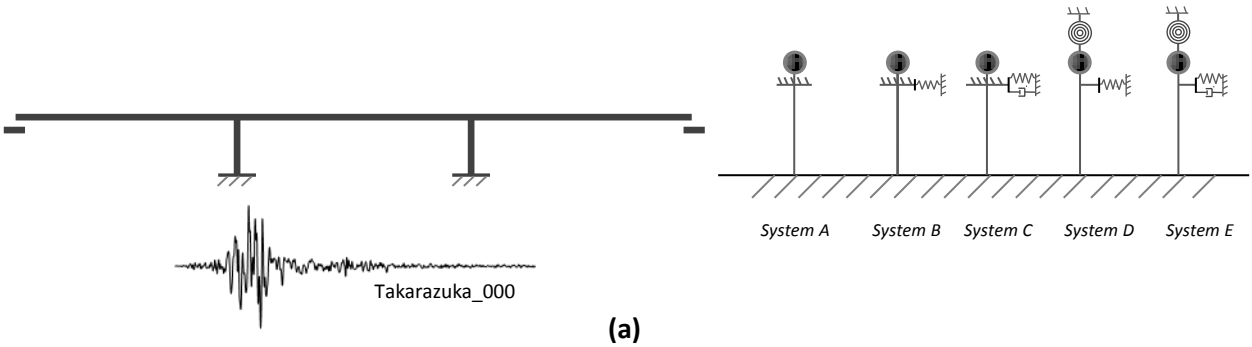

(a)

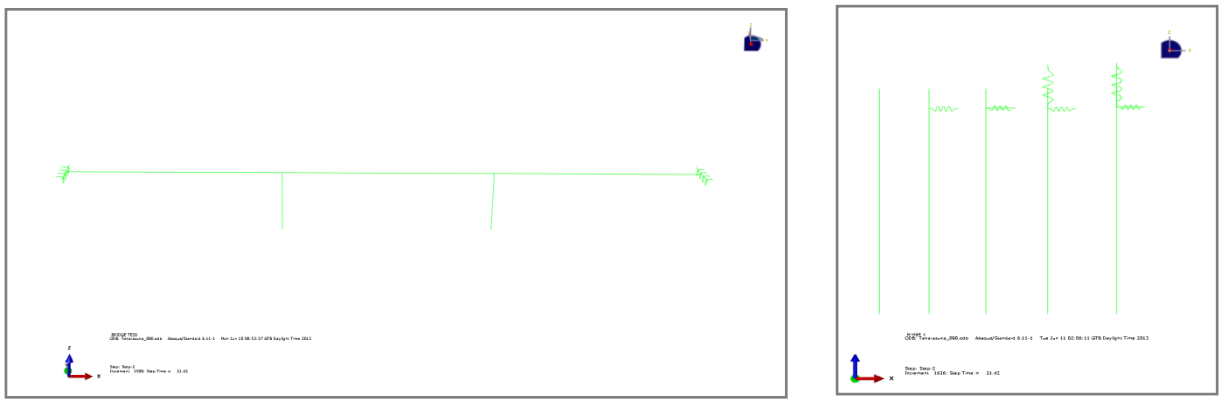

(b)

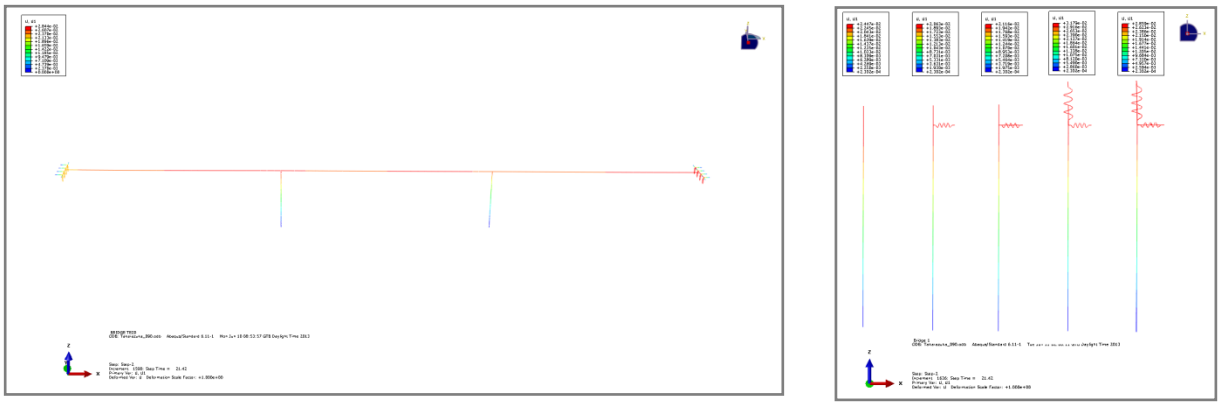

(c)

Figure 5.31 (a),(b) Systems compared in ABAQUS code in longitudinal direction **(c)** Deformed shape for Takarazuka_000 record

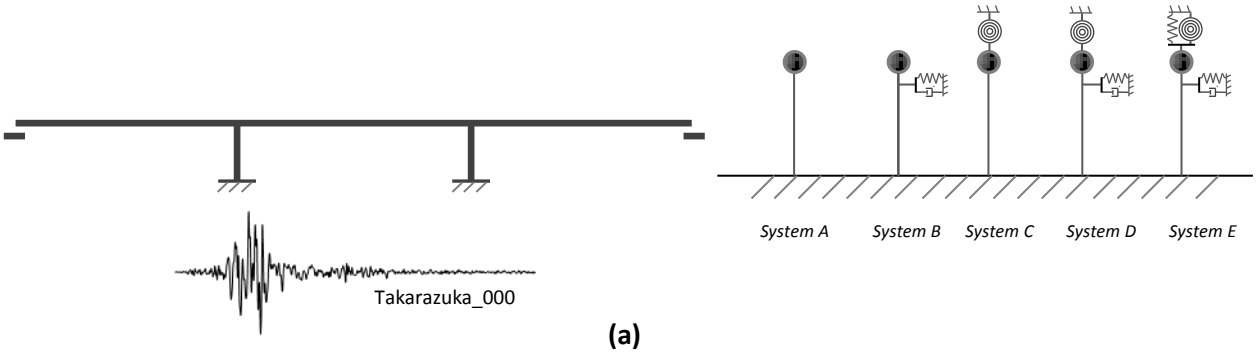

(a)

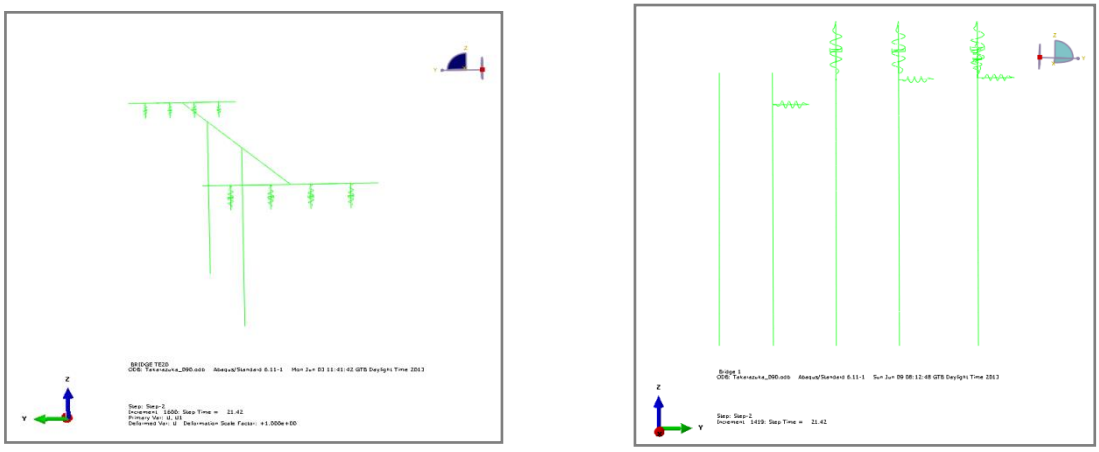

(b)

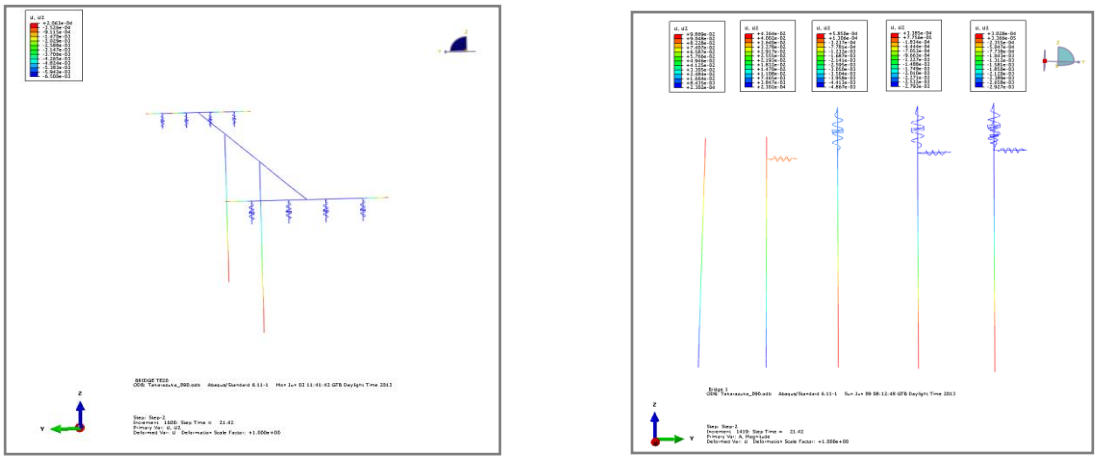

(c)

Figure 5.32 (a),(b) Systems compared in ABAQUS code in transverse direction **(c)** Deformed shape for Takarazuka_000 record (scaled by PGA 50%)

CHAPTER 6

DEVELOPMENT OF 3D MODEL

EFFECT OF SOIL-STRUCTURE INTERACTION

6.1 Development of 3D model

In the previous chapter the impact of the various components of a bridge on its seismic performance was examined and simple models were developed to describe the seismic performance of a whole bridge both in longitudinal and transverse direction. However in all the previous analyses the base of the piers was considered fixed so as the connection of the bearings to the abutments. In this way the effect of soil-structure interaction (SSI) was ignored so as the impact of the retaining walls and the embankments at the abutments to the performance of the whole bridge system. In this chapter a three-dimensional analytical model of the whole bridge system (soil, footings, piers, deck, bearings, retaining walls, access embankments) is generated (Figure 6.1) in order to examine the effect of the previous factors and to develop if necessary new simple models that take into account all the above.

6.1.1 Modeling bridge's deck and piers

The bridge selected was the A01_TE20 bridge of the Greek Metropolitan Motorway ''ATTIKI ODOS'' the same that was used at the previous analyses in order to compare the results. The reason that led to this choice at the first place was that it is a simple and at the same time common case. Its simplicity lies in the symmetry of the bridge and the circular section of the piers. Also each pier consists of a single column which is monolithically connected to the deck while there are bearings at the abutments. The model of the bridge used is the same and is described in detail at chapter 5.

6.1.2 Modeling bridge's footings

Unlike the approach of chapter 5 that the base of the bridge's piers is considered fixed, in this chapter the soil-foundation system is taken into account. The piers of the bridge are connected at their base to a shallow foundation. More specific a square footing of 8 m width and 2 m height is

considered for the base of each pier which was taken from the examined bridge plans. The footings of the piers are modeled in the finite element code ABAQUS using elastic (8-node) continuum elements (C3D8) and are shown in Figure 6.2 (c).

6.1.3 Modeling retaining walls at the abutments

The abutments of the bridge system consist of retaining walls that retain the access embankments, the exact dimensions of which were taken from the examined bridge plans. More specific each wall is of 9 m height and 1.5 m thickness. It is also connected to two side walls of 0.6 m thickness that retain the sides of the embankment. In addition each wall is founded on a rectangular footing of 7 m x 10.4 m and 1.5 m height. Both the retaining walls of the abutments and their footings are modeled in the finite element code ABAQUS using elastic (8-node) continuum elements (C3D8) and are shown in Figure 6.2 (b). The only component of the constructed bridge of Attiki Odos that has not been modeled is the stoppers at the abutments. The reason for this choice is that their impact on the seismic performance of the bridge is dominant and as a result the effect of the rest structural components cannot be examined properly.

6.1.4 Modeling subject soil and embankments

The main objective of this chapter is to examine the effect of soil-structure interaction on the seismic performance of a certain bridge. As a result it is necessary to model the soil subject to the bridge as well as the soil of the embankments at its abutments. For this purpose an idealized homogeneous 20 m stiff clay layer, of undrained shear strength Su=150 kPa is used which is representative soil conditions for which a surface foundation would be a realistic solution. The properties of the soil used are shown on Figure 6.3. The same stiff clay is also used for the embankments, which is not a very realistic approach but it is not of great importance for our purpose. The subject soil and the soil of the embankments are modeled in the finite element code ABAQUS using nonlinear (8-node) continuum elements (C3D8) and are shown in Figure 6.2 (a).

- **Soil behavior**

Soil behavior is modeled through a nonlinear kinematic hardening constitutive model, with a Von Mises failure criterion and associated plastic flow rule (Anastasopoulos et al., 2011). According to the Von Mises failure criterion, the evolution of stresses is described by the relation:

$$\sigma = \sigma_0 + \alpha \quad (1)$$

where σ_0 is the value of stress at zero plastic strain, assumed to remain constant. The parameter α is the "backstress", which defines the kinematic evolution of the yield surface in the stress space. An associated plastic flow rule is assumed:

$$\dot{\varepsilon}^{pl} = \dot{\bar{\varepsilon}}^{pl} \frac{\partial F}{\partial \sigma} \quad (2)$$

where $\dot{\varepsilon}^{pl}$ is the plastic flow rate (obtained through the equivalent plastic work), $\dot{\bar{\varepsilon}}^{pl}$ the equivalent plastic strain rate, and *F* a function defining the pressure-independent yield surface:

$$F = f(\sigma - \alpha) - \sigma_0 \quad (3)$$

The evolution law of the model consists of two components: a nonlinear kinematic hardening component, which describes the translation of the yield surface in the stress space (defined through the backstress α), and an isotropic hardening component, which describes the change of the equivalent stress defining the size of the yield surface σ_0 as a function of plastic deformation. The kinematic hardening component is defined as an additive combination of a purely kinematic term (linear *Ziegler* hardening law) and a relaxation term (the *recall* term), which introduces the nonlinearity. The evolution of the kinematic component of the yield stress is described as follows:

$$\dot{\alpha} = C \frac{1}{\sigma_0} (\sigma - \alpha) \ - \gamma \alpha \quad (4)$$

where C the initial kinematic hardening modulus ($C = \sigma_y / \varepsilon_y = E$) and γ a parameter that determines the rate at which the kinematic hardening decreases with increasing plastic deformation. The evolution of the kinematic and the isotropic hardening components is illustrated in Figures 6.4 (a), (b) and c for unidirectional and multiaxial loading, respectively. The evolution law

for the kinematic hardening component implies that the backstress is contained within a cylinder of radius:

$$\sqrt{\frac{2}{3}a^s} = \sqrt{\frac{2}{3}\frac{C}{\gamma}} \quad (5)$$

where α^s is the magnitude of α at saturation. Since the yield surface remains bounded, this implies that any stress point must lie within a cylinder of radius $\sqrt{2/3}\,\sigma_y$. At large plastic strains, any stress point is contained within a cylinder of radius $\sqrt{2/3}\,(\alpha^s + \sigma^s)$ where σ^s is the equivalent stress defining the size of the yield surface at large plastic strain. The maximum yield stress (at saturation) is:

$$\sigma_y = \frac{C}{\gamma} + \sigma_0 \quad (6)$$

According to the Von Mises yield criterion this ultimate stress is:

$$\sigma_y = \sqrt{3}S_u \quad (7)$$

From Eqs. 6 and 7 we have:

$$\gamma = \frac{C}{\sqrt{3}S_u - \sigma_0} \quad (8)$$

Model parameters are calibrated (Anastasopoulos et al., 2011) to fit published G–γ curves of the literature, following the procedure described in Gerolymos & Gazetas (2005). Figure 6.4 (c) illustrates the validation of the kinematic hardening model (through simple shear finite element analysis) against published G–γ curves by Ishibashi and Zhang (1993).

- **Mesh of the soil model**

The final 3D model of the subject soil is of 155 m length, 40 m width and 20 m depth. The soil model is divided into three volumes: The first volume is a very fine mesh under both footings of 16 m (2B) length and width and 20 m (2.5B) depth, where B is the width of the footing. The elements of this volume are of 0.8 m length and width and 1 m height for the upper 10 m depth of the soil

model and of 2 m height for the rest 10 m depth of the first volume. The second volume is an also very fine mesh under the two embankments of the abutments of 37 m length, 16 m width and 20 m depth. The elements of this volume are of 1 m length, 0.92 m width and 1 m height for the upper 10 m depth of the soil model and of 2 m height for the rest 10 m depth of the second volume. The third volume contains the rest of the subject soil model and consists of cubic elements of 2 m length, width and height. As far as the soil of the embankments is concerned, a 3D soil model is also generated in the finite element code ABAQUS of 30 m length, 9.2 m width and 10.5 m depth for each embankment. The elements of this model are of 1 m length, 0.92 m width and 1 m height. The whole 3D soil model as generated in ABAQUS consists of about 50000 elements and is shown in figure 6.1.

- **Boundaries of the soil model**

The boundaries of the soil model are placed far enough from the bridge model in order not to affect the results of the analysis. In particular ''free-field'' boundaries responding as shear beams are placed at each lateral boundary of the subject soil model and of the embankments, to reproduce free-field conditions. In addition reflections at the base of the formation are avoided by utilizing absorbing boundaries. More specific dashpots are placed under the base of the soil model which damping coefficient is calculated by the following equation:

$$c_{base} = \rho * A * Vs$$

assuming the following parameters:

- ρ=1.6 Mgr/m³, the density of the clay layer
- A, the area of each element of the base
- Vs=255m/s, the shear wave velocity

Due to the fact that for the calculation of the damping coefficient of the dashpot you need to know the area of each element of the base, two different kind of dashpots are used, one for the very fine mesh where the area of each element of the base is A=0.64 m² and one for the rest of the soil base where the area of each element is A=4 m². The kind of dashpots used are node to node ones and

are connected to the nodes of the soil base and to some extra nodes defined which are placed 1 m lower from the soil base. All degree of freedoms of the latter are fixed, while at the nodes of the soil base only the vertical displacement degree of freedom is fixed. The seismic excitation is imposed at the fixed nodes of the dashpots of the soil base.

- **Soil-footing and retaining wall-embankment interfaces**

At the soil-footing and retaining wall-embankment interfaces contact elements are placed. The coefficient of friction at these interfaces is μ=0.7 that allows only small sliding of the foundation and the wall.

6.2 Effect of soil-structure interaction

6.2.1 Seismic performance of 3D model

The seismic performance of the 3D model of the entire bridge-soil system as developed in the finite element code ABAQUS was tested under nonlinear dynamic time history analysis using 3 real earthquake records: One of low intensity (Aegio record), one of moderate intensity (Lefkada_2003 record) and one severe earthquake excitation (Rinaldi_228 record). The 3D model was tested in both longitudinal and transverse direction. The results of the seismic performance of the different components of the 3D model are presented below for the Rinaldi_228 record in both directions.

- **Soil amplification**

There are two alternative ways to impose the seismic excitation. The first is to consider a fixed soil base (bedrock) and impose the seismic excitation there. The second is to consider dashpots at the soil base and to impose the seismic excitation at the fixed nodes of the dashpots below the soil base. The acceleration time histories for the Aegio record for both considerations at the fixed base and at the surface of the soil layer are presented in Figures 6.5 (a), (b) , (c), (d) for both longitudinal and transverse direction. From the comparison of the two alternatives it is concluded that the most

realistic approach is the one with the dashpots at the soil base so this is the one that is finally used. In addition from the comparison of the acceleration time histories for the Rinaldi_228 record at the surface of the subject soil and the surface of the embankment that is shown in Figures 6.6 (a), (b), the additional soil amplification is obvious.

- **Effect of SSI in the natural period of the bridge**

In the previous chapter the base of bridge's piers so as the connections of the bearings at the abutments were considered fixed. The natural period of the bridge system with the fixed base consideration is T=0.55 sec in the longitudinal direction and T=0.66 sec in the transverse. However taking into account the soil-structure interaction it increases to T=0.69 sec in the longitudinal direction and to T=0.78 sec in the transverse. The natural period of the bridge considering soil-structure interaction can be calculated using the equation:

$$T_{ssi} = T_{fixed}\sqrt{1 + \frac{K_{str}}{K_H} + \frac{K_{str}}{K_R}H^2}$$

assuming the following parameters:

- T_{fixed}: the natural period of the superstructure with the fixed base consideration
- K_{str}: the stiffness of the superstructure
- K_H: the stiffness of the horizontal spring that replaces the soil-foundation system
- K_R: the stiffness of the rotational spring that replaces the soil-foundation system
- H: the height of the superstructure

- **Seismic performance of soil-foundation system**

The seismic performance of the whole bridge system depends greatly on the seismic performance of the soil-foundation system. In this case each pier of the bridge is connected at its base to a square footing of 8 m width which is designed according to the provisions of the Greek Code for Reinforced Concrete (ΕΚΩΣ, 2000). The factor of safety (Fs) of the particular soil-footing system

against vertical loading is Fs=6.7. Its seismic performance for the Rinaldi_228 record in both directions is described by the Moment-Rotation and Settlement-Rotation curves that are shown in Figures 6.7 (a), (b) , 6.8 (a), (b). These curves refer to the center point of the soil-footing interface. In addition from the relative horizontal displacement time histories between the footing and the soil that are shown in Figures 6.7 (c), 6.8 (c) for both directions, it is obvious that there is practically no sliding of the footing.

- **Seismic performance of retaining walls**

Each abutment of the 3D bridge-soil model consists of a retaining wall that retains the access embankment. One of the key objectives of this chapter is to examine the effect of the seismic performance of the retaining wall to the performance of the whole bridge system. The seismic performance of each retaining wall for the Rinaldi_228 record in both directions is described by the Settlement-Rotation curves that are shown in Figures 6.9(a), 6.10(a). These curves refer to the center point of the subject soil - retaining wall interface. In addition the relative horizontal displacement time histories between the wall and the deck of the bridge in both directions are shown in Figures 6.9(b), 6.10(b). From these curves it is concluded that both retaining walls don't have significant displacements in comparison to the deck, so the consideration of fixed abutments is a logical and realistic approach.

- **Seismic performance of superstructure**

The present thesis focuses mainly on the structural damage of the superstructure. For this reason great emphasis is given to the seismic performance of the bridge and its components (deck, piers and bearings). The performance of bridge's piers is described for the Rinaldi_228 record in both directions by the Moment-Curvature curve at the base of each pier and the Relative Displacement time histories at the top of each pier, which are shown in Figures 6.11, 6.12. In these figures it is also shown the drift limit at which the stoppers of the bridge at the abutments begin to affect its seismic performance. The structural damage of the piers is expressed in terms of Maximum Drift, Residual Drift and in terms of ductility $\frac{\mu_{demand}}{\mu_{capacity}}$ which can be extruded from the above curves. These values for the Rinaldi_228 record and for both piers and directions are presented in Table

6.1. The deck's seismic performance for the same record in both directions is described by the Moment curves at the time of maximum drift, which are presented in Figures 6.13 (a) and (b), while the performance of the bearings is described by the Relative Displacement time histories of the truss elements that represent the bearings and are shown in Figures 6.13 (c) and (d).

- **Contact pressures at the retaining wall-embankment interface**

The contact pressure time histories at each retaining wall-embankment interface and at different heights for the Rinaldi_228 record in the longitudinal direction are presented in Figure 6.14. These curves refer to the center point of the wall-embankment interface. From the above curves it is obvious that the soil of the abutment is cohesive (clay) as at certain moments and heights the contact pressures drop to zero, which means that the contact between the soil of the embankment and the wall is lost. This is a classic cohesive soil behavior. If the soil of the embankment was sand (noncohesive soil) then these zero values would be less and would appear mainly at the highest points of the interface (top of the wall) as the sand ''follows'' the movement of the wall and ''fills'' the gaps. From the above curves it is also obvious that the two retaining wall-embankment systems at the abutments of the bridge perform different during the earthquake. The observed differences are expected due to the fact that the seismic excitation is imposed in the horizontal direction and as a result the soil layer behind the wall develops passive earth pressure in one abutment and at the same time active earth pressure at the other.

6.2.2 Comparison between fixed base simple models and complete 3D model Effect of soil-structure interaction

In the 5th chapter simple models were developed for both longitudinal and transverse directions that have similar seismic performance to the entire 3D bridge system with the consideration of fixed base conditions. So in this chapter in order to examine the effect of soil-structure interaction the seismic performance of the entire 3D bridge-soil model is compared directly to these simple models and not to the whole 3D bridge system. More specific the simple model that was proven to be the most accurate approach of the 3D bridge model in each direction is chosen to be compared

to the complete 3D bridge-soil model. In both longitudinal and transverse directions the simple model consists of a rotational spring, a rotational dashpot, a horizontal spring and a horizontal dashpot at the top of the pier (8.8m height) that represent the stiffness and the damping of the deck and the stiffness and the damping of the bearings at the abutments as well.

Both the simple models and the complete 3D model were tested under nonlinear time history analysis using three real earthquake records: One of low intensity (Aegio record), one of moderate intensity (Lefkada_2003 record) and one severe earthquake excitation (Rinaldi_228 record). The seismic excitation imposed at the fixed base of the simple models is the acceleration time history at the surface of the soil as resulted from the analysis of the complete model. Finally the same input acceleration time history is imposed to both the base of the pier and the fixed node of the horizontal spring and dashpot. In this way the abutments of the bridge are considered fixed. This is a logical assumption, as explained before, due to the fact that the retaining walls don't have significant displacements in comparison to the deck of the bridge.
As shown in Figures 6.11, 6.12 in the complete model both piers have the same seismic performance in terms of Relative Displacement time history at the top of the pier and Moment-Curvature curve at the base of the pier. So one of them is selected and compared to the simple model. The results of the analysis and the comparison between the simple fixed base model and the complete one in each direction are presented below.

- **Longitudinal direction**

The seismic performance of both the complete model and the simple one is described by the Relative Displacement time histories at the top of the pier and the Moment-Curvature curves at the base of the pier. The above curves for each earthquake record and for both models are presented in Figures 6.15, 6.16. Structural damage of the piers is expressed in terms of Maximum Drift, Residual Drift and in terms of ductility $\frac{\mu_{demand}}{\mu_{capacity}}$ which are extruded from the above curves. These values for each earthquake record and for both models are shown in Table 6.2. In this case for the 2 of the 3 records that demanded less ductility than the capacity of the system, the maximum deviation observed in terms of $\frac{\mu_{demand}}{\mu_{capacity}}$ is 27%, while the average deviation is 19%.

- **Transverse direction**

The seismic performance of both the complete model and the simple one in the transverse direction is also described by the Relative Displacement time histories at the top of the pier and the Moment-Curvature curves at the base of the pier. The above curves for each earthquake record and for both models are presented in Figures 6.17, 6.18. Structural damage of the piers is expressed in terms of Maximum Drift, Residual Drift and in terms of ductility $\frac{\mu_{demand}}{\mu_{capacity}}$ which are extruded from the above curves. These values for each earthquake record and for both models are shown in Table 6.3. In this case for the 2 of the 3 records that demanded less ductility than the capacity of the system, the maximum deviation observed in terms of $\frac{\mu_{demand}}{\mu_{capacity}}$ is 15%, while the average deviation is 9%.

- **Effect of soil-structure interaction**

From the comparison of the fixed base simple model with the complete 3D bridge-soil model in both directions it can be concluded that the effect of soil-structure interaction in the structural damage of the piers and in general in the seismic performance of the superstructure is important and cannot be ignored. More specific it is observed that its effect is beneficial for the superstructure in comparison to the fixed base approach, as it reduces the structural damage of the piers and the ductility demanded by the earthquake. Therefore the following step is to extend the previous simple models in each direction in order to take into account the soil-structure interaction by using springs and dashpots to replace the soil-foundation system.

6.2.3 Use of linear elastic springs and dashpots to consider SSI

The simplest way to take into account the soil-structure interaction is to replace the soil-foundation system by using linear elastic springs and dashpots (Gazetas, 1983). More specific at the base of the simple model horizontal, vertical and rotational springs and dashpots are added to represent the horizontal, vertical and rotational stiffness and damping of the soil-foundation system.

The stiffness of the vertical linear elastic spring is calculated by the following equation (Gazetas, 1983):

$$K_V = \frac{4.54Gb}{1-\nu}$$

assuming the following parameters:

- G=103846 KPa, the shear modulus of elasticity of the soil
- b=B/2=4m, where B is the width of the footing
- v=0.3, the Poisson's ratio

The damping coefficient of the vertical dashpot is calculated by the following equation (Gazetas, 1983):

$$C_V = \frac{2K_V\xi}{\omega}$$

assuming the following parameters:

- K_V=2694066 KN/m, as calculated using the previous equation
- ξ=5%
- $\omega = 2\pi/T_{SSI}$, where T_{SSI} is the natural period of the bridge system in the examined direction considering SSI

The stiffness of the horizontal linear elastic spring is calculated by the following equation (Gazetas, 1983):

$$K_H = \frac{9Gb}{2-\nu}$$

assuming the following parameters:

- G=103846 KPa, the shear modulus of elasticity of the soil
- b=B/2=4m, where B is the width of the footing
- v=0.3, the Poisson's ratio

The damping coefficient of the horizontal dashpot is calculated by the following equation (Gazetas, 1983):

$$C_H = \frac{2K_H\xi}{\omega}$$

assuming the following parameters:

- K_H=2199095 KN/m, as calculated using the previous equation
- ξ=5%
- $\omega = 2\pi/T_{SSI}$, where T_{SSI} is the natural period of the bridge system in the examined direction considering SSI

The stiffness of the rotational linear elastic spring is calculated by the following equation (Gazetas, 1983):

$$K_R = \frac{3.65Gb^3}{1-\nu}$$

assuming the following parameters:

- G=103846 KPa, the shear modulus of elasticity of the soil
- b=B/2=4m, where B is the width of the footing
- v=0.3, the Poisson's ratio

The damping coefficient of the rotational dashpot is calculated by the following equation (Gazetas, 1983):

$$C_R = \frac{2K_R\xi}{\omega}$$

assuming the following parameters:

- K_R=34654945 KNm/rad, as calculated using the previous equation
- ξ=5%
- $\omega = 2\pi/T_{SSI}$, where T_{SSI} is the natural period of the bridge system in the examined direction considering SSI

Due to the change in the natural period of the bridge system considering soil-structure interaction, the damping coefficients of the dashpots that are used in the simple model to represent the different components of the superstructure are also changed.

Both the new simple models and the complete 3D model are tested in both directions under nonlinear time history analysis using the same three real earthquake records. The seismic excitation is imposed at the fixed nodes of the springs and the dashpots that replace the soil-foundation system and the fixed node of the horizontal spring and dashpot that represents the stiffness and damping of the bearings. The input seismic excitation is again the acceleration time history at the surface of the soil as resulted from the analysis of the complete model. The results of the analysis and the comparison between the simple model and the complete one in each direction are presented below.

- **Longitudinal direction**

The seismic performance of both the complete model and the simple one is described by the Rotation time histories of the footing, the Relative Displacement time histories at the top of the pier and the Moment-Curvature curves at the base of the pier. The above curves for each earthquake record and for both models are presented in Figures 6.19, 6.20. Structural damage of the piers is expressed in terms of Maximum Drift, Residual Drift and in terms of ductility $\frac{\mu_{demand}}{\mu_{capacity}}$ which are extruded from the above curves. These values for each earthquake record and for both models are shown in Table 6.4. In this case for the 2 of the 3 records that demanded less ductility than the capacity of the system, the maximum deviation observed in terms of $\frac{\mu_{demand}}{\mu_{capacity}}$ is 18%, while the average deviation is 12%. The maximum deviation is 9% less than the fixed base approach, while the average is 7% less.

- **Transverse direction**

The seismic performance of both the complete model and the simple one in the transverse direction is also described by the Rotation time histories of the footing, the Relative Displacement

time histories at the top of the pier and the Moment-Curvature curves at the base of the pier. The above curves for each earthquake record and for both models are presented in Figures 6.21, 6.22. Structural damage of the piers is expressed in terms of Maximum Drift, Residual Drift and in terms of ductility $\frac{\mu_{demand}}{\mu_{capacity}}$ which are extruded from the above curves. These values for each earthquake record and for both models are shown in Table 6.5. In this case for the 2 of the 3 records that demanded less ductility than the capacity of the system, the maximum deviation observed in terms of $\frac{\mu_{demand}}{\mu_{capacity}}$ is 9%, while the average deviation is 8%. The maximum deviation is 6% less than the fixed base approach, while the average is 1% less.

- **Evaluation of the use of linear elastic springs and dashpots to consider SSI**

From the previous analysis it can be concluded that the use of linear elastic springs and dashpots to replace the soil-foundation system is considered a satisfactory approach for the particular soil-foundation system and for the purposes of the present thesis. The deviations in the structural damage of the superstructure between this approach and the analysis of the entire 3D bridge-soil model are insignificant in comparison to the uncertainties in the properties of the subject soil. However for the sake of completeness a more accurate approach of replacing the soil-foundation system with springs and dashpots is considered in the following section.

6.2.4 Combination of linear elastic and nonlinear springs and dashpots to consider SSI

One more accurate way to take into account the soil-structure interaction is to replace the soil-foundation system by using a combination of linear elastic and nonlinear springs and dashpots (Anastasopoulos & Kontoroupi, 2013). More specific at the base of the simple model horizontal, vertical and rotational springs and dashpots are added to represent the horizontal, vertical and rotational stiffness and damping of the soil-foundation system as before. The horizontal and vertical springs and dashpots are considered linear elastic and have the same stiffness and damping coefficient as in the previous approach, while a nonlinear rotational spring accompanied by a linear

rotational dashpot is added to the simple model calculated according to the methodology described in Anastasopoulos & Kontoroupi (2013). The basic steps of this methodology are presented below.

6.2.4.1 Moment-Rotation Relations

To define the necessary relations to implement this methodology, the *M*–ϑ response of the soil-foundation system is divided in three characteristic phases, which are described in detail in the next sections: (a) quasi–elastic response (for very small rotation $\vartheta \rightarrow 0$), (b) plastic response (referring to the ultimate capacity, for large rotation ϑ) and (c) nonlinear response (which is the intermediate stage between the quasi-elastic and the plastic phases).

- **Quasi–elastic response**

The first phase of response refers to very small rotation ϑ. The effective (secant) rotational stiffness is a function of ϑ and F_S: $K_R = f(\theta, F_S)$. For a given factor of safety F_S, the initial (i.e., for $\vartheta \rightarrow 0$) rotational stiffness can be defined as:

$$K_{R,0} = K_R(0, F_S) \quad (1)$$

As shown in Figure 6.23, for the lightly-loaded (F_S= 10) footing, $K_{R.0}$ is very close to the purely elastic rotational stiffness (Gazetas, 1983):

$$K_{R,elastic} = \frac{3.65Gb^3}{1-\nu} \quad (2)$$

where *b* = *B*/2, *G* is the small strain shear modulus of soil, and *v* the Poisson's ratio. In stark contrast, a substantial difference is observed for the heavily-loaded (F_S = 2) footing. This reduction of $K_{R,0}$ is directly related to the initial soil yielding due to the imposed vertical load *N* (before application of moment loading). Based on the 3D FE analysis results, $K_{R,0}$ can be (approximately) expressed as:

$$K_{R,0} = K_{R,elastic}(1 - 0.8\frac{1}{F_S}) \quad (3)$$

- **Plastic response**

This phase refers to the ultimate capacity of the footing, and is quite straight-forward to define. As thoroughly discussed in Gazetas et al. (2012), the failure envelope can be defined as follows (Figure 6.24):

$$\frac{M_u}{N_{uo}B} = 0.55\left(\frac{N_u}{N_{uo}}\right)\left(1-\frac{N_u}{N_{uo}}\right) \quad (4)$$

where N_{uo} is the bearing capacity for purely vertical loading (Meyerhof, 1953; Gourvenec, 2007):

$$N_{uo} \approx (\pi+3)S_u B^3 \quad (5)$$

- **Nonlinear response**

This corresponds to the intermediate phase, bridging the gap between the quasi-elastic and plastic response. If the soil behaved as an ideally elastic–plastic material, there would be no need to consider this intermediate phase of response, and the previously described solutions would be enough to completely define the necessary *M*–*ϑ* relations. However, as revealed by Figure 6.23, the soil–foundation system exhibits strongly nonlinear response long before reaching its ultimate capacity. Hence, there is a need for a "connection" between the quasi-elastic and the plastic part of the *M*–*ϑ* relations. This is performed on the basis of 3D FE analysis results, following the dimensional formulation presented in Kourkoulis et al. (2012a) and Gazetas et al. (2012).

As shown in Figure 6.23, the initiation of the nonlinear phase is a function of *Fs*. While the lightly-loaded (*Fs* = 10) footing starts exhibiting nonlinear response for *ϑ* ≈ 0.02 x 10-2 rad, in the case of the heavily-loaded (*Fs* = 2) nonlinearity becomes observable much later, for *ϑ* ≈ 0.08 x 10-2 rad. This difference is due to the vertical load *N* acting on the foundation, the increase of which tends to hinder separation and uplifting. In the absence of soil nonlinearity, considering a footing (of any shape) rocking on elastic half-space, the overturning moment to initiate uplifting would be (Apostolou & Gazetas, 2007):

$$M_{uplift} \approx \frac{NB}{4} \quad (6)$$

where *B* is the width of the footing in the direction of rocking. Therefore, the uplifting rotation *ϑuplift* can be defined as:

$$\theta_{uplift} \approx \frac{NB}{4K_{R,elastic}} \quad (7)$$

As previously discussed, the initial quasi-elastic rotational stiffness $K_{R,0}$ decreases with the decrease of F_S due to the increasingly important initial soil yielding (due to the vertical load *N*, before application of moment loading). Therefore, when considering soil inelasticity it is reasonable to assume that the equivalent "uplifting" rotation will be a function of $K_{R,0}$ rather than $K_{R,elastic}$. Hence, combining Eq. 3 and Eq. 7, a characteristic rotation θ_S is defined:

$$\theta_S \approx \frac{NB}{4K_{R,0}} = \frac{NB}{4K_{R,elastic}(1-0.8\frac{1}{F_S})} \quad (8)$$

As shown in Figure 6.25 (a), θ_S can be used to normalize the rotation ϑ, allowing the expression of the *M*–*ϑ* relations in non-dimensional form: $M_u/S_u\,B^3 = f\,(\vartheta/\theta_S)$. Thanks to the normalization of ϑ with θ_S, the shape of the moment–rotation curves is almost identical for all cases examined, irrespective of *Fs*. Hence, if we normalize $M_u/S_u\,B^3$ with the moment capacity $M_u/S_u\,B^3$ of each curve, the moment–rotation curves of Figure 6.25 (a) "collapse" in the single non-dimensional curve of Figure 6.25 (b). The latter is simplified further, being approximated by piecewise linear segments. The resulting non-dimensional *M*–*ϑ* relation encompasses: (a) a quasi-elastic branch, for $\vartheta/\theta_S \leq 1/3$; (b) a plastic branch, for $\vartheta/\theta_S > 10$; and (c) an intermediate nonlinear branch, for $1/3 < \vartheta/\theta_S \leq 10$, consisting of four segments, as illustrated in Figure 6.25 (b).

6.2.4.2 Damping-Rotation Relations

For the rocking-dominated systems considered herein, the damping comprises three different components: (a) radiation damping, (b) hysteretic damping, and (c) damping due to impacts. In the idealized case of elastic soil response (without uplifting or soil inelasticity), radiation is the main source of damping: waves emanating from the dynamically oscillating foundation disperse to infinity, "absorbing" energy from the rocking system (Gazetas, 1983). However, when considering

strongly inelastic response due to material (soil) and geometric nonlinearities (uplifting), radiation damping is practically negligible compared to hysteretic damping. Under strong seismic shaking, which is the main target of the proposed simplified method, the fundamental period *Tsoil* of the soil layer will be significantly lower than both the predominant period *Tp* of the earthquake and the natural period *Tn* of the rocking system—especially in view of the fact that the latter increases substantially due to uplifting. As a result, the system will respond below its "cutoff" frequency (Gazetas, 1983), and radiation damping will be of the order of 1% to 2%. Damping due to impacts is also considered negligible compared to hysteretic damping, being important only when soil inelasticity is limited.

Based on the above, emphasis is placed on the hysteretic component of rotational damping. The latter is computed on the basis of displacement–controlled cyclic pushover analyses, utilizing the rigorous 3D FE model. The FE analyses are conducted for the previously discussed factors of safety against vertical loading *Fs* = 2, 2.5, 3.3, 5, and 10. The rotational damping coefficient is a function of the effective (secant) rotational stiffness K_R, the hysteretic damping ratio ξ, and a characteristic frequency ω:

$$C_R \approx \frac{2K_R\xi}{\omega} \quad (9)$$

While the effective (secant) stiffness K_R is computed utilizing the previously discussed M–ϑ relations, the hysteretic damping ratio ξ is computed through the M–ϑ loops of the cyclic pushover analyses. For this purpose, the SDOF is subjected to cyclic rotation of increasing amplitude. The hysteretic damping ratio ξ is calculated according to its standard definition:

$$\xi \approx \frac{\Delta E/E}{4\pi} \quad (10)$$

where ΔE is the area of the M–ϑ loops, representing the energy consumed during one cycle of loading, and E is the corresponding elastic energy. As discussed in the sequel, the selection of the characteristic frequency ω is not that straightforward.

The results of the analyses are summarized in Figure 6.26 (a), where the hysteretic damping ratio ξ is plotted as a function of the dimensionless cyclic rotation amplitude ϑ/θ_S and the factor of safety against vertical loading *Fs*. As expected, ξ increases with the decrease of *Fs*, since energy dissipation increases with soil nonlinearity (the area enclosed by the M–ϑ loops becomes larger). Exactly for

the same reason, ξ is an increasing function of ϑ/θ_S. Exactly the opposite is observed for the normalized effective (secant) rotational stiffness $K_R/K_{R,elastic}$, which (as also expected) increases with *Fs*, while being a decreasing function of ϑ/θ_S (Figure 6.26 (b)): the increase of soil inelasticity leads to a decrease of the secant stiffness. As a result, being the product of K_R and ξ (Eq. 10) the damping coefficient C_R is not that sensitive to ϑ/θ_S (assuming a constant value of ω). As shown in Figure 6.26 (c), the normalized damping coefficient $C_R/K_{R,elastic}\omega^{-1}$ plotted with respect to ϑ/θ_S is a "bell shaped" curve, with its maximum at $\vartheta/\theta_S \approx 1$. Interestingly, if we plot $C_R/K_{R,elastic}\omega^{-1}$ as a function of the absolute value of ϑ (Figure 6.26 (d)), the maximum is observed for roughly 10^{-3} rad, for all cases examined. The value of the maximum $C_R/K_{R,elastic}\omega^{-1}$ increases with the decrease of *Fs*.

As revealed by the derived C_R–ϑ relations, a nonlinear dashpot would ideally be required. Nevertheless, since most commercial FE codes accept a single value of C_R, a simplifying approximation is proposed in order to maintain simplicity. As discussed in the sequel, the numerical prediction using the simplified model compares well with the results of the rigorous 3D FE model, when the maximum value of the normalized C_R–ϑ curve is adopted. Therefore, in terms of a reasonable simplifying assumption, it is recommended to directly use this value to compute the necessary C_R as a function of *Fs* only, as indicated in Figure 6.26 (d)**.**

Following the previous methodology, to the final simple model used in each direction a nonlinear rotational spring and a linear rotational dashpot are added. The stiffness of the rotational spring is described by the Moment-Angle curve shown in Figure 6.27 for both directions and for Fs=6.7. As far as the rotational dashpot is concerned, its damping coefficient is calculated as described in the previous paragraph. The horizontal and vertical stiffness and damping of the soil-foundation system is considered with the use of the same linear elastic horizontal and vertical springs and dashpots as before.

6.2.4.3 Dynamic Analysis

Both the new simple models and the complete 3D model are tested in both directions under nonlinear time history analysis using the same three real earthquake records. The seismic excitation

is imposed at the fixed nodes of the springs and the dashpots that replace the soil-foundation system and the fixed node of the horizontal spring and dashpot that represents the stiffness and damping of the bearings. The input seismic excitation is again the acceleration time history at the surface of the soil as resulted from the analysis of the complete model. The results of the analysis and the comparison between the simple model and the complete one in each direction are presented below.

- **Longitudinal direction**

The seismic performance of both the complete model and the simple one is described by the Rotation time histories of the footing, the Relative Displacement time histories at the top of the pier and the Moment-Curvature curves at the base of the pier. The above curves for each earthquake record and for both models are presented in Figures 6.28, 6.29. Structural damage of the piers is expressed in terms of Maximum Drift, Residual Drift and in terms of ductility $\frac{\mu_{demand}}{\mu_{capacity}}$ which are extruded from the above curves. These values for each earthquake record and for both models are shown in Table 6.6. In this case for the 2 of the 3 records that demanded less ductility than the capacity of the system, the maximum deviation observed in terms of $\frac{\mu_{demand}}{\mu_{capacity}}$ is 19%, while the average deviation is 13%. These deviations are practically the same with the previous approach of using the linear elastic springs and dashpots by Gazetas (1983).

- **Transverse direction**

The seismic performance of both the complete model and the simple one in the transverse direction is also described by the Rotation time histories of the footing, the Relative Displacement time histories at the top of the pier and the Moment-Curvature curves at the base of the pier. The above curves for each earthquake record and for both models are presented in Figures 6.30, 6.31. Structural damage of the piers is expressed in terms of Maximum Drift, Residual Drift and in terms of ductility $\frac{\mu_{demand}}{\mu_{capacity}}$ which are extruded from the above curves. These values for each earthquake record and for both models are shown in Table 6.7. In this case for the 2 of the 3 records that demanded less ductility than the capacity of the system, the maximum deviation observed in terms

of $\frac{\mu_{demand}}{\mu_{capacity}}$ is 9%, while the average deviation is 9%. These deviations are practically the same with the previous approach of using the linear elastic springs and dashpots by Gazetas (1983).

- **Evaluation of the use of nonlinear rotational spring and linear dashpot**

From the previous analysis it can be concluded that the use of a nonlinear rotational spring and a linear dashpot according to the methodology described in Anastasopoulos & Kontoroupi (2013) instead of the linear elastic ones by Gazetas (1983) has practically no impact in the deviations to the seismic performance between the simple models and the complete 3D model. In addition the computational effort demanded is significant. As a result the simple model that is finally recommended is the one with the linear elastic springs and dashpots by Gazetas (1983) as it combines the simplicity with the effectiveness in achieving similar seismic performance to the entire 3D bridge-soil model, at least for the purposes of the present thesis.

At the end of the chapter are presented both the complete 3D bridge-soil system and the rest systems examined in ABAQUS code (Figures 6.32-6.36).

Chapter 6

Figures

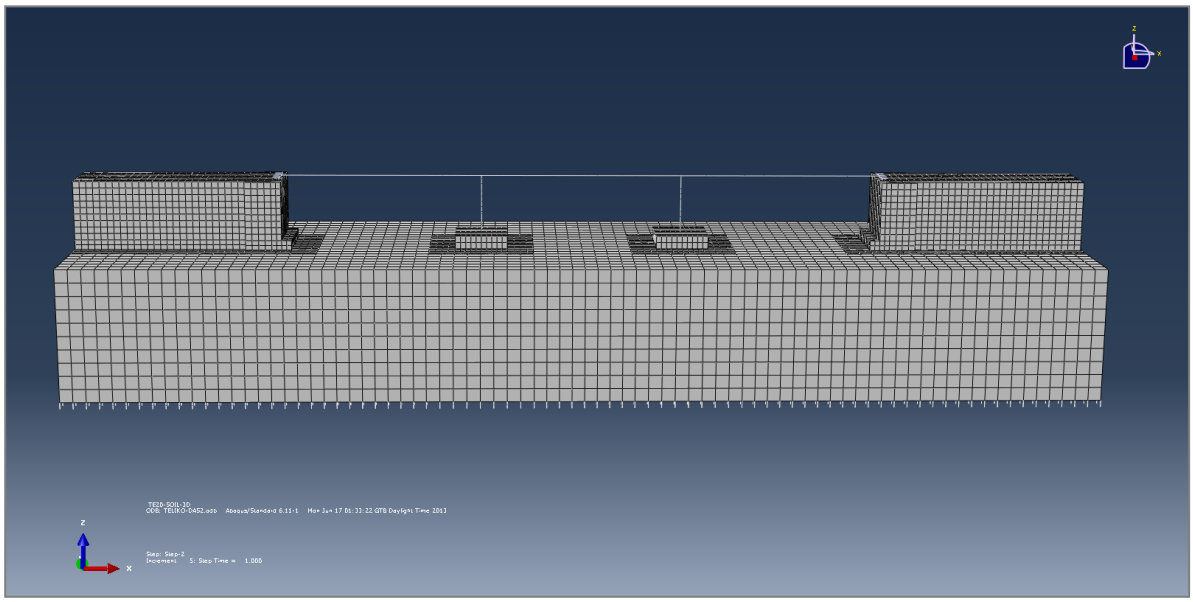

Figure 6.1 . Complete 3D Bridge-Soil Model

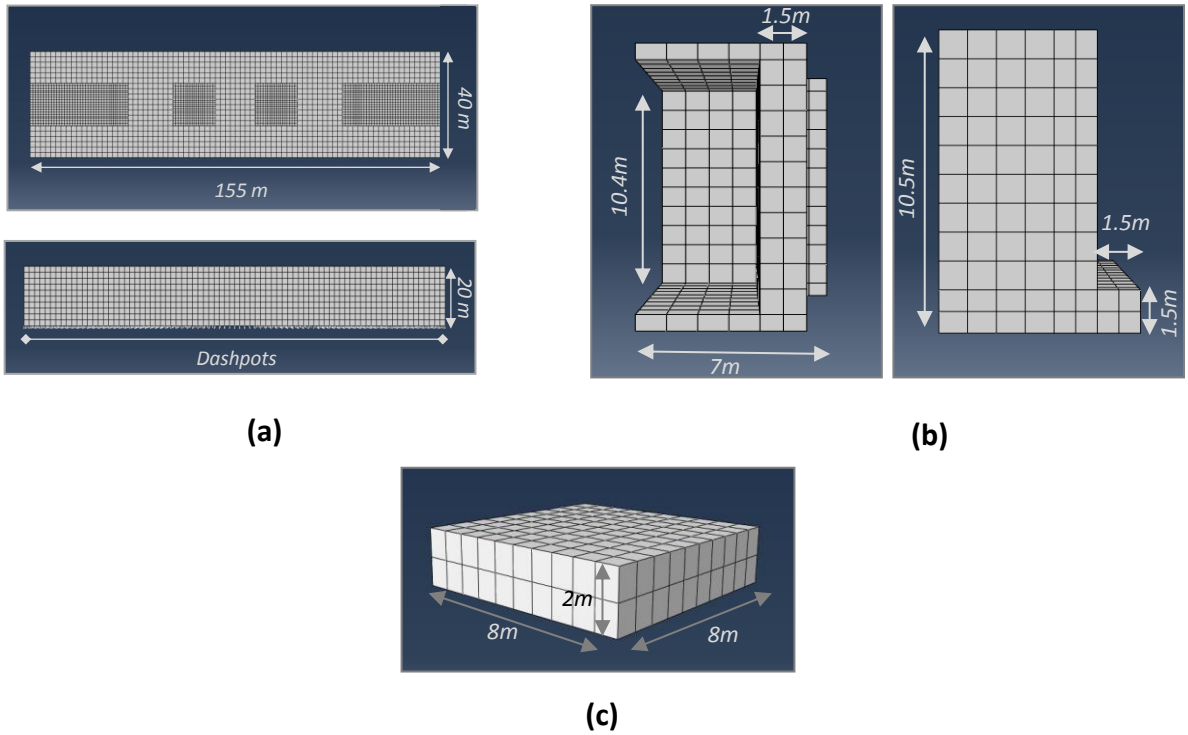

Figure 6.2 . **(a)** Soil Model , **(b)** Model of Retaining Walls, **(c)** Model of Footings

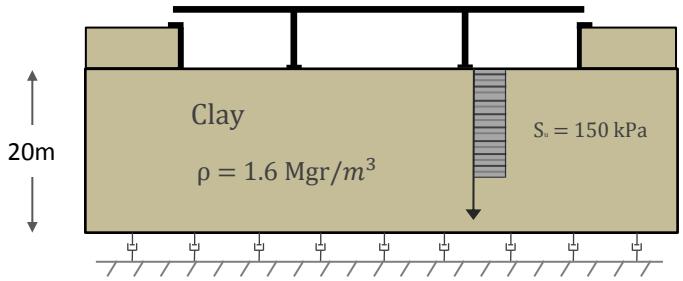

Figure 6.3 Soil Properties

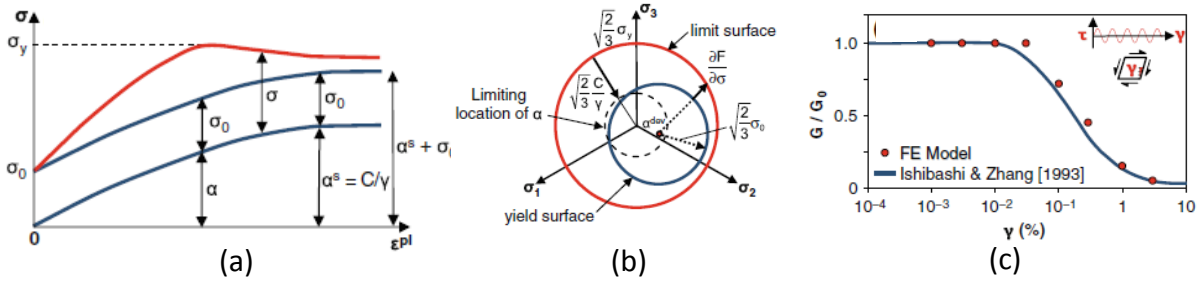

Figure 6.4 **(a),(b)** Simplified 1D and 3D representation of the hardening, **(c)** Calibration of kinematic hardening model for soil (stiff clay, Su =150kPa) against published G–γ (PI=30, σv =100kPa) curves (Ishibashi and Zhang 1993)

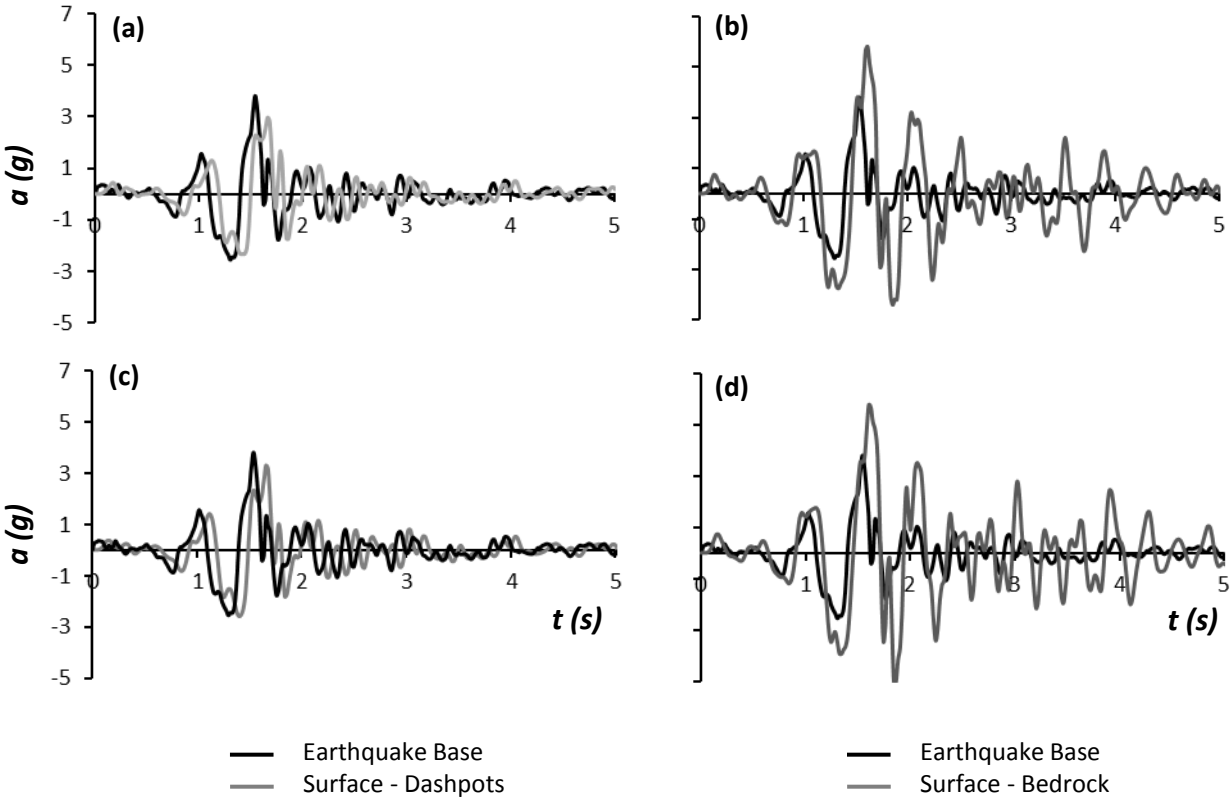

Figure 6.5 Soil amplification with **(a),(c)** and without **(b),(d)** Dashpots at the bottom of the model for Aegio record in longitudinal and transvers direction

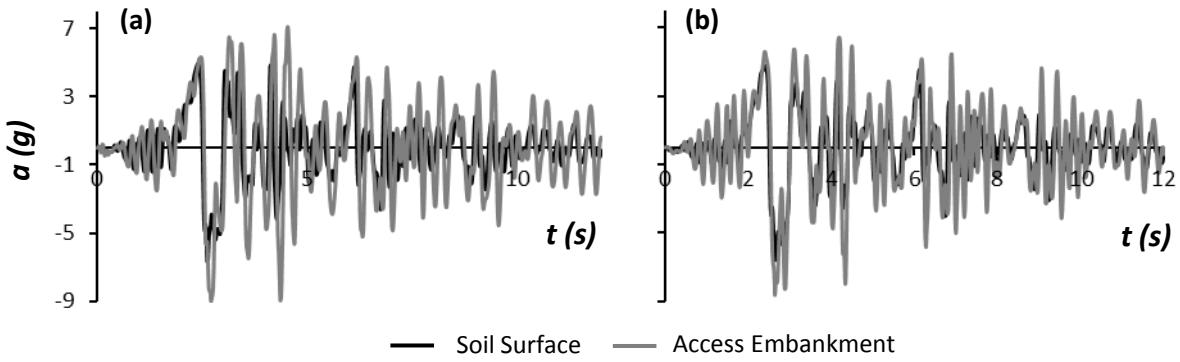

Figure 6.6 Soil amplification for Rinaldi_228 record in **(a)** Longitudinal and **(b**) Transverse direction on access embankment

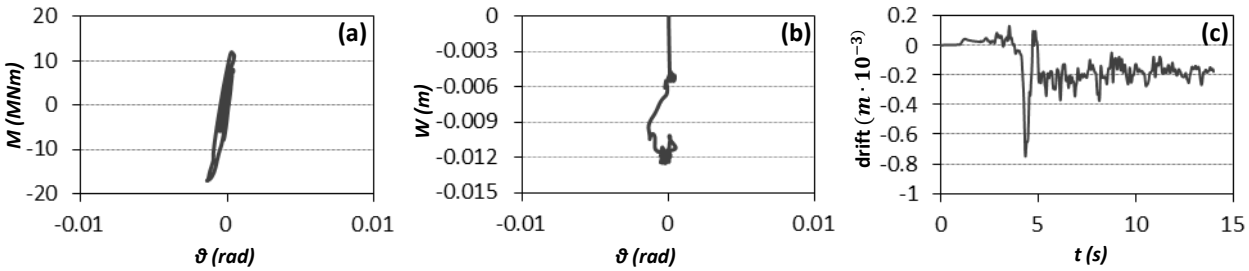

Figure 6.7 **(a)** Moment-Angle, **(b)** Settlement – Angle and **(c)** Horizontal drift curve of surface foundation for Rinaldi_228 record in Longitudinal direction

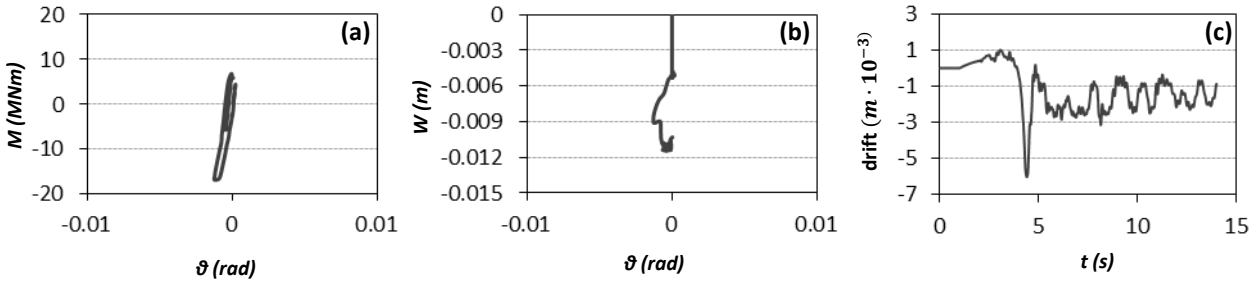

Figure 6.8 **(a)** Moment-Angle, **(b)** Settlement – Angle and **(c)** Horizontal drift curve of surface foundation for Rinaldi_228 record in Transverse direction

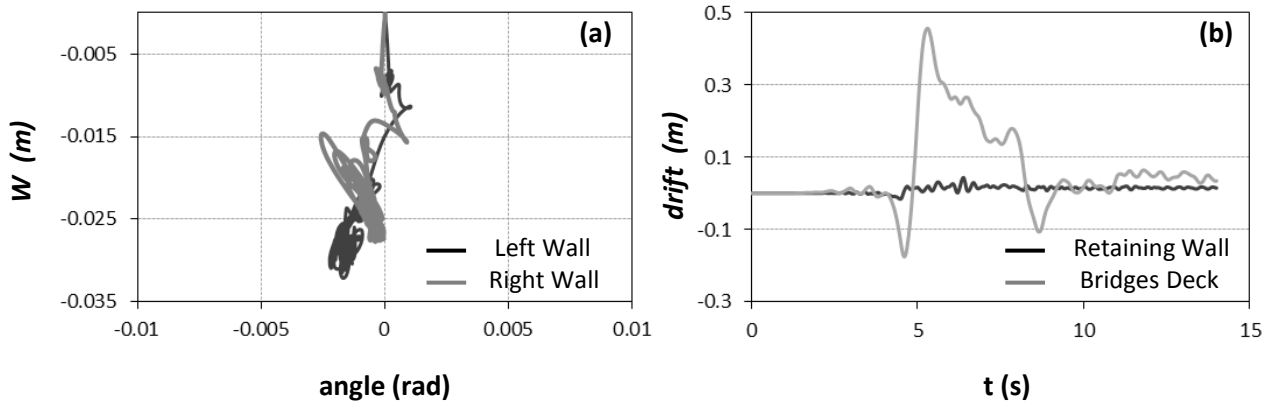

Figure 6.9 (a) Settlement-angle for both retaining walls and **(b)** drift of right retaining wall and displacement of deck for Rinaldi_228 record in Longitudinal direction

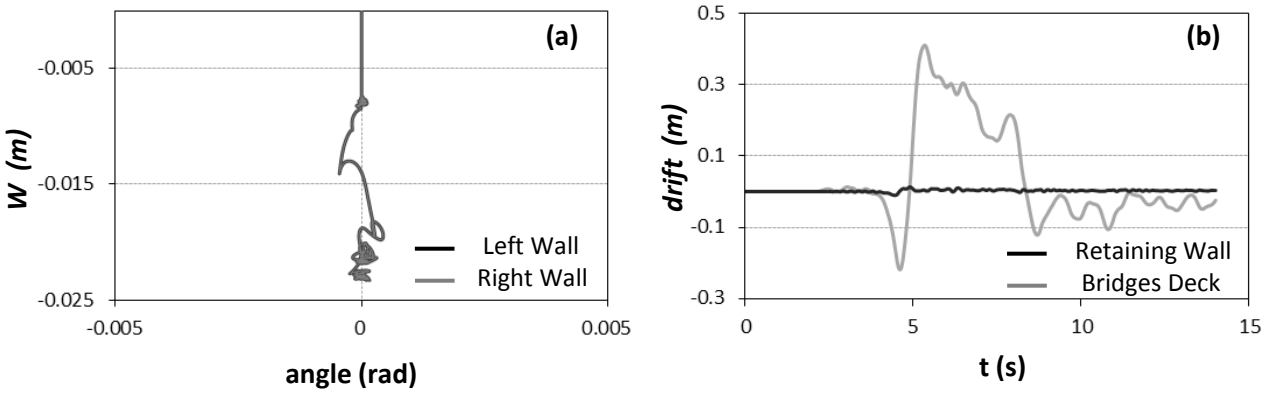

Figure 6.10 (a) Settlement-angle for both retaining walls and **(b)** drift of right retaining wall and displacement of deck for Rinaldi_228 record in Transverse direction

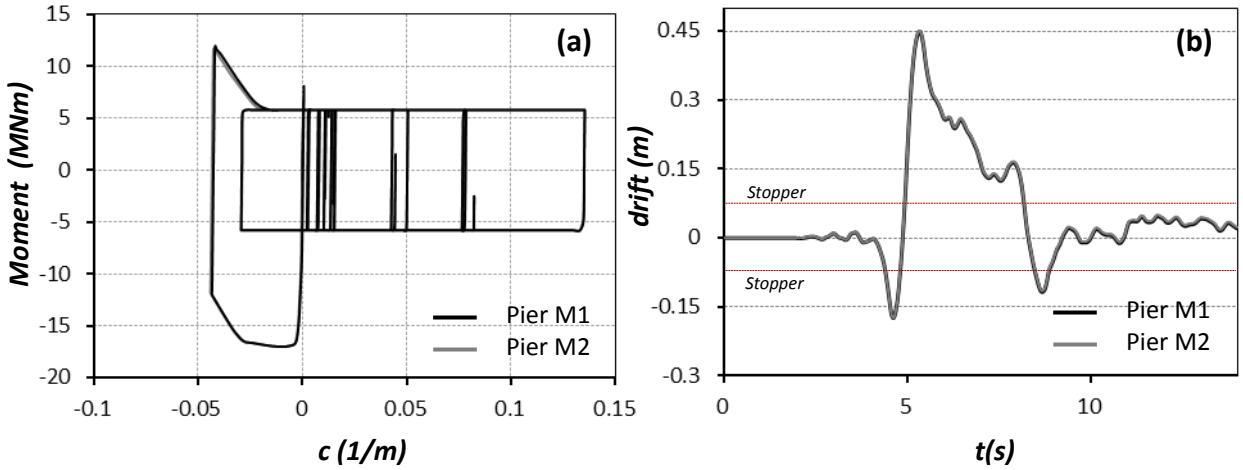

Figure 6.11 (a) Moment-Curvature and **(b)** drift time history for both piers for Rinaldi_228 record in Longitudinal direction

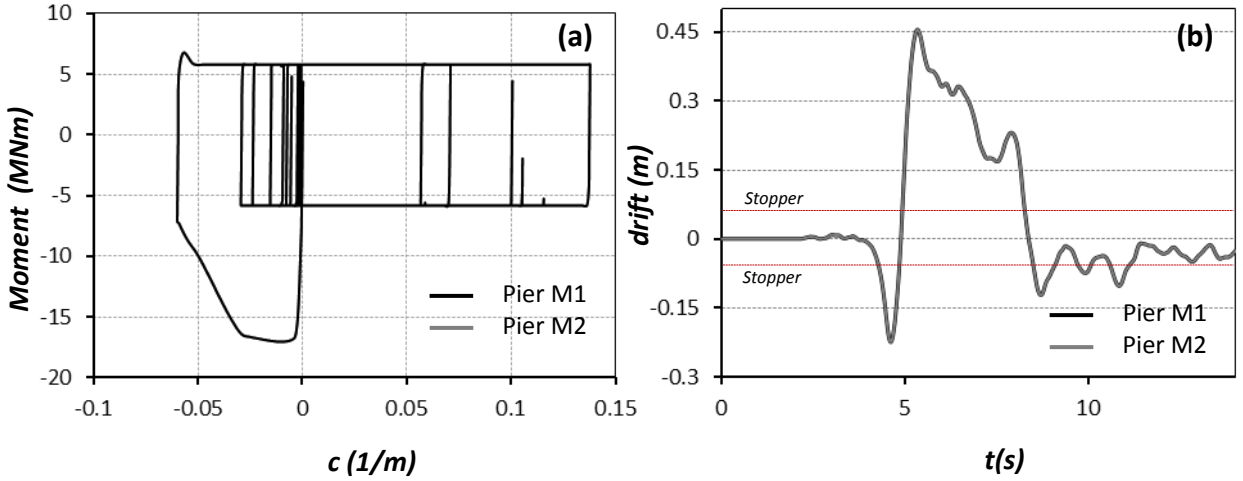

Figure 6.12 (a) Moment-Curvature and **(b)** drift time history for both piers for Rinaldi_228 record in Transverse direction

Rinaldi_228	Longitudinal			Transverse		
	Max Drift	Res Drift	μd/μc	Max Drift	Res Drift	μd/μc
Pier M1	0.45	0.02	5.1	0.46	0.03	5.2
Pier M2	0.45	0.02	5.1	0.46	0.03	5.2

Table 6.1 Seismic Performance of the two piers on Rinaldi_228 record

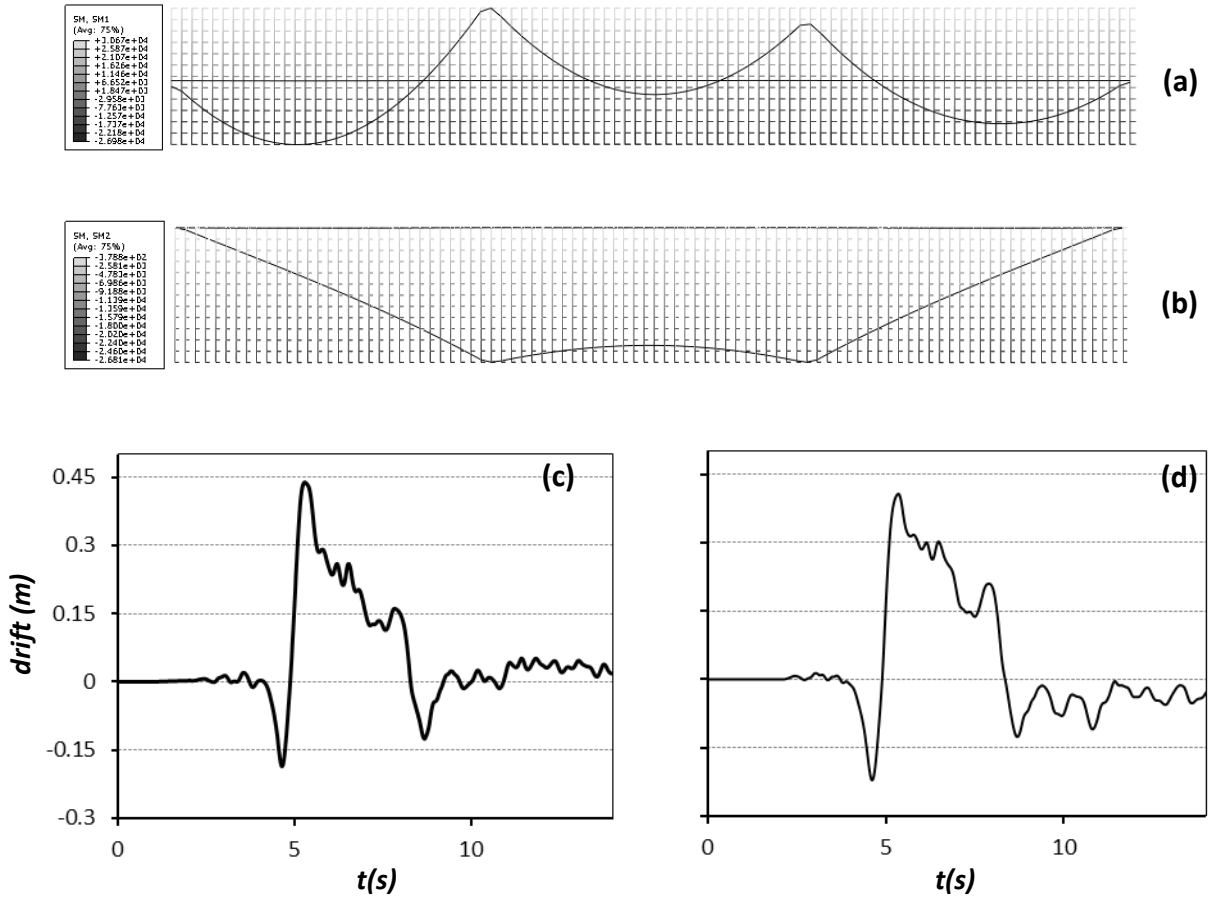

Figure 6.13 Moment curve of deck in **(a)** longitudinal and **(b)** transverse direction and drift time history of bearing in **(c)** longitudinal and **(d)** transverse direction

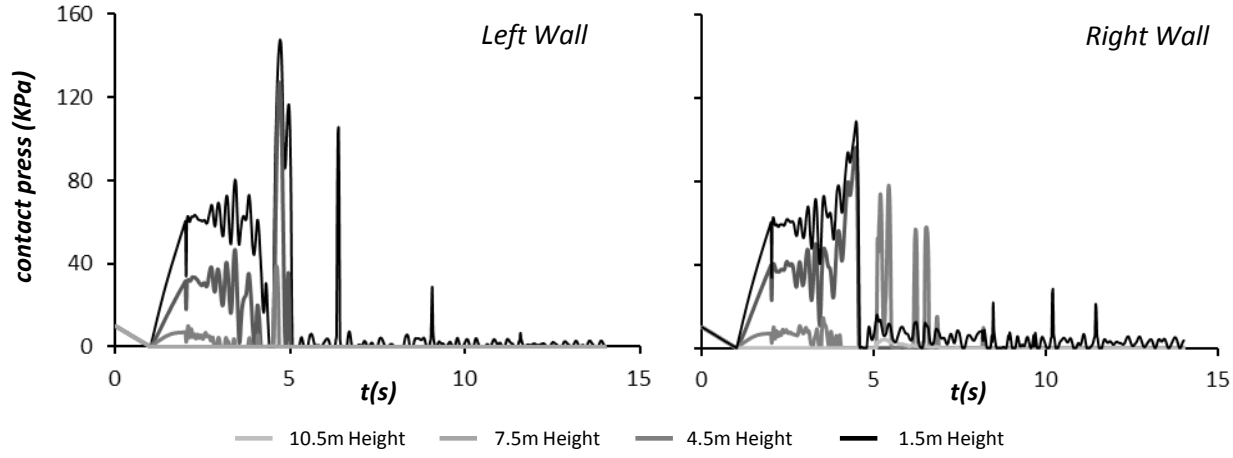

Figure 6.14 Contact Press in both retaining walls in Longitudinal direction for Rinaldi_228 record

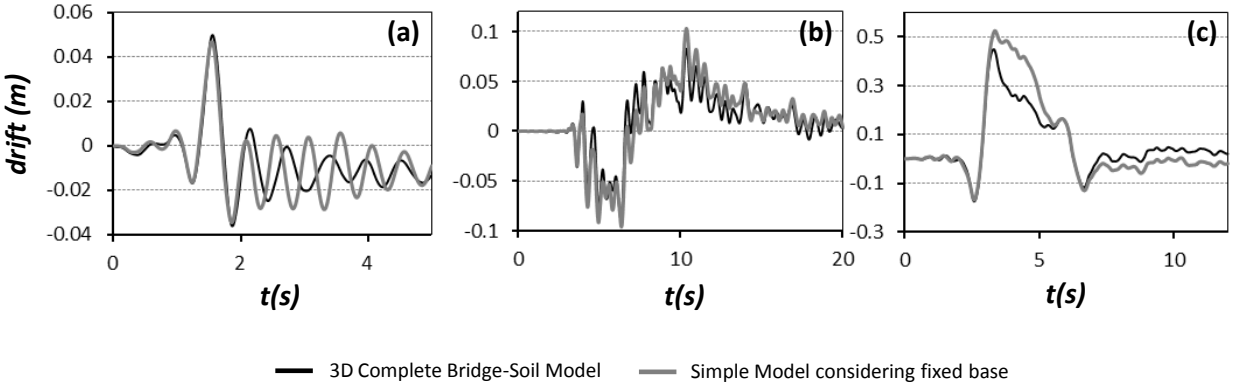

Figure 6.15 Drift time histories of the two models for **(a)** Aegio, **(b)** Lefkada_2003 and **(c)** Rinaldi_228 records in Longitudinal direction

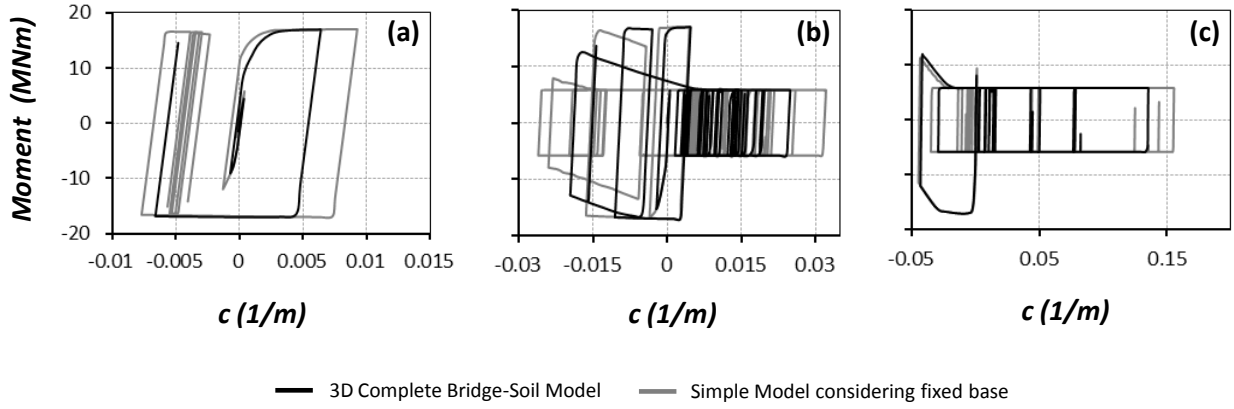

Figure 6.16 Moment-Curvature curves of the two models for **(a)** Aegio, **(b)** Lefkada_2003 and **(c)** Rinaldi_228 records in Longitudinal direction

	3D Complete Bridge-Soil Model				*Simple Model Fixed Base*			
	max Drift (m)	Drift res (m)	μ demand	μ d / μ c	max Drift (m)	Drift res (m)	μ demand	μ d / μ c
AEGIO	0.05	0.01	2.85	0.25	0.05	0.01	4.00	0.35
LEFKADA_2003	0.09	0.00	10.70	0.94	0.10	0.00	13.82	1.21
RINALDI_228	0.45	0.02	58.38	5.12	0.53	0.02	67.06	5.88

Deviations					
max Drift (m)	maxDrift ratio (%)	Drift res (m)	Drift res ratio (%)	μ demand	μ d / μ c
0.00	0.00	0.00	0.00	1.15	0.10
0.01	0.11	0.00	0.01	3.12	0.27
0.08	0.91	0.00	0.02	8.68	0.76

Table 6.2 Seismic Performance and deviations observed between the two Models in Longitudinal direction

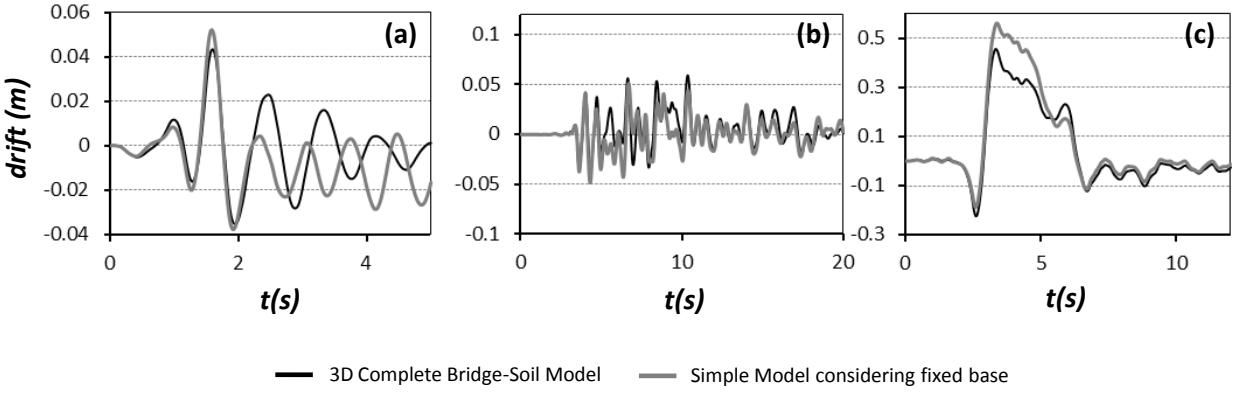

Figure 6.17 Drift time histories of the two models for **(a)** Aegio, **(b)** Lefkada_2003 and **(c)** Rinaldi_228 records in Transverse direction

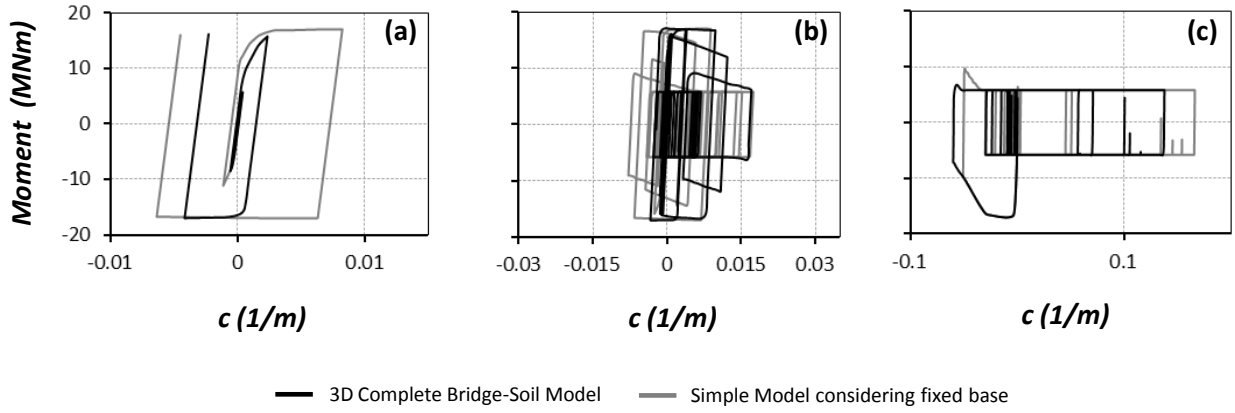

Figure 6.18 Moment-Curvature curves of the two models for **(a)** Aegio, **(b)** Lefkada_2003 and **(c)** Rinaldi_228 records in Transverse direction

	3D Complete Bridge-Soil Model				*Simple Model Fixed Base*			
	max Drift (m)	Drift res (m)	μ demand	μ d / μ c	max Drift (m)	Drift res (m)	μ demand	μ d / μ c
AEGIO	0.04	0.00	1.81	0.16	0.05	0.02	3.55	0.31
LEFKADA_2003	0.06	0.00	7.35	0.64	0.05	0.00	7.52	0.66
RINALDI_228	0.46	0.03	59.42	5.21	0.56	0.01	71.70	6.29

Deviations					
max Drift (m)	maxDrift ratio (%)	Drift res (m)	Drift res ratio (%)	μ demand	μ d / μ c
0.01	0.10	0.02	0.18	1.74	0.15
0.01	0.09	0.00	0.02	0.17	0.02
0.10	1.14	0.01	0.13	12.28	1.08

Table 6.3 Seismic Performance and deviations observed between the two Models in Transverse direction

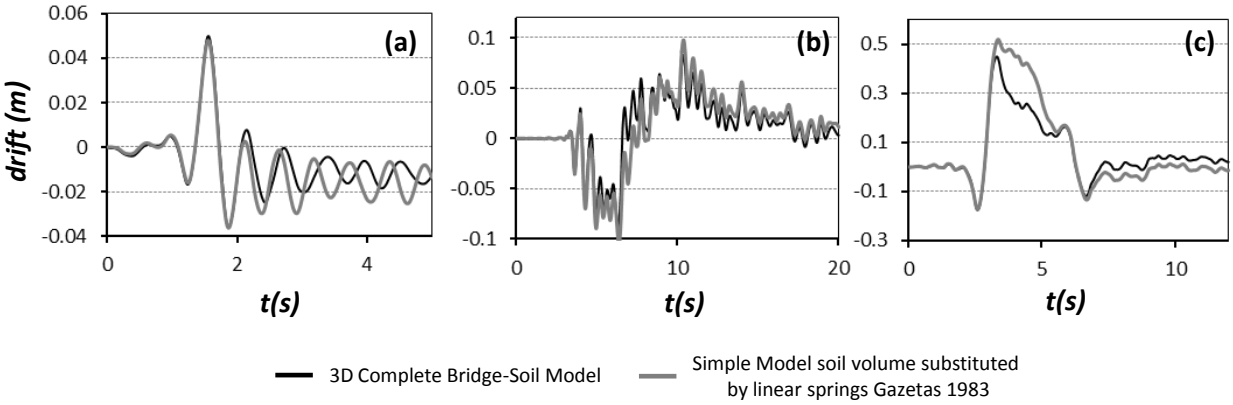

Figure 6.19 Drift time histories of the two models for **(a)** Aegio, **(b)** Lefkada_2003 and **(c)** Rinaldi_228 records in Longitudinal direction

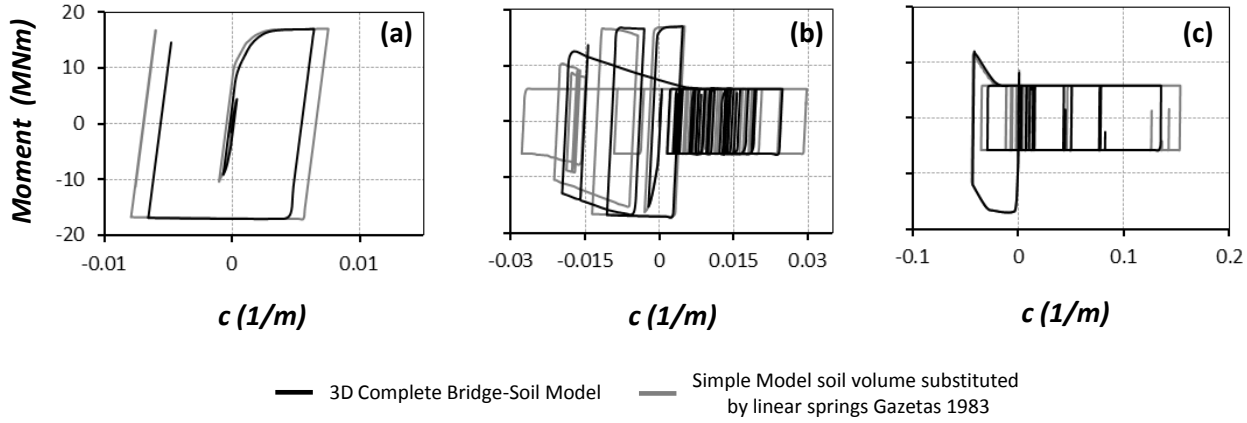

Figure 6.20 Moment-Curvature curves of the two models for **(a)** Aegio, **(b)** Lefkada_2003 and **(c)** Rinaldi_228 records in Longitudinal direction

	3D Complete Bridge-Soil Model				*Simple Model Fixed Base*			
	max Drift (m)	Drift res (m)	μ demand	μ d / μ c	max Drift (m)	Drift res (m)	μ demand	μ d / μ c
AEGIO	0.05	0.01	2.85	0.25	0.05	0.01	3.43	0.30
LEFKADA_2003	0.09	0.00	10.70	0.94	0.11	0.01	12.82	1.12
RINALDI_228	0.45	0.02	58.38	5.12	0.52	0.01	66.22	5.81

Deviations					
max Drift (m)	maxDrift ratio (%)	Drift res (m)	Drift res ratio (%)	μ demand	μ d / μ c
0.00	0.00	0.00	0.00	0.58	0.05
0.02	0.23	0.01	0.09	2.12	0.18
0.07	0.80	0.01	0.09	7.84	0.69

Table 6.4 Seismic Performance and deviations observed between the two Models in Longitudinal direction

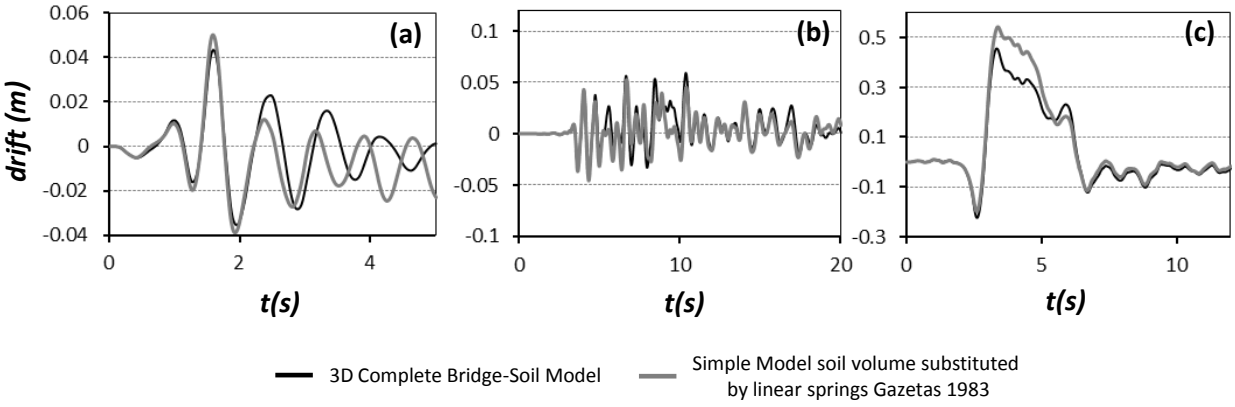

Figure 6.21 Drift time histories of the two models for **(a)** Aegio, **(b)** Lefkada_2003 and **(c)** Rinaldi_228 records in Transverse direction

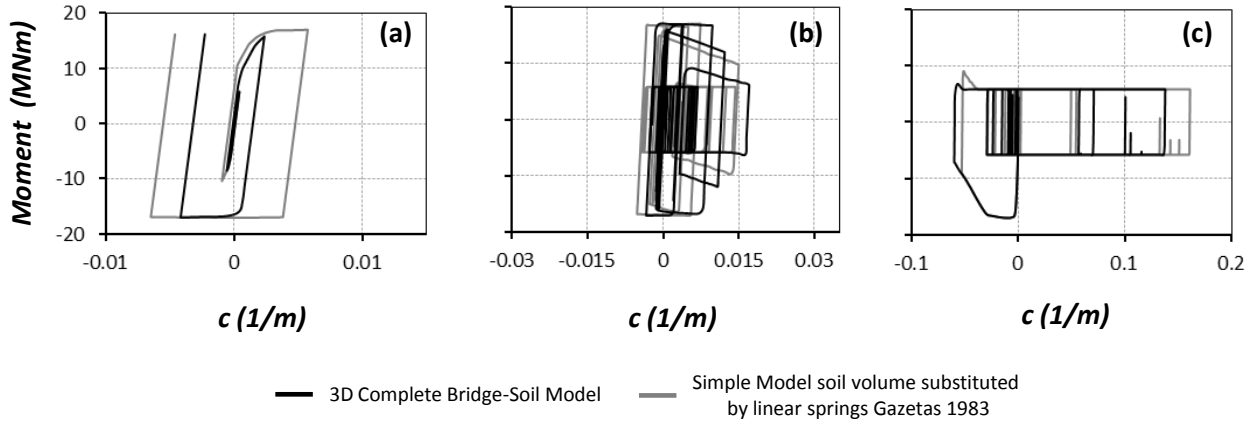

Figure 6.22 Moment-Curvature curves of the two models for **(a)** Aegio, **(b)** Lefkada_2003 and **(c)** Rinaldi_228 records in Transverse direction

	3D Complete Bridge-Soil Model				*Simple Model Fixed Base*			
	max Drift (m)	Drift res (m)	μ demand	μ d / μ c	max Drift (m)	Drift res (m)	μ demand	μ d / μ c
AEGIO	0.04	0.00	1.81	0.16	0.05	0.02	2.81	0.25
LEFKADA_2003	0.06	0.00	7.35	0.64	0.05	0.01	6.46	0.57
RINALDI_228	0.46	0.03	59.42	5.21	0.54	0.02	69.46	6.09

Deviations					
max Drift (m)	maxDrift ratio (%)	Drift res (m)	Drift res ratio (%)	μ demand	μ d / μ c
0.01	0.08	0.02	0.25	1.00	0.09
0.01	0.07	0.01	0.08	0.89	0.07
0.08	0.93	0.01	0.09	10.04	0.88

Table 6.5 Seismic Performance and deviations observed between the two Models in Longitudinal direction

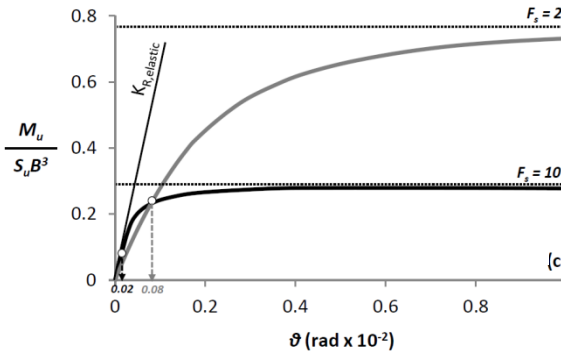

Figure 6.23 Square shallow footing subjected to monotonic pushover loading [Anastasopoulos, Kontoroupi 2013]

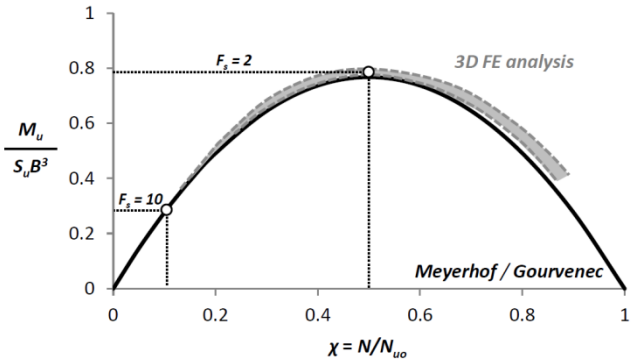

Figure 6.24 Comparison of FE analysis results [Anastasopoulos, Kontoroupi 2013] with published failure envelopes [Meyerhof 1952 ; Gouvernec 2007]

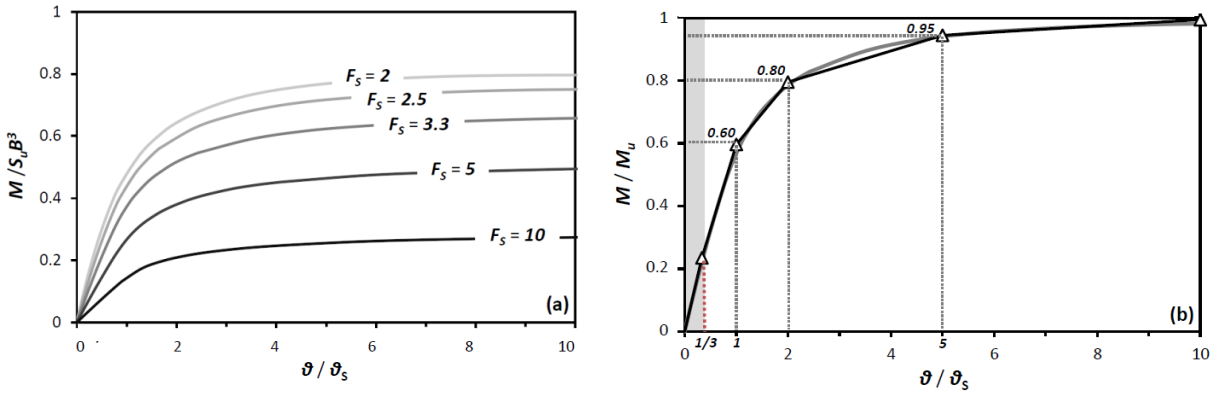

Figure 6.25 (a) Normalized moment-rotation response for different FS and **(b)** non-dimensional unique moment-rotation (M-θ) relation and simplified piecewise approximation [Anastasopoulos, Kontoroupi 2013]

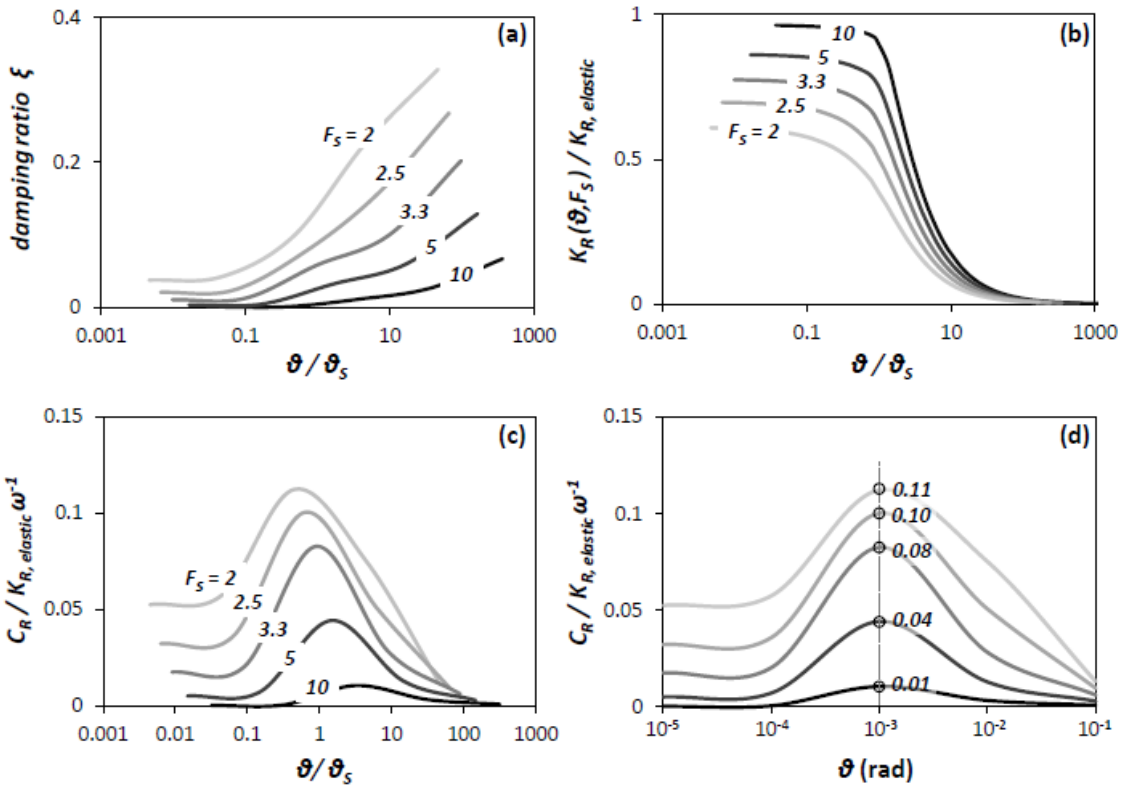

Figure 6.26 (a) Damping ration ξ **(b)** normalized rotational stiffness **(c), (d)** dimensionless damping coefficient with respect to the dimensionless rotation θ/θs and FS and θ and FS [Anastasopoulos, Kontoroupi 2013]

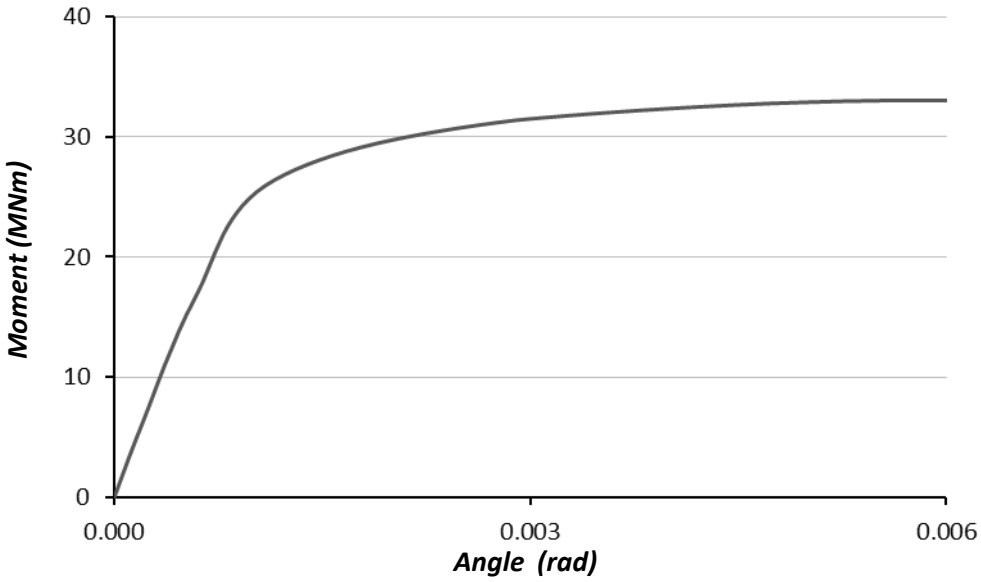

Figure 6.27 Moment-angle curve of the nonlinear rotational spring

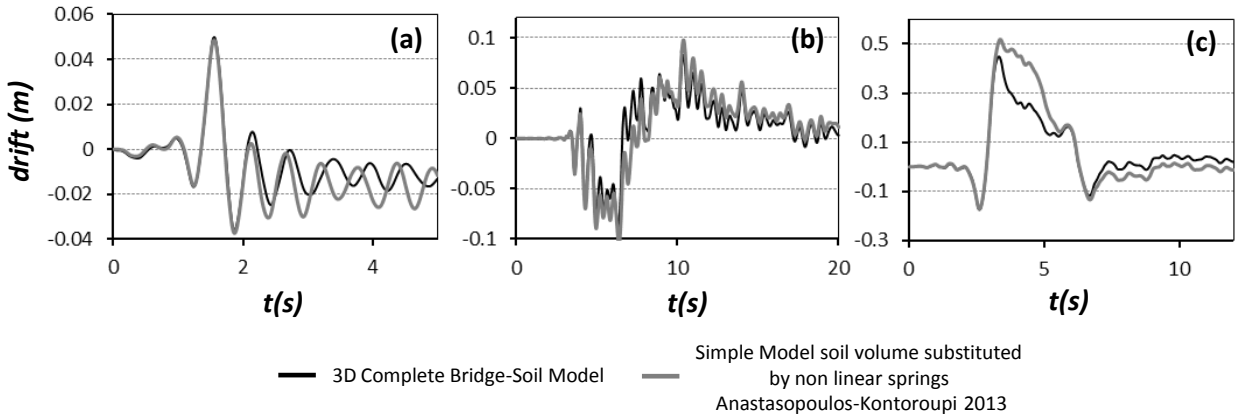

Figure 6.28 Drift time histories of the two models for **(a)** Aegio, **(b)** Lefkada_2003 and **(c)** Rinaldi_228 records in Longitudinal direction

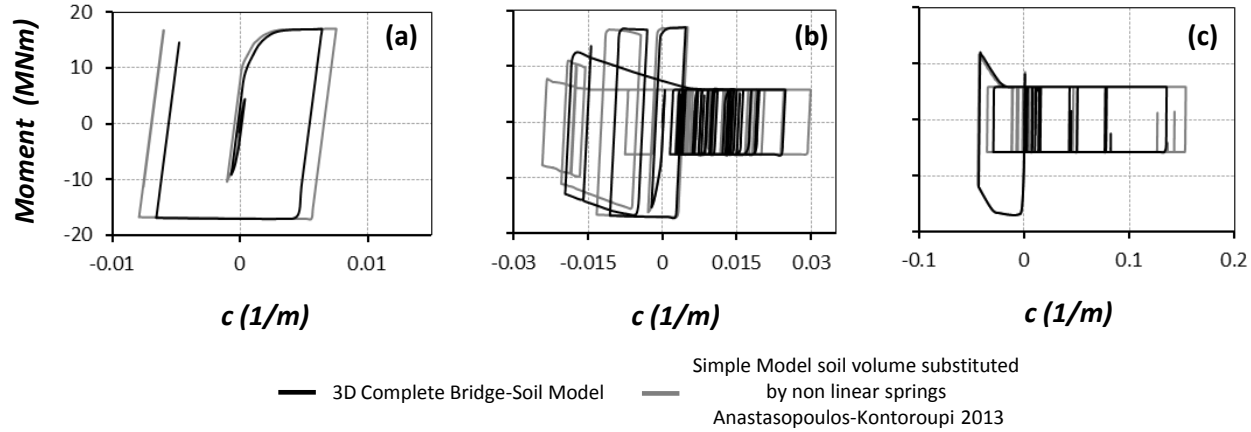

Figure 6.29 Moment-Curvature curves of the two models for **(a)** Aegio, **(b)** Lefkada_2003 and **(c)** Rinaldi_228 records in Longitudinal direction

	3D Complete Bridge-Soil Model				*Simple Model Fixed Base*			
	max Drift (m)	Drift res (m)	μ demand	μ d / μ c	max Drift (m)	Drift res (m)	μ demand	μ d / μ c
AEGIO	0.05	0.01	2.85	0.25	0.05	0.01	3.51	0.31
LEFKADA_2003	0.09	0.00	10.70	0.94	0.10	0.01	12.90	1.13
RINALDI_228	0.45	0.02	58.38	5.12	0.52	0.01	66.23	5.81

Deviations					
max Drift (m)	maxDrift ratio (%)	Drift res (m)	Drift res ratio (%)	μ demand	μ d / μ c
0.00	0.00	0.00	0.00	0.66	0.06
0.01	0.11	0.01	0.09	2.20	0.19
0.07	0.80	0.01	0.10	7.85	0.69

Table 6.6 Seismic Performance and deviations observed between the two Models in Longitudinal direction

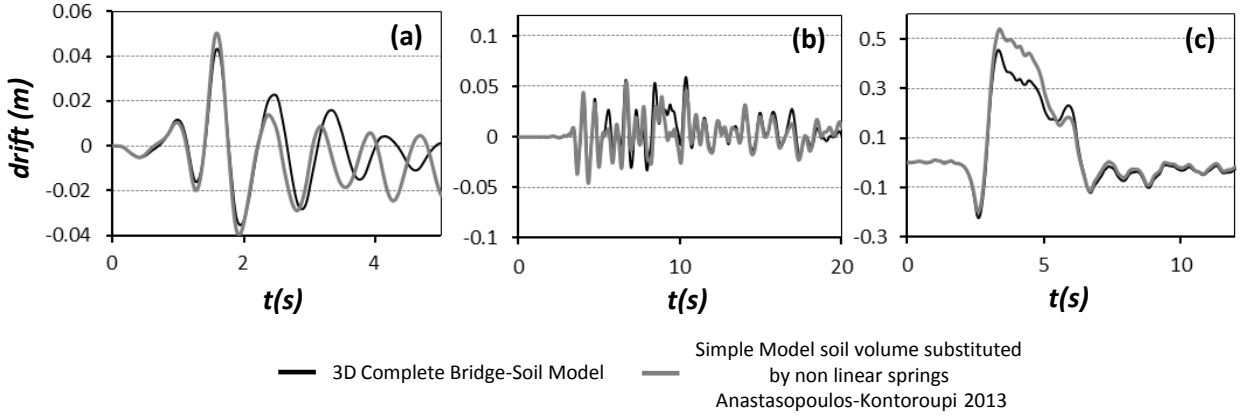

Figure 6.30 Drift time histories of the two models for **(a)** Aegio, **(b)** Lefkada_2003 and **(c)** Rinaldi_228 records in Transverse direction

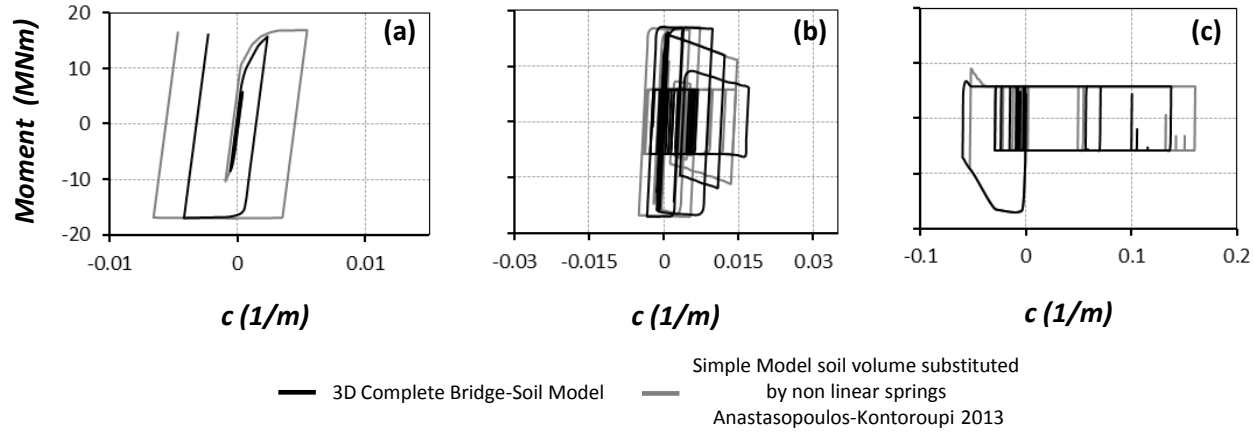

Figure 6.31 Moment-Curvature curves of the two models for **(a)** Aegio, **(b)** Lefkada_2003 and **(c)** Rinaldi_228 records in Transverse direction

	3D Complete Bridge-Soil Model				*Simple Model Fixed Base*			
	max Drift (m)	Drift res (m)	μ demand	μ d / μ c	max Drift (m)	Drift res (m)	μ demand	μ d / μ c
AEGIO	0.04	0.00	1.81	0.16	0.05	0.02	2.84	0.25
LEFKADA_2003	0.06	0.00	7.35	0.64	0.06	0.01	6.35	0.56
RINALDI_228	0.46	0.03	59.42	5.21	0.54	0.02	69.25	6.07

Deviations					
max Drift (m)	maxDrift ratio (%)	Drift res (m)	Drift res ratio (%)	μ demand	μ d / μ c
0.01	0.08	0.02	0.24	1.03	0.09
0.00	0.05	0.01	0.09	1.00	0.08
0.08	0.91	0.01	0.09	9.83	0.86

Table 6.7 Seismic Performance and deviations observed between the two Models in Longitudinal direction

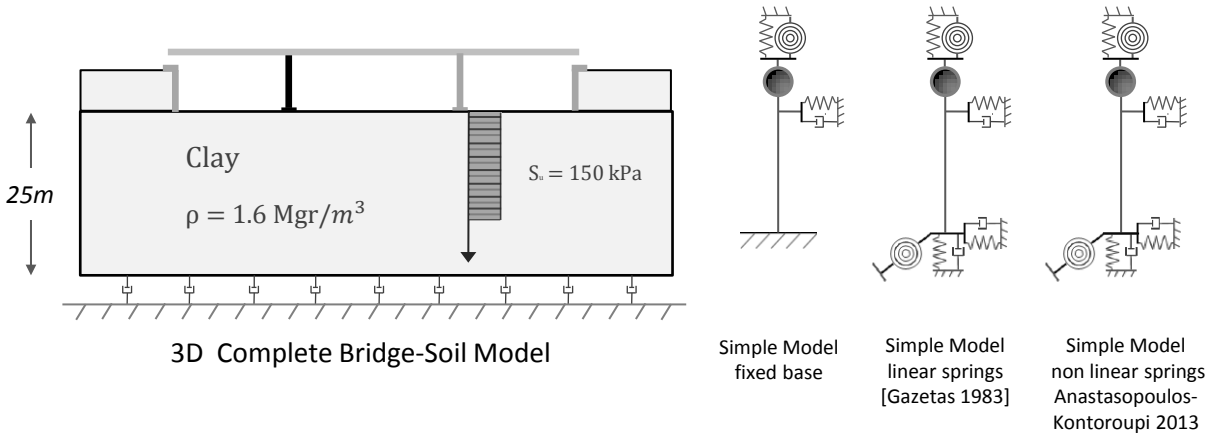

Figure 6.32 Models examined

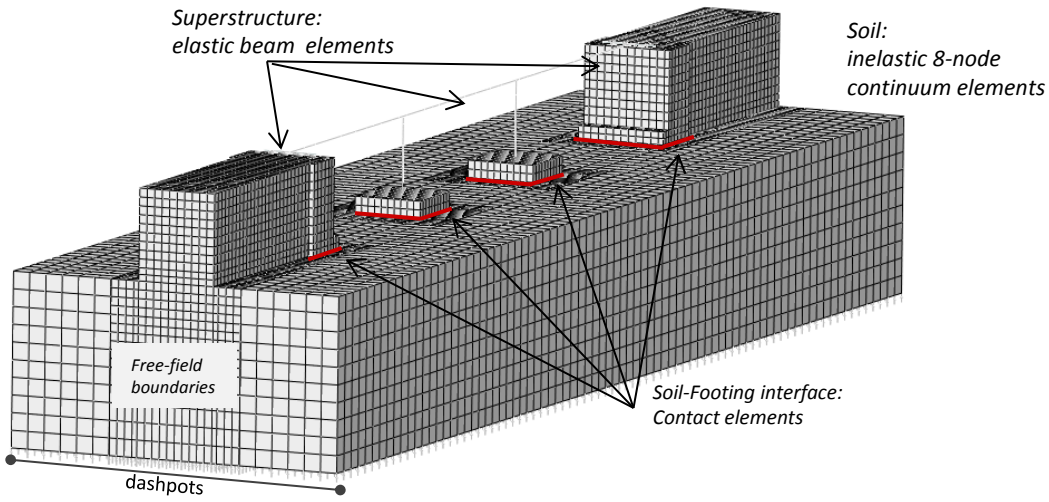

Figure 6.33 Rigorous 3D finite element model comprising the entire soil–foundation–structure system, taking account of material (soil) and geometric nonlinearities (uplifting and P–δ effects).

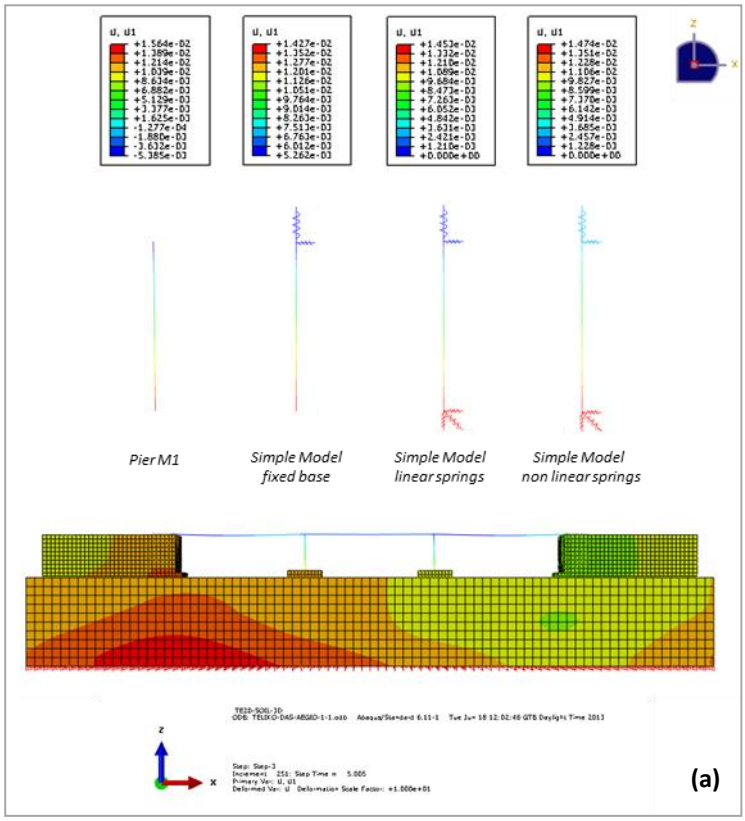

Figure 6.34 Seismic Performance of complete 3D model and simple models for Aegio record in **(a)** Longitudinal and **(b)**Transverse direction

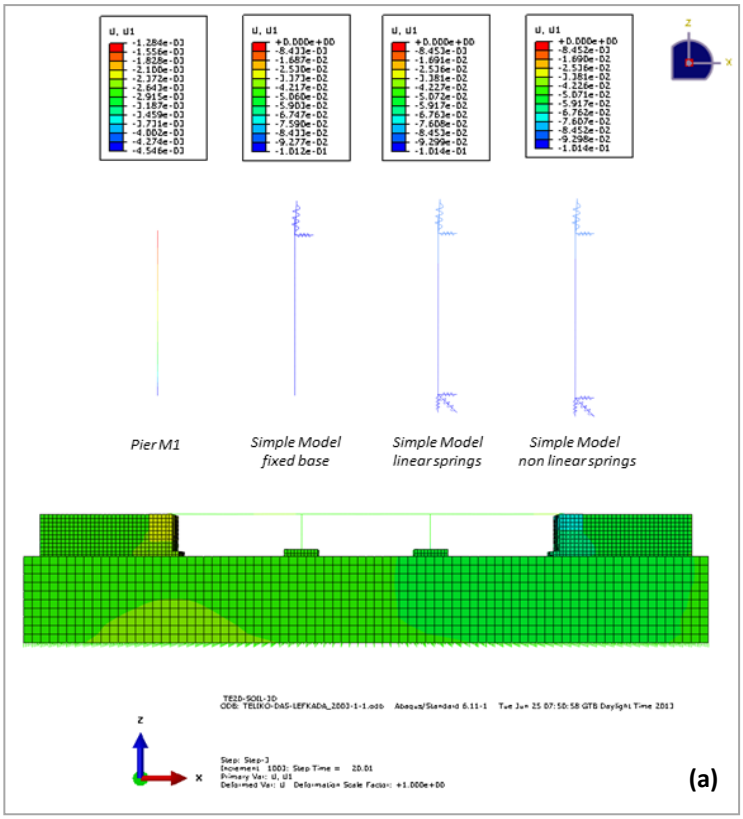

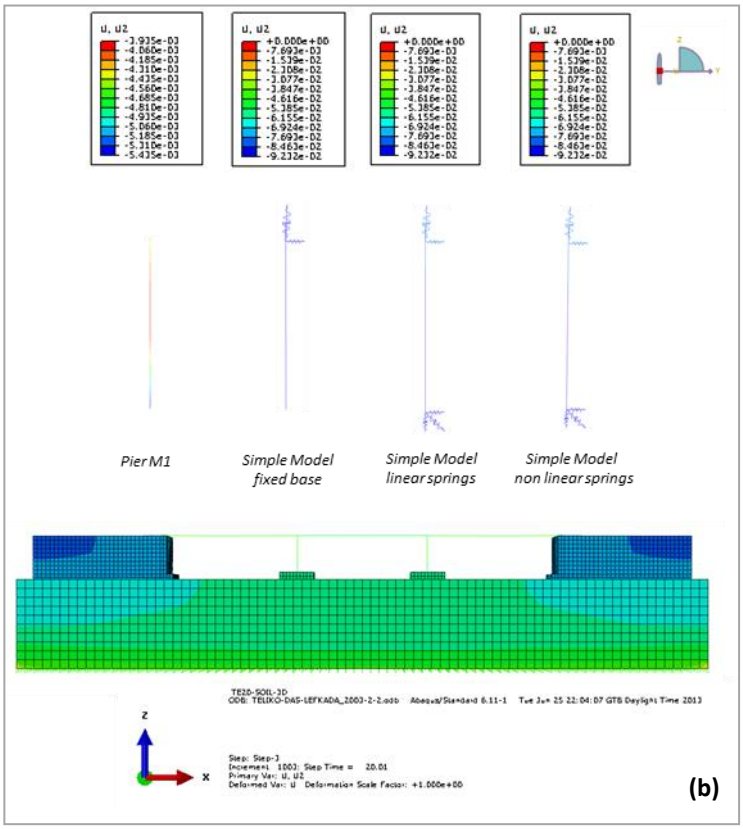

Figure 6.35 Seismic Performance of complete 3D model and simple models for Lefkada_2003 record in **(a)** Longitudinal and **(b)**Transverse direction

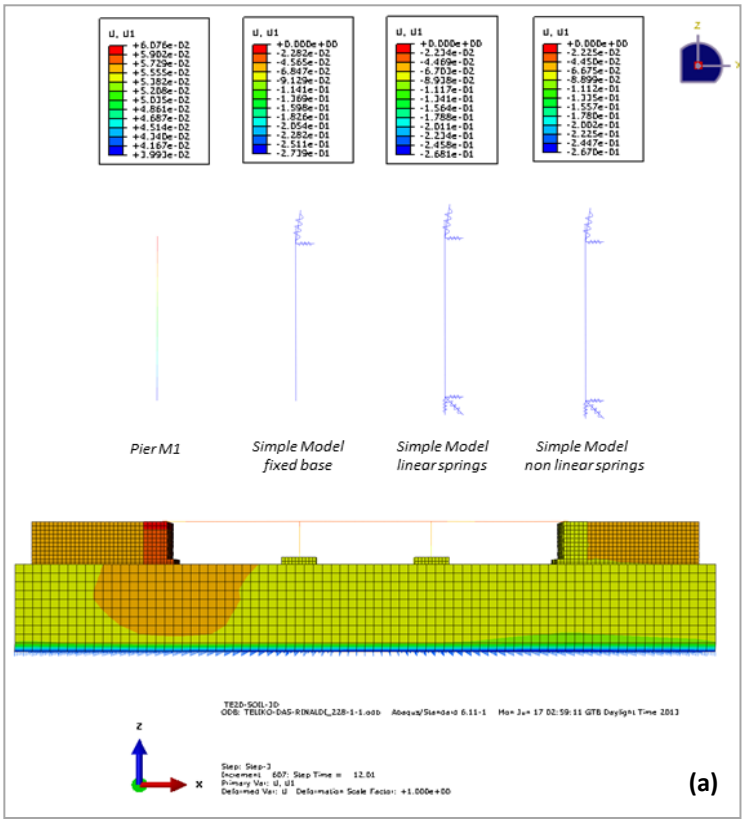

Figure 6.36 Seismic Performance of complete 3D model and simple models for Rinaldi_228 record in **(a)** Longitudinal and **(b)**Transverse direction

CHAPTER 7

PROPOSED METHODOLOGY

CONCLUSIONS

7.1 Proposed Methodology

As presented thoroughly in the 1st chapter the most common way to estimate the seismic vulnerability of a bridge are the Fragility Curves and the Incremental Dynamic Analysis (IDA) Curves. In both cases these curves have been developed using a specific intensity measure (IM), while in most cases a structural component of the bridge (pier) is considered representative of the overall fragility. In the case that the complete model of the bridge is developed, the computational effort increases significantly and therefore limited acceleration time histories are used.

Based on the methodologies available in the literature and the results of the analyses performed in the present thesis, the following simplified methodology is proposed to estimate the seismic vulnerability of bridges considering soil-structure interaction (SSI):

- **Simple Models**

In order to estimate the seismic vulnerability of a bridge, simple models are developed in both directions, as described thoroughly in the 5th chapter, that take into account the contribution of all the structural components of the bridge and the soil-structure interaction.

The development of these simple models requires: (i) a section analysis of the most vulnerable pier of the bridge and (ii) the knowledge of the geometry of the deck and the bearings in order to calculate the relevant springs and dashpots as well as the mass of the deck. Both springs and dashpots can be calculated using the analytical formulations that are presented on Chapter 5. The mass of the deck is distributed to the simple systems according to the final stiffness of the proposed system compared to the overall stiffness of the bridge.

The soil-structure interaction is taken into account using springs and dashpots that are added at the base of the simple models instead of fixed support. The calculation of the above is based on the analytical formulations by Gazetas (1983) and is described in the 6th chapter.

- **Method of analysis**

The seismic performance of the proposed models is examined in a wide range of acceleration time histories of real earthquakes (29 in the present thesis) of varying characteristics. The criterion of selection of these particular 29 acceleration time histories is mentioned in the 2nd chapter. As in most methodologies for the development of Fragility Curves and Incremental Dynamic Analysis (IDA) Curves available in the literature, the chosen accelerograms are scaled by PGA in order to have for each intensity level a wide range of acceleration time histories with different characteristics.

From the above analyses a database is created for the proposed models. Using advanced econometric models it is possible to generate an equation that correlates different intensity measures (IM's) and predicts satisfactory a specific damage index (DI) as described in the 2nd chapter. This equation is the proposed way to express seismic vulnerability of a bridge in both directions taking into account both the impact of each structural component and soil-structure interaction.

- **Advantages of the proposed methodology**

The proposed methodology is based on the relevant methodologies available in the literature, with two main differences:

The first is the fact that it is not tried to specify which intensity measure (IM) is the most appropriate for the examined type of structure. On the contrary a correlation of specific intensity measures that refer to certain characteristics of the seismic excitation is chosen.

The second refers to the model that is chosen as representative of the bridge system. Usually either a certain structural component of the bridge (for example a pier) is selected and is considered as representative of the overall fragility either complete 3D models are developed. In the first case the pier is considered as a cantilever beam (with or without fixed rotational degree of freedom at the top) and a wide range of seismic excitations is used scaled by PGA in most cases. On the contrary in the second due to the significant computational effort the acceleration time histories used are

limited. In the proposed methodology the simplified models in both directions have close seismic performance to the complete 3D model, while the computational effort remains little.

Indicatively for the Aegio record the analysis of the complete 3D bridge-soil model lasted 8 hours, while the analysis of the proposed simple one only 5 minutes. As a result it is possible to perform much more analyses in comparison to the complete model. In this way the uncertainties related to the superstructure but also to the soil properties and the soil-structure interaction are compensated by the wide range of seismic excitations that can be used to the proposed model.

- **Field of application**

The proposed methodology can be used for the purposes of a Rapid Response System for a Metropolitan Motorway. Within the framework of the research program RA.RE. (Rapid Response) in cooperation of Laboratory of Soil Mechanics of National Technical University of Athens (LSM-NTUA), Laboratory of Soil Mechanics, Foundation and Geotechnical Earthquake Engineering of Aristotle University of Thessaloniki (GEO-AUTH), OTM enterprise and Greek metropolitan motorway ''Attiki Odos'' the applicability of the proposed methodology to a portfolio of about 180 bridges of the Greek metropolitan motorway ''Attiki Odos'' can be examined.

For the purposes of the research program within the framework of the present thesis the 180 bridges of the Greek metropolitan motorway ''Attiki Odos'' were recorded, classified with certain criteria (number of spans, continuity of deck, pier-deck connection) and finally a database was created. The whole network is separated in 22 geographical areas and for each bridge the database contains all the basic geometrical data and soil properties as well as data that refer to the type of foundation and seismic design.

Based on the database created it is possible to develop in a straight-forward way the proposed simplified models and thereafter to generate equations for the 180 bridges of the network both in longitudinal and transverse directions.

7.2 Conclusions – Suggestions for further research

A rapid response system is a very useful tool for the operator of a motorway network when a seismic event occurs. Motorway networks consist of a variety of infrastructures and as a result it is very difficult or even impossible in some cases to estimate the seismic vulnerability of each one. Additionally, modeling and testing under a wide range of acceleration time histories complicated structures such as bridges, is difficult due to the high computational effort.

From the previous facts lies the need for:

- Classification of bridges in order to examine some as representative of the others
- Development of simple models representative of the overall fragility of a bridge in order to reduce the computational effort and increase the number of records used

These were two key objectives of the present thesis and the work that followed led to the following conclusions:

- A single pier of a bridge cannot represent precisely the overall fragility of the bridge
- The impact of the rest structural components in the seismic performance of the bridge is significant and therefore cannot be ignored
- The consideration of fixed abutments is a logical and realistic approach
- The consideration of fixed base piers is not a satisfactory approach in this case
- Soil-Structure Interaction cannot be ignored but can easily be considered in this case using elastic springs and dashpots

Another key objective of the present thesis was to examine whether or not a specific Intensity Measure can be used to estimate the seismic vulnerability of S-DOF systems. The results from 377 time histories analyses for the 19 IM's examined led to the following conclusions:

- None of the 19 IM's presented on its own satisfactory correlation with any of the 6 Damage Indexes used

- An attempted correlation of some specific IM's related to different characteristics of the ground motion showed promising results for the purpose of estimating the seismic vulnerability of a S-DOF system, especially for records that didn't exceed system's capacity

As far as classification of S-DOF systems is concerned it was proven that:

- Two S-DOF systems with the same :
  - Natural period (T)
  - Design Spectral Acceleration (SA)
  - and Ductility Capacity ($\mu_{capacity}$)

have very close seismic performance and can be considered as equivalent.

- A S-DOF system cannot represent precisely the seismic performance of a bridge pier and therefore the above conclusion cannot be extended for the entire system of a bridge

• Suggestions for further research

Based on the previous conclusions the following steps would be:

- To investigate the possibility of extending the proposed criterion of equivalence between S-DOF Systems to the simplified models proposed in the present thesis that represent the overall fragility of the bridge
- To examine the applicability of the proposed methodology to a portfolio of bridges of the Greek metropolitan motorway ''Attiki Odos''
- To examine further the effect of soil-structure interaction to the seismic performance of a bridge considering different soil conditions and types of foundation and using more records in both directions

In addition the selected bridge in the present thesis is a common but simple case. Its simplicity lies in the symmetry of the bridge and the circular section of the piers. Therefore the proposed

methodology has to be extended to more complex cases. More specific the impact to the seismic performance of a bridge of different factors like:

- The asymmetry of the bridge
- The existence of bearings in the middle piers of a bridge
- The effect of different geometries of the section of the deck
- The existence of stoppers at the abutments
- The skewness of the bridge
- The type of the piers (single column or multiple column piers)
- The section of the piers (circular, rectangular, etc.)

has to be examined in the future.

References

ABAQUS 6.11. (2011). Standard user's manual. Dassault Systèmes Simulia Corp., Providence, RI, USA.

Anastasopoulos I., Gelagoti F., Kourkoulis R., Gazetas G. (2011). "Simplified Constitutive model for Simulation of Cyclic Response of Shallow Foundations: Validation against Laboratory Tests", *Journal of Geotechnical and Geoenvironmental Engineering*, ASCE, Vol. 137, No. 12, pp. 1154–1168.

Anastasopoulos I., Kokkali P., Tsatsis A. (2011), "Experimental Investigation of Vertical Load Capacity of Surface Footings".

Anastasopoulos I., Kokkali P., Tsatsis A. (2011). "1-dof System Lying on Square Foundation: Monotonic and Cyclic Loading".

Anastasopoulos I., Gazetas G., Loli M., Apostolou M., Gerolymos N. (2010). "Soil failure can be used for seismic protection of structures". *Bulletin of Earthquake Engineering* 8, pp. 309-326.

Applied Technology Council (1985). "Earthquake Damage Evaluation Data for California", *Rep. No. ATC-13, Applied Technology Council, Redwood City, CA.*

Applied Technology Council (1991). "Seismic Vulnerability and Impact of Disruption of Lifelines in the Conterminous United States", *Rep. No. ATC-25, Applied Technology Council, Redwood City, CA.*

Ayyub, B. M. and Lai, K.-L. (1989). "Structural reliability assessment using Latin Hypercube Sampling." *Proceedings of ICOSSAR '89, the 5th International Conference on Structural Safety and Reliability*, Part II , ASCE, New York NY USA , p 1177-1184.

Basoz N. , Kiremidjian, A. S. (1999). "Development of Empirical Fragility Curves for Bridges." *5th US Conference on Lifeline Earthquake Engineering* , ASCE, New York NY USA .

Basoz N., Kiremidjian, A. S. (1997). "Evaluation of Bridge Damage Data From the Loma Prieta and Northridge, CA Earthquakes." *Rep. No. MCEER-98-0004*, John A. Blume Earthquake Engineering Center, Stanford, CA.

Basoz N., Kiremidjian, A. S. (1996). "Risk Assessment for Highway Transportation Systems." *Rep. No. NCEER-118*, JohnA. Blume Earthquake Engineering Center, Stanford, CA.

Broglio, S., Crowley, H., Pinho, R. (2010). "Simplified capacity curves for RC bridges" *Proceedings of the 14th European Conference on Earthquake Engineering*, paper no. 1336, Ohrid, Macedonia.

Chai, Y. H., Priestley, M. J. N., and Seible, F. (1991). "Seismic Retrofit of Circular Bridge Columns for Enhanced Flexural Performance." *ACI Structural Journal (American Concrete Institute),* 88(5), 572-584.

Choi E, DesRoches R, Nielson B (2004). “Seismic fragility of typical bridges in moderate seismic zones”. Engineering Structures ; 26:187–199.

Chopra A. K. (1995): “*Dynamics of structures – Theory and applications to earthquake engineering”*, Prentice-Hall Inc.

Codermatz R., Nicolich R., Slejko D. (2003). “Seismic risk assessments and GIS technology: applications to infrastructures in the Friuli-Venezia Giulia region (NE Italy)”. *Earthquake Engineering and Structural Dynamics,* Vol.32, pp. 1677-1690.

EAK (2000) “Greek Seismic Code”, Organization of Seismic Planning and Protection, Athens (in Greek).

ΕΚΩΣ(2000) “Greek code for reinforced concrete”, Organization of Seismic Planning and Protection, Athens (in Greek).

EN1998-1-1, “Eurocode 8: *Design of structures for earthquake resistance – Part 1 -1”: General rules, seismic actions and rules for buildings, CEN, 2003*.

Erdik M., Fahjan Y., Ozel O., Alcik H., Mert A., Gul M.,(2003). “Istanbul Earthquake Rapid Response and the Early Warning System”, *Bulletin of Earthquake Engineering* **1,** pp. 157-163.

Erdik M., Sesetyan K., Demircioglu M.B., Hancılar U., Zulfikar C. (2010) “Rapid earthquake loss assessment after damaging earthquakes”. *Soil Dynamics and Earthquake Engineering*, Vol. 31, pp. 247-266.

Esposito, S. and Iervolino, I. (2010) “PGA and PGV Spatial Correlation models based on European multi-event datasets”, *Bulletin of the Seismological Society of America*. 101 (5): 2532-2541.

FEMA. (1997). “HAZUS 97 Technical Manual II.” Washington DC, FEMA.

Garini, E. (2011). “Sliding Systems under Near–Fault Ground Shaking: Development and Demonstration of Inelastic Analogues”, *Doctoral Thesis NTUA*.

Gazetas G., Anastasopoulos I, Adamidis O., Kontoroupi T. ,(2013). “Nonlinear rocking stiffness of foundations”*, Soil Dynamics and Earthquake Engineering Volume 47, April 2013, Pages 83–91*

Gazetas G, Anastasopoulos I, Gerolymos N, Mylonakis G, Syngros C. (2005). ”The collapse of the Hanshin expressway (Fukae) bridge, Kobe 1995: soil-foundation-structure interaction, reconstruction, seismic isolation”, *Entwicklungen in der Bodenmechanik, Bodendynamik und Geotechnik, Festschrift zum 60. Geburstag von Univ.-Professor Dr.-Ing.habil. Stavros A. Savidis (Honorary Volume for the 60th Birthday of Professor Savidis)*, Frabk Rackwitz, Springer, pp 93–120.

Gazetas, G. (2005):“Soil Dynamics” Geotechnical Division, National Technical University of Athens, 2005 (in Greek).

Gazetas G, ApostolouM, Anastasopoulos I. (2003). “Seismic uplifting of foundations on soft soil, with examples from Adapazari (Izmit 1999, Earthquake)”. *In: BGA int. conf. on found. innov., observations, design & practice*, Univ. of Dundee, Scotland, September 25, pp 37–50.

Gazetas, G. [1991]. “Formulas and charts for impedances of surface and embedded foundations”, *Journal of Geotechnical Engineering*, ASCE, 117 (9), 1129–1141.

Gazetas G. (1987). “Simple physical methods for foundation impedances.” *Dynamics of Foundations and Buried Structures, Benerjee PK and Butterfield R., editors, ElsevierApplied Science*, Chapter 2, 44-90.

Gazetas, G. (1983). “Analysis of machine foundation vibrations: state of the art,” Soil Dynamics and Earthquake Engineering, 2(1), 2-42.

Gourvenec S. (2007). “Shape effects on the capacity of rectangular footings under general loading”, *Geotechnique 57, No. 8, pp. 637–646.*

Hwang H, Liu JB, Chiu Y-H.(2000) “Seismic fragility analysis of highway bridges”. *MAEC RR-4*, Center for Earthquake Research Information.

Hwang, H., Huo, J. R. (1998). "Probabilistic Seismic Damage Assessment of Highway Bridges." *6th US National Conference on Earthquake Engineering*, EERI, Oakland, CA.

Hwang, H., Jaw, J. W. (1990). "Probabilistic Damage Analysis of Structures." *Journal of Structural Engineering*, 116(7), 1992-2007.

Jacob, K. H. (1992). "Seismic Hazards in the Eastern U.S. and the Impact on Transportation Lifelines." *Lifeline Earthquake Engineering in the Central and Eastern U.S*., Monograph No. 5, ASCE, New York NY USA .

Jernigan JB, Hwang H. (2002) “Development of bridge fragility curves”. *7th US National Conference on Earthquake Engineering*, EERI: Boston, MA, 2002.

Karim, K.R., Yamazaki, F. (2003). “A simplified method of constructing fragility curves for highway bridges”. *Earthquake Engineering and Structural dynamics* **32**, 1603-1626.

Karim, K.R., Yamazaki, F. (2001). “Effect of earthquake ground motions on fragility curves of highway bridge piers based on numerical simulation”. *Earthquake Engineering and Structural dynamics* **30**, 1839-1856.

Kiureghian, A. D. (2002). "Bayesian Methods for Seismic Fragility Assessment of Lifeline Components." Acceptable Risk Processes: Lifelines and Natural Hazards, Monograph No. 21, A. D. Kiureghian, ed., Technical Council on Lifeline Earthquake Engineering, ASCE, Reston VA USA.

Kottegoda N. T. , Rosso, R. (1997). “Statistics, Probability, and Reliability for Civil and Environmental Engineers.” The McGraw-Hill Companies, Inc.

Kourkoulis, R., Anastasopoulos, I., Gelagoti, F., Kokkali, P. (2012). "Dimensional Analysis of SDOF Systems Rocking on Inelastic Soil", *Journal of Earthquake Engineering* (in press).

Koutsourelakis S., Prevost J., Deodatis G. (2002). “Risk assessment of an interacting structure–soil system due to liquefaction Earthquake” *Earthquake Engineering and Structural Dynamics* (2002)31 pp.: 851–879.

Kowalsky, M. J. (2000). "Deformation Limit States for Circular Reinforced Concrete Bridge Columns" *Journal of Structural Engineering*, 126(8), 869-878.

Kwon O, Elnashai A.(2010) , “Fragility analysis of a highway over-crossing bridge with consideration of soil–structure interactions”, *Structure and Infrastructure Engineering Volume 6*, Issue 1-2, 2010 pages 159-178.

Mackie, K. and Stojadinovic, B. (2003). "Seismic Demands for Performance-Based Design of Bridges." Rep. No. PEER 312.

Mackie, K. and Stojadinovic, B. (2001). "Probabilistic Seismic Demand Model for California Bridges." *Journal of Bridge Engineering*, 6(6), 468-480.

Mander, J. B., Kim, D. K., Chen, S. S., Premus, G. J. (1996). “Response of Steel Bridge Bearings to the Reversed Cyclic Loading.” *Rep. No. NCEER 96-0014*, NCEER, Buffalo, NY.

Mander, J. B., Basoz, N. (1999). "Seismic Fragility Curve Theory for Highway Bridges." *5th US Conference on Lifeline Earthquake Engineering* , ASCE, New York NY USA .

Meyerhof, G. G. (1951). "The ultimate bearing capacity of foundations", *Geotechnique*, 2 (4), 301-332.

Moschonas, I.F., Kappos, A.J., Panetsos, P., Papadopoulos, V., Makarios, T. and Thanopoulos, P. (2009). “Seismic fragility curves for greek bridges: methodology and case studies”, *Bulletin of Earthquake Engineering* **7**, pp. 439-468.

Nielson BG. (2005) “Analytical fragility curves for highway bridges in moderate seismic zones”. Ph.D. Thesis, Georgia Institute of Technology, 2005.

Pitilakis, K., Kakderi, K. (2011) “Seismic risk assessment and management of lifelines”, utilities and infrastructures.

Priestley, M.J.N., Seible, F., Calvi, G.M. (1996) “Seismic Design and Retrofit of Bridges,” John Wiley and Sons, New York.

Selva, J., Kakderi, K., Alexoudi, M., Pitilakis, K. (2011). “Seismic Performance of a System of Interdependent Lifeline and Infrastructure Components*”, 8th International Conference on Urban Earthquake Engineering*, March 7-8, 2011, Tokyo Institute of Technology, Tokyo. Japan.

Shinozuka M, Feng MQ, Lee J, Naganuma T.(2000). “ Statistical analysis of fragility curves”. *Journal of Engineering Mechanics*; 126:1224–1231.

Shinozuka M, Feng MQ, Kim H-K, Kim S-H.(2000). Nonlinear static procedure for fragility curve development. *Journal of Engineering Mechanics* 2000; 126:1287–1296.

Shinozuka, M., Feng, M. Q., Dong, X., Uzawa, T., and Ueda, T. (2000). "Damage Assessment of a Highway Network Under Scenario Earthquakes for Emergency Response Decision Support." *Proceedings of SPIE* - The International Society for Optical Engineering, Society of Photo-Optical Instrumentation Engineers , Bellingham WA USA , p264-275.

Vamvatsikos D. , Cornell CA. (2002) “Incremental dynamic analysis Earthquake” *Earthquake Engineering and Structural Dynamics* 31 pp. :491–514.

Vamvatsikos D, Cornell CA.(2001) “Tracing and post-processing of IDA curves: Theory and software implementation” . Report No. RMS-44, RMS Program, Stanford University, Stanford.

Wen, Y. K., Ellingwood, B. R., Veneziano, D., and Bracci, J. (2003). *Rep. No. MAE-FD-2*, Mid-America Earthquake Center, Urbana, IL.

Wen, Y. K. and Wu, C. L. (2001). "Uniform Hazard Ground Motions for Mid-America Cities." *Earthquake Spectra*, 17(2), 359-384.

Yamazaki F, Hamada T, Motoyama H, Yamauchi H.(1999). “Earthquake damage assessment of expressway bridges in Japan”. *Technical Council on Lifeline Earthquake Engineering Monograph* 1999; 361–370.